

ISSN 1881-7815 Online ISSN 1881-7823

BST

BioScience Trends

Volume 11, Number 5
October, 2017



www.biosciencetrends.com

BST

BioScience Trends



ISSN: 1881-7815
Online ISSN: 1881-7823

CODEN: BTIRCZ

Issues/Year: 6

Language: English

Publisher: IACMHR Co., Ltd.

BioScience Trends is one of a series of peer-reviewed journals of the International Research and Cooperation Association for Bio & Socio-Sciences Advancement (IRCA-BSSA) Group and is published bimonthly by the International Advancement Center for Medicine & Health Research Co., Ltd. (IACMHR Co., Ltd.) and supported by the IRCA-BSSA and Shandong University China-Japan Cooperation Center for Drug Discovery & Screening (SDU-DDSC).

BioScience Trends devotes to publishing the latest and most exciting advances in scientific research. Articles cover fields of life science such as biochemistry, molecular biology, clinical research, public health, medical care system, and social science in order to encourage cooperation and exchange among scientists and clinical researchers.

BioScience Trends publishes Original Articles, Brief Reports, Reviews, Policy Forum articles, Case Reports, News, and Letters on all aspects of the field of life science. All contributions should seek to promote international collaboration.

Editorial Board

Editor-in-Chief:

Norihiro KOKUDO
National Center for Global Health and Medicine, Tokyo, Japan

Co-Editors-in-Chief:

Xue-Tao CAO
Chinese Academy of Medical Sciences, Beijing, China
Rajendra PRASAD
University of Delhi, Delhi, India
Arthur D. RIGGS
Beckman Research Institute of the City of Hope, Duarte, CA, USA

Chief Director & Executive Editor:

Wei TANG
The University of Tokyo, Tokyo, Japan

Senior Editors:

Xunjia CHENG
Fudan University, Shanghai, China
Yoko FUJITA-YAMAGUCHI
Beckman Research Institute of the City of Hope, Duarte, CA, USA
Na HE
Fudan University, Shanghai, China
Kiyoshi KITAMURA
The University of Tokyo, Tokyo, Japan
Misao MATSUSHITA
Tokai University, Hiratsuka, Japan
Munehiro NAKATA
Tokai University, Hiratsuka, Japan
Takashi SEKINE

Toho University, Tokyo, Japan
Ri SHO
Yamagata University, Yamagata, Japan
Yasuhiko SUGAWARA
Kumamoto University, Kumamoto, Japan
Ling WANG
Fudan University, Shanghai, China

Managing Editor:

Jianjun GAO
Qingdao University, Qingdao, China

Web Editor:

Yu CHEN
The University of Tokyo, Tokyo, Japan

Proofreaders:

Curtis BENTLEY
Roswell, GA, USA
Christopher HOLMES
The University of Tokyo, Tokyo, Japan
Thomas R. LEBON
Los Angeles Trade Technical College, Los Angeles, CA, USA

Editorial Office

Pearl City Koishikawa 603,
2-4-5 Kasuga, Bunkyo-ku, Tokyo 112-0003, Japan
Tel: +81-3-5840-8764 Fax: +81-3-5840-8765
E-mail: office@biosciencetrends.com

BioScience Trends

Editorial and Head Office

Pearl City Koishikawa 603, 2-4-5 Kasuga, Bunkyo-ku,
Tokyo 112-0003, Japan

Tel: +81-3-5840-8764, Fax: +81-3-5840-8765
E-mail: office@biosciencetrends.com
URL: www.biosciencetrends.com

Editorial Board Members

Girdhar G. AGARWAL <i>(Lucknow, India)</i>	Takahiro HIGASHI <i>(Tokyo, Japan)</i>	Francesco MAROTTA <i>(Milano, Italy)</i>	Shin'ichi TAKEDA <i>(Tokyo, Japan)</i>
Hirotugu AIGA <i>(Geneva, Switzerland)</i>	De-Fei HONG <i>(Hangzhou, China)</i>	Yutaka MATSUYAMA <i>(Tokyo, Japan)</i>	Sumihito TAMURA <i>(Tokyo, Japan)</i>
Hidechika AKASHI <i>(Tokyo, Japan)</i>	De-Xing HOU <i>(Kagoshima, Japan)</i>	Qingyue MENG <i>(Beijing, China)</i>	Puay Hoon TAN <i>(Singapore, Singapore)</i>
Moazzam ALI <i>(Geneva, Switzerland)</i>	Sheng-Tao HOU <i>(Ottawa, Canada)</i>	Mark MEUTH <i>(Sheffi eld, UK)</i>	Koji TANAKA <i>(Tsu, Japan)</i>
Ping AO <i>(Shanghai, China)</i>	Yong HUANG <i>(Ji'ning, China)</i>	Satoko NAGATA <i>(Tokyo, Japan)</i>	John TERMINI <i>(Duarte, CA, USA)</i>
Hisao ASAMURA <i>(Tokyo, Japan)</i>	Hirofumi INAGAKI <i>(Tokyo, Japan)</i>	Miho OBA <i>(Odawara, Japan)</i>	Usa C. THISYAKORN <i>(Bangkok, Thailand)</i>
Michael E. BARISH <i>(Duarte, CA, USA)</i>	Masamine JIMBA <i>(Tokyo, Japan)</i>	Fanghua QI <i>(Ji'nan, Shandong)</i>	Toshifumi TSUKAHARA <i>(Nomi, Japan)</i>
Boon-Huat BAY <i>(Singapore, Singapore)</i>	Kimitaka KAGA <i>(Tokyo, Japan)</i>	Xianjun QU <i>(Beijing, China)</i>	Kohjiro UEKI <i>(Tokyo, Japan)</i>
Yasumasa BESSHO <i>(Nara, Japan)</i>	Ichiro KAI <i>(Tokyo, Japan)</i>	John J. ROSSI <i>(Duarte, CA, USA)</i>	Masahiro UMEZAKI <i>(Tokyo, Japan)</i>
Generoso BEVILACQUA <i>(Pisa, Italy)</i>	Kazuhiro KAKIMOTO <i>(Osaka, Japan)</i>	Carlos SAINZ-FERNANDEZ <i>(Santander, Spain)</i>	Junming WANG <i>(Jackson, MS, USA)</i>
Shiuan CHEN <i>(Duarte, CA, USA)</i>	Kiyoko KAMIBEPPU <i>(Tokyo, Japan)</i>	Yoshihiro SAKAMOTO <i>(Tokyo, Japan)</i>	Xiang-Dong Wang <i>(Boston, MA, USA)</i>
Yuan CHEN <i>(Duarte, CA, USA)</i>	Haidong KAN <i>(Shanghai, China)</i>	Erin SATO <i>(Shizuoka, Japan)</i>	Hisashi WATANABE <i>(Tokyo, Japan)</i>
Naoshi DOHMAE <i>(Wako, Japan)</i>	Bok-Luel LEE <i>(Busan, Korea)</i>	Takehito SATO <i>(Isehara, Japan)</i>	Lingzhong XU <i>(Ji'nan, China)</i>
Zhen FAN <i>(Houston, TX, USA)</i>	Mingjie LI <i>(St. Louis, MO, USA)</i>	Akihito SHIMAZU <i>(Tokyo, Japan)</i>	Masatake YAMAUCHI <i>(Chiba, Japan)</i>
Ding-Zhi FANG <i>(Chengdu, China)</i>	Shixue LI <i>(Ji'nan, China)</i>	Zhifeng SHAO <i>(Shanghai, China)</i>	Aitian YIN <i>(Ji'nan, China)</i>
Xiaobin FENG <i>(Beijing, China)</i>	Ren-Jang LIN <i>(Duarte, CA, USA)</i>	Judith SINGER-SAM <i>(Duarte, CA, USA)</i>	George W-C. YIP <i>(Singapore, Singapore)</i>
Yoshiharu FUKUDA <i>(Ube, Japan)</i>	Lianxin LIU <i>(Harbin, China)</i>	Raj K. SINGH <i>(Dehradun, India)</i>	Xue-Jie YU <i>(Galveston, TX, USA)</i>
Rajiv GARG <i>(Lucknow, India)</i>	Xinqi LIU <i>(Tianjin, China)</i>	Peipei SONG <i>(Tokyo, Japan)</i>	Benny C-Y ZEE <i>(Hong Kong, China)</i>
Ravindra K. GARG <i>(Lucknow, India)</i>	Daru LU <i>(Shanghai, China)</i>	Junko SUGAMA <i>(Kanazawa, Japan)</i>	Yong ZENG <i>(Chengdu, China)</i>
Makoto GOTO <i>(Tokyo, Japan)</i>	Hongzhou LU <i>(Shanghai, China)</i>	Hiroshi TACHIBANA <i>(Isehara, Japan)</i>	Xiaomei ZHU <i>(Seattle, WA, USA)</i>
Demin HAN <i>(Beijing, China)</i>	Duan MA <i>(Shanghai, China)</i>	Tomoko TAKAMURA <i>(Tokyo, Japan)</i>	
David M. HELFMAN <i>(Daejeon, Korea)</i>	Masatoshi MAKUUCHI <i>(Tokyo, Japan)</i>	Tadatoshi TAKAYAMA <i>(Tokyo, Japan)</i>	(as of June 26, 2017)

Review

- 496 - 506 **Chinese single herbs and active ingredients for postmenopausal osteoporosis: From preclinical evidence to action mechanism.**
Jing Lin, Jun Zhu, Yan Wang, Na Zhang, Hans-Jürgen Gober, Xuemin Qiu, Dajin Li, Ling Wang

Original Articles

- 507 - 515 **Social support and care needs of the disabled elderly population: An empirical study based on survey data from Beijing, China.**
Xiaoning Hao, Juan Gu, Xiangji Ying, Tao Bo, Wei Fu
- 516 - 523 **Relationships between neighborhood attributes and subjective well-being among the Chinese elderly: Data from Shanghai.**
Junling Gao, Scott R. Weaver, Hua Fu, Yingnan Jia, Jiang Li
- 524 - 532 **Price adjustment for traditional Chinese medicine procedures: Based on a standardized value parity model.**
Haiyin Wang, Chunlin Jin, Qingwu Jiang
- 533 - 541 **A comparative study on predicting influenza outbreaks.**
Jie Zhang, Kazumitsu Nawata
- 542 - 549 **PCSK9 rs7552841 is associated with plasma lipids profiles in female Chinese adolescents without posttraumatic stress disorder.**
Qiwei Guo, Yanjun Si, Mi Su, Mei Fan, Jia Lin, Nazakat H Memon, Dingzhi Fang
- 550 - 556 **Construction of C35 gene bait recombinants and T47D cell cDNA library.**
Kun Yin, Chao Xu, Gui-Hua Zhao, Ye Liu, Ting Xiao, Song Zhu, Ge Yan
- 557 - 564 **Protective effects of luteolin-7-O-glucoside against starvation-induced injury through upregulation of autophagy in H9c2 Cells.**
Hong Yao, Lichun Zhou, Linlin Tang, Yanhui Guan, Shang Chen, Yu Zhang, Xiuzhen Han
- 565 - 573 **Induction of apoptosis by ethanol extract of *Citrus unshiu* Markovich peel in human bladder cancer T24 cells through ROS-mediated inactivation of the PI3K/Akt pathway.**
Kyu Im Ahn, Eun Ok Choi, Da He Kwon, Hyun HwangBo, Min Yeong Kim, Hong Jae Kim, Seon Yeong Ji, Su-Hyun Hong, Jin-Woo Jeong, Cheol Park, Nam Deuk Kim, Wun Jae Kim, Yung Hyun Choi
- 574 - 580 **Statin use is associated with a reduced risk of hepatocellular carcinoma recurrence after initial liver resection.**
Yoshikuni Kawaguchi, Yoshihiro Sakamoto, Daisuke Ito, Kyoji Ito, Junichi Arita, Nobuhisa Akamatsu, Junichi Kaneko, Kiyoshi Hasegawa, Kyoji Moriya, Norihiro Kokudo

CONTENTS

(Continued)

- 581 - 587 **Indication for surgical resection in patients with hepatocellular carcinoma with major vascular invasion.**
Tokio Higaki, Shintaro Yamazaki, Masamichi Moriguchi, Hisashi Nakayama, Tomoharu Kurokawa, Tadatoshi Takayama
- 588 - 594 **Total bilirubin amount in drainage fluid can be an early predictor for severe biliary fistula after hepatobiliary surgery.**
Toshitaka Sugawara, Junichi Shindoh, Yujiro Nishioka, Masaji Hashimoto

Brief Report

- 595 - 599 **5-aminolevulinic acid (5-ALA) fluorescence-guided Mohs surgery resection of penile-scrotal extramammary Paget's disease.**
Xiaoqiong Peng, Wei Qian, Jiangang Hou

Letter

- 600 - 602 **Non-linear association between alcohol and incident frailty among community-dwelling older people: A dose-response meta-analysis.**
Gotaro Kojima, Steve Iliffe, Ann Liljas, Kate Walters
- 603 - 605 **Activity outside the home, environmental barriers, and healthy aging for community-dwelling elderly individuals in China.**
Yuhong Niu, Na Li, Chunlin Jin, Duo Chen, Yitong Yang, Hansheng Ding

Guide for Authors

Copyright

Chinese single herbs and active ingredients for postmenopausal osteoporosis: From preclinical evidence to action mechanism

Jing Lin^{1,2,3,§}, Jun Zhu^{4,§}, Yan Wang^{1,2,3}, Na Zhang^{1,2,3}, Hans-Jürgen Gober⁵, Xuemin Qiu^{1,2,3}, Dajin Li^{1,2,3}, Ling Wang^{1,2,3,*}

¹Laboratory for Reproductive Immunology, Hospital & Institute of Obstetrics and Gynecology, Shanghai Medical College, Fudan University, Shanghai, China;

²The Academy of Integrative Medicine of Fudan University, Shanghai, China;

³Shanghai Key Laboratory of Female Reproductive Endocrine-related Diseases, Shanghai, China;

⁴Department of Obstetrics and Gynecology, Wenling People's Hospital, Wenzhou Medical University, Zhejiang, China;

⁵Department of Pharmacy, Kepler University Clinic, Neuromed Campus, Linz, Austria.

Summary

Postmenopausal osteoporosis is a systemic metabolic skeletal disease generally ascribable to a dearth of estrogen. Whether traditional Chinese medicine is effective in management of postmenopausal osteoporosis remains unclear. This article reviews the experimental evidence of both *in vitro* and *in vivo* preclinical studies with the theme of the application of Chinese single herbs and active ingredients in postmenopausal osteoporosis. It includes three single herbs (Herba Epimedium, Rhizoma Drynariae, and Salvia miltiorrhiza) and eight active ingredients (saikosaponins, linarin, echinacoside, sweroside, psoralen, poncirin, vanillic acid, and osthole). The experimental studies indicated their potential use as treatment for postmenopausal osteoporosis and investigated the underlying mechanisms including osteoprotegerin/receptor activator of nuclear factor κ B ligand (OPG/RANKL), extracellular-signal-regulated kinase/c-Jun N terminal kinase/mitogen-activated protein kinase (ERK/JNK/MAPK), estrogen receptor (ER), bone morphogenetic protein (BMP), transforming growth factor (TGF)- β , Wnt/ β -catenin, and Notch signaling pathways. This review contributes to a better understanding of traditional Chinese medicine and provides useful information for the development of more effective anti-osteoporosis drugs.

Keywords: Traditional Chinese medicine (TCM), single herbs, active ingredients, postmenopausal osteoporosis, bone morphogenetic protein (BMP), estrogen receptor (ER)

1. Introduction

Postmenopausal osteoporosis is a systemic metabolic skeletal disease characterized by structural deterioration and high fragility of bone tissue, generally ascribable to a dearth of estrogen. Osteoporosis affects 200 million women worldwide, and the probability of women over 50 affected by an osteoporotic fracture has been estimated to approach one third (1). With an aging population, the

economic burden of osteoporosis increases exponentially. It is often associated with pain and fractures leading to reduced quality of life such as depression, morbidity, and increased mortality, which is considered to be an important public health issue.

Therapeutic agents currently used for osteoporosis include menopausal hormone therapy (MHT), bisphosphonates, calcitonin, selective estrogen receptor modulators (SERMs), parathyroid hormone (PTH) analogs, and so on. However, there have been long-term safety concerns about these drugs. Adverse events in clinical use include increased risk of cardiovascular disease, venous thromboembolism, breast and endometrial cancer, and stroke with hormone therapy; gastrointestinal intolerance, jaw osteonecrosis, atypical femoral fractures, and atrial fibrillation with bisphosphonates; a possible oncogenic association with

[§]These authors contributed equally to this work.

*Address correspondence to:

Dr. Ling Wang, Laboratory for Reproductive Immunology, Hospital & Institute of Obstetrics and Gynecology, Fudan University Shanghai Medical College, 413 Zhaozhou Road, Shanghai 200011, China.

E-mail: Dr.wangling@fudan.edu.cn

salmon calcitonin; lower efficacy on fracture prevention and increased risk of venous thrombotic events with SERMs; nausea, headache, dizziness, hypercalcemia, hypercalciuria with PTH analogs (2). Therefore, safer and more effective alternatives for the management of osteoporosis are being explored.

In recent years, a growing interest has risen in the treatment of postmenopausal osteoporosis with traditional Chinese medicine (TCM). Compared with Western medicine, TCM has fewer adverse events with long-term use, for which extensive experience has been accumulated over thousands of years. Chinese medicinal herbs usually exert their therapeutic effects through a "multi-components, multi-pathways, and multi-targets" mode, which is in accordance with the multifactorial and complicated nature of postmenopausal osteoporosis (3). TCM will be continuously adopted as a cost-effective alternative to chemically synthesized medicines as well as excellent and reliable sources for derivation of natural products for the development of new drugs. A meta-analysis in 2009, which included 14 randomized controlled trials involving 780 patients with postmenopausal osteoporosis, suggested that phytotherapy might possess a similar effect as hormone therapy on bone mineral density (BMD) values with a lower incidence of breast pain and uterine bleeding (4). It was later contradicted by new evidence in 2017 which included 10 randomized controlled trials involving 957 patients and concluded that Chinese herbal medicine alone did not significantly improve lumbar spine BMD (5). Further high-quality clinical trials are required in this field.

In TCM, there is no well-defined disease known as postmenopausal osteoporosis. However, symptom profiles in classical records such as low back pain, fracture, spine deformities, and limb atrophy could be the manifestations of osteoporosis. According to the TCM theoretical extraction of pathogenesis and symptoms, postmenopausal osteoporosis belongs to the TCM syndromes of "Gubi", "Gushi (bone loss)", "Guwei (bone atrophy)", "Guku (lack of bone marrow)", and "Guji (bone polarization)" (6). The role of "kidney" in governing the bone and generating marrow was the starting point to understand TCM, proposed in *Su Wen (Plain Questions)* as early as the Spring and Autumn period and the Warring States (more than 2000 years ago) (7). Therefore, "kidney deficiency" is regarded as the underlying cause of all skeletal pathologies, and Chinese herbal medicine accordingly follows the principle of "tonifying the kidney" to treat both the surface symptoms and internal balance in management of postmenopausal osteoporosis (8). The kidney's role in bone metabolism was later recognized by Western medicine, as it discovered the importance of the kidney in regulating calcium-phosphorus homeostasis, generating active metabolites of Vitamin D, and so on (9). It is noteworthy that the "kidney's role" in Chinese

medicine cannot be equated directly with renal function in Western medicine and the kidney in TCM theory involves the neuro-endocrine and reproductive systems.

2. Single herbs commonly used in postmenopausal osteoporosis

2.1. *Herba Epimedium*

Epimedium brevicornum Maxim is a centuries-old traditional herb. Derived from the dried leaf of *Epimedium brevicornum* Maxim, *Herba Epimedium* (known as YinYangHuo in Chinese) is a popular Chinese traditional herb with a broad range of indications, especially for fatigue, sexual dysfunction, rheumatic diseases, and osteoporosis. To date, over 260 individual constituents have been derived from plants of the *Epimedium* genus, including icariin, icaritin, anhydroicaritin, epimedin, and so on (10). According to TCM theory, *Herba Epimedium* could tonify the kidney and expel dampness, which contributes to strengthening tendons and bones.

2.1.1. Clinical trials

To determine the therapeutic effect of *Herba Epimedium* and to provide clear evidence for clinical practice, Wang *et al.* identified 37 clinical trials using *Herba Epimedium* in co-prescription with other TCM herbs as anti-osteoporotic drugs to address postmenopausal and senile osteoporosis whose overall efficacy (with markedly and moderately symptom improvement) was between 73% and 100% (11). And *Herba Epimedium* contributed 4.1% to 21.7% of relative weight in these therapeutic formulas. However, these studies could be further criticized because few of them met the standards of randomized, double-blind, placebo-controlled or involved adequate sample size and treatment duration.

2.1.2. In vivo findings

In vivo studies found that *Herba Epimedium* extract and its bioactive components could prevent ovariectomized (OVX) induced bone loss in rats, as evidenced by the suppression of BMD descent and the improvement of biomechanical properties and trabecular microarchitecture.

In evaluation of bone turnover biomarkers, *Herba Epimedium* was found to decrease serum alkaline phosphatase (ALP) activity and urinary deoxypyridinoline levels compared to the OVX group (12). Total flavones of *Epimedium* (TFE) inhibited reduction of procollagen type I N-terminal propeptide (PINP), and increased serum osteocalcin and type I collagen in OVX rats (13,14). Icariin, one of the major components of *Herba Epimedium*, decreased activities of serum tartrate-resistant acid phosphatase (TRAP) and

bone alkaline phosphatase (BALP), decreased serum osteocalcin and ALP activity, decreased C-terminal telopeptide of type I collagen (CTX) levels compared with the OVX group (15-17). Flavonoid fraction of Epimedium (FE), ipriflavone, and anhydroicaritin inhibited serum ALP and TRAP in OVX rats (18).

For calcium and phosphate homeostasis, Herba Epimedium decreased urinary calcium excretion and corrected serum calcium (12,19). TFE decreased urinary calcium excretion, lowered the urinary calcium/creatinine and phosphate/creatinine ratio, suppressed PTH elevation, increased bone calcium and phosphorus content and serum calcium compared to OVX group (14). Icaritin corrected the decreased serum calcium and phosphate (15). Anhydroicaritin decreased urinary calcium and D-pyruvate/creatinine ratio while increasing bone calcium and phosphate (20). FE prevented osteoporosis independent of intestinal calcium absorption (21,22).

For neuro-endocrine regulation, Herba Epimedium and icaritin corrected estrogen decrease in OVX rats (15). TFE improved serum estrogen and increased estrogen receptor α (ER α) and ER β mRNA expression of hypothalamus and hippocampus (23). Herba Epimedium and TFE inhibited the mRNA expression of interleukin (IL)-6 induced by OVX (14).

In gene profile, TFE enhanced osteoprotegerin (OPG) mRNA expression, increased OPG/receptor activator of nuclear factor κ B ligand (RANKL) ratio, and recovered expression of runt-related transcription factor 2 (Runx2) compared to the OVX group (13,14). FE increased OPG protein expression and reduced the RANKL protein expression in OVX rats (18). Icaritin increased the mRNA expression ratio of OPG/RANKL, up-regulated mRNA expression of low-density lipoprotein receptor-related protein 6 (Lrp6) receptor, while it down-regulated glycogen synthase kinase-3 β and Runx2, following OVX (24,25). Icaritin was also found to up-regulate expression of bone morphogenetic protein 2 (BMP2), BMP4, Runx2, osteocalcin, Wnt1, and Wnt3a in OPG knockout mice, and increase the expression of the direct target genes of β -catenin signaling such as AXIN2, dickkopf-related protein 1 (DKK1), T cell factor 1 (TCF1), and lymphoid enhancer-binding factor 1 (LEF1) (26). Icaritin administration altered 23 proteins in bone and 8 metabolites in serum, involving bone remodeling, energy metabolism, cytoskeleton, lipid metabolism, mitogen-activated protein kinase (MAPK) signaling, and calcium signaling (17). Icaritin increased levels of osteoblast-related gene expression compared to pretreatment OVX levels and decreased adipocyte and osteoclast-related gene expression towards pretreatment sham levels (27).

2.1.3. *In vitro* findings

In vitro studies showed that Herba Epimedium and its

bioactive components could stimulate the proliferation, differentiation and mineralization of osteoblasts (12,28-40), suppress the adipogenesis of bone marrow-derived mesenchymal stem cells (BMSCs) (41-44), inhibit the proliferation and differentiation of osteoclasts (45-47), and induce apoptosis and cell cycle arrest and suppress bone resorption of osteoclasts (48). In addition, icaritin was found to significantly attenuate oxidative stress and apoptosis and preserve viability and osteogenic potential of osteoblasts exposed to hypoxia, which indicated that its anti-osteoporotic effect might be attributed to its anti-hypoxic activity (49).

Taken together, the following pathways were involved in the osteogenesis effect of Herba Epimedium and its constituents: *i*) activate extracellular-signal-regulated kinase (ERK), p38, c-Jun N terminal kinase (JNK)/MAPK pathways in rat BMSCs (50), *ii*) through ER-mediated ERK and JNK signal activation in MC3T3-E1 osteoblastic cell line (51), *iii*) via activating phosphatidylinositol-3-kinase (PI3K)-protein kinase B (AKT)-endothelial nitric oxide synthase (eNOS)-nitric oxide (NO)-cyclic guanosine monophosphate (cGMP)-protein kinase G (PKG) signal pathway in rat BMSCs (36), *iv*) via BMP or Wnt/ β -catenin signaling pathway in human BMSCs (28), rat BMSCs (26), UMR-106 osteoblastic cells, and osteoblasts in neonatal rat calvaria cultures (52), *v*) via BMP2/SMAD4 signal pathway in hFOB 1.19 human osteoblastic cell line (34), *vi*) involve the ER α -Wnt/ β -catenin signaling pathway in rat BMSCs (38), *vii*) through up-regulation of transforming growth factor (TGF)- β 1, BMP2 expression in rabbit BMSCs (30), through up-regulation of BMP2 and Runx2 mRNA expression in calvarial osteoblasts from pups (13), *viii*) via Notch signaling pathway in rat BMSCs (53), *ix*) increase OPG and the OPG/RANKL ratio in UMR-106 osteoblastic cells (12), and *x*) stimulate ER-dependent osteoblastic functions and activate ER in a ligand-independent manner in UMR-106 osteoblastic cells (24,39).

At least three pathways were involved in the inhibition of adipogenesis in rat BMSCs: *i*) reduce peroxisome proliferator-activated receptor γ (PPAR γ) mRNA expression (41), *ii*) down-regulate expression of DKK1 protein (42), and *iii*) activate Wnt/ β -catenin signaling pathway (43).

The following pathways were involved in the anti-resorptive effect of Herba Epimedium and its constituents in co-culture of BMSCs and osteoblasts: *i*) suppress MAPKs/nuclear factor kappa-light-chain-enhancer of activated B cells (NF- κ B) regulated hypoxia inducible factor (HIF)-1 α and prostaglandin E2 (PGE2) synthesis (45), *ii*) inhibit p38 and JNK activation, *iii*) up-regulate expression of OPG while down-regulating RANKL, *iv*) repress the synthesis of cyclooxygenase-2 and PGE2, *v*) inhibit IL-6 and tumor necrosis factor (TNF)- α expression, and *vi*) interact with nuclear ERs via the mitochondrial pathway (48).

2.2. *Rhizoma Drynariae*

The traditional Chinese herb *Rhizoma Drynariae* (Gu-Sui-Bu) is commonly used to manage musculoskeletal traumatic disorders of orthopedics with satisfactory results, as it tonifies the kidney, activates blood circulation, and promotes tissue regeneration. Modern pharmacological studies have revealed more than 300 different constituents in this herb, including flavonoids, triterpenoids, phenylpropanoids, lignans, phenolic acids, and so on (54).

2.2.1. *Clinical findings*

A meta-analysis performed in 2017, which included 6 randomized controlled trials involving 846 patients, showed that both the flavonoids from *Rhizoma Drynariae* and the combined therapy alone were better than conventional treatments in improving BMD value with no severe adverse drug reactions (55). This conclusion needs future research to confirm.

2.2.2. *In vivo preclinical data*

Rhizoma Drynariae had a similar effect compared to estrogen in maintaining normal trabecular structure and connections by inhibiting the increased bone turnover of postmenopausal osteoporosis (56). *Drynariae* total flavonoids could decrease cathepsin K mRNA and increase bending load compared to OVX group (57). *Drynariae* flavonoid fraction exerted dose-dependent effects in improving BMD, bone strength at the femur, tibia and lumbar spine in OVX mice (58). Naringin reversed OVX-induced bone loss *via* increasing BMD, bone volume, trabecular thickness, and mechanical strength (59,60). Naringin up-regulated vascular endothelial growth factor (VEGF) mRNA expression and vascular endothelial growth factor receptor (VEGFR)-2 mRNA and protein expression, which increased the number of vessels, vessel volume, and vessel thickness around the osteoporotic fracture sites (61).

2.2.3. *In vitro preclinical data*

Rhizoma Drynariae and its bioactive constituents were able to promote the osteoblastic proliferation, differentiation, and maturation (56,58,59,62-70), inhibit osteoblastic apoptosis (71), suppress osteoclastogenesis (72-74), promote the apoptosis of osteoclasts (60), stimulate both cellular and humoral immunity (75), and inhibit cathepsins K processing (76,77).

Mechanisms involved in the osteogenesis and osteolysis effect of *Rhizoma Drynariae* and its components included: *i*) promote proliferation, differentiation, and maturation of rat calvarial osteoblasts (64) and UMR-106 osteoblastic cells (58,68) *via* ER pathway, *ii*) promote osteoblastogenesis from rat

BMSCs *via* the Notch signaling pathway (70), *iii*) inhibit osteoclastogenesis of human amniotic fluid-derived stem cells (hAFSCs) *via* elevating OPG/RANKL ratio and induce the osteogenesis of hAFSCs *via* the BMP and Wnt/ β -catenin pathways (72), and *iv*) promote the apoptosis of osteoclasts by regulating the mitochondrial apoptosis pathway using RAW 264.7 cells (60).

2.3. *Salvia miltiorrhiza*

Salvia miltiorrhiza, known as Danshen in Chinese, is one of the best-known Chinese traditional herbs whose root has been clinically exploited in treating postmenopausal syndrome. There are more than 100 compounds isolated from *Salvia miltiorrhiza*, such as tanshinone, salvianic acid, and flavonoids (78). As is recorded in *Qian Jin Fang*, the application of *Salvia miltiorrhiza* for treating blood stasis and injuries dated back over hundreds of years. In TCM, *Salvia miltiorrhiza* has been described to remove blood stasis, promote menstrual blood flow, and reduce pain. It is commonly used in patients with menstrual disorders, blood stasis, and rheumatism.

2.3.1. *Clinical data*

Guo *et al.* reported in 2014 that 25 clinical trials were conducted in which primary osteoporosis was treated with *Salvia miltiorrhiza* plus other herbs with an overall efficacy of 85% to 96% in markedly and moderately symptom improvement (78). Due to the huge variation in trial protocols, the exact therapeutic effects of *Salvia miltiorrhiza* could not be assessed from the available data.

2.3.2. *In vivo preclinical data*

Chae *et al.* demonstrated that the aqueous extracts of *Salvia miltiorrhiza* could enhance bone mechanical strength and prevent trabecular bone resorption in OVX Sprague-Dawley rats (79). Cui *et al.* found that *Salvia miltiorrhiza* prevented OVX-induced bone loss probably due to its anti-oxidative stress and partly *via* modulation of osteoclast maturation and number, because it decreased the osteoclast activation marker TRAP-5b and oxidative stress parameters malondialdehyde (MDA) and NO induced by OVX (80). Individual compound tanshinone also prevented a decrease in trabecular bone volume and trabecular number and an increase in osteoclast surface in vertebra, and partially prevented a decrease in trabecular bone volume and trabecular number in the tibia (81).

2.3.3. *In vitro findings*

Salvia miltiorrhiza increased osteoblast number and inhibited osteoclastogenesis (82). Isolated from *Salvia*

miltiorrhiza Bunge, tanshinone IIA, tanshinone I, cryptotanshinone, 15,16-dihydrotanshinone I, and ferruginol were found to reduce the formation of TRAP positive multinuclear osteoclasts (83). Tanshinol was able to ameliorate the accumulation of reactive oxygen species, decrease in cell viability, cell cycle arrest and apoptosis, and inhibition of osteoblastic differentiation induced by hydrogen peroxide (84). Salvianic acid A increased ALP activity, type I collagen mRNA and OPG mRNA expression, and stimulated nodule mineralization of rat osteoblasts. It stimulated osteogenesis and repressed adipogenesis from BMSCs (85).

Mechanisms involved in the osteogenesis and osteolysis effect of *Salvia miltiorrhiza* and its constituents included: *i*) first down-regulate and then up-regulate OPG/RANKL in MC3T3-E1 osteoblastic cell line (86), *ii*) promote osteogenesis through the ERK signaling pathway in human mesenchymal stem cells (87), *iii*) attenuate oxidative stress *via* down-regulation of forkhead box O3 (FoxO3a) signaling, and rescue the decrease of osteoblastic differentiation through up-regulation of Wnt signal under oxidative stress in pluripotent mesenchymal precursor C2C12 cells and preosteoblastic MC3T3-E1 cells (84), *iv*) inhibit osteoclast formation by inhibiting the expression of c-Fos and nuclear factor of activated T-cells, cytoplasmic 1 (NFATc1) induced by RANKL in a rat BMSCs/calvarial osteoblast co-culture system (88), *v*) prevent osteoclast differentiation by inhibiting RANKL expression and NF- κ B induction in co-culture of monocyte-macrophage cell line RAW 264.7 and osteoblast cell line type CRL 12257 (89), and *vi*) reduce the number and activity of osteoclasts *via* suppression of RANK activated AKT, NF- κ B, and MAPKs signal transduction in rat BMSCs/calvarial osteoblasts co-culture system (90).

3. Active ingredients commonly used in postmenopausal osteoporosis

As forms of Chinese herbal medicine, active ingredients of Chinese medicine are isolated from single herbs or traditional herbal formulas and prepared using modern advanced pharmaceutical technology, such as icariin from *Herba Epimedii*, naringin from *Rhizoma Drynariae*, and tanshinone from *Salvia miltiorrhiza*. Compared to traditional decoctions, active ingredients have various dosage forms including injections, tablets, pills, capsules, and liquids. They are safer, more effective, and easier to use. Thus, active ingredients of Chinese medicine become increasingly popular in China and attract worldwide attention.

3.1. Saikosaponins

Radix Bupleuri, made from dried roots of *Bupleurum scorzoniferifolium* Willd., is commonly used in the

prescriptions of traditional Chinese medicine. It has been utilized to treat various discomforts, including influenza, malaria, chronic hepatitis, and menstrual disorders. Saikosaponins, major bioactive compounds isolated from *Radix Bupleuri*, have exhibited anti-inflammatory, antimycotic, and immuno-regulatory pharmacological properties.

Saikosaponin A and saikosaponin D significantly repressed inducible nitric oxide synthase (iNOS) and cyclooxygenase (COX)-2 expression, reduced TNF- α and IL-6 production, and inhibited NF- κ B translocation in lipopolysaccharide (LPS)-induced murine macrophage cell line RAW264.7 cells (91). *In vitro* study revealed that saikosaponin A suppressed osteoclastogenesis in C57/BL6 mice bone marrow monocytes and mediated osteoclast differentiation through inhibiting RANKL-induced p38, ERK, JNK, and NF- κ B activation in murine RAW264.7 cell line (92). Saikosaponins showed a potent anti-inflammatory and anti-osteoporotic effect as safe and effective agents for management of postmenopausal osteoporosis.

3.2. Linarin

Flos Chrysanthemi Indici, one of the most important drugs in traditional Chinese medicine, possesses biological properties such as antioxidative, antibacterial, antiviral, and antimycotic effects. Linarin, a natural flavonoid compound in *Flos Chrysanthemi Indici*, has been shown to preserve the trabecular bone microarchitecture of OVX C57/BL6 mice. Linarin enhanced osteoblast differentiation and mineralization in MC3T3 E1 cells, mediated by activating the BMP2/Runx2 pathway *via* protein kinase A (PKA) signaling pathway (93).

3.3. Echinacoside

Echinacoside is one of the major constituents of *Herba Cistanches*, a famous traditional Chinese medicine. As a natural polyphenolic compound, echinacoside possesses effective anti-inflammatory, antioxidative, neuroprotective, hepatoprotective, and vasodilative properties. Administration of echinacoside could effectively and safely prevent bone loss in OVX-induced Sprague-Dawley rats through increasing OPG/RANKL ratio, which revealed its potential of developing into a novel agent for treatment in postmenopausal osteoporotic women (94).

3.4. Sweroside

Fructus Corni has wide application in the clinic with a long history, of which Sweroside is an important constituent. Modern pharmacology shows that sweroside has a variety of pharmacological functions including vasorelaxation, antihepatitis, anti-inflammatory, and

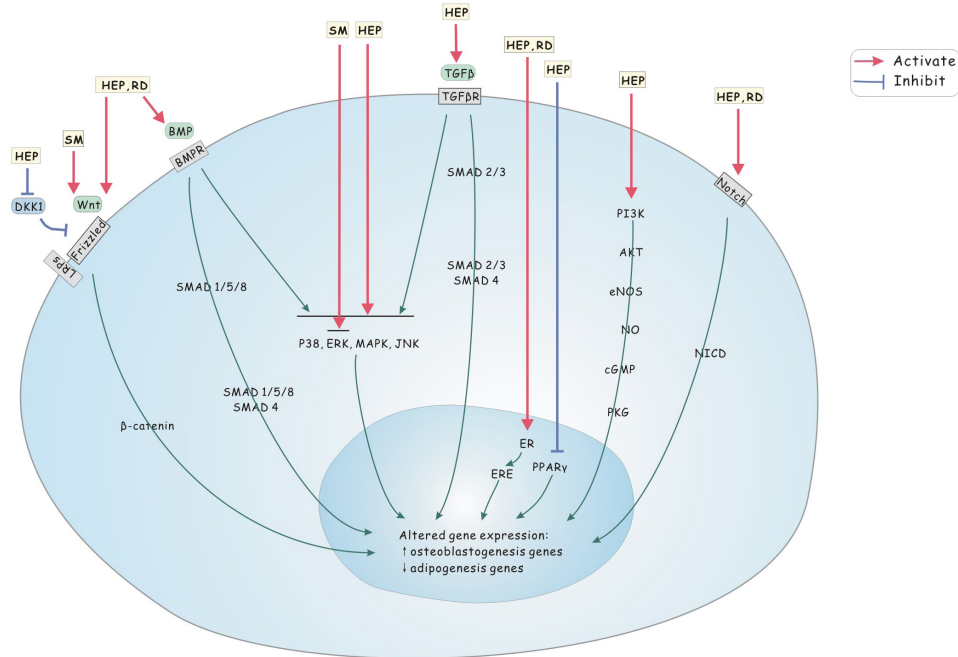


Figure 1. The mechanism of action of Chinese single herbs on pre-osteoblasts. Chinese single herbs interact with at least eight pathways for the treatment of osteoporosis in pre-osteoblasts: *i*) via BMP signaling pathway, *ii*) via Wnt/ β -catenin pathway, *iii*) activate ERK, p38, JNK, MAPK pathways, *iv*) via up-regulation of TGF- β 1 expression, *v*) through ER signal activation, *vi*) activate PI3K-AKT-eNOS-NO-cGMP-PKG signal pathway, *vii*) via Notch signaling pathway, and *viii*) reduce PPAR γ mRNA and DKK1 protein to inhibit adipogenesis. (Abbreviations: HEP, Herba Epimedii; SM, Salvia miltiorrhiza; RD, Rhizoma Drynariae; DKK1, dickkopf-related protein 1; LRP, lipoprotein receptor-related proteins; BMP, bone morphogenetic protein; BMPR, BMP receptor; JNK, c-Jun N terminal kinase; MAPK, mitogen-activated protein kinase; ERK, extracellular-signal-regulated kinase; TGF β , transforming growth factor β ; TGF β R, TGF β receptor; ER, estrogen receptor; ERE, estrogen-response element; PI3K, phosphatidylinositol-3-kinase; AKT, protein kinase B; eNOS, endothelial nitric oxide synthase; NO, nitric oxide; cGMP, cyclic guanosine monophosphate; PKG, protein kinase G; NICD, Notch intracellular domain; PPAR γ , peroxisome proliferator-activated receptor γ .)

antiallergic effects. Sweroside was found to effectively induce proliferation and inhibit apoptosis in human osteosarcoma cell line MG-63 and Wistar rat osteoblastic cells (95), which displayed bright prospects as a therapeutic natural product for osteoporosis.

3.5. Psoralen

Psoralen is extracted from *Psoralea corylifolia*, which is one of the most commonly prescribed herbs for the treatment of bone and joint diseases. Psoralen was found to promote *in vitro* osteoblast differentiation dose-dependently, evidenced by increased ALP activity and enhanced expression of osteoblast-specific marker genes such as type I collagen and osteocalcin. Psoralen might act through the BMP signaling pathway as it could increase the gene expression of BMP2 and BMP4 as well as the protein level of phospho-SMAD1/5/8 (96).

3.6. Poncirin

Poncirin is isolated from *Poncirus trifoliata* and possesses anti-bacterial and anti-inflammatory activities. Studies have showed that poncirin could inhibit adipogenesis and enhance osteoblast differentiation in BMSCs. In C3H10T1/2 mesenchymal stem

cells, poncirin prevented adipocyte differentiation, demonstrated by decreased accumulation of cytoplasm lipid droplets and down-regulated mRNA expression of PPAR- γ and CCAAT-enhancer-binding protein- β (C/EBP- β). In murine BMSCs, poncirin enhanced expression of Runx2, ALP, and osteocalcin, and increased mineral nodule formation (97).

3.7. Vanillic acid

Vanillic acid is a phenolic acid isolated from the bioactive fraction of *Sambucus williamsii* Hance. It stimulated the proliferation and ALP activity in rat osteoblast-like UMR 106 cells, and also increased mRNA expression of genes involved in osteoblast functions and osteoclastogenesis such as Runx2, osteocalcin, and the OPG/RANKL ratio. Its bone protective effects might be mediated through ER and MAPK pathways (98).

3.8. Osthole

Osthole, extracted from *Fructus Cnidii*, was found to notably improve bone microarchitecture, histomorphometric parameters, and biomechanical properties of OVX rats. It could activate Wnt/ β -catenin pathways, up-regulate BMP2 expression, and stimulate

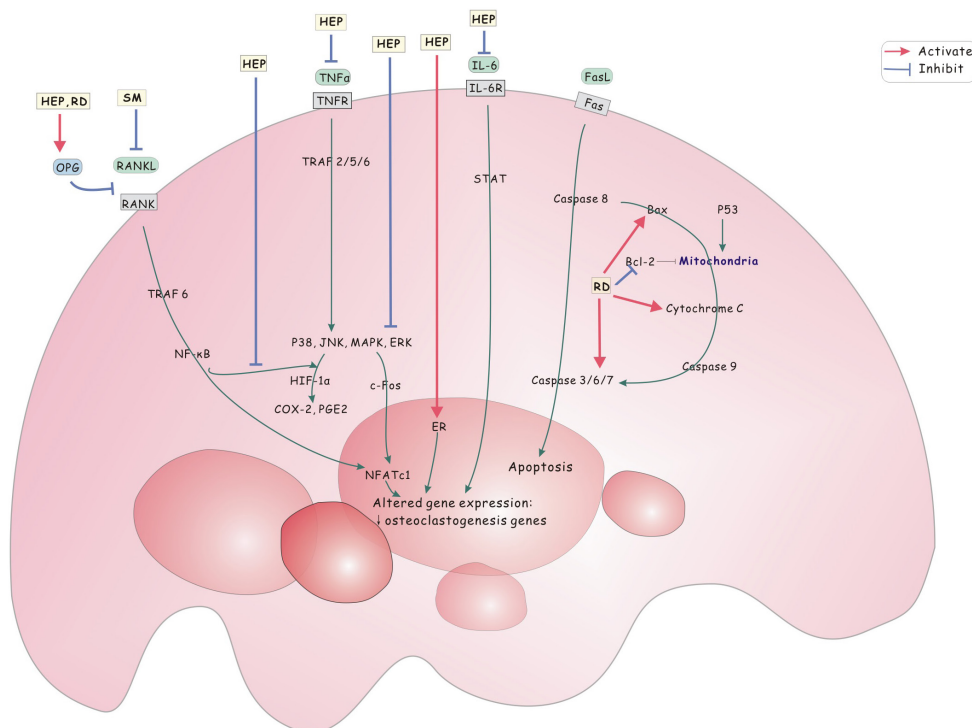


Figure 2. The mechanism of action of Chinese single herbs on pre-osteoclasts. Chinese single herbs interact with at least six pathways in pre-osteoclasts: *i*) up-regulate expression of OPG while down-regulate RANKL, *ii*) suppress MAPKs/NF-κB regulated HIF-1α and PGE2 synthesis, *iii*) inhibit p38, JNK, MAPK, ERK pathways, *iv*) inhibit IL-6 and TNF-α expression, *v*) interact with nuclear ERs, and *vi*) down-regulate the mRNA expression levels of bcl-2 and up-regulate Bax, caspase-3 and cytochrome c. (Abbreviations: HEP, Herba Epimedii; RD, Rhizoma Drynariae; SM, Salvia miltiorrhiza; OPG, osteoprotegerin; RANK, receptor activator of nuclear factor κB; RANKL, RANK ligand; TNF-α, tumor necrosis factor α; TNFR, TNF receptor; TRAF, TNF receptor-associated factor; NF-κB, nuclear factor kappa-light-chain-enhancer of activated B cells; JNK, c-Jun N terminal kinase; MAPK, mitogen-activated protein kinase; ERK, extracellular-signal-regulated kinase; HIF-1α, hypoxia inducible factor 1α; COX-2, cyclooxygenase-2; PGE2, prostaglandin E2; NFATc1, nuclear factor of activated T-cells, cytoplasmic 1; ER, estrogen receptor; IL-6, interleukin 6; IL-6R, IL-6 receptor; STAT, signal transducer and activator of transcription; FasL, Fas ligand.)

osteoblast differentiation *in vitro* (99).

4. Conclusion

In conclusion, Chinese herbal medicine substantially influences postmenopausal osteoporosis as a safer and more effective alternative. However, current clinical studies are not well funded to prove their therapeutic efficacy because most of the studies contain a small sample size and short treatment duration, and their clinical parameters and biomarkers for analysis differ from each other. Both *in vivo* and *in vitro* studies reveal the anti-osteoporotic effect of single herbs targeting different pathways in bone metabolism (Figure 1 and Figure 2). Apart from restoring the balance between osteoblasts and osteoclasts, Chinese single herbs have also been shown to inhibit adipocyte differentiation and exert anti-inflammatory, immuno-regulatory, anti-oxidative, and estrogen-like functions. This review should contribute to a better understanding of Chinese single herbs and active ingredients as treatment for postmenopausal osteoporosis and provide useful information for the development of more effective anti-osteoporosis drugs.

Acknowledgements

This work was supported by the National Natural Science Foundation of China No. 31571196 (to L Wang), the Science and Technology Commission of Shanghai Municipality 2015 YIXUEYINGDAO project No. 15401932200 (to L Wang), the FY2008 JSPS Postdoctoral Fellowship for Foreign Researchers P08471 (to L Wang), the National Natural Science Foundation of China No. 30801502 (to L Wang), the Shanghai Pujiang Program No. 11PJ1401900 (to L Wang), Development Project of Shanghai Peak Disciplines-Integrative Medicine No. 20150407.

References

1. Kanis JA. WHO scientific group technical report: Assessment of osteoporosis at the primary health care level. WHO Collaborating Center for Metabolic Bone Diseases, University of Sheffield, UK. 2007.
2. Gallagher JC, Tella SH. Prevention and treatment of postmenopausal osteoporosis. J Steroid Biochem Mol Biol. 2014; 142:155-170.
3. An J, Yang H, Zhang Q, Liu CC, Zhao JJ, Zhang LL, Chen B. Natural products for treatment of osteoporosis:

- The effects and mechanisms on promoting osteoblast-mediated bone formation. *Life Sci.* 2016; 147:46-58.
4. Xu M, Qi C, Deng B, Deng PX, Mo CW. Phytotherapy versus hormonal therapy for postmenopausal bone loss: A meta-analysis. *Osteoporos Int.* 2009; 20:519-526.
 5. Jin YX, Wu P, Mao YF, Wang B, Zhang JF, Chen WL, Liu Z, Shi XL. Chinese herbal medicine for osteoporosis: A meta-analysis of randomized controlled trials. *J Clin Densitom.* 2017; doi: 10.1016/j.jocd.2017.07.003.
 6. Gao Z, Lu Y, Jin J, Xu D. Study of osteoporosis treatment principles used historically by ancient physicians in Chinese medicine. *Chin J Integr Med.* 2013; 19:862-868.
 7. Wang SJ, Li Y, Liu H, Liu ZH. Mechanism underlying osteoporosis: Understanding according to theory of traditional Chinese medicine. *World Chin Med.* 2013; 8:1044-1048. (in Chinese)
 8. Shu B, Shi Q, Wang YJ. Shen(Kidney)-tonifying principle for primary osteoporosis: To treat both the disease and the Chinese medicine syndrome. *Chin J Integr Med.* 2015; 21:656-661.
 9. Zhang Y, Papasian CJ, Deng HW. Alteration of vitamin D metabolic enzyme expression and calcium transporter abundance in kidney involved in type 1 diabetes-induced bone loss. *Osteoporos Int.* 2011; 22:1781-1788.
 10. Ma HP, He XR, Yang Y, Li MX, Hao DJ, Jia ZP. The genus *Epimedium*: An ethnopharmacological and phytochemical review. *J Ethnopharmacol.* 2011; 134:519-541.
 11. Wang LL, Li Y, Guo YB, Ma RF, Fu M, Niu JZ, Gao SH, Zhang DW. Herba *Epimedii*: An ancient Chinese herbal medicine in the prevention and treatment of osteoporosis. *Curr Pharm Des.* 2016; 22:328-349.
 12. Xie F, Wu CF, Lai WP, Yang XJ, Cheung PY, Yao XS, Leung PC, Wong MS. The osteoprotective effect of Herba *epimedii* (HEP) extract *in vivo* and *in vitro*. *Evid-based Compl Alt.* 2005; 2:353-361.
 13. Qian GF, Zhang XZ, Lu LX, Wu XJ, Li SM, Meng J. Regulation of *Cbfa 1* expression by total flavonoids of Herba *Epimedii*. *Endocr J.* 2006; 53:87-94.
 14. Chen WF, Mok SK, Wang XL, Lai KH, Lai WP, Luk HK, Leung PC, Yao XS, Wong MS. Total flavonoid fraction of the Herba *epimedii* extract suppresses urinary calcium excretion and improves bone properties in ovariectomized mice. *Br J Nutr.* 2011; 105:180-189.
 15. Nian H, Ma MH, Nian SS, Xu LL. Antiosteoporotic activity of icariin in ovariectomized rats. *Phytomedicine.* 2009; 16:320-326.
 16. Li GW, Xu Z, Chang SX, Nian H, Wang XY, Qin LD. Icariin prevents ovariectomy-induced bone loss and lowers marrow adipogenesis. *Menopause.* 2014; 21:1007-1016.
 17. Xue L, Jiang Y, Han T, Zhang N, Qin L, Xin H, Zhang Q. Comparative proteomic and metabolomic analysis reveal the antiosteoporotic molecular mechanism of icariin from *Epimedium brevicornu maxim*. *J Ethnopharmacol.* 2016; 192:370-381.
 18. Zhao BJ, Wang J, Song J, Wang CF, Gu JF, Yuan JR, Zhang L, Jiang J, Feng L, Jia XB. Beneficial effects of a flavonoid fraction of Herba *Epimedii* on bone metabolism in ovariectomized rats. *Planta Med.* 2016; 82:322-329.
 19. Nian H, Xu LL, Ma MH, Qin LP, Zheng HC, Zhang QY. Prevention of bone loss by aqueous extract of *Epimedii sagittatum* in an ovariectomized rat model of osteoporosis. *J Chin Integr Med.* 2006; 4:628-633.
 20. Wu MS, Zhao SZ, Ren LZ, Wang R, Bai X, Han HW, Li B. Experimental study on effect of anhydroicaritin phytosomes in preventing and treating bone loss and enhancing bone quality in ovariectomized osteoporosis rats. *China J Chin Materia Medica.* 2013; 38:2163-2168. (in Chinese)
 21. Qin L, Zhang G, Wang XL, Shi YY, Kong YY, Yang XE, Sheng H, Liang BZ, Liang GS, Yao XS. *Epimedium*-derived flavonoids prevent ovariectomy-induced osteoporosis in rats independent of its enhancement in intestinal calcium absorption. *Natl Med J China.* 2008; 88:1772-1777. (in Chinese)
 22. Zhang G, Qin L, Hung WY, Shi YY, Leung PC, Yeung HY, Leung KS. Flavonoids derived from herbal *Epimedium Brevicornum Maxim* prevent OVX-induced osteoporosis in rats independent of its enhancement in intestinal calcium absorption. *Bone.* 2006; 38:818-825.
 23. Wu M, Zhao S, Ren L. Effects of total flavonoids of *Epimedium sagittatum* on the mRNA expression of the estrogen receptor alpha and beta in hypothalamus and hippocampus in ovariectomized rats. *J Cent South Univ (Med Sci).* 2011; 36:15-20.
 24. Mok S, Chen W, Lai W, Leung P, Wang X, Yao X, Wong M. Icariin protects against bone loss induced by oestrogen deficiency and activates oestrogen receptor-dependent osteoblastic functions in UMR 106 cells. *Br J Pharmacol.* 2010; 159:939-949.
 25. Chen G, Wang C, Wang J, Yin S, Gao H, Xiang LU, Liu H, Xiong Y, Wang P, Zhu X, Yang LI, Zhang R. Antiosteoporotic effect of icariin in ovariectomized rats is mediated *via* the Wnt/beta-catenin pathway. *Exp Ther Med.* 2016; 12:279-287.
 26. Li XF, Xu H, Zhao YJ, Tang DZ, Xu GH, Holz J, Wang J, Cheng SD, Shi Q, Wang YJ. Icariin Augments Bone Formation and Reverses the Phenotypes of Osteoprotegerin-Deficient Mice through the Activation of Wnt/ beta -Catenin-BMP Signaling. *Evid-based Compl Alt.* 2013; 2013:652317.
 27. Peng S, Zhang G, Zhang B, Guo B, He Y, Bakker AJ, Pan X, Zhen W, Hung L, Qin L, Leung W. The beneficial effect of Icariin on osteoporotic bone is dependent on the treatment initiation timing in adult ovariectomized rats. *Bone.* 2013; 55:230-240.
 28. Zhang JF, Li G, Chan CY, Meng CL, Lin MC, Chen YC, He ML, Leung PC, Kung HF. Flavonoids of Herba *Epimedii* regulate osteogenesis of human mesenchymal stem cells through BMP and Wnt/beta-catenin signaling pathway. *Mol Cell Endocrinol.* 2010; 314:70-74.
 29. Wang R, Luo J, Kong L. An MC3T3-E1 cell line biomembrane extraction and HPLC-ESI-MS (n) method for simultaneous analysis of potential anti-osteoporosis components of *Epimedium koreanum*. *Chromatographia.* 2012; 75:607-615.
 30. Wu H, Zha ZG, Yao P. Experimental study of icariin in inducing bone marrow mesenchymal stem cell differentiation. *Chin J Integr Tradit West Med.* 2010; 30:410-415. (in Chinese)
 31. Ma HP, Ming LG, Ge BF, Zhai YK, Song P, Xian CJ, Chen KM. Icariin is more potent than genistein in promoting osteoblast differentiation and mineralization *in vitro*. *J Cell Biochem.* 2011; 112:916-923.
 32. Xiao Q, Chen A, Guo F. Effects of Icariin on expression of OPN mRNA and type I collagen in rat osteoblasts *in vitro*. *J Huazhong Univ Sci Technolog Med Sci.* 2005; 25:690-692.
 33. Hsieh T, Sheu S, Sun J, Chen M, Liu M. Icariin isolated

- from *Epimedium pubescens* regulates osteoblasts anabolism through BMP-2, SMAD4, and Cbfa1 expression. *Phytomedicine*. 2010; 17:414-423.
34. Liang W, Lin M, Li X, Li C, Gao B, Gan H, Yang Z, Lin X, Liao L, Yang M. Icariin promotes bone formation *via* the BMP-2/Smad4 signal transduction pathway in the hFOB 1.19 human osteoblastic cell line. *Int J Mol Med*. 2012; 30:889-895.
 35. Cao H, Ke Y, Zhang Y, Zhang CJ, Qian W, Zhang GL. Icariin stimulates MC3T3-E1 cell proliferation and differentiation through up-regulation of bone morphogenetic protein-2. *Int J Mol Med*. 2012; 29:435-439.
 36. Zhai Y, Guo X, Ge B, Zhen P, Ma X, Zhou J, Ma H, Xian CJ, Chen K. Icariin stimulates the osteogenic differentiation of rat bone marrow stromal cells *via* activating the PI3K-AKT-eNOS-NO-cGMP-PKG. *BONE*. 2014; 66:189-198.
 37. Chen KM, Ge BF, Ma HP, Liu XY, Bai MH, Wang Y. Icariin, a flavonoid from the herb *Epimedium* enhances the osteogenic differentiation of rat primary bone marrow stromal cells. *Pharmazie*. 2005; 60:939-942.
 38. Wei Q, Zhang J, Hong G, Chen Z, Deng W, He W, Chen MH. Icariin promotes osteogenic differentiation of rat bone marrow stromal cells by activating the ERalpha-Wnt/beta-catenin signaling pathway. *Biomed Pharmacother*. 2016; 84:931-939.
 39. Xiao HH, Fung CY, Mok SK, Wong KC, Ho MX, Wang XL, Yao XS, Wong MS. Flavonoids from *Herba epimedii* selectively activate estrogen receptor alpha (ERalpha) and stimulate ER-dependent osteoblastic functions in UMR-106 cells. *J Steroid Biochem Mol Biol*. 2014; 143:141-51.
 40. Liu M, Xu H, Ma Y, Cheng J, Hua Z, Huang G. Osteoblasts proliferation and differentiation stimulating activities of the main components of *epimedii folium*. *Pharmacogn Mag*. 2017; 13:90-94.
 41. Liu HQ, Qin JJ, Wu Q. Effect of herb *epimedii* on expression of PPAR gamma mRNA of MSCs during adipogenesis in postmenopausal osteoporosis rats. *Tradit Chin Drug Res Clin Pharm*. 2013; 24:382-385. (in Chinese)
 42. Xu YX, Xu B, Wu CL, Wu Y, Tong PJ, Xiao LW. Dynamic expression of DKK1 protein in the process whereby *Epimedium*-derived flavonoids up-regulate osteogenic and down-regulate adipogenic differentiation of bone marrow stromal cells in ovariectomized rats. *Orthop Surg*. 2011; 3:119-126.
 43. Xu YX, Wu CL, Wu Y, Tong PJ, Jin HT, Yu NZ, Xiao LW. *Epimedium*-derived flavonoids modulate the balance between osteogenic differentiation and adipogenic differentiation in bone marrow stromal cells of ovariectomized rats *via* Wnt/beta-catenin signal pathway activation. *Chin J Integr Med*. 2012; 18:909-917.
 44. Zhang S, Feng P, Mo G, Li D, Li Y, Mo L, Yang Z, Liang. Icariin influences adipogenic differentiation of stem cells affected by osteoblast-osteoclast co-culture and clinical research adipogenic. *Biomed Pharmacother*. 2017; 88:436-442.
 45. Hsieh T, Sheu S, Sun J, Chen M. Icariin inhibits osteoclast differentiation and bone resorption by suppression of MAPKs/NF-kappa B regulated HIF-1 alpha and PGE2 synthesis. *Phytomedicine*. 2011; 18:176-185.
 46. Zhang JF, Li G, Meng CL, Dong Q, Chan CY, He ML, Leung PC, Zhang YO, Kung HF. Total flavonoids of *Herba Epimedii* improves osteogenesis and inhibits osteoclastogenesis of human mesenchymal stem cells. *Phytomedicine*. 2009; 16:521-529.
 47. Liu YQ, Yang QX, Cheng MC, Xiao HB. Synergistic inhibitory effect of Icariside II with Icaritin from *Herba Epimedii* on pre-osteoclastic RAW264.7 cell growth. *Phytomedicine*. 2014; 21:1633-1637.
 48. Zhang D, Zhang J, Fong C, Yao X, Yang M. *Herba epimedii* flavonoids suppress osteoclastic differentiation and bone resorption by inducing G2/M arrest and apoptosis. *Biochimie*. 2012; 94:2514-2522.
 49. Ma HP, Ma XN, Ge BF, Zhen P, Zhou J, Gao YH, Xian CJ, Chen KM. Icariin attenuates hypoxia-induced oxidative stress and apoptosis in osteoblasts and preserves their osteogenic differentiation potential *in vitro*. *Cell Prolif*. 2014; 47:527-539.
 50. Wu Y, Xia L, Zhou Y, Xu Y, Jiang X. Icariin induces osteogenic differentiation of bone mesenchymal stem cells in a MAPK-dependent manner. *Cell Prolif*. 2015; 48:375-384.
 51. Song LG, Zhao JS, Zhang XZ, Li H, Zhou Y. Icariin induces osteoblast proliferation, differentiation and mineralization through estrogen receptor-mediated ERK and JNK signal activation. *Eur J Pharmacol*. 2013; 714:15-22.
 52. Li M, Zhang ND, Wang Y, Han T, Jiang YP, Rahman K, Qin LP, Xin HL, Zhang QY. Coordinate regulatory osteogenesis effects of icariin, timosaponin B II and ferulic acid from traditional Chinese medicine formulas on UMR-106 osteoblastic cells and osteoblasts in neonatal rat calvaria cultures. *J Ethnopharmacol*. 2016; 185:120-131.
 53. Bian Q, Huang JH, Liu SF, Ning Y, Yang Z, Zhao YJ, Shen ZY, Wang YJ. Different molecular targets of icariin on bMSCs in CORT and OVX-rats. *Front Biosci (Elite Ed)*. 2012; 4:1224-1236.
 54. Qiao X, Lin XH, Liang YH, Dong J, Guo DA, Ye M. Comprehensive chemical analysis of the rhizomes of *Drynaria fortunei* by orthogonal pre-separation and liquid chromatography mass spectrometry. *Planta Med*. 2014; 80:330-336.
 55. Zhang YL, Jiang JJ, Shen H, Chai Y, Wei X, Xie YM. Total flavonoids from *Rhizoma Drynariae* (Gusuibu) for treating osteoporotic fractures: Implication in clinical practice. *Drug Des Devel Ther*. 2017; 11:1881-1890.
 56. Wang XL, Wang NL, Zhang Y, Gao H, Pang WY, Wong MS, Zhang G, Qin L, Yao XS. Effects of eleven flavonoids from the osteoprotective fraction of *Drynaria fortunei* (KUNZE) J. SM. on osteoblastic proliferation using an osteoblast-like cell line. *Chem Pharm Bull (Tokyo)*. 2008; 56:46-51.
 57. He WT, Zhou JX, Ding XH, Wang HF, Liang B. Experimental study of *drynaria fortunei* J. SM for the prevention of postmenopausal osteoporosis. *Chin J Osteoporos*. 2012; 444-446+457. (in Chinese)
 58. Wong KC, Pang WY, Wang XL, Mok SK, Lai WP, Chow HK, Leung PC, Yao XS, Wong MS. *Drynaria fortunei*-derived total flavonoid fraction and isolated compounds exert oestrogen-like protective effects in bone. *Br J Nutr*. 2013; 110:475-485.
 59. Li N, Jiang Y, Wooley PH, Xu Z, Yang SY. Naringin promotes osteoblast differentiation and effectively reverses ovariectomy-associated osteoporosis. *J Orthop Sci*. 2013; 18:478-485.
 60. Li F, Sun X, Ma J, Ma X, Zhao B, Zhang Y, Tian P, Li Y, Han Z. Naringin prevents ovariectomy-induced osteoporosis and promotes osteoclasts apoptosis through

- the mitochondria-mediated apoptosis pathway. *Biochem Biophys Res Commun.* 2014; 452:629-635.
61. Song N, Zhao Z, Ma X, Sun X, Ma J, Li F, Sun L, Lv J. Naringin promotes fracture healing through stimulation of angiogenesis by regulating the VEGF/VEGFR-2 signaling pathway in osteoporotic rats. *Chem Biol Interact.* 2017; 261:11-17.
 62. Jeong J, Lee J, Yoon C, Kim H, Kim C. Drynariae Rhizoma promotes osteoblast differentiation and mineralization in MC3T3-E1 cells through regulation of bone morphogenetic protein-2, alkaline phosphatase, type I collagen and collagenase-1. *Toxicol in Vitro.* 2004; 18:829-834.
 63. Jeong JC, Lee JW, Yoon CH, Lee YC, Chung KH, Kim MG, Kim CH. Stimulative effects of Drynariae Rhizoma extracts on the proliferation and differentiation of osteoblastic MC3T3-E1 cells. *J Ethnopharmacol.* 2005; 96:489-495.
 64. Zhai YK, Niu YB, Pan YL, Li CR, Wu XL, Mei QB. Effects of naringin on proliferation, differentiation and maturation of rat calvarial osteoblasts *in vitro*. *China J Chin Materia Medica.* 2013; 38:105-111. (in Chinese)
 65. Zhang P, Dai KR, Yan SG, Yan WQ, Zhang C, Chen DQ, Xu B, Xu ZW. Effects of naringin on the proliferation and osteogenic differentiation of human bone mesenchymal stem cells. *Eur J Pharmacol.* 2009; 607:1-5.
 66. Chen L, Lei L, Ding P, Tang Q, Wu Y. Osteogenic effect of Drynariae rhizoma extracts and Naringin on MC3T3-E1 cells and an induced rat alveolar bone resorption model. *Arch Oral Biol.* 2011; 56:1655-1662.
 67. Chang EJ, Lee WJ, Cho SH, Choi SW. Proliferative effects of flavan-3-ols and propelargonidins from rhizomes of Drynaria fortunei on MCF-7 and osteoblastic cells. *Arch Pharm Res.* 2003; 26:620-630.
 68. Wang X, Zhen L, Zhang G, Wong MS, Qin L, Yao X. Osteogenic effects of flavonoid aglycones from an osteoprotective fraction of Drynaria fortunei--an *in vitro* efficacy study. *Phytomedicine.* 2011; 18:868-872.
 69. Li L, Zeng Z, Cai G. Comparison of neoeriocitrin and naringin on proliferation and osteogenic differentiation in MC3T3-E1. *Phytomedicine.* 2011; 18:985-989.
 70. Yu GY, Zheng GZ, Chang B, Hu QX, Lin FX, Liu DZ, Wu CC, Du SX, Li XD. Naringin stimulates osteogenic differentiation of rat bone marrow stromal cells *via* activation of the Notch signaling pathway. *Stem Cells Int.* 2016; 2016:7130653.
 71. Huang ZM, Ouyang GL, Xiao LB, Li NL, Gao HL, He Y, Huang Z, Huang XX. Effects of Drynaria total flavonoids on apoptosis of osteoblasts mediated by tumor necrosis factor-alpha. *J Chin Integr Med.* 2011; 9:173-178. (in Chinese)
 72. Liu M, Li Y, Yang S. Effects of naringin on the proliferation and osteogenic differentiation of human amniotic fluid-derived stem cells. *J Tissue Eng Regen Med.* 2017; 11:276-284.
 73. Qiu ZC, Dong XL, Dai Y, Xiao GK, Wang XL, Wong KC, Wong MS, Yao XS. Discovery of a new class of Cathepsin K inhibitors in Rhizoma Drynariae as potential candidates for the treatment of osteoporosis. *Int J Mol Sci.* 2016; 17:2116-2134.
 74. Sun J, Dong G, Lin C, Sheu S, Lin F, Chen L, Chang WH, Wang Y. The effect of Gu-Sui-Bu (Drynaria fortunei J. Sm) immobilized modified calcium hydrogenphosphate on bone cell activities. *Biomaterials.* 2003; 24:873-882.
 75. Jeong J, Lee B, Yoon C, Kim H, Kim C. Effects of Drynariae rhizoma on the proliferation of human bone cells and immunomodulatory activity. *Pharmacol Res.* 2005; 51:125-136.
 76. Jeong J, Kang S, Youn C, Jeong C, Kim H, Lee Y, Chang Y, Kim C. Inhibition of Drynariae Rhizoma extracts on bone resorption mediated by processing of cathepsin K in cultured mouse osteoclasts. *Int Immunopharmacol.* 2003; 3:1685-1697.
 77. Jeong JC, Yoon CH, Jeong CW, Lee YC, Chang YC, Kim CH. Inhibitory activity of Drynariae rhizoma extracts on cathepsin having bone resorption activity. *Immunopharmacol Immunotoxicol.* 2004; 26:373-385.
 78. Guo YB, Li Y, Xue LM, Severino RP, Gao SH, Niu JZ, Qin LP, Zhang DW, Brömme D. Salvia miltiorrhiza: An ancient Chinese herbal medicine as a source for anti-osteoporotic drugs. *J Ethnopharmacol.* 2014; 155:1401-1416.
 79. Chae HJ, Chae SW, Yun DH, Keum KS, Yoo SK, Kim HR. Prevention of bone loss in ovariectomized rats: The effect of Salvia miltiorrhiza extracts. *Immunopharm Immunot.* 2004; 26:135-144.
 80. Cui Y, Bhandary B, Marahatta A, Lee GH, Li B, Kim DS, Chae SW, Kim HR, Chae HJ. Characterization of Salvia Miltiorrhiza ethanol extract as an anti-osteoporotic agent. *BMC Complement Altern Med.* 2011; 11:120-130.
 81. Cui L, Wu T, Liu YY, Deng YF, Ai CM, Chen HQ. Tanshinone prevents cancellous bone loss induced by ovariectomy in rats. *Acta Pharmacol Sin.* 2004; 25:678-684.
 82. Kim HK, Woo ER, Lee HW, Park HR, Kim HN, Jung YK, Choi JY, Chae SW, Kim HR, Chae HJ. The correlation of Salvia miltiorrhiza extract-induced regulation of osteoclastogenesis with the amount of components tanshinone I, tanshinone IIA, cryptotanshinone, and dihydrotanshinone. *Immunopharm Immunot.* 2008; 30:347-364.
 83. Lee SY, Choi DY, Woo ER. Inhibition of osteoclast differentiation by tanshinones from the root of Salvia miltiorrhiza Bunge. *Arch Pharm Res.* 2005; 28:909-913.
 84. Yang Y, Su Y, Wang D, Chen Y, Wu T, Li G, Sun X, Cui L. Tanshinol attenuates the deleterious effects of oxidative stress on osteoblastic differentiation *via* Wnt/FoxO3a signaling. *Oxid Med Cell Longev.* 2013; 2013:351895.
 85. Cui L, Liu YY, Wu T, Ai CM, Chen HQ. Osteogenic effects of D+beta-3,4-dihydroxyphenyl lactic acid (salvianic acid A, SAA) on osteoblasts and bone marrow stromal cells of intact and prednisone-treated rats. *Acta Pharmacol Sin.* 2009; 30:321-332.
 86. Chin A, Yang YQ, Chai L, Wong RWK, Rabie ABM. Effects of medicinal herb Salvia Miltiorrhiza on osteoblastic cells *in vitro*. *J Orthop Res.* 2011; 29:1059-1063.
 87. Xu D, Xu L, Zhou C, Lee WY, Wu T, Cui L, Li G. Salvianolic acid B promotes osteogenesis of human mesenchymal stem cells through activating ERK signaling pathway. *Int J Biochem Cell Biol.* 2014; 51:1-9.
 88. Lee S. Tanshinone IIA inhibits osteoclast differentiation through down-regulation of c-Fos and NFATc1. *Exp Mol Med.* 2006; 38:256-264.
 89. Nicolin V, Dal Piaz F, Nori SL, Narducci P, De Tommasi N. Inhibition of bone resorption by Tanshinone VI isolated from Salvia miltiorrhiza Bunge. *Eur J Histochem.* 2010; 54:e21.
 90. Kim HH, Kim JH, Kwak HB, Huang H, Han SH, Ha H, Lee SW, Woo ER, Lee ZH. Inhibition of osteoclast

- differentiation and bone resorption by tanshinone IIA isolated from *Salvia miltiorrhiza* Bunge. *Biochem Pharmacol.* 2004; 67:1647-1656.
91. Lu CN, Yuan ZG, Zhang XL, Yan R, Zhao YQ, Liao M, Chen JX. Saikosaponin a and its epimer saikosaponin d exhibit anti-inflammatory activity by suppressing activation of NF-kappaB signaling pathway. *Int Immunopharmacol.* 2012; 14:121-126.
92. Zhou C, Liu WG, He W, Wang HB, Chen QQ, Song HP. Saikosaponin a inhibits RANKL-induced osteoclastogenesis by suppressing NF-kappaB and MAPK pathways. *Int Immunopharmacol.* 2015; 25:49-54.
93. Li J, Hao LY, Wu JH, Zhang JQ, Su JS. Linarin promotes osteogenic differentiation by activating the BMP-2/RUNX2 pathway *via* protein kinase A signaling. *Int J Mol Med.* 2016; 37:901-910.
94. Yang XL, Li F, Yang YN, Shen JY, Zou R, Zhu PP, Zhang CF, Yang ZL, Li P. Efficacy and safety of echinacoside in a rat osteopenia model. *Evid Based Complement Alternat Med.* 2013; 2013:926928.
95. Sun H, Li LJ, Zhang AH, Zhang N, Lv HT, Sun WJ, Wang XJ. Protective effects of sweroside on human MG-63 cells and rat osteoblasts. *Fitoterapia.* 2013; 84:174-179.
96. Tang DZ, Yang F, Yang Z, Huang J, Shi Q, Chen D, Wang YJ. Psoralen stimulates osteoblast differentiation through activation of BMP signaling. *Biochem Biophys Res Commun.* 2011; 405:256-261.
97. Yoon HY, Yun SI, Kim BY, Jin Q, Woo ER, Jeong SY, Chung YS. Poncirin promotes osteoblast differentiation but inhibits adipocyte differentiation in mesenchymal stem cells. *Eur J Pharmacol.* 2011; 664:54-59.
98. Xiao HH, Gao QG, Zhang Y, Wong KC, Dai Y, Yao XS, Wong MS. Vanillic acid exerts oestrogen-like activities in osteoblast-like UMR 106 cells through MAP kinase (MEK/ERK)-mediated ER signaling pathway. *J Steroid Biochem Mol Biol.* 2014; 144:382-391.
99. Tang DZ, Hou W, Zhou Q, Zhang M, Holz J, Sheu TJ, Li TF, Cheng SD, Shi Q, Harris SE, Chen D, Wang YJ. Osthole stimulates osteoblast differentiation and bone formation by activation of beta-catenin-BMP signaling. *J Bone Miner Res.* 2010; 25:1234-1245.

(Received September 5, 2017; Revised October 18, 2017; Accepted October 23, 2017)

Social support and care needs of the disabled elderly population: An empirical study based on survey data from Beijing, China

Xiaoning Hao^{1,2,*}, Juan Gu³, Xiangji Ying¹, Tao Bo⁴, Wei Fu¹

¹ China National Health Development Research Center, National Health and Family Planning Commission, Beijing, China;

² School of Public Health, Shandong University, Ji'nan, Shandong, China;

³ School of Public Administration, Chongqing University, Chongqing, China;

⁴ College of Politics and Public Administration, Qingdao University, Qingdao Shandong, China.

Summary

In order to describe and examine differences in social support and care needs among disabled Chinese elderly, the current study used stratified sampling to survey local residents of Beijing age 60 or over in the districts of Xicheng, Chaoyang, and Tongzhou in 2016. Structured in-person interviews were conducted with a 7-domain questionnaire. Multiple logistic regressions were used to compare social support and care needs among functioning, partially disabled, and completely disabled elderly. All statistical analyses were performed using SPSS 19.0 with a significance level of 0.05 (two-sided). One thousand and eighty-three residents completed the survey. Based on Activities of Daily Living (ADL) scores, 736 (68.0%) respondents were functioning (ADL score = 14), 167 (15.4%) were partially disabled ($14 < \text{ADL score} < 22$), and 180 (16.6%) were fully disabled (ADL score ≥ 22). Most of the disabled had formal financial support, they received daily care at home, and they received modest emotional support. After controlling for confounding factors, fully disabled respondents were 2.35 times ($p = 0.018$) more likely to receive financial support and 3.65 times ($p = 0.003$) more likely to receive emotional support than functioning respondents. However, the fully functioning and partially disabled did not differ significantly in terms of financial or emotional support. Compared to fully functioning respondents, partially disabled respondents were 0.49 ($p < 0.001$) times less likely to be fully satisfied with their daily care while fully disabled respondents were 0.37 ($p < 0.001$) times less likely to be fully satisfied with that care. The current study provided a thorough depiction of the current status of social support and care needs of disabled Chinese elderly. More attention should be paid to social support for the partially disabled and daily care for both the partially and fully disabled.

Keywords: Disabled elderly, social support, population aging

1. Introduction

China is witnessing the aging of its population. The country now has the largest population age 60 or over of any country worldwide. In 2015, its population age 60 or over was 211.9 million, accounting for approximately 15% of the total population (1).

Meanwhile, aging in China has occurred faster than in any other country. The population age 60 or over is expected to account for 35% of the total population by 2050 (1).

Functional ability or disability has been identified as an indicator of overall health status among older adults. The disabled elderly need to receive support and care from family members, relatives, and society for the rest of their lives. According to survey data from the China National Committee on Aging, there were approximately 33.5 million partially or fully disabled elderly living in urban or rural areas of China by the end of 2010; these individuals accounted for 19% of the total elderly

*Address correspondence to:

Dr. Hao Xiaoning, China National Health Development Research Center, National Health and Family Planning Commission, Beijing 100191, China.
E-mail: xnhao5421@163.com

population and included 10.8 million elderly who were fully disabled and who represented 6.25% of all elderly (2). The Report on China's Efforts to Address Aging (2013) indicated that the number of disabled elderly in China has been increasing and reached 37.5 million in 2013 (3).

The association between social support and functional ability has garnered increased attention due to rapid population aging around the world. Except for a few studies (4), most studies have found high levels of social support and connections help sustain good health and functional ability, along with other physiological and behavioral factors (5-11). Numerous studies have identified several components of social support that are associated with future functional status, including financial support, instrumental support such as house-cleaning, preparing meals, and provision of transportation (12,13), as well as emotional support (14).

Most previous studies have focused on finding social support factors that predict future functional ability among elderly, whereas few have focused on the status of social support of disabled older adults. The current study therefore aims to describe and examine differences in the extent of social support among disabled elderly in the Beijing area to help create a better social support system for the disabled older population in China.

2. Materials and Methods

2.1. Data collection

This study was conducted from February 2016 until the end of April 2016. Individuals age 60 or over who lived in the districts of Xicheng (including the former Xuanwu district), Chaoyang, and Tongzhou of Beijing were surveyed. Beijing was chosen as the survey site because of the prominent aging of its population. A variety of neighborhoods were sampled, including recently constructed neighborhoods, old neighborhoods, suburban neighborhoods, mixed neighborhoods, and villages. The current study used two-stage sampling. First, two urban districts (Xicheng and Chaoyang) and one suburban district (Tongzhou) were chosen in light of Beijing's functional districts. Neighborhoods from the districts were then chosen and equidistant sampling was used to select families from these neighborhoods to serve as the final sample. Data were obtained through structured face-to-face interviews with a 7-domain questionnaire. The research team provided quality control and 20 investigators visited homes to conduct interviews. Of 1,185 potential participants, 1,085 individuals agreed to participate in this study (response rate: 91.6%).

2.2. Measures

2.2.1. Activities of Daily Living (ADL) Scale score

The definition of disability is inconsistent across the domestic and international literature. In aging studies and practical applications, disability usually refers to an inability of elderly individuals to continue living independently. ADL scales have been widely used around the world as an effective measurement tool to assess the extent of disability among the elderly, which contain two parts, the Physical Self-Maintenance Scale (PSMS) and the Instrumental Activities of Daily Living (IADL) Scale, originally developed by Lawton and Brody in 1969 (15). Accordingly, the current survey consisted of 14 items to assess disability and was divided into two parts: one was the PSMS, which includes six domains – toilet use, eating, dressing, grooming, walking, and bathing, and the other was the IADL Scale, which includes eight dimensions – ability to use a telephone, shopping, food preparation, housework, laundry, mode of transportation, responsibility for taking one's own medications, and the ability to handle one's finances. Each question on the scale was scored from 1 (indicating complete functioning) to 4 (indicating complete disability). The total score ranged from 14 to 56. A total score of 14 points indicates complete functioning, a score between 15 and 21 indicates disability to some extent, and a score ≥ 3 on two or more questions or total score > 22 indicates complete disability.

2.2.2. Social support

The definition and measures of social support are similarly inconsistent across the literature (16). In the current study, social support was defined as "elderly receiving support from other people, organizations, or society, including financial support, routine support, and emotional support, as part of their daily lives or when they face a crisis". Variables for social support were thus divided into three categories: financial support, routine support, and emotional support. Based on the extent to which support was official, social support was also classified as formal or informal support (this mainly applied to financial support). Formal financial support (e.g. a salary, pension, or earnings) is the main source of funds for the elderly while informal financial support, usually from a spouse, son(s)/daughter(s), grandchildren, or other relatives, is an important source of funds for the elderly. Table 1 shows the categories of social support and variables for needs.

2.3. Data processing and analysis

EpiData 3.1 was used to create a database. Data entry was completed by two independent research assistants and a logical review was conducted by a third member of the research team. Descriptive statistical analysis, chi-square tests, and logistic regression analysis were performed using SPSS 19.0 with a significance level

Table 1. Categories of social support and variables for care needs

Type	Variable	Applicable questions
Financial support	Variables for financial support	Disposable income Financial status Satisfaction with medical insurance coverage
	Formal financial support	Salary, pension, etc. Having medical insurance
	Informal financial support	Source of funds
Routine support	Routine support	Living arrangements Receiving help from son(s)/daughter(s) Main caregiver when sick Satisfaction with the quality of care provided by a caregiver
Emotional support	Emotional support	Number of close friends Willingness to ask for help from son(s)/daughter(s) Relationship with neighbors

Table 2. ADL scale score for respondents as a whole and by gender (n = 1,083)

ADL category*	Total	Male	Female	Percentage (%)
ADL score = 14	736	388	348	68.0
14 < ADL score < 22	167	70	97	15.4
ADL score ≥ 22	180	82	98	16.6
Total	1,083	540	543	100

*ADL scale score = 14: fully functioning; 14 < ADL score < 22: partially disabled; ADL score ≥ 22: fully disabled. ADL, Activities of Daily Living.

of 0.05 (two-sided). Relevant variables were converted when necessary.

3. Results

3.1. Descriptive statistics

Of 1,085 elderly who initially agreed to participate in this study, 1,083 completed the survey ($n = 350$ in Xicheng and Xuanwu, $n = 506$ in Chaoyang, and $n = 227$ in Tongzhou). Of the respondents, 736 (68.0%) were fully functioning (ADL score of 14 points; 388 males, 348 females), 167 (15.4%) were partially disabled (14 points < ADL score < 22 points; 70 males, 97 females), and 180 (16.6%) were fully disabled (ADL score ≥ 22 points; 82 males, 98 females) (Table 2). Results indicated that female respondents had a greater level of disability than male respondents.

Table 3 shows descriptive statistics regarding the disabled elderly. Disabled adults over the age of 70 accounted for 89% of the sample. Elderly respondents were less able to live alone and were more likely to be disabled with increasing age. Eight percent of respondents ages 60-69 were disabled, 38.7% of respondents ages 70-79 were disabled, and 80.3% of respondents age 80 or over were disabled. Eleven-point-five percent of the disabled elderly had no chronic diseases. A higher percentage of the fully disabled elderly had more than three chronic diseases (52.8%) in comparison to the partially disabled elderly (38.9%).

A point worth mentioning is that the self-rated ability to live independently was greater than the score on the ADL scale. Only 1.4% respondents described themselves as fully disabled. However, 16.5% of respondents were fully disabled according to the ADL scale.

3.2. Current status of social support among disabled Chinese elderly

3.2.1. Financial support

Table 4 shows the current status of financial, routine, and emotional support by the extent of disability. Most of the disabled elderly (92.2% of the fully disabled, 90.4% of the partially disabled) responded that they had a middle or low level of monthly disposable income (in US dollars). Prior group interviews indicated that some elderly individuals had financial problems if they did not have a pension and they relied solely on government subsidies. When asked to rate their financial status, 46.7% of the partially disabled elderly and 45% of the fully disabled elderly responded they could basically balance their income and expenditures. Seventeen percent of the partially disabled elderly and 24.6% of the fully disabled elderly responded that they were currently struggling financially and could not balance their income and expenditures. This apparent difference between partially and fully disabled elderly in terms of self-perceived financial difficulty might be

Table 3. Baseline characteristics of the disabled elderly in Beijing (n = 347)

Item	Total (n = 347)		Partially disabled elderly (n = 167)		Fully disabled elderly (n = 180)	
	n	%	n	%	n	%
Gender						
Female	195	56.2	97	58.1	98	54.4
Age						
60-69	38	11.0	29	17.4	9	5
70-79	166	47.8	97	58.1	69	38.3
≥ 80	143	41.2	41	24.5	102	56.7
Marital status						
Spouse	177	51.0	105	62.9	72	40.0
No spouse	170	49.0	62	37.1	108	60.0
Level of education						
Less than primary school	254	73.2	110	65.9	144	80.0
Middle school	80	23.1	48	28.7	32	17.8
College or higher	13	3.7	9	5.4	4	2.2
Income (per month, in USD)						
< 300	158	45.5	69	41.3	89	49.4
301-500	119	34.3	64	38.3	55	30.6
501-600	40	11.5	18	10.8	22	12.2
≥ 601	30	8.6	16	9.6	14	7.8
Number of diseases						
None	40	11.5	22	13.2	18	10.0
1	64	18.4	31	18.6	33	18.3
2	83	23.9	49	29.3	34	18.9
≥ 3	160	46.1	65	38.9	95	52.8

due to the fact that the fully disabled elderly had higher medical expenses as part of their daily lives than the partially disabled elderly had. Respondents described their out-of-pocket medical expenditures as 4,053 yuan on average, accounting for 31% of the total treatment costs. One hundred and sixty-five fully disabled elderly and 177 partially disabled elderly answered the question "how satisfied are you with your medical insurance coverage?" Fifty-one-point-five percent of the fully disabled and 54.8% of the partially disabled responded that they were "somewhat satisfied" or "dissatisfied".

As shown in Table 4, 69.7% of the disabled elderly had formal financial support such as a salary or pension (71.9% of the partially disabled elderly, 67.8% of the fully disabled elderly). Ninety-eight-point-six percent of the disabled elderly participated in medical insurance (98.8% of the partially disabled elderly, 98.3% of the fully disabled elderly). The top two types of insurance that most respondents had were Urban Employee Medical Insurance (57% of all respondents, 60.6% of the partially disabled elderly, 53.7% of the fully disabled elderly) and New Rural Cooperative Medical Insurance (22.5% of all respondents, 23% of the partially disabled elderly, 22% of the fully disabled elderly). Other types of insurance included Serious Illness Insurance for the Elderly and Elderly-Children Insurance.

In terms of informal financial support, 61.1% of the disabled elderly received financial help from the local government or community (61.7% of the partially disabled elderly, 60.3% of the fully disabled elderly). Thirty-point-five percent of the disabled elderly

received financial help from their son(s)/daughter(s) (27.7% of the partially disabled elderly, 32.8% of the fully disabled elderly), and 8.4% received financial help from their spouses (10.2% of the partially disabled elderly, 6.9% of the fully disabled elderly). None (0%) of the partially or fully disabled elderly received financial help from their grandchildren or other relatives.

3.2.2. Routine support

Overall, most elderly individuals lived with family. Although 10.1% of the elderly lived alone, most lived with immediate family, relatives, or a care worker (92.2% of the partially disabled elderly, 87.8% of the fully disabled elderly). Eighty-four-point-one percent of the disabled elderly (two partially disabled elderly individuals with no son(s)/daughter(s)) responded that they could often receive help from their son(s)/daughter(s) (81.8% of the partially disabled elderly, 86.1% of the fully disabled elderly), 14.8% responded that they could occasionally receive help from their son(s)/daughter(s) (16.4% of the partially disabled elderly, 13.3% of the fully disabled elderly), and 1.1% responded that they could not receive help from their son(s)/daughter(s) (1.8% of the partially disabled elderly, 0.6% of the fully disabled elderly). Most elderly chose their son(s)/daughter(s) (58.7% of the partially disabled elderly, 75.6% of the fully disabled elderly) as their main caregiver when sick, followed by their spouse (38.3% of the partially disabled elderly, 20.6% of the fully disabled elderly). One-point-eight percent

Table 4. Descriptive statistics regarding social support for the disabled elderly in Beijing (n = 347)

Item	Total (n = 347)		Partially disabled (n = 167)		Fully disabled (n = 180)	
	n	%	n	%	n	%
<i>Financial support</i>						
Disposable monthly income						
Low (< 300 USD)	158	45.5	69	41.3	89	49.4
Middle (301-600 USD)	159	45.8	82	49.1	77	42.8
High (> 601 USD)	30	8.6	16	9.6	14	7.8
Financial status						
Well-off	127	36.6	72	43.1	55	30.6
Modest	159	45.8	78	46.7	81	45.0
Struggling	61	17.6	17	10.2	44	24.4
Satisfaction with medical insurance coverage*						
Fully satisfied	160	46.1	80	48.5	80	45.2
Somewhat satisfied	109	31.4	55	33.3	54	30.5
Dissatisfied	73	21.0	30	18.2	43	24.3
<i>Formal financial support</i>						
Have a salary, pension, etc. (yes)	242	69.7	120	71.9	122	67.8
Have medical insurance (yes)	342	98.6	165	98.8	177	98.3
<i>Informal financial support</i>						
Source of funds						
Local government or community	212	61.1	103	61.7	109	60.3
Son(s)/daughter(s)	106	30.5	47	27.7	59	32.8
Spouse	29	8.4	17	10.2	12	6.9
Grandchildren or other relatives	0	0	0	0	0	0
<i>Routine support</i>						
Living arrangements						
Living alone	35	10.1	13	7.8	22	12.2
Residing with relatives	312	89.9	154	92.2	158	87.8
Receiving help from son(s)/daughter(s)						
Often	290	83.6	135	81.8	155	86.1
Occasionally	51	14.7	27	16.4	24	13.3
Never	4	1.2	3	1.8	1	0.6
Main caregiver when sick						
Spouse	101	29.1	64	38.3	37	20.6
Son(s)/daughter(s)	234	67.4	98	58.7	136	75.6
Someone else	9	2.6	2	1.2	7	3.9
None	3	0.9	3	1.8	0	0
Satisfaction with the quality of care						
Fully satisfied	136	39.2	70	43.2	66	36.7
Somewhat satisfied	189	54.5	83	51.2	106	58.9
Dissatisfied	17	4.9	9	5.6	8	4.4
<i>Emotional support</i>						
Number of close friends						
0	65	18.7	12	7.2	53	29.4
1-2	96	27.7	47	28.1	49	27.2
3-5	160	46.1	96	57.5	64	35.6
≥ 6	26	7.5	12	7.2	14	7.8
Willingness to ask for son(s)/daughter(s)' help (yes)	318	91.6	146	88.5	172	95.6
Relationship with neighbors						
Amicable	196	56.5	104	62.3	92	51.1
Passing acquaintance only	93	26.8	47	28.1	46	25.6
Poor	58	16.7	16	9.6	42	23.3

*Refers to the elderly who choose to purchase medical insurance.

of the partially disabled elderly had no caregiver or received care from a nurse/social services while 2.6% of the fully disabled elderly had no caregiver or received care from a nurse/social services. One could argue that the main caregiver for the disabled elderly was a family member and that the community and other social factors had a limited influence. Most of the disabled elderly were fully satisfied or somewhat satisfied with the help that they received for the 14 daily tasks listed in the ADL scale (94.4% of the partially disabled

elderly, 95.6% of the fully disabled elderly).

3.2.3. Emotional support

Few disabled elderly respondents had a large number of friends. Seven-point-two percent of the partially disabled and 29.4% of the fully disabled had no close friends. Twenty-eight-point-one percent of the partially disabled elderly and 27.2% of the fully disabled elderly said they had only 1-2 close friends. Only a few

Table 5. Relationships constituting the emotional support network of disabled elderly (n = 347)

Relationships	n	% of total	% of relatives	% of non-relatives
Immediate family	1,209	98.5	100	
Spouse	140	11.4	11.6	
Son	459	37.4	38.0	
Daughter	383	31.2	31.7	
Daughter-in-law	119	9.7	9.8	
Son-in-law	45	3.7	3.7	
Grandchildren	46	3.7	3.8	
Other relatives	17	1.4	1.4	
Non-relatives	19	1.5		100
Neighbors	11	0.9		57.9
Colleagues	3	0.2		15.8
Friends	2	0.2		10.5
Nurse	2	0.2		10.5
Someone else	1	0.1		5.3
Total	1,228			

Table 6. Bivariate analyses of social support factors in relation to ADL scale score for the elderly

Social support factors	Normal	Partially disabled	Fully disabled	χ^2	p
<i>Financial support</i>					
Source of income				16.046	< 0.001
Pension or other remuneration	769 (71.0%)	156 (14.4%)	158 (14.6%)		
Other sources	626 (57.8%)	205 (18.9%)	252 (23.3%)		
<i>Routine support</i>					
Main caregiver when sick				64.828	< 0.001
Spouse	865 (79.8%)	136 (12.6%)	82 (7.6%)		
Someone else	632 (58.4%)	192 (17.7%)	259 (23.9%)		
<i>Emotional support</i>					
Willingness to talk to someone else when upset				10.293	0.006
Yes	754 (69.6%)	164 (15.1%)	165 (15.3%)		
No	631 (58.3%)	179 (16.6%)	273 (25.2%)		

ADL, Activities of Daily Living.

disabled elderly respondents responded that they had more than six friends (7.5% of all respondents, 7.2% of the partially disabled elderly, 7.8% of the fully disabled elderly). When they faced difficulties, 92.2% of the disabled elderly were willing to ask a son(s)/daughter(s) for help (88.5% of the partially disabled elderly, 95.6% of the fully disabled elderly). Most of the disabled elderly responded that they were on friendly terms with their neighbors (62.3% of the partially disabled elderly, 51.1% of the fully disabled elderly).

In this study, social support networks were measured using the technique devised by Poel, which involves identification of the people in one's personal network (17). A typical question about one's emotional support network asked elderly respondents "when you are not in a good mood, who would you like to talk to?" Respondents were allowed multiple answers from among 12 possible answers: spouse, son(s)/daughter(s), parents, siblings, other relatives, colleagues, superiors, subordinates, classmates, friends, neighbors, and other non-relatives. As shown in Table 5, relatives were chosen most often (98.5%); a son was chosen most often (38%), followed by a daughter (31.7%), and a spouse (11.6%). Relationships with non-relatives played a relatively minor role in the support network;

neighbors accounted for the highest proportion (57.9%) of non-relatives.

3.3. Bivariate analysis of the association between social support and disability

Table 6 shows the results of bivariate analysis of the association between social support factors and the ADL score for the elderly. The ADL score for elderly respondents with personal income (including a salary, pension, or earnings) was lower than that of elderly respondents who received financial support from their spouse, son(s)/daughter(s), or the government ($p < 0.001$). Disabled elderly respondents who were mainly cared for by their spouse had a significantly higher ADL score than disabled elderly who were cared for by someone else ($p < 0.001$). Disabled elderly who were willing to talk to someone else when upset had a lower ADL score than disabled elderly who were reluctant to talk when upset ($p = 0.006$).

3.4. Multivariate analysis of the association between social support and disability

Table 7 shows the results of multivariate logistic

Table 7. Multivariate logistic regressions of the effect of receiving social support on ALD scale score for the disabled elderly

ADL category*	OR (95% CI)		
	Financial support	Routine support	Emotional support
ADL score = 14	Referent	Referent	Referent
14 < ADL score < 22	0.706 (0.432, 1.154)	0.485 (0.325, 0.724)	0.808 (0.469, 1.394)
ADL score ≥ 22	2.346 (1.160, 4.743)	0.369 (0.236, 0.578)	3.648 (1.560, 8.532)

*ADL scale score = 14: fully functioning; 14 < ADL score < 22: partially disabled; ADL score ≥ 22: fully disabled. ADL, Activities of Daily Living.

regression analysis of the effect of receiving social support on the ALD score for the disabled elderly. After adjusting for gender, age, level of education, marital status, and monthly income, fully disabled respondents were 2.346 times more likely to receive financial support than fully functioning respondents ($p = 0.018$, 95% CI: 1.160-4.743). However, the partially disabled elderly and the fully disabled elderly did not differ significantly in terms of financial support ($p = 0.165 > 0.05$). Partially disabled respondents were 0.485 ($p < 0.001$) times and fully disabled respondents were 0.369 ($p < 0.001$) times less likely to be fully satisfied with daily care than fully functioning respondents. In addition, fully disabled respondents were 3.648 times more likely to receive emotional support than fully functioning respondents ($p = 0.003$, 95% CI: 1.560-8.532). However, the partially disabled elderly and the fully disabled elderly did not differ significantly in terms of emotional support ($p = 0.444 > 0.05$).

4. Discussion

Most of the respondents had formal financial support such as a salary and pension, they had medical insurance, and they received financial support from the local government or community, but respondents also had a middle or low level of income and their insurance was insufficient. Multivariate analysis revealed significant differences between fully functioning and disabled individuals, but the financial support received by the partially disabled elderly did not differ significantly from that received by respondents who were able to live independently. Thus, under current conditions in China where "aging of the population is proceeding faster than the pace of development," there is an imminent need for a better financial support system for the disabled elderly, and especially those who are partially disabled or in financial distress.

Moreover, the current long-term care service for disabled elderly is not reimbursed by medical insurance. Disabled elderly had to cover medical expenses resulting from hospitalization due to an illness through out-of-pocket payments or payments by their families. Although such solutions are feasible at present, the increase in the disabled elderly population and the decrease in the number of son(s)/daughter(s) will result

in a greater financial burden posed by the long-term care needs of the disabled elderly as well as increasing reliance on nursing homes. Thus, a helpful approach would be for medical insurance to cover long-term care in the future. Other potential solutions could be the establishment of an independent insurance system for long-term care or a combination of long-term care insurance and social care insurance for the disabled elderly.

The extent of routine support was somewhat greater than the extent of financial support. Most elderly respondents lived with their family/children, they responded that they could often receive help from their son(s)/daughter(s), they were cared by their son(s)/daughter(s) or spouse when sick, and they were fully satisfied or somewhat satisfied with the help they received. A point worth mentioning is that care by one's family or son(s)/daughter(s) was the main form of routine support received by the disabled elderly. Previous studies have found older Chinese with the ability to live independently also tend to reside with family rather than live in a nursing home (18). This phenomenon can be explained by the fact that residing with and caring for elderly parents is still the predominant way that adult son(s)/daughter(s) in modern China express filial piety - a key virtue in Chinese culture (19).

However, the current analysis indicated that partially or fully disabled respondents were much less likely to be fully satisfied with daily care, which was mainly care provided by their family, compared to functioning respondents. Previous studies have suggested that the disabled elderly who need long-term care and who heavily depend on daily care probably need institutional care. As an example, a study in Taiwan found that caring for stroke patients in their own homes was both more expensive and also less effective in improving ADL scores than caring for patients in nursing homes or in chronic care units of hospitals (20). In the current study, nearly 30% of the respondents who would have preferred to live in a nursing home (results not published). Asked further about their reasons for not living in a nursing home, nearly half of the disabled elderly responded they could not afford that care (results not published). Thus, improving the affordability of institutional care is likewise essential for improvement

of the recovery, quality of life, and survival of disabled older adults.

Almost one third of the fully disabled had no close friends and nearly half were not on good terms with their neighbors. A study on non-institutionalized, fully functioning Japanese elderly found that among all social support and network characteristics, adequacy of emotional support contributed the most to the prevention of depression and suicide among older adults (21). The current bivariate analysis likewise found that disabled elderly who were willing to talk to someone else when they were not in a good mood had a lower ADL score than that of disabled elderly who were reluctant to talk. This finding is consistent with a previous study suggesting that emotional support was not associated with disability but did it did prevent a decrease in ADL (14). Since the physical activity and social interaction of disabled elderly are limited, the lack of emotional support for the disabled is a pressing issue. Moreover, multivariate analysis suggested that partially disabled respondents needed more emotional support than fully functioning respondents but that the two groups did not differ in terms of the emotional support they actually received. All of these findings emphasize the need to provide sufficient emotional support to the fully disabled elderly as well as to the partially disabled elderly.

In addition, the emotional support network of the disabled elderly mainly consisted of immediate family and relatives, suggesting a lack of diversity in their social network. Though evidence is inconsistent across the literature (22), most studies have pointed out the importance of diversity in the social networks of the elderly (23,24). Increasing the diversity of social networks may prevent disability among older people.

There are several limitations inherent in the current study. First, data were collected using a cross-sectional survey. With such data, only associations, as opposed to causality, could be inferred. Second, the nature of the questionnaire inevitably led to certain drawbacks, including recall bias and social desirability bias. Third and last, China is a large country with significant differences among its regions and areas. Although Beijing is a cosmopolitan city, caution should be taken in generalizing findings from the Beijing area to other areas of China.

In summary, the current study provided a thorough look at the current status of social support among disabled Chinese elderly. The results highlight the need to pay greater attention to social support for partially disabled individuals and daily care for both partially and fully disabled individuals.

Acknowledgements

This study was funded by grants from the National Nature Science Foundation of China (71373184,

71774034), the think tank project of the Data Center for Management Science, NSFC-PKU of the National Nature Science Foundation of China (2015KEY05), and the Beijing Natural Science Foundation (9162018).

References

1. Fang EF, Scheibye-Knudsen M, Jahn HJ, Li J, Ling L, Guo H, Zhu X, Preedy V, Lu H, Bohr VA, Chan WY, Liu Y, Ng TB. A research agenda for aging in China in the 21st century. *Ageing Res Rev.* 2015; 24:197-205.
2. China Research Center on Aging. <http://www.crca.cn> (accessed September 1, 2017).
3. Wu YS. Report on China's Efforts to Address Aging. Social Sciences Academic Press (Beijing), 2013. (in Chinese)
4. Kempen GI, Ranchor AV, van Sonderen E, van Jaarsveld CH, Sanderman R. Risk and protective factors of different functional trajectories in older persons: Are these the same? *J Gerontol B Psychol Sci Soc Sci.* 2006; 61:P95-101.
5. Stuck AE, Walthert JM, Nikolaus T, Bula CJ, Hohmann C, Beck JC. Risk factors for functional status decline in community-living elderly people: A systematic literature review. *Soc Sci Med.* 1999; 48:445-469.
6. McLaughlin D, Leung J, Pachana N, Flicker L, Hankey G, Dobson A. Social support and subsequent disability: It is not the size of your network that counts. *Age Ageing.* 2012; 41:674-677.
7. Levasseur M, Genereux M, Bruneau JF, Vanasse A, Chabot E, Beaulac C, Bedard MM. Importance of proximity to resources, social support, transportation and neighborhood security for mobility and social participation in older adults: Results from a scoping study. *BMC Public Health.* 2015; 15:503.
8. Zunzunegui MV, Rodriguez-Laso A, Otero A, Pluijm SMF, Nikula S, Blumstein T, Jylha M, Minicuci N, Deeg DJH, Group CW. Disability and social ties: Comparative findings of the CLESA study. *Eur J Ageing.* 2005; 2:40-47.
9. James BD, Boyle PA, Buchman AS, Bennett DA. Relation of late-life social activity with incident disability among community-dwelling older adults. *J Gerontol A Biol Sci Med Sci.* 2011; 66:467-473.
10. Mendes de Leon CF, Glass TA, Berkman LF. Social engagement and disability in a community population of older adults: The New Haven EPESE. *Am J Epidemiol.* 2003; 157:633-642.
11. Hsu HC, Tung HJ. What makes you good and happy? Effects of internal and external resources to adaptation and psychological well-being for the disabled elderly in Taiwan. *Aging Ment Health.* 2010; 14:851-860.
12. Mendes de Leon CF, Glass TA, Beckett LA, Seeman TE, Evans DA, Berkman LF. Social networks and disability transitions across eight intervals of yearly data in the New Haven EPESE. *J Gerontol B Psychol Sci Soc Sci.* 1999; 54:S162-172.
13. Avlund K, Lund R, Holstein BE, Due P. Social relations as determinant of onset of disability in aging. *Arch Gerontol Geriatr.* 2004; 38:85-99.
14. Mendes de Leon CF, Gold DT, Glass TA, Kaplan L, George LK. Disability as a function of social networks and support in elderly African Americans and Whites:

- The Duke EPSE 1986--1992. *J Gerontol B Psychol Sci Soc Sci.* 2001; 56:S179-190.
15. Lawton MP, Brody EM. Assessment of older people: Self-maintaining and instrumental activities of daily living. *Gerontologist.* 1969; 9:179-186.
 16. Berkman LF, Glass T, Brissette I, Seeman TE. From social integration to health: Durkheim in the new millennium. *Soc Sci Med.* 2000; 51:843-857.
 17. Poel M. Personal Networks: A Rational-Choice Explanation of their Size and Composition. Swets and Zeitlinger (Lisse), 1993.
 18. Zhang L, Zeng Y, Fang Y. The effect of health status and living arrangements on long term care models among older Chinese: A cross-sectional study. *PLoS One.* 2017; 12:e0182219.
 19. Zhang Z, Gu D, Luo Y. Coresidence with elderly parents in contemporary China: The role of filial piety, reciprocity, socioeconomic resources, and parental needs. *J Cross Cult Gerontol.* 2014; 29:259-276.
 20. Chiu L, Shyu WC, Liu YH. Comparisons of the cost-effectiveness among hospital chronic care, nursing home placement, home nursing care and family care for severe stroke patients. *J Adv Nurs.* 2001; 33:380-386.
 21. Oxman TE, Berkman LF, Kasl S, Freeman DH, Jr., Barrett J. Social support and depressive symptoms in the elderly. *Am J Epidemiol.* 1992; 135:356-368.
 22. Rafnsson SB, Shankar A, Steptoe A. Longitudinal influences of social network characteristics on subjective well-being of older adults: Findings from the ELSA study. *J Aging Health.* 2015; 27:919-934.
 23. Simons RL. Specificity and substitution in the social networks of the elderly. *Int J Aging Hum Dev.* 1983; 18:121-139.
 24. Escobar-Bravo MA, Puga-Gonzalez D, Martin-Baranera M. Protective effects of social networks on disability among older adults in Spain. *Arch Gerontol Geriatr.* 2012; 54:109-116.

(Received September 20, 2017; Revised October 17, 2017; Accepted October 26, 2017)

Relationships between neighborhood attributes and subjective well-being among the Chinese elderly: Data from Shanghai

Junling Gao¹, Scott R. Weaver², Hua Fu^{1,*}, Yingnan Jia¹, Jiang Li¹

¹Institute of Health Communication, School of Public Health, Fudan University, Shanghai, China;

²School of Public Health, Georgia State University, Atlanta, GA, USA.

Summary

It has been hypothesized that subjective well-being (SWB) is determined by a combination of individual characteristics, social environment, and physical environment. However, few studies have simultaneously examined the relationships of the social and physical attributes of a neighborhood with SWB. Accordingly, the present study aimed to examine these relationships among Chinese elders. A total of 2,719 elders aged 60 years or older were recruited from 47 neighborhoods in the Xinhua subdistrict of Shanghai by two-stage stratified random sampling and interviewed between July and September 2014. The social and physical attributes of each neighborhood were assessed using validated and psychometrically tested measures. The Chinese version of the international Personal Wellbeing Index was used to assess SWB. Control variables included sex, age, marital status, education level, years living in the neighborhood, self-rated health, chronic conditions, and leisure-time physical activity. Multilevel linear regression analysis was conducted to explore whether social and physical attributes were associated with SWB. The average level of SWB was $74.2 \pm 15.7\%$ of the scale maximum. After controlling for individual covariates, individual-level social cohesion and social interaction were positively correlated with SWB, and both individual-level and neighborhood-level aesthetic quality was positively correlated with SWB. In conclusion, both social and physical attributes of neighborhoods were associated with SWB among Chinese elderly. These findings suggest that creating aesthetic and cohesive neighborhoods may encourage Chinese elders to participate in social activities and promote their SWB.

Keywords: Neighborhood attributes, social capital, subjective wellbeing, aging

1. Introduction

Regarded as a key dimension of quality of life, subjective well-being (SWB) has been defined as "good mental states, including all of the various evaluations, positive and negative, that people make of their lives and the affective reactions of people to their experiences" (1). Based on a substantial body of research that has found strong associations of this characteristic with longer survival and several other health indicators (2,3), SWB has been designated as

an important indicator of societal progress and a target for improvement by health care systems (2,4). As the prevalence of chronic illness increases with advancing age and treatments for life-threatening disease become more effective, the issue of maintaining well-being at advanced ages is growing in importance (2). This has led to increased efforts to develop appropriate measures of SWB and gain an increased understanding of determinants of well-being worldwide.

SWB is thought to be determined by a multitude of individual factors as well as social and physical environmental factors (5,6). Several studies have focused on demographic factors that may affect SWB – such as gender, age, income, and marital status – but they have found that these factors generally explain less than 20% of the variance in SWB (7). Furthermore, the relationships found between demographic factors and SWB were not consistent. For example, the quadratic

Released online in J-STAGE as advance publication October 11, 2017.

*Address correspondence to:

Dr. Hua Fu, School of Public Health, Fudan University, PO Box 248 138 Yixueyuan Road, Shanghai 200032, China.
E-mail: hfu@fudan.edu.cn

relationship between SWB and age in high-income English-speaking countries was not replicated in other regions (2). Studies of SWB have also examined its association with environmental factors, with an emphasis on the importance of the geographically proximal environment for older adults, particularly those who are retired or becoming frail and therefore likely to be spending more time in their immediate neighborhood (8). Several studies showed that certain physical attributes of the neighborhood, such as quality public transportation (9) and access to green/recreational areas (10,11), were positively associated with higher levels of SWB.

There is limited evidence on the relationship between perceived aspects of the neighborhood and mental health in older people, but findings from a few studies have linked self-reported neighborhood problems (12), poor social environment in a neighborhood (13), and low sense of belonging to a neighborhood (14) with psychological distress in older people. This suggests that how individuals feel about the physical and social environment in which they live may be associated with their mental health just as strongly as objective, area-level measures of neighborhood deprivation (15). These associations with mental health could be expected to extend to SWB. This has been supported by cross-sectional studies, which have found that perceived neighborhood cohesion was positively associated with SWB among elders (8,15,16), and a longitudinal study in England (17), which found that negative neighborhood perceptions were associated with poorer SWB. Another longitudinal study in the Netherlands (18) found that social cohesion and social belonging were positively associated with SWB.

Physical and social environments are thought not only to influence health outcomes and health behaviors, but also to be interrelated and influence each other (19,20). One study (21) found that adults living in high-walkable neighborhoods reported higher levels of knowing their neighbors, political participation, trust in other people, and social participation compared to participants living in low-walkable neighborhoods. Other studies have also supported the hypothesis that pedestrian-friendly environments are related to increased social capital (22,23). However, few studies have simultaneously examined the unique effects of individual, physical, and social neighborhood characteristics on SWB among elders.

While some studies have found individual characteristics (such as gender, age, and education) (24-26), social support (26,27), social belonging (28), economic openness (29), and atmospheric pollution (30) to be associated with SWB among urban Chinese people, research focusing specifically on the neighborhood environment and SWB among elders in China has been limited. In fact, we could only find one such study (27), and this study did not

examine individual, physical, and social environmental characteristics simultaneously. The objective of the present study is to address a gap in the SWB literature with a cross-sectional study examining the effects of neighborhood social cohesion, social interaction, aesthetic quality (AQ), and walkability on SWB in a sample of elders from Shanghai, China.

2. Methods

2.1. Participants and study design

The present study was conducted in the Xinhua subdistrict of Shanghai from July to September 2014. The Xinhua subdistrict with mature physical structure is aging subdistrict of approximately 2.2 km² located in southwest Shanghai. It consists of 198 neighborhoods with approximately 78,000 residents, of whom 16% are over 65 years old (<http://www.xhjd.org/>). The subdistrict has a stable population structure and built environment, which make it a suitable place to examine the effects of the perceived social and physical attributes of a neighborhood on health. The study design and sampling approach has been described previously (31). Briefly, the first stage consisted of the selection of 47 neighborhoods by purposive sampling that took into account environmental factors such as accessibility to services, aesthetics, and street connectivity. In the second stage, we randomly sampled 120 elders aged 60 years or older from each neighborhood that had more than 120 elders; in neighborhoods with fewer than 120 elders, all elders living in the neighborhood were selected. In total, 2,839 elders were sampled from 47 neighborhoods; however, 120 elders were excluded from analysis because of incomplete data, resulting in a final analytic sample consisting of 2,719 elders for the current study.

Informed consent was obtained from all participants, and face-to-face interviews were used to collect data. The study was approved by the Institutional Review Board of the School of Public Health at Fudan University.

2.2. Measurements

2.2.1. Subjective well-being

The Chinese version of the Personal Wellbeing Index (CPWI) (32) was used to measure subjective well-being. The CPWI used in the current study consisted of seven core domains (standard of living, health, life achievement, personal relationships, personal safety, feeling part of the community, and future security), measured on an 11-point Likert-type scale, with numerical ratings ranging from 0 (*extremely dissatisfied*) to 10 (*extremely satisfied*). A previous study found the CPWI to have acceptable reliability, Cronbach's $\alpha = 0.81$ (24). In the present study, Cronbach's $\alpha = 0.92$ for our

sample. The Likert scale data were standardized into units of percentage of scale maximum (% SM) on a 0-100 distribution using the equation

$$\frac{X - K^{min}}{K^{max} - K^{min}} \times 100 \quad (32),$$

where X is the score to be converted, $K^{min} = 0$ (the minimum score possible on the scale), and $K^{max} = 10$ (the maximum score possible on the scale).

2.2.2. Attributes of neighborhood

In the present study, we mainly focused on two physical dimensions of neighborhoods (aesthetic quality and walkability) and two social dimensions (social interaction with neighbors and social cohesion). The scales used to measure these dimensions were developed by Mujahid and colleagues (33). As described in detail previously (31), the original scale was initially translated into Chinese, and the Chinese version was then translated back into English to verify that the content of the original scale was maintained. The aesthetic quality (AQ) subscale consisted of 5 items, the walkability subscale consisted of 7 items, the social interaction with neighbors subscale consisted of 5 items, and the social cohesion subscale consisted of 4 items. The Cronbach's α s for these subscales in our sample were 0.74, 0.81, 0.87, and 0.88, respectively.

Due to the relationship between neighborhood characteristics and individual-level characteristics (33,34), with varying perceptions of the same reality by different individuals, the averaging of responses across multiple persons within a neighborhood reduces measurement error due to individual subjectivity (33). In the present study, all attributes of the neighborhood were assessed in two alternative ways: (a) individual-level attributes were assessed by calculating the mean score of each individual's own assessments on the corresponding scale's items; (b) neighborhood-level attributes for participant i were measured as the mean perceived individual-level attributes for all participants from the same neighborhood as participant i , excluding participant i . Previous studies indicated that objective neighborhood measures were significantly correlated with subjective perceptions of neighborhood quality (35) – for example, a participant with higher neighborhood-level AQ would generally indicate that she/he lived in a more aesthetic neighborhood. For analysis, both individual and neighborhood-level attribute scores were converted into quartiles, with the highest quartile indicating the highest level of neighborhood attributes.

2.2.3. Covariates

We selected the following variables as potential confounders for statistical control: sex, age (categorized in 5-year intervals), marital status (married or cohabiting

vs. other), education level (elementary school, junior high school, senior high school, and university or higher), and years living in the neighborhood (categorized in 10-year intervals). Additionally, a previous study indicated that both comorbidity and self-rated health were associated with SWB (36); therefore, we also controlled for the number of self-reported chronic diseases (0, 1, 2 or more) and self-rated health. Self-rated health was assessed by the single item, "Would you say that in general your health is excellent, very good, good, fair, or poor?" From this item, we created a dichotomous measure (0 = fair or poor; 1 = excellent, very good, or good). Finally, we controlled for leisure-time physical activity (LTPA), which was assessed by the Chinese long form of the International Physical Activity Questionnaire (37). Consistent with previous research (38), self-reported minutes of recreational walking and moderate- and vigorous-intensity physical activity in the past week were used to estimate a LTPA score, which was dichotomized into high or low. High LTPA was defined as at least 150 minutes of leisure-time physical activity per week. This criterion is in accordance with the current recommendations for physical activity (39).

2.2.4. Statistical analyses

Our data had a multilevel structure comprising elders (the first level) nested within neighborhoods (the second level). We fitted the data using multilevel linear regression models, adjusting for both individual- and neighborhood-level variables as fixed effects and allowing for a random intercept for SWB. The analyses of the relationships between attributes of a neighborhood and SWB involved estimating multiple sequential models (40). After examining the neighborhood-level variance in SWB without including any explanatory variables (empty model), we examined the relationship between individual- and neighborhood-level attributes of the neighborhood with SWB (Models 1 and 2, respectively) after controlling for individual covariates. Finally, we modeled all individual- and neighborhood-level variables simultaneously (Model 3). We used $-2 \log$ likelihood ($-2LL$) and Akaike information criterion (AIC) to compare the goodness of fit of each model (40). STATA version 13.1 was used for all analyses (StataCorp, Texas, USA). For all models, the unstandardized coefficient (B) and corresponding 95% confidence interval were reported. Results were considered statistically significant if the two-sided p values were < 0.05 .

3. Results

3.1. Demographic characteristics and subjective well-being of the sample

The demographic characteristics of the sample and univariate relationships between demographic

Table 1. Demographic differences in subjective well-being

Items	N, %	Subjective well-being (mean and <i>SD</i>)	<i>p</i> value
Overall	2,719	74.2 (15.7)	
Sex			
Men	1,124 (41.3)	74.8 (14.8)	0.082
Women	1,595 (58.7)	73.8 (15.2)	
Age (years)			
60-64	722 (26.6)	75.2 (14.5)	0.023
65-69	590 (21.7)	74.8 (14.0)	
≥ 70	1,407 (51.8)	73.5 (15.7)	
Education level			
Elementary school	844 (31.0)	71.2 (16.4)	< 0.001
Junior high school	963 (35.4)	74.3 (14.1)	
Senior high school	473 (17.4)	76.5 (13.1)	
University	439 (16.2)	77.4 (15.2)	
Marital status			
Married or cohabiting	2,183 (80.3)	74.9 (14.7)	< 0.001
Other	536 (19.7)	71.4 (15.8)	
Self-rated health			
Poor	1,785 (65.7)	73.2 (15.1)	< 0.001
Good	934 (34.4)	76.3 (14.7)	
Number of chronic diseases			< 0.001
None	640 (23.5)	77.8 (13.2)	
One	1,093 (40.2)	74.7 (14.8)	
Two or more	986 (36.5)	71.3 (15.7)	
Years living in the neighborhood			
< 10	305 (11.2)	68.5 (15.7)	< 0.001
10-19	1,141 (42.0)	73.3 (14.7)	
20-29	582 (21.4)	76.0 (14.3)	
30-39	342 (12.6)	76.7 (15.4)	
≥ 40	349 (12.8)	77.0 (14.9)	
Leisure-time physical activity			
Low	1,281 (47.1)	71.7 (15.4)	< 0.001
High	1,438 (52.9)	76.4 (14.3)	

characteristics and SWB are shown in Table 1. Overall, 58.7% of the subjects were women, and more than half (51.8%) were 70 years old or older. Only 16.2% had graduated from university. More than 70% reported having at least one chronic disease, and 65.7% reported poor self-rated health. More than half of subjects had lived in the neighborhood for 20 years or longer. The average level of SWB was $74.2 \pm 15.7\%$ SM. SWB was significantly higher among those who were married/cohabiting ($74.9 \pm 14.7\%$ SM) than among their unmarried counterparts ($71.4 \pm 15.8\%$ SM); it was also significantly higher among those with higher education levels ($p < 0.001$). Subjects with good self-rated health also reported significantly higher levels of SWB than subjects with poor self-rated health. Additionally, SWB was significantly higher among people with high LTPA ($76.7 \pm 14.4\%$ SM) than among their low-LTPA counterparts ($72.0 \pm 15.2\%$ SM). SWB was negatively correlated with age group and number of chronic diseases (both $p < 0.05$), and positively correlated with years living in the neighborhood ($p < 0.05$).

3.2. Univariate analysis of neighborhood attributes and SWB

Univariate analyses showed that SWB increased

Table 2. Univariate relationships between perceived neighborhood attributes and subjective well-being

Items	N, %	Subjective well-being (mean and <i>SD</i>)	<i>p</i> value
Physical characteristics			
Aesthetic quality			
1 st quartile	641 (23.6)	70.6 (15.0)	< 0.001
2 nd quartile	612 (22.5)	71.2 (15.7)	
3 rd quartile	649 (23.9)	74.0 (12.6)	
4 th quartile	817 (30.1)	79.6 (14.8)	
Walking environment			
1 st quartile	666 (24.5)	72.7 (15.2)	< 0.001
2 nd quartile	661 (24.3)	72.0 (15.0)	
3 rd quartile	693 (25.5)	73.8 (13.8)	
4 th quartile	699 (25.7)	78.2 (15.4)	
Social characteristics			
Social cohesion			
1 st quartile	670 (24.6)	68.6 (16.4)	< 0.001
2 nd quartile	480 (17.7)	71.9 (13.6)	
3 rd quartile	481 (17.7)	73.9 (14.7)	
4 th quartile	1088 (40.0)	78.9 (13.4)	
Social interaction			
1 st quartile	646 (23.8)	71.0 (15.7)	< 0.001
2 nd quartile	544 (20.0)	72.9 (15.0)	
3 rd quartile	677 (24.9)	74.5 (13.8)	
4 th quartile	852 (31.3)	77.4 (14.8)	

significantly with higher individual perceptions of AQ, walkability, social cohesion, and social interaction (Table 2). For example, the SWB levels among participants in the first (lowest), second, third, and fourth (highest) quartiles of perceived neighborhood AQ were $70.6 \pm 15.0\%$ SM, $71.2 \pm 15.7\%$ SM, $74.0 \pm 12.6\%$ SM, and $79.6 \pm 14.8\%$ SM, respectively.

3.3. Multilevel linear regressions of the relationship between neighborhood attributes and SWB

The results of the multilevel linear regression models are shown in Table 3. The empty model (not shown in Table 3) indicated that there was significant variation in SWB across neighborhoods ($\chi^2 = 149.78$, $p < 0.001$); the interclass correlation coefficient (ICC) was 0.084, indicating that 8.4% of the variance in SWB was explained by a random effect for neighborhoods.

Model 1 indicated that individual-level social cohesion, social interaction, and AQ were positively associated with SWB, but individual-level walkability was not associated with SWB after controlling for individual covariates. For example, compared with participants in the lowest quartile of social cohesion, the regression coefficients of participants in the second, third, and fourth quartiles were 2.34 (95% CI: 0.71-3.98), 3.03 (95% CI: 1.32-4.73), and 6.90 (95% CI: 5.38-8.42), respectively. However, Model 2, which included the neighborhood-level attributes and individual covariates, found that only neighborhood-level AQ was significantly and positively correlated with SWB after controlling for individual covariates.

Table 3. Multilevel regression models of relationships between neighborhood attributes and subjective well-being*

Items	Model 1: <i>B</i> , 95%CI	Model 2: <i>B</i> , 95%CI	Model 3: <i>B</i> , 95%CI
Fixed effects			
Individual-level variables			
Social cohesion			
1 st quartile	Reference		Reference
2 nd quartile	2.34 (0.71-3.98)		2.31 (0.68-3.95)
3 rd quartile	3.03 (1.32-4.73)		2.87 (1.15-4.59)
4 th quartile	6.90 (5.38-8.42)		6.79 (5.24-8.33)
Social interaction			
1 st quartile	Reference		Reference
2 nd quartile	1.20 (0.76-1.36)		1.17 (0.73-1.40)
3 rd quartile	1.90 (0.98-2.46)		1.04 (0.53-2.61)
4 th quartile	2.76 (1.16-4.36)		2.72 (1.14-4.23)
Aesthetic quality			
1 st quartile	Reference		Reference
2 nd quartile	0.43 (0.09-1.95)		0.46 (0.15-1.98)
3 rd quartile	1.63 (0.07-3.18)		1.69 (0.12-3.26)
4 th quartile	4.50 (2.86-6.14)		4.59 (2.81-6.17)
Walkability			
1 st quartile	Reference		Reference
2 nd quartile	- 0.10 (- 1.61-1.41)		0.18 (- 1.34-1.70)
3 rd quartile	- 0.90 (- 2.44-0.63)		- 0.64 (- 2.20-0.91)
4 th quartile	1.44 (- 0.18-3.07)		1.70 (- 0.04-3.36)
Neighborhood level variables			
Social cohesion			
1 st quartile		Reference	Reference
2 nd quartile		0.55 (- 2.44-3.54)	- 0.02 (- 2.95-2.91)
3 rd quartile		2.81 (- 0.17-5.78)	1.45 (- 1.48-4.37)
4 th quartile		2.95 (- 0.43-6.33)	0.16 (- 3.20-3.52)
Social interaction			
1 st quartile		Reference	Reference
2 nd quartile		- 1.34 (- 4.21-1.53)	- 2.18 (- 4.99-0.62)
3 rd quartile		- 1.49 (- 4.27-1.30)	- 2.11 (- 4.85-0.62)
4 th quartile		- 2.07 (- 5.05-0.91)	- 3.42 (- 6.37-0.47)
Aesthetic quality			
1 st quartile		Reference	Reference
2 nd quartile		1.06 (0.64-1.21)	1.03 (0.64-1.16)
3 rd quartile		1.24 (1.15-1.67)	1.17 (1.08-1.47)
4 th quartile		2.76 (1.46-3.98)	2.38 (1.38-3.58)
Walkability			
1 st quartile		Reference	Reference
2 nd quartile		- 2.24 (- 5.26-0.78)	- 2.66 (- 5.62-0.29)
3 rd quartile		- 2.22 (- 5.29-0.84)	- 2.29 (- 5.31-0.73)
4 th quartile		- 1.30 (- 4.18-1.58)	- 2.29 (- 5.16-0.59)
Random effects			
Neighborhood-level variance (<i>SE</i>)	11.11 (3.11)	6.55 (2.23)	6.33 (2.10)
ICC (<i>SE</i>)	0.06 (0.02)	0.03 (0.01)	0.03 (0.01)
Model fit			
-2LL	21841.61	22060.48	21824.16
AIC	21887.61	22106.48	21894.16

-2LL: -2 Log Likelihood (smaller is better); AIC: Akaike information criterion (smaller is better); *Gender, age, marital status, educational attainment, self-reported chronic diseases, self-rated health, number of years in the neighborhood and leisure-time physical activity were adjusted in all models.

In Model 3, the individual- and neighborhood-level attributes of each neighborhood were entered simultaneously. After controlling for individual-level covariates, individual-level social cohesion, social interaction, and AQ were still positively correlated with SWB. However, the regression coefficients of individual-level social cohesion and social interaction in Model 3 were slightly lower than those in Model 2, and the regression coefficient of individual-level AQ was slightly higher than that in Model 2. For example, compared with

participants in the lowest quartile of social cohesion, the regression coefficients of participants in the second, third, and fourth quartiles were 2.31 (95% CI: 0.68-3.95), 2.87 (95% CI: 1.15-4.59), and 6.79 (95% CI: 5.24-8.33), respectively. Meanwhile, neighborhood-level AQ was also positively correlated with SWB; compared with participants in the lowest quartile, the regression coefficients of participants in the second, third, and fourth quartiles were 1.03 (95% CI: 0.64-1.16), 1.17 (95% CI: 1.08-1.47), and 2.38 (95% CI: 1.38-3.58), respectively.

4. Discussion

With the largest and most rapidly growing aging population in the world (41), China is undergoing a rapid transition from a rural to an urban society. The growth of the aging population coupled with rapid urbanization simultaneously presents challenges and opportunities for maintaining the well-being of elders in China (42). Because elders spend a greater proportion of their lives in their neighborhoods than younger adults, neighborhood environments are critical sources of support systems for elders, whose declining health may lead to frailty, social isolation, as well as limited mobility, financial strain, and/or limited access to transportation. Exploring the unique effects of neighborhood attributes on elders' well-being could be helpful to urban planners and public health officials in their efforts to build age-friendly neighborhoods and cities.

Accumulating evidence suggests that the physical and social attributes of the neighborhood play a role in the health of older individuals. However, research on the relationship between subjective well-being and individual perceptions of the neighborhood is limited (43). To our knowledge, this is the first study in China to simultaneously examine the effects of the perceptions of the social and physical attributes of one's neighborhood on well-being among older adults.

Neighborhood aesthetic quality has been shown to influence health behaviors such as physical activity (44,45) and fruit and vegetable consumption (46). Another study in Taiwan (47) found that high fruit and vegetable consumption combined with high LTPA could reduce the likelihood of developing new depressive symptoms among elders. Our study also found that high LTPA was associated with high SWB, which is consistent with previous studies (48,49). After accounting for demographic characteristics, years living in the neighborhood, physical activity, comorbidity, and self-reported health, we found that good perceived aesthetic quality of one's neighborhood was associated with high SWB, which is consistent with the finding of another study that the mental well-being of residents of deprived areas in Glasgow was higher when the respondents considered their neighborhood to have very good aesthetic qualities (50). Furthermore, we also found that high neighborhood-level aesthetic quality was associated with high SWB. These findings suggest that building aesthetic neighborhoods may promote better SWB among elders, which should be considered during urban planning and construction in China.

Our study also found that perceived social cohesion and social interaction were positively associated with SWB, which was consistent with our hypotheses and previous studies (16,18,51,52). Social cohesion and social interaction may influence elders' SWB in several

ways. First, social cohesion positively impacts the strength of relationships and social interaction as well as collective attachment to the neighborhood, and is thus expected to enhance individuals' well-being (53). Second, elders living in more cohesive communities may receive more instrumental and affective support (16), which are resources that can contribute to SWB (49,51). Third, neighborhood social cohesion and social interaction may promote physical activity among elders (45,54). Previous studies (48,55) and our study have found physical activity to be positively associated with SWB.

No neighborhood-level social attributes were found to be associated with elders' SWB in our study. Research has shown Chinese people to be more collectivistic (56) than Westerners, but social capital in China resides largely in families and other narrow circles of social relationships, which implies that people may only trust those who belong to the same in-group and may not participate social activities outside of their circles (57). When individual-level social interaction and social cohesion are aggregated to the neighborhood level, their effect on SWB may become diluted and less relevant. Hence, there was no relationship between neighborhood-level social interaction or social cohesion and SWB.

This study is not without limitations. First, the direction of causality could not be addressed due to the cross-sectional study design. Second, neighborhood attributes were measured by validated self-reported questionnaires (33) rather than independent neighborhood measures. However, prior research has found that perceptions of one's neighborhood are more strongly related to health than objective neighborhood measures (58). Finally, a large sample from 47 neighborhoods was used, but the study was conducted in only one administrative district of Shanghai, which may not be representative of the overall elderly population or other neighborhoods in China. Well-designed, multicenter prospective studies of the neighborhood correlates of SWB should be conducted in the future.

In conclusion, despite the aforementioned limitations, this study provides new findings on the relationships between the social and physical attributes of neighborhoods and SWB among the Chinese elderly. Building aesthetic and cohesive neighborhoods may facilitate the participation of Chinese elders in the social activities of their neighborhoods and thereby enhance their SWB.

Acknowledgements

The authors disclose receipt of the following source of financial support for the research, authorship, and/or publication of this article: The Major Program of the National Natural Science Foundation of China (Grant No. 71490735).

References

1. OECD. OECD Guidelines on Measuring Subjective Well-being. OECD Publishing, Paris, France, 2013. <http://dx.doi.org/10.1787/9789264191655-en> (accessed July 14, 2017).
2. Steptoe A, Deaton A, Stone AA. Subjective wellbeing, health, and ageing. *Lancet*. 2015; 385:640-648.
3. Wang X, Jia X, Zhu M, Chen J. Linking health states to subjective well-being: An empirical study of 5854 rural residents in China. *Public Health*. 2015; 129:655-666.
4. Stiglitz JE, Sen A, Fitoussi J-P. Report by the Commission on the Measurement of Economic Performance and Social Progress. <http://www.uit.no/studier/emner/sv/ekonomi/ECON4270/h09/Report%20in%20English.pdf> (accessed July 10, 2017).
5. Lorenc T, Clayton S, Neary D, Whitehead M, Petticrew M, Thomson H, Cummins S, Sowden A, Renton A. Crime, fear of crime, environment, and mental health and wellbeing: Mapping review of theories and causal pathways. *Health Place*. 2012; 18:757-765.
6. Nguyen-Viet H, Zinsstag J, Schertenleib R, Zurbrugg C, Obrist B, Montangero A, Surkinkul N, Kone D, Morel A, Cisse G, Koottatep T, Bonfoh B, Tanner M. Improving environmental sanitation, health, and well-being: A conceptual framework for integral interventions. *Ecohealth*. 2009; 6:180-191.
7. Wang P, Vanderweele TJ. Empirical research on factors related to the subjective well-being of Chinese urban residents. *Soc Indic Res*. 2011; 101:447-459.
8. Elliott J, Gale CR, Parsons S, Kuh D; HALCYON Study Team. Neighbourhood cohesion and mental wellbeing among older adults: A mixed methods approach. *Soc Sci Med*. 2014; 107:44-51.
9. Green J, Jones A, Roberts H. More than A to B: The role of free bus travel for the mobility and wellbeing of older citizens in London. *Ageing Soc*. 2014; 34:472-494.
10. Mitchell RJ, Richardson EA, Shortt NK, Pearce JR. Neighborhood environments and socioeconomic inequalities in mental well-being. *Am J Prev Med*. 2015; 49:80-84.
11. Marselle MR, Irvine KN, Lorenzo-Arribas A, Warber SL. Moving beyond green: Exploring the relationship of environment type and indicators of perceived environmental quality on emotional well-being following group walks. *Int J Environ Res Public Health*. 2014; 12:106-130.
12. Schieman S, Meersman SC. Neighborhood problems and health among older adults: Received and donated social support and the sense of mastery as effect modifiers. *J Gerontol B Psychol Sci Soc Sci*. 2004; 59:S89-S97.
13. Brown SC, Mason CA, Spokane AR, Cruza-Guet MC, Lopez B, Szapocznik J. The relationship of neighborhood climate to perceived social support and mental health in older Hispanic immigrants in Miami, Florida. *J Aging Health*. 2009; 21:431-459.
14. Young AF, Russell A, Powers JR. The sense of belonging to a neighbourhood: Can it be measured and is it related to health and well being in older women? *Soc Sci Med*. 2004; 59:2627-2637.
15. Gale CR, Dennison EM, Cooper C, Sayer AA. Neighbourhood environment and positive mental health in older people: The Hertfordshire Cohort Study. *Health Place*. 2011; 17:867-874.
16. Cramm JM, van Dijk HM, Nieboer AP. The importance of neighborhood social cohesion and social capital for the well being of older adults in the community. *Gerontologist*. 2013; 53:142-152.
17. Toma A, Hamer M, Shankar A. Associations between neighborhood perceptions and mental well-being among older adults. *Health Place*. 2015; 34:46-53.
18. Cramm JM, Nieboer AP. Social cohesion and belonging predict the well-being of community-dwelling older people. *BMC geriatrics*. 2015; 15:30.
19. Alfonzo MA. To walk or not to walk? The hierarchy of walking needs. *Environment & Behavior*. 2005; 37:808-836.
20. Dannenberg AL, Howard F, Jackson RJ. Making Healthy Places: Designing and Building for Health, Well-being, and Sustainability. Island Press, Washington, USA, 2011.
21. Leyden KM. Social capital and the built environment: The importance of walkable neighborhoods. *Am J Public Health*. 2003; 93:1546-1551.
22. Lund H. Testing the claims of new urbanism: Local access, pedestrian travel, and neighboring behaviors. *J Am Plann Assoc*. 2003; 69:414-429.
23. Rogers S, Halstead J, Gardner K, Carlson C. Examining walkability and social capital as indicators of quality of life at the municipal and neighborhood scales. *Applied Research in Quality of Life*. 2011; 6:201-213.
24. Smyth R, Nielsen I, Zhai Q. Personal well-being in urban China. *Soc Indic Res*. 2010; 95:231-251.
25. Wang P, Vanderweele TJ. Empirical research on factors related to the subjective well-being of Chinese urban residents. *Soc Indic Res*. 2011; 101:447-459.
26. Hsu HC, Chang WC, Chong YS, An JS. Happiness and social determinants across age cohorts in Taiwan. *J Health Psychol*. 2016; 21:1828-1839.
27. Deng J, Hu J, Wu W, Dong B, Wu H. Subjective well-being, social support, and age-related functioning among the very old in China. *Int J Geriatr Psychiatry*. 2010; 25:697-703.
28. Mak WW, Cheung RY, Law LS. Sense of community in Hong Kong: Relations with community-level characteristics and residents' well-being. *Am J Community Psychol*. 2009; 44:80-92.
29. Smyth R. Economic openness and subjective well-being in China. *China & World Economy*. 2010; 18:22-40.
30. Smyth R, Mishra V, Qian X. The environment and well-being in urban China. *Ecological Economics*. 2008; 68:547-555.
31. Gao J, Fu H, Li J, Jia Y. Association between social and built environments and leisure-time physical activity among Chinese older adults—a multilevel analysis. *BMC public health*. 2015; 15:1317.
32. International Wellbeing Group. Personal Wellbeing Index-Adult (Cantonese). The Australian Centre on Quality of Life, Deakin University, Australia, 2006. <http://www.deakin.edu.au/research/acqol/instruments/wellbeing-index.htm> (accessed July 10, 2017).
33. Mujahid MS, Diez Roux AV, Morenoff JD, Raghunathan T. Assessing the measurement properties of neighborhood scales: From psychometrics to ecometrics. *Am J Epidemiol*. 2007; 165:858-867.
34. Sampson RJ, Raudenbush SW, Earls F. Neighborhoods and violent crime: A multilevel study of collective efficacy. *Science*. 1997; 277:918-924.
35. Wen M, Hawkley LC, Cacioppo JT. Objective and perceived neighborhood environment, individual SES and psychosocial factors, and self-rated health: An analysis of

- older adults in Cook County, Illinois. *Soc Sci Med.* 2006; 63:2575-2590.
36. Iecovich E, Cwikel J. The relationship between well-being and self-rated Health among middle-aged and older women in israel. *Clinical Gerontologist.* 2010; 33:255-269.
 37. Macfarlane D, Chan A, Cerin E. Examining the validity and reliability of the Chinese version of the International Physical Activity Questionnaire, long form (IPAQ-LC). *Public Health Nutr.* 2011; 14:443-450.
 38. Branco JC, Jansen K, Oses JP, de Mattos Souza LD, da Silva Alves Gdel G, Lara DR, da Silva RA. Practice of leisure-time physical activities and episodes of mood alteration amongst men and women. *J Affect Disord.* 2014; 169:165-169.
 39. Nelson ME, Rejeski WJ, Blair SN, Duncan PW, Judge JO, King AC, Macera CA, Castaneda-Sceppa C, American College of Sports M, American Heart A. Physical activity and public health in older adults: Recommendation from the American College of Sports Medicine and the American Heart Association. *Circulation.* 2007; 116:1094-1105.
 40. Wang J, Xie H, Jiang F. *Multilevel models: Methods and applications.* Hiher Education Press, Beijing, China, 2008. (in Chinese).
 41. WHO. Good health adds life to years Global brief for World Health Day 2012. WHO Publisher, Geneva, 2012.
 42. Zhu YG, Ioannidis JP, Li H, Jones KC, Martin FL. Understanding and harnessing the health effects of rapid urbanization in China. *Environ Sci Technol.* 2011; 45:5099-5104.
 43. Toma A, Hamer M, Shankar A. Associations between neighborhood perceptions and mental well-being among older adults. *Health Place.* 2015; 34:46-53.
 44. Ball K, Bauman A, Leslie E, Owen N. Perceived environmental aesthetics and convenience and company are associated with walking for exercise among Australian adults. *Prev Med.* 2001; 33:434-440.
 45. Cerin E, Lee KY, Barnett A, Sit CH, Cheung MC, Chan WM. Objectively-measured neighborhood environments and leisure-time physical activity in Chinese urban elders. *Prev Med.* 2013; 56:86-89.
 46. Litt JS, Soobader MJ, Turbin MS, Hale JW, Buchenau M, Marshall JA. The influence of social involvement, neighborhood aesthetics, and community garden participation on fruit and vegetable consumption. *Am J Public Health.* 2011; 101:1466-1473.
 47. Chi SH, Wang JY, Tsai AC. Combined association of leisure-time physical activity and fruit and vegetable consumption with depressive symptoms in older Taiwanese: Results of a national cohort study. *Geriatr Gerontol Int.* 2016; 16:244-251.
 48. Fox K, Stathi A, McKenna J, Davis M. Physical activity and mental well-being in older people participating in the better ageing project. *Eur J Appl Physiol.* 2007; 100:591-602.
 49. McAuley E, Blissmer B, Marquez DX, Jerome GJ, Kramer AF, Katula J. Social relations, physical activity, and well-being in older adults. *Preventive medicine.* 2000; 31:608-617.
 50. Bond L, Kearns A, Mason P, Tannahill C, Egan M, Whitley E. Exploring the relationships between housing, neighbourhoods and mental wellbeing for residents of deprived areas. *BMC public health.* 2012; 12:48.
 51. Lee GR, Ishii-Kuntz M. Social interaction, loneliness, and emotional well-being among the elderly. *Res Aging.* 1987; 9:459-482.
 52. Nezlek JB, Richardson DS, Green LR, Schatten-Jones EC. Psychological well-being and day-to-day social interaction among older adults. *Personal Relationships.* 2002; 9:57-71.
 53. Sampson RJ. Local friendship ties and community attachment in mass society: A multilevel systemic model. *American Sociological Review.* 1988; 53:766-779.
 54. Mendes de Leon CF, Cagney KA, Bienias JL, Barnes LL, Skarupski KA, Scherr PA, Evans DA. Neighborhood social cohesion and disorder in relation to walking in community-dwelling older adults: A multilevel analysis. *J Aging Health.* 2009; 21:155-171.
 55. Mcauley E, Rudolph D. Physical activity, aging, and psychological well-being. *J Aging Phys Act.* 1995; 3:67-96.
 56. Oyserman D, Coon HM, Kimmelmeier M. Rethinking individualism and collectivism: Evaluation of theoretical assumptions and meta-analyses. *Psychol Bull.* 2002; 128:3-72.
 57. Allik J, Realo A. Individualism-collectivism and social capital. *J Cross Cult Psychol.* 2004; 35:29-49.
 58. Weden MM, Carpiano RM, Robert SA. Subjective and objective neighborhood characteristics and adult health. *Soc Sci Med.* 2008; 66:1256-1270.
- (Received July 26, 2017; Revised September 21, 2017; Accepted October 1, 2017)

Price adjustment for traditional Chinese medicine procedures: Based on a standardized value parity model

Haiyin Wang^{1,2}, Chunlin Jin^{2,*}, Qingwu Jiang^{1,*}

¹ School of Public Health, Fudan University, Shanghai, China;

² Shanghai Health Development Research Center (Shanghai Medical Information Center), Shanghai, China.

Summary

Traditional Chinese medicine (TCM) is an important part of China's medical system. Due to the prolonged low price of TCM procedures and the lack of an effective mechanism for dynamic price adjustment, the development of TCM has markedly lagged behind Western medicine. The World Health Organization (WHO) has emphasized the need to enhance the development of alternative and traditional medicine when creating national health care systems. The establishment of scientific and appropriate mechanisms to adjust the price of medical procedures in TCM is crucial to promoting the development of TCM. This study has examined incorporating value indicators and data on basic manpower expended, time spent, technical difficulty, and the degree of risk in the latest standards for the price of medical procedures in China, and this study also offers a price adjustment model with the relative price ratio as a key index. This study examined 144 TCM procedures and found that prices of TCM procedures were mainly based on the value of medical care provided; on average, medical care provided accounted for 89% of the price. Current price levels were generally low and the current price accounted for 56% of the standardized value of a procedure, on average. Current price levels accounted for a markedly lower standardized value of acupuncture, moxibustion, special treatment with TCM, and comprehensive TCM procedures. This study selected a total of 79 procedures and adjusted them by priority. The relationship between the price of TCM procedures and the suggested price was significantly optimized ($p < 0.01$). This study suggests that adjustment of the price of medical procedures based on a standardized value parity model is a scientific and suitable method of price adjustment that can serve as a reference for other provinces and municipalities in China and other countries and regions that mainly have fee-for-service (FFS) medical care.

Keywords: Traditional Chinese medicine (TCM), prices of medical procedures, standardized value parity model, mechanism of price adjustment

1. Introduction

Traditional Chinese medicine (TCM) has gradually developed and advanced into a system of medical

theories through long-standing medical practices. TCM is an important part of the medical system of China (1). TCM plays an important role in the control of infectious diseases and chronic diseases and it is widely used to treat cerebrovascular disease, bone, joint and muscle diseases, multiple sclerosis, and other conditions (2,3). Due to the prolonged low price of TCM procedures and the lack of an effective mechanism of dynamic price adjustment (4-6), traditional calculation of costs did not reflect the value of TCM care and other factors, causing the development of TCM to lag markedly behind Western medicine. In 2014, the World Health Organization (WHO) formulated the *WHO Traditional Medicine Strategy: 2014-2023*;

Released online in J-STAGE as advance publication October 24, 2017.

*Address correspondence to:

Dr. Qingwu Jiang, School of Public Health, Fudan University, 130 Dong'an Road, Shanghai, China.

E-mail: jiangqw@fudan.edu.cn

Dr. Chunlin Jin, Shanghai Health Development Research Center, Shanghai Medical Information Center, 1477 Beijing Road (west), Shanghai, China.

E-mail: jinchunlin@shdrc.org

World Health Assembly resolution WHA62.13 on traditional medicine emphasized that the Member States should actively formulate policies and implement an action plan to enhance the role of alternative and traditional medicine in maintaining public health (7). At the Chinese Sanitation and Health Conference in 2015, Chinese President Xi Jinping pointed out that "sustained prevention is needed first; that traditional Chinese medicine and Western medicine should both be emphasized, and that health should be integrated into all policies". In 2016, the State Council of China issued *Guidelines on Developing Traditional Chinese Medicine from 2016-2030* (8). *The Law of the People's Republic of China on Traditional Chinese Medicine* was enacted that same year (9); it clearly sought to develop TCM and it represented a major breakthrough in legislation on TCM.

In the context of this reform, establishing a scientific and appropriate mechanism for adjustment and management of the prices of TCM procedures in order to promote changes in the ways in which prices of TCM procedures are adjusted and managed is crucial to guiding the development of TCM. In 2012, the National Development and Reform Commission, the National Health and Family Planning Commission of the People's Republic of China, the State Administration of Traditional Chinese Medicine issued the *Manual on National Standards for the Prices of Medical Procedures (2012 Edition)* (denoted here as the *2012 Manual on the Prices of Medical Procedures*). The *2012 Manual on the Prices of Medical Procedures* required provinces and municipalities to organize and standardize prices of medical procedures and to apply new standards for prices of medical procedures (10,11). Shanghai has the highest best concentration of medical resources in China. Fees for medical procedures and their management are consistent with most provinces and municipalities in China. Shanghai is able to lead and influence the country in terms of adjusting the prices of TCM procedures. Therefore, the current study has used Shanghai, China as an example. Based on the *2012 Manual on the Prices of Medical Procedures*, this study has attempted to create a value parity model for the price of TCM procedures in order to provide evidence for creation of a mechanism of price management that accord with the characteristics of TCM practices and the characteristics of the value of TCM procedures.

2. Materials and Methods

2.1. Sources of data and creation of a database

Data in this study came from the *2012 Manual on the Prices of Medical Procedures* (12), and the *Compilation of Medical Procedures and Prices at Medical Facilities in Shanghai (2014)* (denoted here as the *Shanghai Compilation of Medical Procedures and Prices*) (13).

Variables obtained from the *2012 Manual on the Prices of Medical Procedures* included the name of the procedure, what the procedure entailed, the unit of pricing, basic manpower expended and time spent, technical difficulty (referring to the relative degree of difficulty entailed in a given procedure through a combination of factors such as the degree of complexity, the degree of skill involved, and requirements for practitioners; difficulty was rated from 1-100), and the degree of risk (referring to a comprehensive assessment of the probability of complications and the severity of adverse outcomes as well as the degree of relative risk of a given procedure; risk was rated from 1-100). Variables obtained from the *Shanghai Compilation of Medical Procedures and Prices* included the name of the procedure, what the procedure entailed, and the unit of pricing. Based on what the procedure entailed and the unit of pricing, procedures in the *2012 Manual on the Prices of Medical Procedures* were matched with procedures in the *Shanghai Compilation of Medical Procedures and Prices*. A database of corresponding procedures (referring to matching TCM procedures in the *Shanghai Compilation of Medical Procedures and Prices* and *2012 Manual on the Prices of Medical Procedures* in terms of what the procedure entailed and the unit of pricing) was created.

2.2. Determining indices for analysis and creation of a standardized value parity model

Indices used to calculate the value of procedures included basic allocation of medical personnel (physicians, nurses, medical technicians, and other personnel), the duration of the basic procedure (minutes), the technical difficulty score, the risk score, the annual salary of medical personnel at different hospitals, and the proportion of different types of medical personnel.

The standardized value referred to the measured value of a procedure in terms of resources consumed in a normal flow and under normal conditions. The standardized value had two components: medical care provided and the cost of resources consumed (14). The standardized value of medical care provided was mainly based on determination of the basic manpower expended and time spent while also considering technical difficulty and risk. The standardized value of medical care provided involved: i) calculation of all salary parameters based on the *Shanghai Reform Plan for Salary Systems at Public Health Facilities*. A physician's salary was calculated as 3.2 RMB per minute; the salary ratio for a physician:nurse:medical technician:other personnel was 1:0.7:0.6:0.5; and ii) calculation of a model:

$$Y = \sum_{i=1}^n \frac{X_i}{\text{mos.} \cdot \text{days} \cdot \text{hrs worked}} (K_i \cdot T \cdot L_i) * \left(1 + L_g \frac{\text{technical difficulty of a procedure} \cdot \text{technical risk}}{\text{technical difficulty of a standard procedure} \cdot \text{technical risk}} \right)$$

In the above formula, X_i is the target salary of a hospital physician; K_i is the number of medical personnel

allocated; T is the duration of the procedure; L_i is the type and position of personnel. Data on the basic manpower expended, the duration of the procedure, technical difficulty, and risk were from the *2012 Manual on the Prices of Medical Procedures*. Months, days, and hours worked were determined according to the *Regulations on Public Holidays for National Annual Festivals and Memorial Days* (State Council Decree No. 513).

The cost of direct materials consumed was calculated using Activity-based Costing. The cost of resources was apportioned to medical procedures based on the resources consumed while primarily providing medical care. Medical products used and medical care provided was ultimately used to apportion costs to medical procedures. Cost data were collected from 5 pilot hospitals in Shanghai (15). The cost of direct materials consumed did not include separate charges for consumables, energy consumption, and premises, and it did not include expenses for administration and logistics, expenditure of financial subsidies, or depreciation of fixed assets and amortization of intangible assets.

The current price and standardized value of a TCM procedure were used to calculate the relative price ratio of the current price to the standardized value. The relative price ratio was obtained by dividing the current price ratio by the standardized value. The difference in price levels and the relative price ratio were used to comprehensively assess and select procedures for price adjustment.

$$\text{Relative price ratio} = \frac{\text{current price/average current price}}{\text{standardized value/average standardized value}}$$

2.3. Selection of procedures for price adjustment and the suggested price

The principle for selection of procedures for price adjustment was: *i*) a relative price ratio < 0.5 and *ii*) a current price lower than the standardized value. The formula for calculation of the suggested adjusted price was: adjusted price = the current price + (standardized value - current price) × α . A preliminary study noted a large gap between the standard value and the current price. Directly assuming the standardized value would have considerably impacted the price. In accordance with a partial adjustment strategy and budget constraints, the gap between the standardized value and the current price served as the range of price adjustment. Based on stepwise adjustment of coefficient α , α was set at 0.3. In theory, a distribution of the current price that was closed to the distribution of the standardized value would result in a symmetrical distribution with the relative price ratio tending to be 1 and less dispersion.

2.4. Statistical analysis

Frequency and proportion were used to describe the

number of corresponding procedures in the *Shanghai Compilation of Medical Procedures and Prices* and the *2012 Manual on the Prices of Medical Procedures* and the number of parameter adjustments. The mean difference and the relative ratio were used to compare the current price and standardized value. A ladder function was used to obtain the square root of the relative price ratio of the current price and the suggested adjusted price. A kernel density curve (kdensity) was fitted to the plotted probability distribution of the relative price ratio. A paired *t*-test was used to compare differences in the distribution of the relative price ratio of the current price to the suggested adjusted price. $p < 0.05$ was considered to indicate a significant difference. The interquartile range was used to describe changes in the dispersion of the relative price ratio. Analysis was performed using the software Stata 10.0.

3. Results

3.1. Basic information

One hundred and forty-four procedures (45% of all TCM procedures) in the *2012 Manual on the Prices of Medical Procedures and the Shanghai Compilation of Medical Procedures and Prices* matched (for specific procedures, see Supplemental Table S1, <http://www.biosciencetrends.com/action/getSupplementalData.php?ID=14>). Corresponding procedures were categorized into a total of seven categories: topical treatment with TCM, TCM for orthopedic injuries, acupuncture and moxibustion, massage therapy, anorectal treatment with TCM, special treatment with TCM, and comprehensive TCM. Seventy-nine percent of TCM procedures for orthopedic injuries matched, 66% of the forms of massage therapy matched, and 46% of the forms of topic treatment with TCM matched (Table 1).

3.2. Comparison of the current price and standardized value

The standardized value of TCM procedures in a given category mainly consisted of the standardized value of medical care provided. The standardized value of medical care provided accounted for 89% of the standardized value of a TCM procedure, on average. Direct materials consumed accounted for relatively high proportion (80%) of the standardized value of anorectal treatment with TCM. Medical care provided accounted for more than 85% of the standardized value of other procedures. Medical care provided accounted for almost all (97%) of the value of acupuncture and moxibustion (Table 2).

The current price level of TCM procedures tended to be low. The current price represented 56% of the standardized value. The current price of acupuncture

Table 1. Corresponding categories in the Shanghai Compilation of Medical Procedures and Prices and the 2012 Manual on the Prices of Medical Procedures*

Procedure Category	Number of Procedures in the 2012 Manual on the Prices of Medical Procedures (procedures)	Number of Corresponding Procedures **(procedures)	Percentage (%)
Topical Treatment with Traditional Chinese Medicine	35	16	45.7
Traditional Chinese Medicine for Orthopedic Injuries	70	55	78.6
Acupuncture and Moxibustion	70	19	27.1
Naprapathy	67	44	65.7
Anorectal Treatment with Traditional Chinese Medicine	41	3	7.3
Special Therapy with Traditional Chinese Medicine	20	6	30.0
Comprehensive TCM	19	1	5.3
Total	322	144	44.7

*The Shanghai Compilation of Medical Procedures and Prices refers to the Compilation of Medical Procedures and Prices at Medical Facilities in Shanghai (2014). The 2012 Manual on the Prices of Medical Procedures refers to the Manual on National Standards for the Prices of Medical Procedures (2012 Edition). **The Number of Corresponding Procedures refers to corresponding procedures in the Shanghai Compilation of Medical Procedures and Prices and the 2012 Manual on the Prices of Medical Procedures.

Table 2. The current price and standardized value of corresponding procedures in seven major categories of TCM procedures in the Shanghai Compilation of Medical Procedures and Prices and the 2012 Manual on the Prices of Medical Procedures

Procedure Category	Current Price*	Standardized Value**	Standardized Value of Medical Care Provided (%)	Cost of Direct Materials Consumed (%)
Acupuncture and Moxibustion	24	142	138 (97)	5 (3)
Anorectal Treatment with Traditional Chinese Medicine	120	696	137 (20)	559 (80)
Traditional Chinese Medicine for Orthopedic Injuries	98	521	484 (93)	38 (7)
Special Therapy with Traditional Chinese Medicine	6	102	98 (96)	4 (4)
Massage Therapy with Traditional Chinese Medicine	48	58	51 (88)	7 (12)
Topical Treatment with Traditional Chinese Medicine	39	191	180 (94)	11 (6)
Comprehensive TCM	3	54	51 (94)	3 (6)
Total	62	276	246 (89)	30 (11)

*The Current Price is the price of the procedure in the Shanghai Compilation of Medical Procedures and Prices and the current price charged by public hospitals. **The Standardized Value is the sum of the Standardized Value of Medical Care Provided and the Cost of Direct Materials Consumed. Figures are the average for each procedure in each category. Specific procedures and the method of calculation are shown in Supplementary Table S1.

Table 3. Comparison of the current price and standardized value of corresponding procedures in seven major categories of TCM procedures in the Shanghai Compilation of Medical Procedures and Prices and the 2012 Manual on the Prices of Medical Procedures

Procedure Category	Sample Size	Current Price*		Standardized Value**	
		Median	Interquartile Range	Median	Interquartile Range
Acupuncture and Moxibustion	19	10	5	67	25
Anorectal Treatment with Traditional Chinese Medicine	3	100	140	751	270
Traditional Chinese Medicine for Orthopedic Injuries	55	100	90	512	471
Special Therapy with Traditional Chinese Medicine	6	6	1	96	192
Massage Therapy with Traditional Chinese Medicine	44	50	15	52	7.5
Topical Treatment with Traditional Chinese Medicine	16	11	24	63	87
Comprehensive TCM	1	2.5	0	52	0
Total	144	52.5	80	94.5	371

*The Current Price is the price of the procedure in the Shanghai Compilation of Medical Procedures and Prices and the current price charged by public hospitals. **The Standardized Value is the sum of the Standardized Value of Medical Care Provided and the Cost of Direct Materials Consumed. Figures are the average for each procedure in each category. Specific procedures and the method of calculation are shown in Supplementary Table S1.

and moxibustion, special treatment with TCM, TCM for orthopedic injuries, and comprehensive TCM procedures was markedly low. The lowest current price level represented only 3% of the standardized value. Closed reduction and percutaneous internal fixation of a tubular bone fracture required three physicians and one nurse, the procedure took 50 minutes, the technical

difficulty score was 70 and the risk score was 58, and the coefficient to adjust for technical difficulty and risk was 0.8. The standardized value of the procedure was 1,205 RMB while the current price was only 150 RMB, so the current price represented for 12% of the standardized value. Acupuncture in the neck required one physician, it took 20 minutes, the technical

difficulty score was 53 and the risk score was 40, and the coefficient to adjust for technical difficulty and risk was 0.7. The standardized value of the procedure was 77 RMB while the current price was only 20 RMB, so current price represented 26% of the standardized value. "Nourishing" therapy required one physician and one nurse, it took 30 minutes, the technical difficulty score was 77 and the risk score was 40, and the coefficient to adjust for technical difficulty and risk was 0.7. The standardized value of the procedure was 201 RMB while the current price was only 6 RMB, so the current price represented only 3% of the standardized value. The current price of massage therapy with TCM was basically the same as its standardized value (*i.e.* the current price represented 96% of the standardized value) (Table 2 and Table 3). Massage therapy for a headache required one physician, it took 15 minutes, the technical difficulty score was 38 and the risk score was 14, and the coefficient to adjust for technical difficulty and risk was 0.4. The standardized value of the procedure was 51 RMB while the current price was only 55 RMB, so the current price was 8% higher than the standardized value (for specific procedures and the method of calculation, see Supplemental Table S1, <http://www.biosciencetrends.com/action/getSupplementalData.php?ID=14>).

3.3. Selection of procedures for price adjustment and the suggested price

Seventy-nine procedures (55% of all corresponding procedures) were performed less often (accounting for less than 0.5 of procedures) and those procedures had a low average price level. Many of the selected procedures involved TCM for orthopedic injuries (50.6%), acupuncture and moxibustion (20.2%), or topical treatment with TCM (17.7%). The average ratio for selected procedures was 0.27. Few of the selected procedures involved comprehensive TCM, special treatment with TCM, or acupuncture and moxibustion (the lowest proportion was 0.08). The suggested price increase was an average of 234%. The lowest increase was for massage therapy with TCM (an increase of 79%) while the highest increase was for special treatment with TCM (an increase of 713%) (Table 4). The current price of manipulative reduction of a distal radius and ulna joint dislocation was 24 RMB while its standardized value was 601 RMB; the price difference was 577 RMB. The suggested price increase was 173 RMB (30% of the difference). The suggested price was 197 RMB, representing a 721% increase. The current price of wound debridement with TCM (an especially large wound) was 192 RMB while its standardized value was 1330 RMB; the price difference was 1138 RMB. The suggested increase was 341 RMB (30% of the difference). The suggested price was 533 RMB, an increase of 178%. The current price of "thunder-fire" moxibustion was 15 RMB

Table 4. Selection of procedures by priority, suggested increases, and the adjusted relative price ratio

Procedure Category	Number (proportion in %)	Mean Current Price*	Mean Ratio of the Current Price**	Mean Standardized Value#	Mean Ratio of the Standardized Value##	Mean Relative Price Ratio*	Suggested Increase (%)	Mean Adjusted Relative Price Ratio
Acupuncture and Moxibustion	16 (20.2)	16	0.29	160	1.7	0.24	215	0.68
Anorectal Treatment with Traditional Chinese Medicine	3 (3.8)	120	2.26	696	7.4	0.31	189	0.72
Traditional Chinese Medicine for Orthopedic Injuries	40 (50.6)	94	1.77	614	6.53	0.27	228	0.69
Special Therapy with Traditional Chinese Medicine	4 (5.1)	6	0.11	149	1.58	0.08	713	0.57
Massage Therapy with Traditional Chinese Medicine	1 (1.3)	55	1.04	200	2.13	0.49	79	0.85
Topical Treatment with Traditional Chinese Medicine	14 (17.7)	34	0.64	191	2.03	0.34	132	0.74
Comprehensive TCM	1 (1.3)	3	0.05	54	0.57	0.08	618	0.57
Total	79 (100)	62	1.17	414	4.41	0.27	234	0.69

*The Mean Current Price is the mean current price of procedures by priority from among 7 major categories of corresponding procedures in traditional Chinese medicine. Current price data are from the *Shanghai Compilation of Medical Procedures and Price*. **The Mean Ratio of the Current Price is the ratio of the current price of each selected procedure to the mean current price; this index is a relative ratio. ##The Mean Standardized Value is the mean standardized value of a selected procedure from among corresponding procedures. The standardized value is the sum of the standardized value of medical care provided and the cost of direct materials consumed. ###The Mean Ratio of the Standardized Value is the ratio of the standardized value of the selected procedure to the mean standardized value; this index is a relative ratio. ####The Mean Relative Price Ratio is the mean ratio of the current price divided by the mean ratio of standardized value. A value less than 1 indicates that the current price is low; this ratio is an index of the price relationship. Figures are the average for each category. Specific procedures and the method of calculation are shown in Supplementary Table S1. The Suggested Increase (%) is the rate of increase (%) in the suggested price relative to the current price. The method of calculation for specific procedures and the suggested price are shown in Supplementary Table S2. The Mean Adjusted Relative Price Ratio is the mean relative price ratio of each procedure based on the suggested price. The relative price ratio based on the suggested price for a specific procedure is shown in Supplementary Table S3.

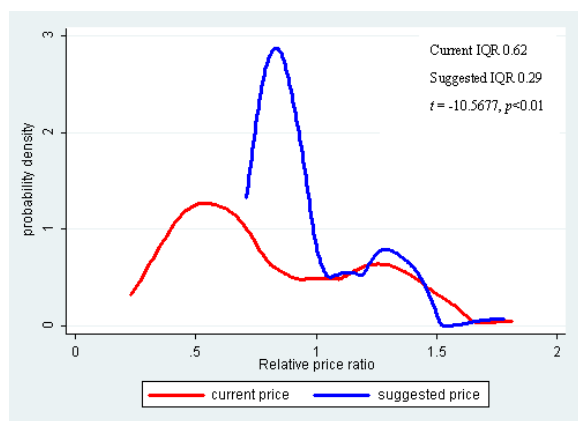


Figure 1. Current price and changes in the relative price ratio based on the suggested price. Changes in the relative price ratio of the current price to the suggested price indicated that the relative price ratio of the current price was concentrated at 0.5 and 1.4 and that the relative price ratio of the suggested price tended to be concentrated at 1, *i.e.* at 0.7 and 1.4. The interquartile range decreased from 0.62 to 0.29. Changes in the relative price ratio differed significantly ($t = -10.5677$, $p < 0.01$).

while its standardized value was 112 RMB; the price difference was 97 RMB. The suggested increase was 29 RMB (30% of the difference). The suggested price was 44 RMB, an increase of 194% (specific procedures and the method of calculation are shown in Supplemental Table S2, <http://www.biosciencetrends.com/action/getSupplementalData.php?ID=14>).

3.4. Relationship between prices of procedures before and after adjustment

In accordance with adjustment to the suggested price, the distribution of the price parity between procedures tended to be concentrated at 1. The distribution of the relative price ratio differed significantly ($t = -10.5677$, $p < 0.01$) between the current price and the suggested adjusted price. After data were converted, the relative price ratio of the current price was mainly concentrated at 0.5 to 1.4 and the suggested adjusted price was concentrated at 0.8 to 1.4. There was less dispersion of the suggested adjusted price. The adjusted interquartile range was 0.29 and the current price was 0.62 (Figure 1). The relative price ratio was 0.27 of the current price and the recommended adjusted price was 0.69. The relative price ratio changed markedly for integrated traditional Chinese and Western medicine (from 0.08 to 0.57), special treatment with TCM (from 0.08 to 0.57), and acupuncture and moxibustion (from 0.24 to 0.68) (Table 4). The relative price ratio of manipulative reduction of a distal radius and ulna joint dislocation changed from 0.07 to 0.56, the relative price ratio of massage therapy for a cervical facet joint disorder changed from 1.39 to 1.34, and the relative price ratio of "nourishing" therapy changed from 0.05 to 0.55 (see Supplemental Table S3 for specific items, <http://www.biosciencetrends.com/action/getSupplementalData.php?ID=14>).

4. Discussion

Over the past few years, remuneration of public hospitals for medical care has changed as public hospitals in China have gradually been reformed (16-18). Remuneration has changed from three avenues - service charges, additional income from pharmaceuticals, and government subsidies - to two avenues - service fees and government subsidies (19). Government financing currently accounts for around 9% of the income of public hospitals, and pharmaceuticals account for a large proportion (45%) of hospital income (20). In 2011, public hospitals lost 55.2 billion RMB, and losses from medical procedures were directly related to the low pricing of medical procedures (21). A domestic study found that the prices of medical procedures at 288 medical facilities in 30 provinces and cities were not adjusted at fixed intervals or were adjusted at intervals longer than two years (89%) (5). Public TCM hospitals are the main providers of TCM care. Due to the small number of TCM procedures, low pricing, and prolonged lack of price adjustment, TCM hospitals have gradually adopted Western medicine instead, and the development of TCM practices is seriously lagging. A key issue that China needs to urgently address is the gradual increase in the proportion of income that TCM hospitals are receiving from laboratory diagnostic testing and surgery as the use of TCM procedures and the proportion of income they represent are gradually decreasing (22,23).

The current results indicated that the value of a TCM procedure is mainly the medical care provided. The value of medical care provided represents 97% of the value of acupuncture and moxibustion, 88% of the value of massage therapy with TCM, and 94% of the value of integrated traditional Chinese and Western medicine. The results were consistent with the characteristics of TCM practices. Calculating the current cost does not properly reflect the value of care provided by medical personnel, and calculations deviate widely from the value of TCM procedures (24,25). The current study found that the current price does not fully reflect the value of medical care provided. The average price of special therapy with TCM was 6 RMB while the value of direct materials consumed was 4 RMB and the standardized value of medical care provided was 98 RMB. The current price mainly reflects the value of materials consumed without fully taking into account the value of medical care provided. The current price of "thunder-fire" moxibustion was 15 RMB while its standardized value was 112 RMB. The cost of direct materials consumed was 11 RMB and the value of medical care provided was 101 RMB (the procedure requires 1 physician, it takes 30 minutes, and the technical difficulty score is 46 and the risk score is 24). Pricing of procedures mainly considers the price of supplies but not the value of medical care provided. China's current system of provincial pricing of medical procedures is based on a single price. There is

no distinction between the components of the value of a procedure, such as medical care provided and materials consumed. The current study analyzed the value of medical care provided and the cost of direct materials consumed, and it devised a method of adjusting the prices of medical procedures based on a standardized value parity model. The United States and other countries use a pricing theory based on relative units (26,27). A relative value unit (RVU) is assigned to the three components of medical services - work, practice expense, and professional liability insurance - resulting in work RVUs, practice expense RVUs, and professional liability insurance RVUs. The current study is the first to classify components of domestic prices, producing a system with two types of values: the value of medical care provided and the value of materials consumed. Since domestic medical liability insurance is in its initial stages and that liability insurance is not yet a major component of the value system, medical liability insurance was not included in the standardized value of a procedure in this study.

The current study found a large gap between the current price and the standardized value of TCM procedures; the current price was significantly lower. The value of acupuncture and moxibustion was 6.7 times its current price, the value of anorectal treatment with TCM was 7.5 times its current price, the value of TCM for orthopedic injuries was 51 times its current price, and the value of integrated traditional Chinese and Western medicine was 20 times its current price. Closed reduction and percutaneous internal fixation of a tubular bone fracture requires 3 physicians and 1 nurse, it takes 50 minutes, and the technical difficulty score is 70 and the risk score is 58. In accordance with revised salary levels in Shanghai, the standardized value of that procedure was 1,205 RMB but its current price was 150 RMB (*i.e.* 8 times the current price). A study of TCM in Shandong Province, China found that the prices of acupuncture and comprehensive TCM procedures at medical facilities were lower than the cost of those procedures. Municipal hospitals recovered 32% of the cost of moxibustion and 35% of the cost of topical treatment with TCM; township hospitals recovered only 7% of the cost of comprehensive TCM (28). Determination of the cost of TCM procedures in Chongqing indicated that charges for TCM were generally low, and this was especially true for surgery and treatment with TCM (29). Costs were 2-5 times the current price. Calculations of the standardized value in the current study were similar to the results of previous studies.

Through stepwise adjustments, the current study gradually gained insight into price parity. Based on the labor theory of value and drawing on the values and factors used in the resource-based relative value scale (RBRVS) and the concept of standard clinical pathways, this study quickly determined the value of procedures in terms of the medical care provided. That

value was combined with data on price factors in the 2012 *Manual on the Prices of Medical Procedures* and data on salary reform by provinces and cities. This study also focused on the relationship between the value of marginal resources invested in medical procedures and rational prices based on Ramsey's theory of pricing (30). The current study created a model of price adjustment based on a ratio. Theoretically, if the current price of a procedure is close to parity with its standardized value, then the ratio will mainly have a symmetrical distribution concentrated at 1. If the ratio is far below 1, then the pricing is markedly lower. Data based on the relative price ratio can be used to select procedures by priority and correct the price relationship. This study found that the current price parity was not reasonable. The current price of TCM with packets of herbs (small) was 6 RMB while its standardized value was 35 RMB. The current price ratio was 0.11, the standardized value ratio was 0.37, and the relative price ratio was 0.3. The current price of massage therapy for lumbar muscle strain was 50 RMB while its standardized value was 61 RMB. The current price ratio was 0.94, the standardized value ratio was 0.65, and the relative price ratio was 1.45.

Based on selection criteria, this study identified a total of 79 procedures that need price adjustment first. The main categories of those procedures were TCM for orthopedic injuries, topical treatment with TCM, and acupuncture and moxibustion. Consistent with the results of a preliminary study, the current study found a large gap between the current price and standardized value. Directly adjusting the current price to the standardized value could result in massive price fluctuations. The current price of wound debridement with TCM (an especially large wound) was 192 RMB while its standardized value was 1,330 RMB; the absolute price increase would be 1,138 RMB (590%) if the current price is changed to the standardized value. The current price of manipulative reduction of an ankle fracture and dislocation was 156 RMB while its standardized value was 1,208 RMB; the absolute price increase would be 1,052 RMB (670%) if the current price was changed to the standardized value. Therefore, this study suggested that the gap between the current price and the standardized value represents a range. Given a coefficient for relative adjustment, the price could be gradually adjusted to a target standardized value. As mentioned above, the adjusted price for wound debridement with TCM (an especially large wound) would be 533 RMB (an increase of 178%) and the adjusted price for manipulative reduction of an ankle fracture and dislocation would be 471 RMB (an increase of 201%). The suggested price of special treatment with TCM and topical treatment with TCM increased significantly (713% for special treatment and 618% for topical treatment), and this is related to their significantly lower current price. The price of "nourishing" therapy changed from 6 RMB to 65 RMB; its standardized

value was 201 RMB. The price increase would be 59 RMB, representing an increase of 975%. The price of a manmade decoction changed from 2.5 RMB to 18 RMB; its standardized value was 54 RMB. The price increase would be 15.5 RMB, representing an increase of 618%. The increase was substantial since the current price was markedly low. However, the absolute value of the suggested adjusted price was within the acceptable range, which is not unusual, and there is some leeway to reach the target value. Therefore, the price suggested in this study was reasonable. In terms of the price relationship based on the suggested price, the distribution of the relative price ratio tends to be 1, representing an increase from 0.27 to 0.69, and the dispersion decreases from 0.62 to 0.29. The distribution of the relative price ratio coincided with marked optimization, suggesting that the mechanism of selecting certain procedures for price adjustment mechanism and the suggested price were reasonable and feasible. Therefore, other areas can refer to this model, in conjunction with local parameters for calculation and selection, to adjust the price of medical procedures in a stepwise manner.

The current study had two limitations: *i*) this study used data parameters from the *2012 Manual on the Prices of Medical Procedures* and it did not fully create a database of procedure parameters from the *Shanghai Compilation of Medical Procedures and Prices* and *ii*) the standardized value was mainly combined with the characteristics of TCM and it measured the value of medical care provided and the value of direct materials consumed. However, material costs were not comprehensively calculated. These two aspects may have biased the results, so these aspects need to be studied further and improved in future research.

In summary, the current study matched data from the *2012 Manual on the Prices of Medical Procedures and the Shanghai Compilation of Medical Procedures and Prices* and this study created a database for calculation of the value of 144 TCM procedures. Based on the standardized value parity model, 79 procedures were selected for initial price adjustment. On average, the suggested price increase was 234%. Price parity between TCM procedures was significantly optimized at the suggested price ($p < 0.01$). The current results indicated that a strategy for adjustment of the distribution of the price ratio in a standardized value parity model is a scientific and suitable approach. Other regions should refer to the model in order to devise their own system of value and to gradually create a mechanism of dynamic price adjustment.

Acknowledgements

This work was supported by a grant from the City of Shanghai for Evidence-based Public Health Care and Health Economics (15GWZK0901), a grant from the United States China Medical Foundation for the second

round of cooperative projects to transform health care research and policymaking (Establishing a Network to Transform Chinese Health Care Policy (CMB-CP 14-190), and a grant for Creation of a System to Support Health Care Decision-making based on Big Data in Shanghai (GWIV-33). The authors wish to thank Rong Yan, Wei Wang, Gong Li, and Yuanfeng He for their expert advice.

References

1. Xu Q, Bauer R, Hendry BM, Fan TP, Zhao Z, Duez P, Simmonds MS, Witt CM, Lu A, Robinson N, Guo DA, Hylands PJ. The quest for modernisation of traditional Chinese medicine. *BMC Complement Altern Med*. 2013; 13:132.
2. Zhu AS, Chen ZH, Pei YP, Yang GL. Review and discussion of a strategy to develop a basic theory of traditional Chinese medicine. *China Journal of Traditional Chinese Medicine and Pharmacy*. 2016; 7:2467-2471. (in Chinese)
3. Zhang Q, Zhu L, Wim Van der L. The importance of traditional Chinese medicine services in health care provision in China. *Universitas Forum*. 2011; 2:1-8.
4. Liu Y, Jiang LJ, Wang LJ, Ma Y, Xu AJ. Current status of and thoughts on the prices of traditional Chinese medicine procedures. *Chinese Health Economics*. 2017; 36:63-65. (in Chinese)
5. Xu T, Qi W, Huang XC, Chen X, Cao LQ. Study on the mechanism of dynamic adjustment of the prices of medical procedures. *Chinese Health Economics*. 2017; 36:67-69. (in Chinese)
6. Ma Y, Xu AJ. Review of the prices of Chinese medical procedures. *Prices Monthly*. 2017; 03:36-40. (in Chinese)
7. World Health Organization. WHO Traditional Medicine Strategy: 2014-2023. <http://www.who.int/medicines/areas/traditional/en/index.html> (accessed June 14, 2017).
8. The State Council of China. Guideline on Developing Traditional Chinese Medicine from 2016-2030. http://www.gov.cn/zhengce/content/2016-02/26/content_5046678.htm (accessed June 15, 2017). (in Chinese)
9. The National People's Congress (NPC) Standing Committee of China. The Law on Traditional Chinese Medicine 2016. http://news.xinhuanet.com/english/2016-12/25/c_135931387.htm (accessed June 16, 2017). (in Chinese)
10. Zheng GL, Zhang Y, Yang YS, Xiao MX, Chen LJ. Analysis of TCM procedures in the 2012 National Medical Fee Schedule. *Chinese Health Service Management*. 2014; 4:269-270, 93. (in Chinese)
11. Zou LA. Analysis of policy characteristics of the National Standards for the Prices of Medical Procedures (2012 Edition). *Chinese Health Economics*. 2013; 32:71-73. (in Chinese)
12. The National Development and Reform Commission, National Health and Family Planning Commission, the State Administration of Traditional Medicine of China. Notice on management of the prices of specified medical procedures and related issues. http://www.ndrc.gov.cn/rdzt/2012xxgkgz/jgsfxxgk/201205/t20120510_499420.html (accessed August 1, 2017). (in Chinese)
13. Shanghai Municipal Health and Family Planning

- Commission. Compilation of Medical Procedures and Prices at Medical Facilities in Shanghai. <http://www.wsjsw.gov.cn/wsj/n473/n1978/index.html> (accessed August 1, 2017). (in Chinese)
14. Wang HY, Jin CL, Wang W, Gong L, He YF, Peng Y. Development of a system to compare the prices of medical procedures in Shanghai. Chinese Journal of Hospital Administration. 2015; 31:635-638. (in Chinese)
 15. Peng Y, Li X, Wang HY, Yang ZH, Huang LP, Jin CL. Analysis of calculations of the cost of medical procedures at 5 pilot hospitals in Shanghai. Chinese Hospital Management. 2017; 37:5-9. (in Chinese)
 16. Li L, Fu H. China's health care system reform: Progress and prospects. Int J Health Plann Manage. 2017; 32:240-253.
 17. Blumenthal D, Hsiao W. Lessons from the East – China's rapidly evolving health care system. N Engl J Med. 2015; 372:1281-1285.
 18. Barber SL, Borowitz M, Bekedam H, Ma J. The hospital of the future in China: China's reform of public hospitals and trends from industrialized countries. Health Policy Plan. 2014; 29:367-378.
 19. Liu GG, Vortherms SA, Hong X. China's health reform update. Annu Rev Public Health. 2017; 38:431-448.
 20. Ministry of Health of the People's Republic of China. Public hospital income and expenditures (4-4-1). In: 2013 China Health Statistics Yearbook. Peking Union Medical College Press, Beijing, China, 2013; pp.121-24. (in Chinese)
 21. Tan J, Xiang Q. Analysis of the income and expenditures and budget surpluses at public hospitals in China. Chinese Health Economics. 2014; 33:78-79. (in Chinese)
 22. Shen JJ, Wang Y, Lin F, Lu J, Moseley CB, Sun M, Hao M. Trends of increase in western medical services in traditional medicine hospitals in China. BMC Health Serv Res. 2011; 11:212.
 23. Wang L, Suo S, Li J, Hu Y, Li P, Wang Y, Hu H. An investigation into traditional Chinese medicine hospitals in China: Development trend and medical procedures innovation. Int J Health Policy Manag. 2017; 6:19-25.
 24. Dou L, Yin AT, Liu YX, Liu Q. Study on calculation of the costs of traditional Chinese medical procedures and specific features of methods of calculation. Chinese Health Economics. 2012; 31:76-78. (in Chinese)
 25. Long YX. Creation and empirical study of a model of price adjustment for traditional Chinese medicine procedures in Hubei Province. Journal Hubei University of Chinese Medicine, Wuhan, China, 2016; pp.21-36. (in Chinese)
 26. Baadh A, Peterkin Y, Wegener M, Flug J, Katz D, Hoffmann JC. The relative value unit: History, current use, and controversies. Curr Probl Diagn Radiol. 2016; 45:128-132.
 27. Baltic, S. Pricing Medicare services: Insiders reveal how it's done. Managed Healthcare Executive. 2013. High Beam Research. <https://www.highbeam.com/doc/1P3-3127446971.html> (accessed August 1, 2017).
 28. Dou L, Liu Q, Yin AT, Liu YX. Analysis of the status of profits and losses from traditional Chinese medicine procedures and reasons for losses. Chinese Health Economics. 2012; 31:82-84. (in Chinese)
 29. Huang Y, Duan XK. Study on calculation of fees for and costs of traditional Chinese medicine procedures in Chongqing. Chinese Health Resources. 2015; 18:266-267. (in Chinese)
 30. Cui L. Study of price regulations for Chinese medical procedures: An analysis based on the Ramsey Pricing method. Chinese Health Economics. 2015; 34:49-51. (in Chinese)
- (Received July 31, 2017; Revised September 13, 2017; Accepted October 1, 2017)

A comparative study on predicting influenza outbreaks

Jie Zhang*, Kazumitsu Nawata

Graduate School of Engineering, University of Tokyo, Tokyo, Japan.

Summary

Worldwide, influenza is estimated to result in approximately 3 to 5 million annual cases of severe illness and approximately 250,000 to 500,000 deaths. We need an accurate time-series model to predict the number of influenza patients. Although time-series models with different time lags as feature spaces could lead to varied accuracy, past studies simply adopted a time lag in their models without comparing or selecting an appropriate number of time lags. We investigated the performance of adopting 6 different time lags in 6 different models: Auto-Regressive Integrated Moving Average (ARIMA), Support Vector Regression (SVR), Random Forest (RF), Gradient Boosting (GB), Artificial Neural Network (ANN), and Long Short Term Memory (LSTM) with hyperparameter adjustment. To the best of our knowledge, this is the first time that LSTM has been used to predict influenza outbreaks. As a result, we found that the time lag of 52 weeks led to the lowest Mean Absolute Percentage Error (MAPE) in the ARIMA, ANN and LSTM, while the machine learning models (SVR, RF, GB) achieved the lowest MAPEs with a time lag of 4 weeks. We also found that the MAPEs of the machine learning models were less than ARIMA, and the MAPEs of the deep learning models (ANN, LSTM) were less than those of the machine learning models. In all the models, the LSTM model of 4 layers reached the lowest MAPE of 5.4%, and the LSTM model of 5 layers with regularization reached the lowest root mean squared error (RMSE) of 0.00210.

Keywords: Time series, Influenza-Like Illness, time lag, Long Short Term Memory (LSTM)

1. Introduction

Influenza, commonly known as flu, is a contagious respiratory illness caused by influenza viruses (1,2). Influenza virus spreads through air from coughs or sneezes as well as by touching surfaces contaminated with influenza virus and then touching mouths or eyes (3,4). The strong infectivity and annual outbreak of flu are estimated to result in approximately 3 to 5 million annual cases of severe illness and approximately 250,000 to 500,000 deaths worldwide (1). The resultant high levels of worker/school absenteeism and productivity losses lead to direct costs of lost productivity and associated medical treatment and indirect costs of preventative measures. In the U.S., flu is responsible

for a total cost of over \$10 billion per year, and a future flu pandemic is estimated to cost hundreds of billions of dollars in direct and indirect costs (5). Clinics and hospitals are overwhelmed during peak illness periods. The impeding of transmission routes, especially via school closures, and influenza immunizations effectively prevent the propagation of the flu (6-8). To help governments, hospitals, clinics, pharmaceutical companies, and others prepare for flu outbreaks efficiently and restrict routes of transmission in a timely manner, we need an accurate time-series model to predict influenza outbreaks.

Time-series models can be categorized into 3 types by using different features. The first type of model is an autoregressive model, which uses the numbers of patients in the past as features ("Xs") and forecasts the number of patients in the future as the response (y). Typical examples include the Auto-Regressive Integrated Moving Average (ARIMA) model and the Vector Auto-Regression model (VAR). The second type of model uses other parameters (such as temperature, humidity, etc.) instead of past flu data as features for regression models (e.g., linear regression, random forest, etc.). The famous

Released online in J-STAGE as advance publication October 24, 2017.

*Address correspondence to:

Jie Zhang, Department of Technology Management for Innovations, Graduate School of Engineering, University of Tokyo, 7-3-1, Hongo, Bunkyo-ku Tokyo, 113-8656, Japan.
E-mail: jie-zhang@g.ecc.u-tokyo.ac.jp

example is "Google Flu Trends", which used search engine query data (9) as features and a linear regression model. The third type of model is a combination of the first and second types. It uses the numbers of flu patients in the past as features (as in the first type) and regression models (as in the second type) (10). In this study, we adopted the third model type and tried 6 different models with hyperparameter adjustments, including: Auto-Regressive Integrated Moving Average (ARIMA), Support Vector Regression (SVR), Random Forest (RF), Gradient Boosting (GB), Artificial Neural Network (ANN), and Long Short Term Memory (LSTM). To the best of our knowledge, this is the first time LSTM has been used to predict influenza outbreaks.

Time-series models with different time lags usually result in different levels of accuracy. The selection of time lags can be essential to improve the accuracy of predications. However, past studies simply adopted a time lag for models without comparing or selecting an appropriate number of time lags, which could make the model misunderstand past outbreak patterns. Therefore, in this study, we investigated the performance of 6 different time lags in each of the models we tried: 2 weeks (approximately 0.5 month), 4 weeks (approximately 1 month), 9 weeks (approximately 2 months), 13 weeks (approximately 3 months), 26 weeks (approximately 6 months), and 52 weeks (approximately 12 months). We hoped we would find some clues from our studies for future studies, which leverage machine learning (ML) and deep learning (DL) models for predicting epidemic outbreaks.

2. Methodology

2.1. Data

We collected the U.S. flu season data from the "FluView" Portal of the website for the Centers for Disease Control and Prevention (CDC) (11). The data are posted "weekly" with "not available" (N/A) values from the 21st week to the 39th week from 1998, 1999, 2000, 2001, and 2002. Therefore, we only used the U.S. Flu Season Data without any N/As, *i.e.* the U.S. Flu Season Data from the 40th week of 2002 to the 30th week of 2017.

To remove any possible variations in populations, we adopted the Influenza-Like Illness (ILI) rates as the response (y) of our models.

$$\text{ILI rate} = \frac{\text{The number of ILI}}{\text{Total number of Illness}}$$

Figure 1(a) illustrates the raw data. The Y-axis represents the weekly ILI rate, and the X-axis represents the time series. The seasonality appears obvious, except in 2009 when swine flu occurred. The swine flu (also called the 2009 flu pandemic) was an influenza pandemic, and the

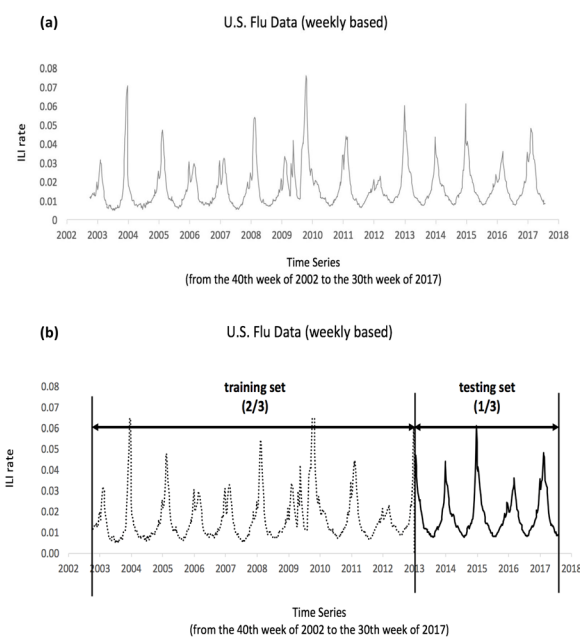


Figure 1. The U.S. flu season data from the 40th week of 2002 to the 30th week of 2017. (a). The Y-axis represents the weekly ILI rate, and the X-axis represents the time series. **(b).** The dashed line is the first 2/3 used for the training set, and the solid line is the last 1/3 used for the testing set. The Y-axis represents the weekly ILI rate, and the X-axis represents the time series.

second of two pandemics involving the H1N1 influenza virus (the first was the 1918 flu pandemic), albeit a new variety.

We split the data into two parts: the first 2/3 was the training set and the last 1/3 was the testing set, as shown in Figure 1(b).

2.2. Models

Table 1 illustrates the models, programming languages, libraries, and hyperparameter adjustments we used in this study.

We trained the ARIMA model in R Programming Language (version 3.4.1) and the "forecast" package (version 8.1) (12). The function of "auto.arima" in the "forecast" package of R automatically performs a stepwise regression and selects the best hyperparameters based on the Bayesian Inference Criteria (BIC). For SVR, we applied the caret package (Version 6.0-76) in R. For RF and GB, we used Python (Version 3.6.0) and the Scikit-Learn package (Version 0.18.1) with a grid search. For ANN and LSTM, we used Python and the Keras package (Version 2.0.4) based on Tensorflow (Version 1.1.0) and adopted an "early-stopping" algorithm with a "patience" of 100 epochs (for a total of 1000 epochs).

2.3. Metrics

We compared different models and different time lags using the Mean Absolute Percentage Error (MAPE) and

Table 1. The models, programming languages, libraries, and hyperparameter adjustments we used in this study

Models	Programming Languages	Programming Libraries	Hyperparameter Adjustment
ARIMA	R (Version 3.4.1)	Forecast (Version 8.1)	<ul style="list-style-type: none"> ● auto.arima
SVR	R (Version 3.4.1)	Caret (Version 6.0-76)	<ul style="list-style-type: none"> ● cross validation ($n = 3$)
RF	Python (Version 3.6.0)	Scikit Learn (Version 0.18.1)	<ul style="list-style-type: none"> ● cross validation ($n = 3$) ● grid search <ul style="list-style-type: none"> ● n_estimators ● max_features ● max_depth
GB	Python (Version 3.6.0)	Scikit Learn (Version 0.18.1)	<ul style="list-style-type: none"> ● cross validation ($n = 3$) ● grid search <ul style="list-style-type: none"> ● learning rate ● subsample ● n_estimators ● max_features ● max_depth
ANN	Python (Version 3.6.0)	Keras (Version 2.0.4) Tensorflow (Version 1.1.0)	<ul style="list-style-type: none"> ● different layers (up to 5 layers) ● with/without dropout, ● with/without regularization ● with/without batch normalization
LSTM	Python (Version 3.6.0)	Keras (Version 2.0.4) Tensorflow (Version 1.1.0)	<ul style="list-style-type: none"> ● different layers (up to 10 layers) ● with/without dropout, ● with/without regularization ● with/without batch normalization

Root Mean Squared Error (RMSE) as Key Performance Indicators (KPIs).

$$\text{MAPE} = \frac{1}{n} \sum_{t=1}^n \left| \frac{F_t - A_t}{A_t} \right| * 100\%$$

$$\text{RMSE} = \sqrt{\frac{1}{n} \sum_{t=1}^n (F_t - A_t)^2}$$

where A_t is the actual value and F_t is the forecasted value.

Figure 2 illustrates the histogram of the weekly ILI rates of the U.S. flu data. In our opinion, comparing models using MAPEs reflects the difference based on the median, and comparing models using RMSE is based on means. In this study, the histogram is right skewed. Furthermore, we performed the Kolmogorov-Smirnov Test to examine the data distribution, and the p -value is < 0.001 . Therefore, we concluded that the distribution is a non-normal distribution, and we therefore regard the MAPE as the first KPI and the RMSE as an assistant KPI in this study.

2.4. Feature space

2.4.1. Time lags

Influenza seasonality is an annually recurring time period characterized by the prevalence of outbreaks of influenza. Therefore, in this study, we reviewed a maximum of 52 weeks (approximately 1 year). We tried using time lags of 2 weeks (around half a month), 4 weeks (approximately 1 month), 9 weeks

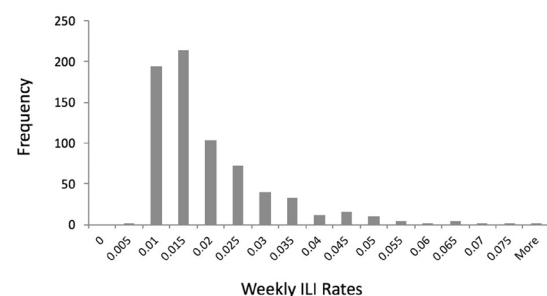
Histogram of Weekly ILI Rates

Figure 2. The histogram of weekly ILI Rates from U.S. flu data. The histogram is right skewed. Furthermore, we performed the Kolmogorov-Smirnov Test to examine the data distribution. The p -value is < 0.001 , and we therefore concluded that the distribution is a non-normal distribution.

(approximately 2 months), 13 weeks (approximately 3 months), 26 weeks (around half a year), and 52 weeks (approximately 1 year) for model training and compared the results.

2.4.2. First-order differences

Some previous studies found that first-order differences helped improve the results of the prediction models for influenza data (13). We also included the first-order differences as a part of the feature spaces.

In this study, we reviewed a maximum of 52 weeks. In the case of the time lag of 52 weeks, we used (I) the ILI rate of the current week, (II) the ILI rates of the past 52 weeks, and (III) the 52 first-order differences. In total,

Table 2. In the case of the time lag of 52 weeks, in all, we have 105 predictors (I + II + III) for use as feature spaces: (I) the ILI rate of the current week, (II) the ILI rates of the past 52 weeks, and (III) the 52 first-order differences. We dropped the first 52 rows (the first 52 weeks), since we are unable to calculate the first-order differences for the first 52 rows (the first 52 weeks). We also dropped the last row (the last week), since the source data ends at the 30th week of 2017, and we have no data for the 31st week in 2017 and therefore cannot calculate the MAPE or RMSE

		Feature space, <i>i.e.</i> Xs									
		Response, <i>i.e.</i> , "y"			Current data & historic data			First-order difference			
Year	Week	Monday of week (Year/Month/Date)	ILI rates (1 week previous)	ILI rates (this week)	ILI rates (1 week ago)	ILI rates (2 weeks ago)	ILI rates (52 weeks ago)	(This week) (1 week ago)	(This week) (2 weeks ago)	...	(This week) (52 weeks ago)
2002	40	2002/09/30	0.0122	0.0117	N/A	N/A	N/A	N/A	N/A	...	N/A
2002	41	2002/10/07	0.0113	0.0122	0.0117	N/A	N/A	0.000	N/A	...	N/A
2002	42	2002/10/14	0.0125	0.0113	0.0122	0.0117	N/A	-0.001	0.000	...	N/A
...	39
2003	40	2003/09/29	0.0096	0.0075	0.0064	0.0064	N/A	0.001	0.001
2003	41	2003/10/06	0.0104	0.0096	0.0075	0.0064	0.0117	0.002	0.003	...	N/A
2003	41	2003/10/06	0.0105	0.0104	0.0096	0.0075	0.0122	0.001	0.003	...	-0.0021
...	29
2017	29	2017/07/17	0.0088	0.0085	0.0084	0.0104	0.0084	0.000	-0.002	...	0.0000
2017	30	2017/07/24	N/A	0.0088	0.0085	0.0084	0.0083	0.000	0.000	...	0.0004

we have 105 predictors (I + II + III) for use as feature spaces. Since we are unable to calculate the first-order differences for the first 52 rows (the first 52 weeks), we dropped these data. Table 2 illustrates the pretreatment of the source data.

In the case of the time lag of 52 weeks, we had 105 predictors and had to drop the first 52 rows (the first 52 weeks), since we are unable to calculate the first-order differences for the first 52 rows (the first 52 weeks). Similarly, in the case of the time lag of 2, 4, 9, 13, 26 weeks, we had 5, 9, 19, 27, 53 predictors and had to dropped the first 2, 4, 9, 13, 26 rows (the first 2, 4, 9, 13, 26 weeks) since we are unable to calculate the first-order differences for the first 2, 4, 9, 13, 26 rows (the first 2, 4, 9, 13, 26 weeks). As a result, the models with fewer time lags could have more training data, which was considered unfair when we compared the predicting accuracy of the models since models (especially DL models) with more training data usually brought better accuracy (14). To fairly compare the predicting accuracy of adopting different time lags, we uniformly removed the first 52 rows (the first 52 weeks) from the training set of all the models.

3. Results

3.1. ARIMA, SVR, RF, GB, and ANN

Table 3(a) and Table 3(b) present the MAPE and RMSE of ARIMA, SVR, RF, GB, ANN. When increasing the time lags in the ARIMA models, we found obvious decreases in the MAPE and RMSE. We achieved the lowest MAPE (8.36%) and the lowest RMSE (0.00364) when using the time lag of 52 weeks, and we found a similar phenomenon when performing the ANN models, where we achieved the lowest MAPE (5.79%) and the lowest RMSE (0.002411) when using the time lag of 52 weeks. Regarding the ML models (*i.e.*, SVR, RF, and GB), all of them reached their lowest MAPE (6.75%, 6.75%, 6.58%, respectively) when we used the time lag of 4 weeks. The SVR reached the lowest RMSE (0.002271) when we used the time lag of 52 weeks. The RF reached the lowest RMSE (0.002417) when we used the time lag of 2 weeks. The GB reached the lowest RMSE (0.002351) when we used the time lag of 4 weeks. The cells with the gray background in Table 3(a) are the lowest MAPEs in the ARIMA, SVR, RF, GB, and ANN models, while the cells with the gray background in Table 3(b) are the lowest RMSEs in the ARIMA, SVR, RF, GB, and ANN models.

Figure 3(a), 3(b), 3(c), 3(d), and 3(e) compares the actual and the predicted outcomes when we used the time lag of 52 weeks in ARIMA, the time lag of 4 weeks in SVR, the time lag of 4 weeks in RF, the time lag of 4 weeks in GB, and the time lag of 52 weeks in ANN. All the time lags we adopted in Figure 3 achieved the lowest MAPE in the respective model.

Table 3(a). The MAPEs of the testing set for ARIMA, SVR, RF, GB, and ANN. When performing the ARIMA models, we achieved the lowest MAPE (8.36%) when using the time lag of 52 weeks. We achieved the lowest MAPE (6.75%, 6.75%, and 6.58%) of all the ML models when we used the time lag of 4 weeks. When performing the ANN models, we achieved the lowest MAPE (5.79%) when using the time lag of 52 weeks. The cells with the gray background are the lowest MAPEs in the ARIMA, SVR, RF, GB, and ANN models

	Time lags (Weeks)	2	4	9	13	26	52
Models	ARIMA MAPE (%)	13.46	11.90	9.14	8.72	8.58	8.36
	SVR MAPE (%)	6.76	6.75	6.99	6.90	6.85	6.86
	RF MAPE (%)	7.36	6.75	6.95	7.82	7.07	6.92
	GB MAPE (%)	6.96	6.58	7.24	6.92	7.67	7.02
	ANN MAPE (%)	6.65	6.50	6.32	6.34	6.16	5.79

Table 3(b). The RMSEs of the testing set for ARIMA, SVR, RF, GB, ANN. The ARIMA reached the lowest RMSE (0.003285) when we used the time lag of 13 weeks. The SVR reached the lowest RMSE (0.002271) when we used the time lag of 2 weeks. The RF reached the lowest RMSE (0.002417) when we used the time lag of 4 weeks. The GB reached the lowest RMSE (0.002351) when we used the time lag of 4 weeks. The ANN reached the lowest RMSE (0.002411) when we used the time lag of 4 weeks. The cells with the gray background are the lowest RMSEs in the ARIMA, SVR, RF, GB, and ANN models

	Time lags (Weeks)	2	4	9	13	26	52
Models	ARIMA RMSE	0.004437	0.004099	0.003665	0.003285	0.003428	0.003642
	SVR RMSE	0.002558	0.002554	0.002536	0.002526	0.002514	0.002271
	RF RMSE	0.002417	0.002522	0.002582	0.002692	0.002554	0.002591
	GB RMSE	0.002378	0.002351	0.002652	0.002586	0.002732	0.002511
	ANN RMSE	0.002590	0.002552	0.002574	0.002549	0.002516	0.002411

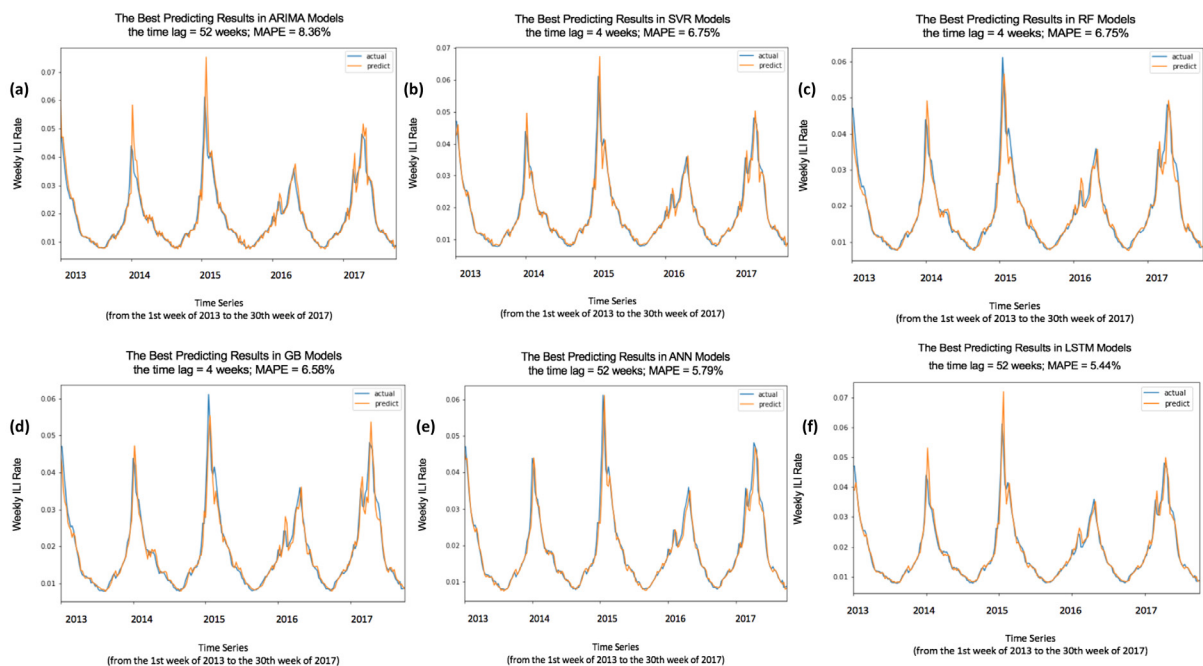


Figure 3. The actual and the predicted outcomes when we use the time lag of 52 weeks in ARIMA, the time lag of 4 weeks in SVR, the time lag of 4 weeks in RF, the time lag of 4 weeks in GB, the time lag of 52 weeks in ANN, and the time lag of 52 weeks in the LSTM model (4 layers). All the time lags we adopted achieved the lowest MAPE in ARIMA, SVR, RF, GB, and ANN, respectively. The X-axis represents the time series (from the 1st week of 2013 to the 30th week of 2017) of the testing set. The Y-axis represents the weekly ILI rates.

3.2. LSTM results

We performed a variety of LSTM models: 3 layers, 4 layers, 4 layers with dropout, 4 layers with regularization, 5 layers, 5 layers with regularization, 6 layers with regularization, and 10 layers with regularization. Table

4(a) and Table 4(b) present the MAPEs and RMSEs of all the LSTM models with different hyperparameters, as previously mentioned. All the LSTM models achieved the lowest MAPEs (6.71%, 5.44%, 6.27%, 5.45%, 6.28%, 5.53%, 5.46%, and 5.72%) when we adopted a time lag of 52 weeks. The cells with the gray background are

Table 4(a). The MAPEs of all the LSTM models: 3 layers, 4 layers, 4 layers with dropout, 4 layers with regularization, 5 layers, 5 layers with regularization, 6 layers with regularization, and 10 layers with regularization. All the LSTM models achieved the lowest MAPEs (6.71%, 5.44%, 6.27%, 5.45%, 6.28%, 5.53%, 5.46%, and 5.72%) when we adopted a time lag of 52 weeks. The cells with the gray background are the lowest MAPEs in the different LSTM models

Time lags	2	4	9	13	26	52	Mean MAPE of Different LSTM Structures
3 layers MAPE (%)	6.80	7.00	7.00	6.87	6.93	6.71	6.89
4 layers MAPE (%)	6.69	6.42	6.28	6.17	6.06	5.44	6.18
LSTM Structures 4 layers with dropout MAPE (%)	7.62	7.17	7.26	7.18	6.56	6.27	7.01
4 layers with regularization MAPE (%)	6.74	6.32	6.22	6.09	6.07	5.45	6.15
5 layers MAPE (%)	6.85	6.61	7.20	6.64	6.53	6.28	6.69
5 layers with regularization MAPE (%)	6.56	6.38	6.11	6.01	5.91	5.53	6.08
6 layers with regularization MAPE (%)	6.61	6.52	6.20	6.12	5.91	5.46	6.14
10 layers with regularization MAPE (%)	6.46	6.42	5.98	5.90	5.75	5.72	6.04
Mean MAPE of Different Time Lags MAPE (%)	6.79	6.61	6.53	6.37	6.22	5.86	

Table 4(b). The RMSEs of all the LSTM models: 3 layers, 4 layers, 4 layers with dropout, 4 layers with regularization, 5 layers, 5 layers with regularization, 6 layers with regularization, and 10 layers with regularization. All the LSTM models achieved the lowest MAPEs when we adopted a time lag of 52 weeks, except for the 4 layers with regularization and 5 layers with regularization, which reached their lowest MAPEs when we used a time lag of 13 weeks. The cells with the gray background are the lowest RMSEs (0.002102, 0.002431, 0.002352, 0.002499, 0.002099, 0.002439, 0.002438, 0.002274) in the different LSTM models

Time lags	2	4	9	13	26	52	Mean MAPE of Different LSTM Structures
3 layers RMSE	0.002534	0.002535	0.002497	0.002490	0.002411	0.002102	0.002428
4 layers RMSE	0.002611	0.002581	0.002570	0.002572	0.002516	0.002431	0.002547
LSTM Structures 4 layers with dropout RMSE	0.002528	0.002517	0.002518	0.002499	0.002462	0.002352	0.002479
4 layers with regularization RMSE	0.002621	0.002563	0.002505	0.002499	0.002632	0.002559	0.002563
5 layers RMSE	0.002504	0.002486	0.002458	0.002434	0.002408	0.002099	0.002398
5 layers with regularization RMSE	0.002663	0.002549	0.002556	0.002439	0.002590	0.002566	0.002560
6 layers with regularization RMSE	0.002593	0.002561	0.002503	0.002479	0.002521	0.002438	0.002516
10 layers with regularization RMSE	0.002460	0.002390	0.002312	0.002325	0.002296	0.002274	0.002343
Mean MAPE of Different Time Lags	0.002564	0.002523	0.002490	0.002467	0.002480	0.002353	

the lowest MAPEs in the different LSTM models. All the LSTM models achieved the lowest MAPEs when we adopted a time lag of 52 weeks, except the 4 layers with regularization and the 5 layers with regularization, which reached their lowest MAPEs when we used a time lag of 13 weeks. The cells with the gray background are the lowest RMSEs (0.002102, 0.002431, 0.002352, 0.002499, 0.002099, 0.002439, 0.002438, and 0.002274) in the different LSTM models.

Figure 3(f) compares the actual and the predicted outcomes when we used the time lag of 52 weeks in the LSTM model (4 layers). The X-axis represents the time series (from the 1st week of 2013 to the 30th week of 2017) of the testing set. The Y-axis represents the weekly ILI rates

4. Discussion

4.1. Time lag selection in ARIMA, SVR, RF, GB, and ANN

The MAPEs of the ARIMA model decreased significantly (from 13.46% to 8.36%) when we increased the time lags from 2 weeks to 52 weeks. (Figure 4) The probable explanation for this phenomenon is that ARIMA is an autoregressive model focusing on seasonality. The

closer the feature spaces to a complete seasonality, the lower the MAPE will be. In other words, when training ARIMAs for time-series prediction, at the least, we need a complete duration. Similar to those of the ARIMA models, the MAPEs of the ANN models also decreased (from 13.46% to 8.36%) when we increased the time lag from 2 weeks to 52 weeks. (Figure 4)

Regarding the ML models (SVR, RF, and GB), the MAPEs were always approximately 7%, with almost no changes as we increased the time lags (Figure 4), likely because the ML models usually cannot learn the seasonality but can learn the trend of the data by inputting the first-order differences into the training and testing.

4.2. With and without regularization

We calculated the standard deviations of the MAPEs of the LSTM models of 3, 4, and 5 layers without regularization and of 4, 5, 6, and 10 layers with regularization when using the time lags of 2, 4, 9, 13, 26, and 52 weeks. (Table 5) We found the standard deviations of the MAPEs of the LSTM models with regularization were less than those of the LSTM models without regularization when we used almost all the time lags except the time lag of 2 weeks. (Figure 5a) The

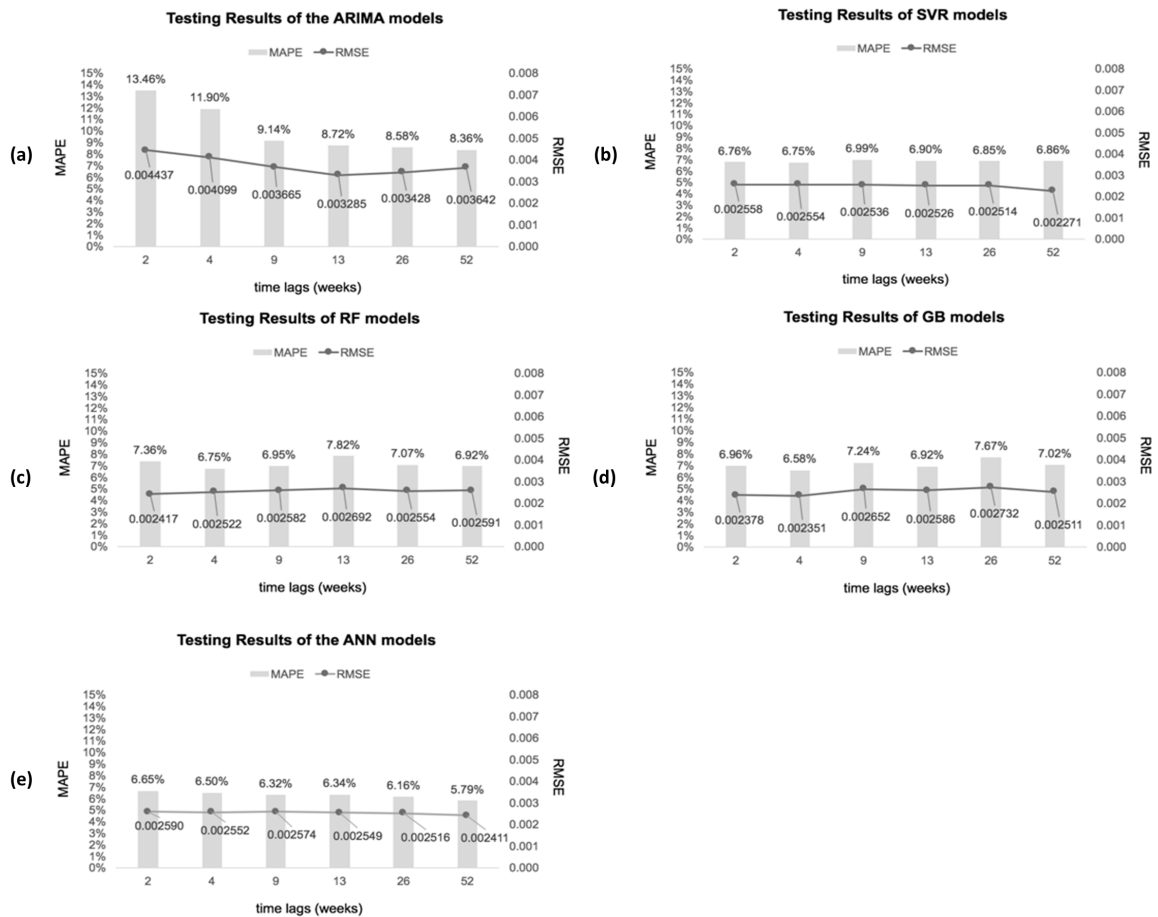


Figure 4. The MAPEs and RMSEs of the ARIMA, SVR, RF, GB, and ANN models with the different time lags as the feature spaces.

Table 5. The standard deviations of the MAPEs of the LSTM models of 3, 4, and 5 layers without regularization and of 4, 5, 6, and 10 layers with regularization

Time lags		2	4	9	13	26	52	Mean MAPE of Different LSTM Structures
LSTM Structures	3 layers MAPE (%)	6.80	7.00	7.00	6.87	6.93	6.71	6.89
	4 layers MAPE (%)	6.69	6.42	6.28	6.17	6.06	5.44	6.18
	5 layers MAPE (%)	6.85	6.61	7.20	6.64	6.53	6.28	6.69
Standard Deviation of MAPEs of LSTM without Regularization of 3, 4, 5 Layers (%)		0.08	0.30	0.49	0.36	0.44	0.64	0.37
LSTM Structures	4 layers with regularization MAPE (%)	6.74	6.32	6.22	6.09	6.07	5.45	6.15
	5 layers with regularization MAPE (%)	6.56	6.38	6.11	6.01	5.91	5.53	6.08
	6 layers with regularization MAPE (%)	6.61	6.52	6.20	6.12	5.91	5.46	6.14
	10 layers with regularization MAPE (%)	6.46	6.42	5.98	5.90	5.75	5.72	6.04
Standard Deviation of MAPEs of LSTM with Regularization of 4, 5, 6, 10 Layers MAPE (%)		0.12	0.08	0.11	0.10	0.13	0.12	0.05

probable explanation for this finding is that regularization made the models more robust, and the robust models made the results (*i.e.*, the MAPEs in this study) relatively stable.

Although we achieved the lowest MAPE (5.44%) when we used the 4-layer LSTM model without

regularization, the gap between the MAPEs of the 4-layer LSTM model without and with regularization is very limited (5.45% - 5.44% = 0.01%). Considering that unstable models may lead to poor accuracy if we changed the testing data, we recommend the use of the model with regularization for U.S. flu prediction.

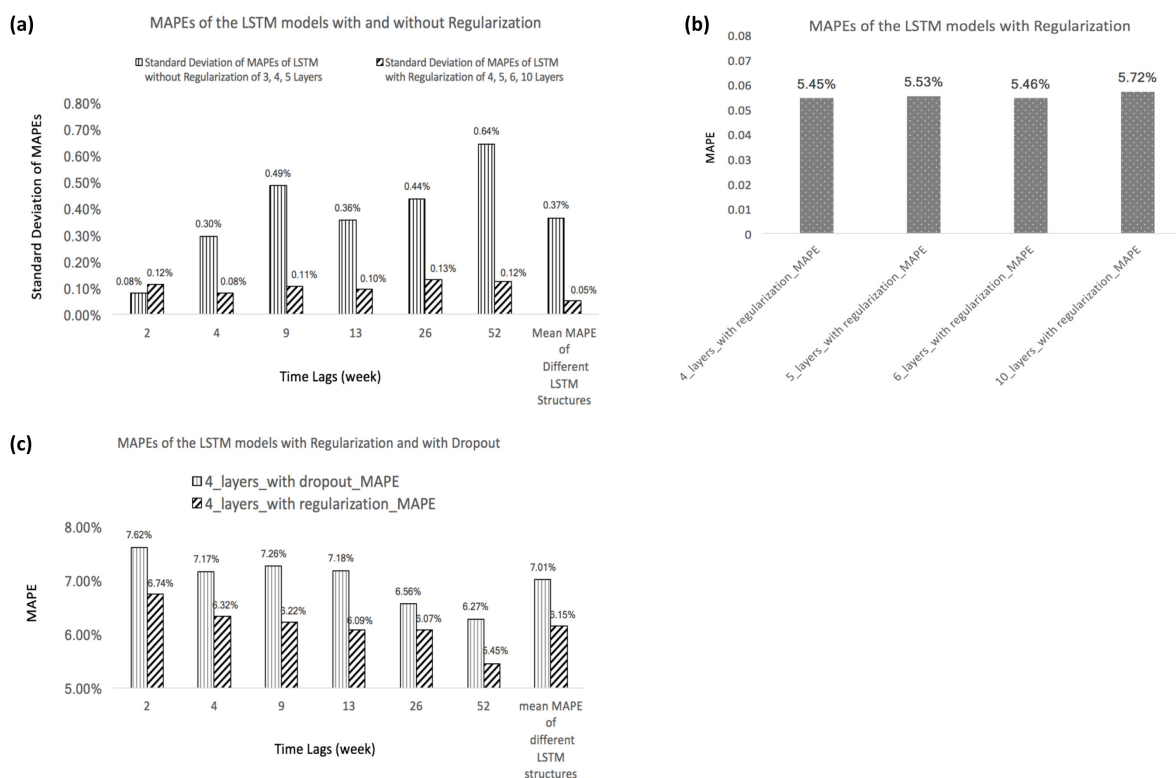


Figure 5. Comparison of LSTM Predicting Accuracy. (a). MAPEs of the LSTM models with and without regularization. The standard deviations of the MAPEs of the LSTM models with regularization were less than those of the LSTM models without regularization when we used almost all the time lags except the time lag of 2 weeks. (b). MAPEs of the LSTM models with different number of layers with regularization. (c). MAPEs of the LSTM models with Regularization and with Dropout.

4.3. LSTM structure (Layers)

After comparing the MAPEs of the LSTM models with and without regularization, we compared the different layers for the LSTM with regularization. (Figure 5b) We found extra layers (more than 4 layers) contributed little to improve the predicting accuracy. In other words, the LSTM models of 4 to 5 layers are considered sufficient for U.S. flu prediction.

4.4. Regularization and dropout

In addition to regularization, dropout can also usually help prevent overfitting and make the model more robust. We found that the MAPE of the LSTM models with regularization is obviously lower than those with dropout. "Dropout" randomly drops neurons, while "Regularization" selectively drops neurons. Although both suppress the number of neurons, in this study, the selective dropping performed much better than the random dropping.

4.5. Feature spaces

Comparing results, we found that the MAPE of ARIMA > MAPEs of SVR, RF, and GBM > MAPEs of ANN and LSTM. Although the different models have totally different algorithms, the increasing feature space and

the increasing model parameters are considered other factors that impact the models' accuracy. In ARIMA, we only have very limited feature spaces. The number of features is equal to the lag times, *i.e.*, 3, 5, 10, 14, 27, or 53. In the ML models (SVR, RF, and GB), we added the first-order differences, including more information in the models, and we clearly found that the ML models with 105 features resulted in lower MAPEs. In DL models, we used 255 neurons in every LSTM layer, which included more parameters in the models. To achieve better epidemic predictions, more neurons can perform more linear and non-linear combinations of past data, create more "artificial" feature spaces, and provide better results.

4.6. More time lags

Why not adopt more time lags such as 104 weeks (around 2 years) or more? For one things, the models with the time lag of 52 weeks (around 1 year) have brought an accuracy of about 95% (*i.e.* 1 - MAPE). For another thing, we have to drop more training data (the first 104 rows) if we adopt a time lag of 104 week or more. Although a longer time lag might help improve the accuracy, the less training data would also setback the accuracy. We suppose whether the accuracy would be better or worse depends on different data. However, a time lag including a complete periodicity is

recommended for ARIMA, ANN, and LSTM.

5. Conclusion

In this study, we performed ARIMA, SVM, RF, GB, ANN, and LSTM models with different time lags (2, 4, 9, 13, 26, 52 weeks) to forecast the weekly ILI rate of U.S. flu data. We found the ARIMA, ANN and LSTM models with a lag time of 52 weeks (*i.e.*, the periodicity of the flu season) resulted in the best MAPEs, while SVR, RF, and GB performed with almost no changes when we used the time lags. We also found the MAPEs of the ML models (SVR, RF, and GB) with the first differences were lower than those of ARIMA, and the MAPEs of the deep learning models (ANN and LSTM) with multiple layers were lower than those of the ML models (SVR, RF, and GB). To the best of our knowledge, this is the first time LSTM has been used to predict influenza outbreaks. In all the models (with different model types, different hyperparameters, and different time lags), the LSTM model of 4 layers reached the lowest MAPE of 5.4%, and the LSTM model of 5 layers with regularization reached the lowest RMSE of 0.00210. Additionally, the LSTM models with 4 ~ 6 layers with regularization resulted in very low MAPEs of approximately 5.4 ~ 5.5%, and more than 6 layers contributed little to improving the predictive accuracy.

References

1. World Health Organization. Influenza (Seasonal) fact sheet. <http://www.who.int/mediacentre/factsheets/fs211/en/> (accessed August 23, 2017).
2. Longo D. Harrison's principles of internal medicine. (18th ed., Fauci A, Kasper D, Hauser S, Jameson J, Loscalzo J, eds.). McGraw-Hill, New York, 2012; 187:1442.
3. Centers for disease control and prevention. Key facts about influenza (Flu). <https://www.cdc.gov/flu/keyfacts.htm> (accessed Aug 23, 2017).
4. Brankston B, Gitterman L, Hirji Z, Lemieux C, Gardam M. Transmission of influenza A in human beings. *Lancet Infect Dis.* 2007; 4:257-265.
5. Statement from president George W. Bush on Influenza". <http://www.presidency.ucsb.edu/ws/index.php?pid=65259> (accessed August 23, 2017).
6. Earn DJ, He D, Loeb MB, Fonseca K, Lee BE, Dushoff J. Effects of school closure on incidence of pandemic influenza in Alberta, Canada. *Ann Intern Med.* 2012; 156:173-181
7. Cauchemez S, Valleron AJ, Boëlle PY, Flahault A, Ferguson NM. Estimating the impact of school closure on influenza transmission from Sentinel data. *Nature.* 2008; 452:750-754.
8. Heymann A, Hoch I, Valinsky L, Kokia E, Steinberg DM. School closure may be effective in reducing transmission of respiratory viruses in the community. *Epidemiol Infect.* 2009; 137:1369-1376.
9. Ginsberg J, Mohebbi MH, Patel RS, Brammer L, Smolinski MS, Brilliant L. Detecting influenza epidemics using search engine query data. *Nature.* 2009; 457:1012-1014
10. Kane MJ, Price N, Scotch M, Rabinowitz P. Comparison of ARIMA and random forest time series models for prediction of avian influenza H5N1 outbreaks. *BMC Bioinformatics.* 2014; 15:276.
11. "FluView" portal of centers for disease control and prevention (CDC). <https://www.cdc.gov/flu/weekly/fluviewinteractive.htm> (accessed Jun 7, 2017).
12. Hyndman R. Package 'forecast' Ver 8.1. CRAN. <https://cran.r-project.org/web/packages/forecast/index.html> (accessed Oct 2, 2017).
13. Wu H, Cai Y, Wu Y, Zhong R, Li Q, Zheng J, Lin D, Li Y. Time series analysis of weekly influenza-like illness rate using a one-year period of factors in Random forest regression. *Biosci Trends.* 2017. 11:292-296
14. Andrew NG, What Data Scientists Should Know about Deep Learning. <https://www.slideshare.net/ExtractConf/andrew-ng-chief-scientist-at-baidu> (accessed Sep 21, 2017).

(Received September 25, 2017; Revised October 9, 2017; Accepted October 20, 2017)

PCSK9 rs7552841 is associated with plasma lipids profiles in female Chinese adolescents without posttraumatic stress disorder

Qiwei Guo, Yanjun Si, Mi Su, Mei Fan, Jia Lin, Nazakat H Memon, Dingzhi Fang*

Department of Biochemistry and Molecular Biology, West China School of Basic Medical Sciences & Forensic Medicine, Sichuan University, Chengdu, China.

Summary

To explain the inconsistent relationship between *proprotein convertase subtilisin/kexin type 9* (PCSK9) rs7552841 and plasma lipids profiles, we hypothesized that interplays might occur among gender, PCSK9 rs7552841 and posttraumatic stress disorder (PTSD) on plasma lipids levels. To test this hypothesis, a population of 704 Chinese Han high school students was used, which had been recruited after the 2008 Wenchuan Earthquake. In this population, the plasma levels of glucose, triglyceride (TG), total cholesterol (TC), high-density lipoprotein cholesterol (HDL-C) and low-density lipoprotein cholesterol (LDL-C) had been measured by routine methods. PTSD had been assessed by the PTSD Checklist Civilian Version (PCL-C). PCSK9 rs7552841 was analyzed by polymerase chain reaction-restriction fragment length polymorphism analyses and verified by DNA sequencing. The T allele carriers had significantly higher levels of TG, TC, LDL-C, and glucose than the CC homozygotes of PCSK9 rs7552841 after the adjustment for age and BMI in the female students, but not in the male students. When PTSD was taken into consideration, the female T allele carriers had significantly higher TG, TC, LDL-C and glucose than the female CC homozygotes after the adjustment for age and BMI only in the subjects without PTSD, but not in the PTSD patients. No significant differences were observed in the male students regardless of PTSD and the adjustment for age and BMI. These results suggest that PCSK9 rs7552841 is associated with plasma lipids profiles only in female adolescents, but not in male students. This association can be modified and negated by PTSD.

Keywords: PCSK9 rs7552841, genetic variation, gender, PTSD, blood lipids

1. Introduction

Posttraumatic stress disorder (PTSD) is a serious chronic anxiety problem (1) that develops in some people after experiencing extremely traumatic events such as serious injury, actual or threatened death, childhood abuse and natural disasters (2-4). Numerous studies indicated that individuals with PTSD exhibited higher levels of triglyceride (TG), total cholesterol (TC) and low-density lipoprotein cholesterol (LDL-C) but lower levels of high

density lipoprotein cholesterol (HDL-C) than healthy control subjects (5-7). However, Jendricko *et al.* (8) reported that there were no differences of plasma TG, TC, HDL-C and LDL-C between the male war veterans with PTSD and the control subjects. Jergovic *et al.* (9) also reported that plasma lipids did not differ between PTSD patients and controls in individual time points. The mechanism of the discrepancy has not been elucidated yet.

In recent years, proprotein convertase subtilisin/kexin type 9 (PCSK9) has emerged as a new, promising key therapeutic target to reduce the plasma levels of TC, especially LDL-C (10,11). PCSK9, also known as neural apoptosis-regulated convertase 1, is a serine protease mostly secreted by liver that plays a critical role in cholesterol metabolism (12). In particular, PCSK9 promotes the degradation of cell-surface LDL receptor (LDL-R), resulting in reduced clearance of

Released online in J-STAGE as advance publication October 29, 2017.

*Address correspondence to:

Dr. Dingzhi Fang, Department of Biochemistry and Molecular Biology, West China School of Basic Medical Sciences & Forensic Medicine, Sichuan University, Chengdu 610041, China.

E-mail: dzfang@scu.edu.cn

LDL-C from circulation through a post-transcriptional mechanism (12-14). Human PCSK9 gene (*PCSK9*) is located on chromosome 1p32, expanding promoter region and 12 exons (15). Gain-of-function mutations of *PCSK9* were found to increase the degradation of LDL-R, resulting in autosomal dominant hypercholesterolemia. These findings were confirmed by mice experiments using the wild-type and mutant genes such as S127R and F216L (15-17). Conversely, heterozygous patients with loss-of-function mutations had lower plasma LDL-C levels and decreases of 80-90% risk of coronary heart disease (16,18). Furthermore, previous studies have demonstrated that PCSK9 is not only take part in the regulation of lipids profiles, but also associated with mental disorders. Kang *et al.* (19) reported that plasma levels of PCSK9 were increased in both Alzheimer's disease (AD) and mild cognitive impairment patients. It was also shown recently that AD patients had significantly higher levels of PCSK9 in cerebrospinal fluid than non-AD subjects (20). However, there are no existing reports about the relationship between PCSK9 and PTSD.

In addition, over 40 single nucleotide polymorphisms have been found at *PCSK9*. Much more recently, *PCSK9* rs7552841 in the intron region with a thymine (T) to cytosine (C) transition has been reported to be associated with statin response in European individuals (21). Significant differences of plasma levels of TG, TC and LDL-C were also observed between the T allele carriers and the CC homozygotes of *PCSK9* rs7552841 in a Chinese Jing population (22). Furthermore, the distribution of the T allele carriers and the CC homozygotes were significantly different between hypercholesterolaemic and control subjects or between hypertriglyceridaemic and control subjects. After adjusting age, gender, body mass index (BMI), smoking and alcohol consumption, *PCSK9* rs7552841 was found to be associated with not only hypercholesterolaemia but also hypertriglyceridaemia (23). On the other hand, no significant differences of plasma lipid levels were observed between the T allele carriers and the CC homozygotes in a Chinese Han population (22), and in 101 Chilean hypercholesterolaemic individuals before or after 10 mg/day of atorvastatin therapy although the T allele carrier showed a trend towards less increases of HDL-C after the treatment (24). Obviously, more studies are needed to clarify the above discrepancies of the associations reported before between *PCSK9* rs7552841 and plasma lipids profiles.

To explain the discrepancies of the associations between PTSD and plasma lipids profiles, and between *PCSK9* rs7552841 and plasma lipids profiles reported previously by others, we hypothesized that interplays might occur between *PCSK9* rs7552841 and PTSD to influence plasma lipids profiles. The present study was to test the hypothesis. In fact, we had a population of

high school students experiencing the 2008 Wenchuan earthquake, which we had explored the PTSD characteristics in 2008 and 2009, and reported them (25). We also had measured the plasma lipids profiles after sampling in 2008 (26). In the present study, we genotyped *PCSK9* rs7552841 and analyzed the plasma lipids profiles in the students with different genotypes of *PCSK9* rs7552841 and with or without PTSD. To our knowledge, this is the first study exploring the interaction between PTSD and *PCSK9* rs7552841 on plasma lipids profiles.

2. Materials and Methods

2.1. Study population

As reported before (25), the population was from a boarding high school after the 2008 Wenchuan earthquake. The devastating earthquake occurred in the afternoon of 12 May 2008, measuring 8.0 on the Richter scale and led to 69,227 deaths, 17,923 missing and 374,643 injured. The earthquake extended about 10 thousand km² and covered 254 towns in 21 counties, which destroyed 6.5 million houses. About 5 million people were evacuated and lived in temporary shelters after the earthquake. The school is located only 10 km away from the epicenter of the earthquake and was severely damaged during the earthquake. All the teaching halls and students dormitories were destroyed by the earthquake. The students lived and studied in temporary houses.

Although PTSD characteristics had been measured at 6, 12 and 18 months after the earthquake (25), only the data at 6 months were used to test the hypothesis in the present study, which included 746 students from grade 11. Among them, 737 (98.8%) had completed the questionnaires evaluating their demographic characteristics and PTSD status. Recruitment criteria were understanding of the procedures involved, no history of metabolic disease and providing written consents and blood samples. The students with cardiovascular, renal, or endocrinological diseases, or diabetes, and the students who took lipid-lowering drugs or hormones, consumed alcohol and smoked were excluded. In the end, 704 students were included in the present study. They were all Chinese Han adolescents at the age of 15 to 18 years with an average of 16.86 ± 0.59 years. There were 310 male students (44.03%) and 394 female students (55.97%). Written consents had been provided by all the participants of the study and their guardians. This study was approved by the Human Research Ethics Committee of Sichuan University, ratifying our lab to analyze not only the psychological characteristic, genetic variations and plasma lipids profiles, but also the interplays psychological characteristic, genetic variations on plasma lipids profiles (26).

2.2. Measurements

The measurement instrument was composed of two parts, which was reported previously (25). The first part had been used to assess measures including demographic characteristics such as gender, age, body weight and height. Body mass index (BMI) had been calculated. The PTSD Checklist-Civilian Version (PCL-C) (27) had been used to assess PTSD in the second part, which corresponds to Diagnostic and Statistical Manual of Mental Disorders, 4th edition (DSM-IV) criteria (2). The PCL-C includes 17 self-report items. The total score ranges from 17 to 85. A total score of 38 was defined as the cutoff point of PTSD in this study (28). The assessments had been finished in 2008 and the existing data were used for the present study.

2.3. Blood collection and laboratory analyses

Twelve-hour fasting venous bloods had been sampled. The levels of plasma glucose, TG and TC had been measured using enzymatic methods. The levels of HDL-C had been determined after separated by phosphotungstate-magnesium chloride precipitation method. The levels of LDL-C had been examined using the polyvinyl sulfate precipitation method. All the samples had been measured 3 times and the average values were used for statistical analyses. All the measurements had been finished after sampling in 2008 and the existing data were used for the present study.

2.4. DNA extraction and genotyping

Genetic DNA had been isolated after sampling by others in the lab from peripheral blood leucocytes using a DNAout kit (Tiandz, China) and stored at -80°C . In the present study, the stored genetic DNA was used for the genotyping of *PCSK9* rs7552841. The genotypes of *PCSK9* rs7552841 were determined by polymerase chain reaction-restriction fragment length polymorphism method and verified by DNA sequencing. The following PCR primers were used for the amplifications of DNA containing *PCSK9* rs7552841 locus: forward primer, 5'-AGGGAAGGGCACGGTTAG-3', reverse primer, 5'-TGCCAGTTCCTCCACCAC-3'. The PCR cycling parameters were denaturation at 95°C for 2 min, 30 subsequent cycles of denaturation at 95°C for 30 sec, annealing at 60°C for 30 sec and extension at 72°C for 30 sec, and a final extension at 72°C for 2 min. The resulting PCR products were DNA fragments of 496 bp. The identification of the genotypes was performed by the restriction digestion with *MspI*. The digested products were separated by electrophoresis on 1.5% agarose gel. As a result, the digested PCR products with the CC genotype migrated as one band of 496 bp, the

TT genotype as two bands of 320 and 176 bp and the CT genotype as three bands of 496, 320 and 176 bp.

2.5. Statistical analyses

The results were expressed as mean \pm standard deviation (SD) unless otherwise stated. Log power transformations were applied to the levels of TG because they were in positively skewed distribution. The genotype and allele frequencies were determined by counting. The agreement of the genotype distribution of *PCSK9* rs7552841 with Hardy-Weinberg equilibrium was assessed by chi-squared goodness-of-fit tests. Differences of genotype frequencies as well as allele distribution between the male and female students were estimated using Chi-Square (χ^2) tests. Independent-samples *t* tests were used to compare all the other quantitative variables between the male and female students and between the individuals with different genotypes of *PCSK9* rs7552841. Covariance analyses were used to eliminate the potentially confounding bias of age and BMI on biochemical characteristics. The level of statistical significance was set at 0.05.

3. Results

3.1. Characteristics of the study population

The levels of plasma lipids and the related metabolic variables in the study population are shown in Table 1. The male subjects were significantly older than the female subjects in the present study. The levels of BMI, TG, TC, HDL-C and LDL-C were significantly higher, but glucose was significantly lower in the female students when compared with those of the male students.

3.2. Genotype and allele frequencies of *PCSK9* rs7552841

The genotype and allele frequencies of *PCSK9* rs7552841 in the adolescents are presented in Table 2. No deviation was found from Hardy-Weinberg equilibrium of the distribution of the genotypes of *PCSK9* rs7552841 in the study population ($\chi^2 = 0.17$). There were no statistically significant differences in the genotype and allele frequencies between the male and female subjects. As there were limited subjects with the TT genotype, they were combined with the subjects with the CT genotype and defined as the T allele carriers for further analyses and presented as CT/TT in the tables.

3.3. Prevalence of PTSD in the subjects with different genotypes of *PCSK9* rs7552841

According to the assessment of PCL-C, the prevalence of PTSD in the students with different genotypes of

Table 1. Characteristics of the study population

Variables	All	Males	Females	p-Value ^a
n	704	310	394	--
age	16.86 ± 0.59	16.95 ± 0.61	16.78 ± 0.56	< 0.001
BMI, kg/m ²	20.28 ± 2.31	19.81 ± 2.29	20.66 ± 2.27	< 0.001
TG, mmol/L	1.12 ± 0.44	0.96 ± 0.35	1.24 ± 0.47	< 0.001
TC, mmol/L	3.58 ± 0.57	3.41 ± 0.51	3.72 ± 0.58	< 0.001
HDL-C, mmol/L	1.41 ± 0.28	1.36 ± 0.26	1.45 ± 0.29	< 0.001
LDL-C, mmol/L	1.67 ± 0.49	1.61 ± 0.46	1.71 ± 0.50	0.011
Glucose, mmol/L	5.07 ± 0.44	5.15 ± 0.45	5.01 ± 0.42	< 0.001

^a comparisons between those of the male subjects and those of the female subjects (independent-samples *t* test).

Table 2. Genotype and allele frequencies of PCSK9 rs7552841 in the study population

Genotype	Total (n = 704) n (%)	Hardy-Weinberg p	Males (n = 310) n (%)	Females (n = 394) n (%)	p ^a
Genotype Frequencies					
CC	510 (72.4)		221 (71.3)	289 (73.4)	
CT	180 (25.6)		84 (27.1)	96 (24.4)	0.606
TT	14 (1.99)	0.683	5 (1.60)	9 (2.30)	
Allele Frequencies					
C	1,200 (85.2)		526 (84.8)	674 (85.5)	0.715
T	208 (14.8)		94 (15.2)	114 (14.5)	

Data are presented as n (%). ^a Male students vs. female students by Chi-Square tests.

Table 3. Prevalence of PTSD in the subjects with different genotypes of PCSK9 rs7552841

Group	All		Males		Females	
	CC	CT/TT	CC	CT/TT	CC	CT/TT
Control	346 (67.8)	136 (70.1)	166 (75.1)	71 (79.8)	180 (62.3) ^a	65 (61.9) ^a
PTSD	164 (32.2)	58 (29.9)	55 (24.9)	18 (20.2)	109 (37.7)	40 (38.1)

Data are expressed as n (%). ^a p < 0.05 when compared with that of the male students (Chi-Square test).

PCSK9 rs7552841 is shown in Table 3. No significant difference of prevalence was found between the CC homozygotes and the T allele carriers in all the students, the male or the female subjects. The PTSD prevalence of female subjects was significantly higher than the male subjects in both the CC homozygotes ($p = 0.002$) and the T allele carriers ($p = 0.008$).

3.4. Plasma lipids profiles and the related metabolic variables of the subjects with different genotypes of PCSK9 rs7552841

Table 4 shows age, BMI, plasma lipids and plasma glucose of the subjects with different genotypes of PCSK9 rs7552841. The female T allele carriers had higher levels of TC and LDL-C than the female CC homozygotes. After the adjustment for age and BMI, the female T allele carriers had significantly higher levels of TG, TC, LDL-C and glucose than the female CC homozygotes. However, there were no significant

differences between the T allele carriers and the CC homozygotes in the male subjects regardless of the adjustment for age and BMI.

3.5. Effects of PTSD on the association of PCSK9 rs7552841 polymorphism with plasma lipids profiles and the related metabolic variables

As shown in Table 5, no significant differences were found between the CC homozygotes and the T allele carriers in the male students regardless of PTSD and the adjustment for age and BMI. However, the T allele carriers had higher levels of BMI, TG, TC, and LDL-C than the CC homozygotes in the female subjects without PTSD, but not in the female students with PTSD. After the adjustment for age and BMI, the female T allele carriers had significantly higher levels of TG, TC, LDL-C, and glucose than the female CC homozygotes in the students without PTSD. Still, no significant differences were observed after the adjustment for

Table 4. Serum Lipids Profiles and the Related Metabolic Variables of the subjects with different genotypes of PCSK9 rs7552841

Variables	Males				Females			
	CC	CT/TT	p-Value ^a	ANCOVA p-Value ^b	CC	CT/TT	p-Value ^a	ANCOVA p-Value ^b
n	221	89	--	--	289	105	--	--
Age, year	16.95 ± 0.61	16.96 ± 0.62	0.950	--	16.79 ± 0.59	16.76 ± 0.49	0.635	--
BMI, kg/m ²	19.83 ± 2.36	19.76 ± 2.11	0.810	--	20.74 ± 2.22	20.44 ± 2.38	0.254	--
TG, mmol/L	0.95 ± 0.34	0.98 ± 0.37	0.545	0.486	1.21 ± 0.46	1.31 ± 0.47	0.055	0.025
TC, mmol/L	3.41 ± 0.52	3.41 ± 0.48	0.950	0.975	3.68 ± 0.56	3.85 ± 0.64	0.008	0.004
HDL-C, mmol/L	1.35 ± 0.25	1.36 ± 0.28	0.819	0.867	1.46 ± 0.29	1.43 ± 0.28	0.316	0.212
LDL-C, mmol/L	1.62 ± 0.48	1.60 ± 0.43	0.686	0.717	1.66 ± 0.48	1.82 ± 0.54	0.004	0.002
Glucose, mmol/L	5.15 ± 0.41	5.14 ± 0.52	0.862	0.873	4.98 ± 0.41	5.08 ± 0.43	0.051	0.047

^a Comparisons between those of the CC homozygotes and those of the T allele carriers (independent-samples *t* test). ^b Analyses of covariance with the adjustment for age and BMI.

Table 5. Effects of PTSD on the association of PCSK9 rs7552841 with anthropometric and biochemical characteristics

Variables	Group	Males				Females			
		CC	CT/TT	p-Value ^a	ANCOVA p-Value ^b	CC	CT/TT	p-Value ^a	ANCOVA p-Value ^b
n	Control	166	71	--	--	180	65	--	--
	PTSD	55	18	--	--	109	40	--	--
Age, year	Control	16.96 ± 0.62	16.93 ± 0.66	0.752	--	16.78 ± 0.58	16.75 ± 0.50	0.717	--
	PTSD	16.93 ± 0.57	17.06 ± 0.42	0.384	--	16.81 ± 0.60	16.78 ± 0.48	0.760	--
BMI, kg/m ²	Control	19.68 ± 2.06	19.58 ± 1.99	0.727	--	20.69 ± 2.08	19.97 ± 2.31	0.021	--
	PTSD	20.25 ± 3.09	20.44 ± 2.46	0.816	--	20.81 ± 2.44	21.21 ± 2.31	0.371	--
TG, mmol/L	Control	0.94 ± 0.28	0.98 ± 0.35	0.312	0.265	1.20 ± 0.42	1.33 ± 0.46	0.036	0.014
	PTSD	1.00 ± 0.49	0.97 ± 0.42	0.836	0.792	1.23 ± 0.52	1.28 ± 0.49	0.579	0.799
TC, mmol/L	Control	3.37 ± 0.52	3.42 ± 0.49	0.506	0.464	3.67 ± 0.64	3.84 ± 0.62	0.042	0.031
	PTSD	3.53 ± 0.52	3.36 ± 0.41	0.208	0.183	3.68 ± 0.59	3.87 ± 0.67	0.090	0.135
HDL-C, mmol/L	Control	1.35 ± 0.25	1.35 ± 0.28	0.992	0.929	1.47 ± 0.28	1.42 ± 0.28	0.234	0.095
	PTSD	1.37 ± 0.26	1.41 ± 0.29	0.562	0.411	1.44 ± 0.30	1.44 ± 0.28	0.907	0.960
LDL-C, mmol/L	Control	1.59 ± 0.47	1.62 ± 0.43	0.659	0.588	1.66 ± 0.45	1.81 ± 0.54	0.041	0.012
	PTSD	1.71 ± 0.49	1.51 ± 0.46	0.127	0.087	1.67 ± 0.52	1.85 ± 0.57	0.079	0.117
Glucose, mmol/L	Control	5.12 ± 0.41	5.14 ± 0.52	0.804	0.833	4.98 ± 0.37	5.09 ± 0.46	0.057	0.041
	PTSD	5.25 ± 0.40	5.16 ± 0.56	0.479	0.463	5.00 ± 0.47	5.06 ± 0.40	0.431	0.484

^a Comparisons between those of the CC homozygotes and those of the T allele carriers (independent-samples *t* test). ^b Analyses of covariance with the adjustment for age and BMI.

age and BMI between the T allele carriers and the CC homozygotes in the female students with PTSD.

4. Discussion

In the present study, we used the population that we had reported the PTSD characteristics (25) and had measured the lipids profiles (26). We genotyped PCSK9 rs7552841 and analyzed the plasma lipids profiles in the students with different genotypes of PCSK9 rs7552841 and with or without PTSD. To our best knowledge, these analyses have not been reported before. In fact, PTSD characteristics had been measured in the population at 6, 12 and 18 months after the earthquake (25). However, only the data at 6 months were used in the present study because the purpose was to test our hypothesis that interplays might occur between PCSK9 rs7552841 and PTSD to influence plasma lipids

profiles. Although the follow-up might provide more information about the changes of PTSD and lipids profiles, analyzing the interplays of course, PTSD and PCSK9 rs7552841 was not the purpose of the present study.

It has been reported that PCSK9 can regulate plasma levels of LDL-C, while some of the single nucleotide polymorphisms at PCSK9 are associated with plasma lipids profiles (12-14,16,29). Recently, the association of PCSK9 rs7552841 polymorphism with plasma lipids has been explored in two laboratories in China and Chile (22-24). Significant differences were found by the Chinese laboratory of the plasma levels of TG, TC and LDL-C between the T allele carriers and the CC homozygotes of PCSK9 rs7552841 in a Chinese Jing population, but not in Chinese Han population (22). The results reported by the Chilean laboratory showed that there were no significant differences

of plasma lipids between the T allele carriers and the CC homozygotes of *PCSK9* rs7552841 in 101 Chilean hypercholesterolaemic individuals before and after 10 mg/day of atorvastatin therapy (24). These discrepancies may be explained by ethnicities, healthy status, medication status and even the sample size because the Chilean investigation was carried out in a smaller population. However, other confounding factors such as age, BMI, gender or psychological factors were not included in all the above analyses, which have been generally accepted to be important factors associated with plasma lipids profiles (30-34). In the present study, the female students had significantly higher levels of TG, TC, HDL-C and LDL-C but lower levels of glucose than the male students in the whole study population (Table 1). These results confirm again that gender serves as an important confounding factor and influences the levels of plasma lipids. Therefore, we examined the differences of plasma lipids between the T allele carriers and the CC homozygotes of *PCSK9* rs7552841 in the male and female students separately. To eliminate the influence of confounders such as age and BMI on plasma lipids, the adjustment was made of age and BMI. The results show that the female T allele carriers had significantly higher levels of TG, TC, LDL-C and glucose than the female CC homozygotes after the adjustment for age and BMI. Nevertheless, no significant differences were observed between the T allele carriers and the CC homozygotes in the male subjects regardless of the adjustment for age and BMI (Table 4). These results suggest that *PCSK9* rs7552841 may interplay with gender to influence plasma lipids profiles. And therefore, *PCSK9* rs7552841 is associated with plasma lipids in a gender-dependent manner. This finding may be one of the explanations of the discrepancies reported before of the associations between *PCSK9* rs7552841 and the levels of plasma lipids.

Although a biopsychosocial medical model was proposed by Engel in 1977 (35), much less efforts have been made to explore the interplays between biomedical factors and psychological factors on plasma lipids profiles. Therefore, in the present study, PTSD was selected as a psychological factor to study its interplays with gender and *PCSK9* rs7552841 on the levels of plasma lipids in a biological-psychological approach. The results indicate that the female T allele carriers had significantly higher levels of TG, TC, LDL-C and glucose than the female CC homozygotes after the adjustment for age and BMI only in the subjects without PTSD, but not in the PTSD patients (Table 5). No significant differences were observed between the male T allele carriers and the male CC homozygotes regardless of PTSD and the adjustment for age and BMI. These results suggest that *PCSK9* rs7552841 may interplay with not only gender but also PTSD to affect plasma levels of TG, TC, LDL-C and glucose. More

specifically, the association between *PCSK9* rs7552841 and plasma lipids profiles in female subjects may be modified or eliminated by PTSD. These findings may be one of the explanations that no associations were found between *PCSK9* rs7552841 and the levels of plasma lipids in the same ethnicity reported before (22). Therefore, in the future study, gender and psychological factors should be taken into account when the relationship is tested between *PCSK9* rs7552841 and plasma lipids profiles.

Cunningham *et al.* (36) reported that the mutant with the gain-of-function mutation D374Y could bind LDL receptor more tightly than the wild-type *PCSK9*, resulting in the increment of plasma LDL-C. On the other hand, Suzanne *et al.* (37) found that *PCSK9* with the natural mutation F216L could increase the levels of circulating LDL-C through resisting to furin digestion and increasing plasma *PCSK9* levels. In addition, some other gain-of-function mutations were also reported to increase the levels of plasma LDL-C (16,38-40). As the variation of *PCSK9* rs7552841 is located at the intron region, the molecular mechanism of its effects on plasma lipids profiles cannot be the gain-of-function mutation of *PCSK9*. The possible mechanism may be that its mRNAs are more stable since higher stabilities of mutant intron-containing RNAs have been found to promote translation, resulting in more protein production (41,42). Other mechanisms such as linkage disequilibrium should also be taken into consideration.

There were some limitations in the present study. Firstly, only adolescents were included in the present study. The metabolic characteristics of this population may be different from adults. Secondly, the plasma levels of *PCSK9* and the levels of *PCSK9* mRNA in liver tissues were not measured. Thirdly, other psychological factors such as depression were not included, which had been reported to be related to dyslipidemia (43,44). These measurements are recommended for future studies in this field.

In conclusion, there may be interactions among gender, PTSD and *PCSK9* rs7552841 on plasma lipids profiles. *PCSK9* rs7552841 is associated with plasma lipids profiles in a gender-dependent manner in Chinese Han adolescents without PTSD, but not in Chinese Han adolescents with PTSD. The T allele of *PCSK9* rs7552841 may be a risk factor to increase the levels of plasma TG, TC, LDL-C and glucose in healthy female subjects. This finding may provide novel insights into the regulation of lipids metabolisms by *PCSK9* in younger populations, and pave the way for the precision prevention to reduce risks of CVD in adolescents, especially in a country with a quarter of the world's population.

Acknowledgements

This study was supported by the Program of Sichuan

Province for International Cooperation and Exchanges of Sciences and Technologies (Grant no. 2017HH0074). Professor Dingzhi Fang is the recipient of the grant.

References

- Davis LL, Suris A, Lambert MT, Heimberg C, Petty F. Post-traumatic stress disorder and serotonin: New directions for research and treatment. *J Psychiatry Neurosci.* 1997; 22:318-326.
- APA. Diagnostic and Statistical Manual of Mental Disorders, DSM-IV-TR Fourth Edition. American Psychiatric Association, Washington, DC, 2000, USA.
- Lancaster CL, Teeters JB, Gros DF, Back SE. Posttraumatic Stress Disorder: Overview of Evidence-Based Assessment and Treatment. *J Clin Med.* 2016; 5: pii: E105.
- Neumeister A, Seidel J, Ragen BJ, Pietrzak RH. Translational evidence for a role of endocannabinoids in the etiology and treatment of posttraumatic stress disorder. *Psychoneuroendocrinology.* 2015; 51:577-584.
- Levine AB, Levine LM, Levine TB. Posttraumatic stress disorder and cardiometabolic disease. *Cardiology.* 2014; 127:1-19.
- Dennis PA, Ulmer CS, Calhoun PS, Sherwood A, Watkins LL, Dennis MF, Beckham JC. Behavioral health mediators of the link between posttraumatic stress disorder and dyslipidemia. *J Psychosom Res.* 2014; 77:45-50.
- Maia DB, Marmar CR, Mendlowicz MV, Metzler T, Nobrega A, Peres MC, Coutinho ES, Volchan E, Figueira I. Abnormal serum lipid profile in Brazilian police officers with post-traumatic stress disorder. *J Affect Disord.* 2008; 107:259-263.
- Jendricko T, Vidovic A, Grubisic-Ilic M, Romic Z, Kovacic Z, Kozaric-Kovacic D. Homocysteine and serum lipids concentration in male war veterans with posttraumatic stress disorder. *Prog Neuropsychopharmacol Biol Psychiatry.* 2009; 33:134-140.
- Jergovic M, Bendelja K, Savic Mlakar A, Vojvoda V, Aberle N, Jovanovic T, Rabatic S, Sabioncello A, Vidovic A. Circulating levels of hormones, lipids, and immune mediators in post-traumatic stress disorder - A 3-month follow-up study. *Front Psychiatry.* 2015; 6:49.
- Nissen SE, Dent-Acosta RE, Rosenson RS, *et al.* Comparison of PCSK9 Inhibitor Evolocumab vs Ezetimibe in Statin-Intolerant Patients: Design of the Goal Achievement After Utilizing an Anti-PCSK9 Antibody in Statin-Intolerant Subjects 3 (GAUSS-3) Trial. *Clin Cardiol.* 2016; 39:137-144.
- Norata GD, Ballantyne CM, Catapano AL. New therapeutic principles in dyslipidaemia: Focus on LDL and Lp(a) lowering drugs. *Eur Heart J.* 2013; 34:1783-1789.
- Peterson AS, Fong LG, Young SG. PCSK9 function and physiology. *J Lipid Res.* 2008; 49:1152-1156.
- Park SW, Moon YA, Horton JD. Post-transcriptional regulation of low density lipoprotein receptor protein by proprotein convertase subtilisin/kexin type 9a in mouse liver. *J Biol Chem.* 2004; 279:50630-50638.
- Lagace TA, Curtis DE, Garuti R, McNutt MC, Park SW, Prather HB, Anderson NN, Ho YK, Hammer RE, Horton JD. Secreted PCSK9 decreases the number of LDL receptors in hepatocytes and in livers of parabiotic mice. *J Clin Invest.* 2006; 116:2995-3005.
- Abifadel M, Varret M, Rabes JP, *et al.* Mutations in PCSK9 cause autosomal dominant hypercholesterolemia. *Nat Genet.* 2003; 34:154-156.
- Benjannet S, Rhoads D, Essalmani R, *et al.* NARC-1/PCSK9 and its natural mutants: Zymogen cleavage and effects on the low density lipoprotein (LDL) receptor and LDL cholesterol. *J Biol Chem.* 2004; 279:48865-48875.
- Maxwell KN, Breslow JL. Adenoviral-mediated expression of Pcsk9 in mice results in a low-density lipoprotein receptor knockout phenotype. *Proc Natl Acad Sci U S A.* 2004; 101:7100-7105.
- Zhao Z, Tuakli-Wosornu Y, Lagace TA, Kinch L, Grishin NV, Horton JD, Cohen JC, Hobbs HH. Molecular characterization of loss-of-function mutations in PCSK9 and identification of a compound heterozygote. *Am J Hum Genet.* 2006; 79:514-523.
- Kang S, Jeong H, Baek JH, Lee SJ, Han SH, Cho HJ, Kim H, Hong HS, Kim YH, Yi EC, Seo SW, Na DL, Hwang D, Mook-Jung I. PiB-PET Imaging-Based Serum Proteome Profiles Predict Mild Cognitive Impairment and Alzheimer's Disease. *J Alzheimers Dis.* 2016; 53:1563-1576.
- Zimetti F, Caffarra P, Ronda N, Favari E, Adorni MP, Zanotti I, Bernini F, Barocco F, Spallazzi M, Galimberti D, Ricci C, Ruscica M, Corsini A, Ferri N. Increased PCSK9 Cerebrospinal Fluid Concentrations in Alzheimer's Disease. *J Alzheimers Dis.* 2017; 55:315-320.
- Thompson JF, Hyde CL, Wood LS, Paciga SA, Hinds DA, Cox DR, Hovingh GK, Kastelein JJ. Comprehensive whole-genome and candidate gene analysis for response to statin therapy in the Treating to New Targets (TNT) cohort. *Circ Cardiovasc Genet.* 2009; 2:173-181.
- Guo T, Yin RX, Huang F, Yao LM, Lin WX, Pan SL. Association between the *DOCK7*, *PCSK9* and *GALNT2* Gene Polymorphisms and Serum Lipid levels. *Sci Rep.* 2016; 6:19079.
- Guo T, Yin R-X, Lin W-X, Wang W, Huang F, Pan S-L. Association of the variants and haplotypes in the *DOCK7*, *PCSK9* and *GALNT2* genes and the risk of hyperlipidaemia. *J Cell Mol Med.* 2016; 20:243-265.
- Cuevas A, Fernández C, Ferrada L, Zambrano T, Rosales A, Saavedra N, Salazar LA. HMGCR rs17671591 SNP Determines Lower Plasma LDL-C after Atorvastatin Therapy in Chilean Individuals. *Basic Clin Pharmacol Toxicol.* 2016; 118:292-297.
- Zhang Z, Ran MS, Li YH, Ou GJ, Gong RR, Li RH, Fan M, Jiang Z, Fang DZ. Prevalence of post-traumatic stress disorder among adolescents after the Wenchuan earthquake in China. *Psychol Med.* 2012; 42:1687-1693.
- Fan M, LiRH, Hu MS, Fang DZ. Effects of interactions between post-traumatic stress disorder with brain-derived neurotrophic factor gene Val66Met polymorphism on serum lipid profiles in adolescents. *China Sciencepaper.* 2015; 10:2876-2879. (in Chinese)
- Blanchard EB, Jones-Alexander J, Buckley TC, Forneris CA. Psychometric properties of the PTSD Checklist (PCL). *Behav Res Ther.* 1996; 34:669-673.
- Tian Y, Wong TK, Li J, Jiang X. Posttraumatic stress disorder and its risk factors among adolescent survivors three years after an 8.0 magnitude earthquake in China. *BMC public health.* 2014; 14:1073.
- Scartezini M, Hubbard C, Whittall RA, Cooper JA,

- Neil AH, Humphries SE. The *PCSK9* gene R46L variant is associated with lower plasma lipid levels and cardiovascular risk in healthy U.K. men. *Clin Sci (Lond)*. 2007; 113:435-441.
30. Wenger NK. Gender disparity in cardiovascular disease: Bias or biology? *Expert Rev Cardiovasc Ther*. 2012; 10:1401-1411.
31. Zheng J, Gao Y, Jing Y, Zhou X, Shi Y, Li Y, Wang L, Wang R, Li M, Xiao C, Li Y, Li R. Gender differences in the relationship between plasma lipids and fasting plasma glucose in non-diabetic urban Chinese population: A cross-section study. *Front Med*. 2014; 8:477-483.
32. Fall T, Hagg S, Ploner A, *et al*. Age- and sex-specific causal effects of adiposity on cardiovascular risk factors. *Diabetes*. 2015; 64:1841-1852.
33. Engebretson TO, Stoney CM. Anger expression and lipid concentrations. *Int J Behav Med*. 1995; 2:281-298.
34. Chikani V, Reding D, Gunderson P, McCarty CA. Wisconsin rural women's health study psychological factors and blood cholesterol level: Difference between normal and overweight rural women. *Clin Med Res*. 2004; 2:47-53.
35. Engel GL. The need for a new medical model: A challenge for biomedicine. *Science*. 1977; 196:129-136.
36. Cunningham D, Danley DE, Geoghegan KF, *et al*. Structural and biophysical studies of PCSK9 and its mutants linked to familial hypercholesterolemia. *Nat Struct Mol Biol*. 2007; 14:413-419.
37. Benjannet S, Rhainds D, Hamelin J, Nassoury N, Seidah NG. The proprotein convertase (PC) PCSK9 is inactivated by furin and/or PC5/6A: Functional consequences of natural mutations and post-translational modifications. *J Biol Chem*. 2006; 281:30561-30572.
38. Leren TP. Mutations in the *PCSK9* gene in Norwegian subjects with autosomal dominant hypercholesterolemia. *Clin Genet*. 2004; 65:419-422.
39. Timms KM, Wagner S, Samuels ME, Forbey K, Goldfine H, Jammulapati S, Skolnick MH, Hopkins PN, Hunt SC, Shattuck DM. A mutation in PCSK9 causing autosomal-dominant hypercholesterolemia in a Utah pedigree. *Hum Genet*. 2004; 114:349-353.
40. Berge KE, Ose L, Leren TP. Missense mutations in the *PCSK9* gene are associated with hypocholesterolemia and possibly increased response to statin therapy. *Arterioscler Thromb Vasc Biol*. 2006; 26:1094-1100.
41. Manthey GM, McEwen JE. The product of the nuclear gene *PET309* is required for translation of mature mRNA and stability or production of intron-containing RNAs derived from the mitochondrial COX1 locus of *Saccharomyces cerevisiae*. *EMBO J*. 1995; 14:4031-4043.
42. Le Hir H, Nott A, Moore MJ. How introns influence and enhance eukaryotic gene expression. *Trends Biochem Sci*. 2003; 28:215-220.
43. Almeida OP, Alfonso H, Flicker L, Hankey GJ, Norman PE. Cardiovascular disease, depression and mortality: The Health In Men Study. *Am J Geriatr Psychiatry*. 2012; 20:433-440.
44. Chuang CS, Yang TY, Muo CH, Su HL, Sung FC, Kao CH. Hyperlipidemia, statin use and the risk of developing depression: A nationwide retrospective cohort study. *Gen Hosp Psychiatry*. 2014; 36:497-501.

(Received September 19, 2017; Revised October 15, 2017; Accepted October 21, 2017)

Construction of C35 gene bait recombinants and T47D cell cDNA library

Kun Yin^{1,§}, Chao Xu^{1,§}, Gui-Hua Zhao¹, Ye Liu², Ting Xiao¹, Song Zhu¹, Ge Yan^{1,*}

¹Shandong Institute of Parasitological Disease, Shandong Academy of Medical Sciences, Jining, Shandong, China;

²The First People's Hospital of Jining City, Jining, Shandong, China.

Summary

C35 is a novel tumor biomarker associated with metastasis progression. To investigate the interaction factors of C35 in its high expressed breast cancer cell lines, we constructed bait recombinant plasmids of C35 gene and T47D cell cDNA library for yeast two-hybrid screening. Full length C35 sequences were subcloned using RT-PCR from cDNA template extracted from T47D cells. Based on functional domain analysis, the full-length C35_{1-348bp} was also truncated into two fragments C35_{1-153bp} and C35_{154-348bp} to avoid auto-activation. The three kinds of C35 genes were successfully amplified and inserted into pGBKT7 to construct bait recombinant plasmids pGBKT7-C35_{1-348bp}, pGBKT7-C35_{1-153bp} and pGBKT7-C35_{154-348bp}, then transformed into Y187 yeast cells by the lithium acetate method. Auto-activation and toxicity of C35 baits were detected using nutritional deficient medium and X- α -Gal assays. The T47D cell ds cDNA was generated by SMARTTM technology and the library was constructed using *in vivo* recombination-mediated cloning in the AH109 yeast strain using a pGADT7-Rec plasmid. The transformed Y187/pGBKT7-C35_{1-348bp} line was intensively inhibited while the truncated Y187/pGBKT7-C35 lines had no auto-activation and toxicity in yeast cells. The titer of established cDNA library was 2×10^7 pfu/mL with high transformation efficiency of 1.4×10^6 , and the insert size of ds cDNA was distributed homogeneously between 0.5-2.0 kb. Our research generated a T47D cell cDNA library with high titer, and the constructed two C35 "baits" contained a respective functional immunoreceptor tyrosine based activation motif (ITAM) and the conserved last four amino acids Cys-Ile-Leu-Val (CILV) motif, and therefore laid a foundation for screening the C35 interaction factors in a BC cell line.

Keywords: C35 gene, bait construction, T47D cDNA library, breast carcinoma, yeast strain

1. Introduction

Breast carcinoma (BC) is the most common cancer and the first killer of women's health in both the developed and developing countries. According to the statistics from World Health Organization published in 2013 (1), BC was responsible for approximately 508,000 female deaths in 2011 in the world. In China, the incidence

of BC has been increasing in recent years, more than 1.6 million patients were diagnosed and 1.2 million death cases occurred each year, among those the newly diagnosed cases accounted for 12.2% (2). C35 is a novel identified tumor biomarker for prediction and early diagnosis of either breast carcinoma (3) or other cancers such as colorectal and prostate cancer (4,5). By comparing 38 kinds of human normal tissue cells including brain cerebellum, endothelium and skeletal muscle, Evans *et al.* revealed that almost all normal cells were negative for C35 expression, with the exception of human leydig cells (6). Parallel experiments were also conducted in 10 kinds of human mammary carcinoma cell lines such as BT-20, MCF7 and T47D, and the C35 gene was abundantly expressed in 7 kinds of mammary carcinoma cells, but no obvious

Released online in J-STAGE as advance publication October 16, 2017.

[§]These authors contributed equally to this work.

*Address correspondence to:

Dr. Ge Yan, Shandong Institute of Parasitological Disease, Shandong Academy of Medical Sciences, 11 Taibai Middle Road, Jining 272033, Shandong, China.

E-mail: geyan1965@163.com

expression was detected in adjacent normal breast epithelium (6). In particular, the expression level of C35 gene in T47D cell line was 10 to 70 times more than in the H16N2 normal mammary epithelial cell line, and more frequent in infiltrating ductal carcinoma and invasive lobular carcinoma (6). Moreover, Kun *et al.* reported that overexpression frequency of C35 was associated with clinical Tumor Node Metastasis staging and Scarff-Bloom-Richardson grade ($p < 0.05$), indicated that C35 may take part in transforming normal cells into tumor progression and lymph node metastasis (3).

C35 gene is located on the minus region of human chromosome 17q12 (7). The full length of C35 transcript consists of 776 nucleotides and 4 exons, encoding a 12 kDa membrane-anchored protein. *In-situ* hybridization by Evans *et al.* indicated that gene expression and regulation of C35 was correlated with chromosomal amplification, especially overexpression of C35 was accompanied by amplification of the *ERBB2* gene, consistent with the fact that C35 location is bounded by the oncogene *ERBB2* and growth factor receptor-bound protein 7 (*GRB7*) (6). The C-terminal end of C35 contains a conserved canonical immunoreceptor tyrosine based activation motif (ITAM) and a tiny functional domain made up of the last four amino acids Cys-Ile-Leu-Val (CVIL), these two domains were proved to have an important role in cancer progression and metastasis (5,8). By prediction of the functional sites and conserved domain of C35, Dasgupta *et al.* speculated that C35 may participate in four important physiological pathways including apoptosis, cell transformation, cytoskeleton remodeling and vesicle trafficking (5), yet the molecular mechanisms and interaction factors of C35 in regulation of those pathways are still unknown.

In this study, we have constructed 3 bait recombinant plasmids of C35 according to its functional domains and a T47D cell cDNA library in order to conduct a yeast-two hybrid system, for screening the interaction factors of C35 in its over-expressed cell line. The extensive detection of auto-activation and toxicity for the three baits were also performed to evaluate their application value. Our study laid a foundation for the following screening research.

2. Materials and Methods

2.1. Cell culture conditions

Human T47D breast cancer cell line (supplied by the Institute of Basic Medicine, Shandong Academy of Medical Sciences, Ji'nan, China) was cultured in DMEM (Gibco, Grand Island, NY, USA), supplemented with 10% FBS (Gibco, Grand Island, NY, USA), 100 U/mL of penicillin (Hyclone, Logan, UT, USA), and 100 U/mL of streptomycin (Hyclone, Logan, UT, USA), in an

incubator with 5% CO₂ at 37°C. For maintenance and subculture, T47D cells in exponential phase were treated with 0.25% trypsin solution containing 0.02% EDTA. After reaching 80% confluence, the cells were collected.

2.2. Extraction of T47D cells mRNA

The T47D cells (1×10^7) were harvested for mRNA extraction using the Oligotex Direct mRNA kit (Qiagen, Hilden, Germany). Extraction of T47D cells mRNA was conducted according to the kit instructions. The amount and quality of product was analyzed by using the NanoDrop 2000 spectrophotometer (Thermo Fisher Scientific, Wilmington, DE, USA). Then it was first reverse transcribed into cDNA using a MuV reverse transcriptase kit (Fermentas, Burlington, Ontario, Canada) according to the protocol.

2.3. Amplification of C35 gene

The entire open reading frame of C35 gene was amplified using a DNA thermal cycler (Applied Biosystems, San Diego, CA, USA). The primers sequences corresponded to the registered C35 gene sequence in GeneBank (ID: 84299): C35-1bp-*EcoR* I-5': 5'-CGGAATTCATGAGCGGGGAGCCGG-3'; C35-348bp-*Sal* I-3': 5'-ACGCGTCTCGACTCACAGGATGACGCAGGGA-3' (the underlined were sequences of restriction sites *EcoR* I and *Sal* I respectively). PCR was performed in a 50 μ L reaction volume containing 37 μ L ddH₂O, 5 μ L 10 \times Buffer, 2 μ L deoxy-ribonucleoside triphosphate (dNTP), 1 μ L each of C35 primer (50 mmoL/L), 2 μ L DMSO (Sigma, USA), 1 μ L cDNA template, and 1 μ L Pfu DNA polymerase (Takara, Japan). The PCR reaction condition was: 95°C for 5 min, 30 cycles of 94°C for 1min, 56°C for 30 s, 72°C for 1min, with a final extension at 72°C for 5 min. PCR products were detected using 1.2% agarose gel electrophoresis with ethidiumbromide staining, and visualized under an ultraviolet transilluminator (Bio-Rad, USA).

2.4. C35 bait plasmids construction

Analysis of C35 functional and conserved domain was performed by the online software PROSITE (<http://www.expasy.org/prosite>) and the DNASTar Lasergene software v7.1 respectively. Two kinds of truncated C35 fragments were designed as C35_{1-153bp} and C35_{154-348bp}. The primers of C35 truncated fragments were as follows: C35-153bp-*Sal* I-3': 3'-ACGCGTCTCGACCGGATACTGCTCCTTACA; C35-154bp-*EcoR* I-5': 5'-CGGAATTCGGCATCGAGATCGAGTC. PCR amplification C35_{1-348bp}, C35_{1-153bp} and C35_{154-348bp} were performed and detected as described previously (section 2.3). All of the three PCR products were digested with *EcoR* I and *Sal* I (Takara, Japan), then inserted

into the corresponding sites of the bait expression vector pGBKT7 using T4 DNA ligase (Takara, Japan) to construct recombinant plasmids pGBKT7-C35_{1-348bp}, pGBKT7-C35_{1-153bp} and pGBKT7-C35_{154-348bp} respectively. The three plasmids were transformed into *E. coli* DH5 α competent cells respectively and the positive clones were identified by colony's PCR and double digested with *EcoR* I and *Sal* I enzymes, then further verified by a commercial sequencing service (BGI Corporation, Beijing, China). The sequencing results were analyzed using Chromas 2.2 Software (Technelysium Pty Ltd, Australia).

2.5. Yeast strain transformation

Preparation of the Y187 and AH109 yeast competent cells and chemical transformation using the lithium acetate method were performed according to the Matchmaker™ Library Construction & Screening Kits User Manual (Cat # PT3955-1) and Yeast Protocols Handbook (Cat # PT3024-1) by Clontech Company (Palo Alto, CA, USA). A total of 5 kinds of plasmids pGBKT7-C35_{1-348bp}, pGBKT7-C35_{1-153bp}, pGBKT7-C35_{154-348bp}, pGBKT7-53 (positive control, Clontech) and pGBKT7-Lam (negative control, Clontech) were transformed into the Y187 competent cells respectively.

2.6. Autoactivation and toxicity detection of C35 baits

After transformation, five kinds of transformants were spread onto SD/-Trp/X- α -Gal plates respectively and cultivated at 30°C for 3-5 d, then the colony with the largest diameter was transferred on SD/-His/-Trp/X- α -Gal and SD/-Ade/-Trp/X- α -Gal plates (Sigma, USA). To estimate the optimal concentration of 3-AT (Sigma, USA), the largest colonies were also cultivated on SD/-His/-Trp/-3-AT plates respectively at 30°C for 3-5 d, with a 3-AT concentration gradient of 0, 2.5, 5.0, 7.5, 10.0, 12.5, 15.0 mM. The positive colonies with more than 2 mm diameter were picked out and inoculated at 250-270 rpm/min in 50 mL SD/-Trp/-Kan media (20 μ g/mL) for 16-24 h at 30°C to measure the A₆₀₀ values.

2.7. Generation of T47D cells ds cDNA

The first strand cDNA of T47D cells was synthesized with SMART™ technology by using Moloney Murine Leukemia Virus (MMLV) reverse transcriptase and CDS III primer (Clontech, Palo Alto, CA, USA) according to the manual's instructions. Then the LD-PCR was used to amplify ds cDNA using the first-strand cDNA as template and the advantage 2 polymerase mixture. The reaction condition was performed according to the instruction of PT3955-1, and detected using 1.0% agarose gel electrophoresis. The ds cDNA products were purified by CHROMA SPIN™+TE-400 columns to remove small DNA molecules less than 200 bp. The

amount of ds cDNA was assessed by a NanoDrop 2000 spectrophotometer.

2.8. Library construction and titer detection

20 μ L of ds cDNA (2-5 μ g) and 6 μ L of pGADT7-Rec plasmid (0.5 μ g/ μ L) were co-transformed into competent AH109 yeast cells. The transformed cells were resuspended in 15 mL of 0.9% NaCl. Every 100 μ L of a 1/10, 1/100, 1/1,000 and 1/10,000 dilution of transformed cells was spread on a 100 mm SD/-Leu/plate and grown at 30°C for 3-4 days to determine independent colonies (Formula: Number of cfu/mL on SD/-Leu \times 15 mL) which indicated transformation efficiency. The remainder of the transformed cells were spread on 150 mm SD/-Leu plates (a total of 100 plates) with 150 μ L cells per plate and incubated at 30°C for 3-4 d. The transformants in each 150 mm plate were harvested in 5 mL of freezing YPDA medium containing 25% glycerol and isolated using sterile glass beads, the cell density was calculated with a hemocytometer. After that, all liquids of the library were divided into 1 mL aliquots for library screening or stored at -80°C. To determine the library titer (cfu/mL), every 100 μ L of a 1/100, 1/1,000 and 1/10,000 dilution of the aliquot was spread on a 100 mm SD/-Leu/ plate (Formula: number of colonies/plating volum (mL) \times dilution factor). 20 colonies were randomly picked up from the plates to check the insert size using Matchmaker™ Insert Check PCR Mix 2 Kit (Clontech, Palo Alto, CA, USA).

3. Results

3.1. Amplification of C35 and its truncated fragments

The mRNA isolated from T47D cells was identified by spectrophotometer and the OD₂₆₀/OD₂₈₀ value was 1.944, indicating that the quality of the extracted mRNA met the requirement for being the template of the following RT-PCR and LD-PCR. The full-length sequences of C35 were amplified by RT-PCR of the cDNA. Analysis of the RT-PCR products using 1.2% agarose gel electrophoresis showed positive bands with the expected 348 bp size (Figure 1A). Based on the results of conserved domain analysis, C35 protein contains two functional motifs, ITAM and CVIL. The ITAM motif in sequence ₃₆EATYLELASAVKEQYPGIEI₅₃ conforms to a prototypical immunoreceptor tyrosine-based activation consensus sequence with the Tyr39 as a tyrosine kinase activity site. The COOH-terminal "CVIL" sequence fits the prenylation motif CAAX and may take part in the membrane combining process. Since the kinase domain usually induces an auto-activation activity in the yeast system, we designed two truncated fragments of C35_{1-153bp} and C35_{154-348bp}. These two truncated fragments were amplified and verified by the same protocols as the full-length one. The

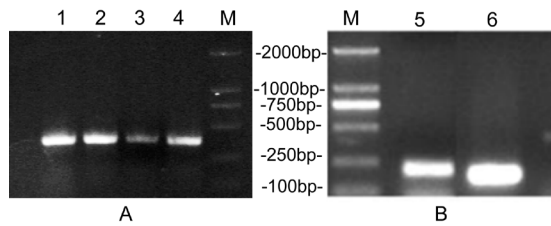


Figure 1. PCR amplification results of C35 gene. (A): PCR products of full-length C35 gene. 1-4: C35_{1-348bp}; M: DL 2000 DNA marker. **(B):** PCR products of truncated C35 fragments. 5: C35_{154-348bp}; 6: C35_{1-153bp}.

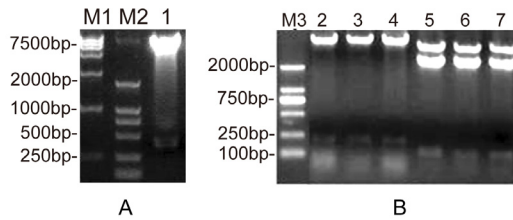


Figure 2. Identification of the C35 bait recombinant plasmids pGBKT7-C35 by restriction enzyme digestion with *EcoR* I and *Sal* I. (A): Gel electrophoresis of double digested pGBKT7-C35_{1-348bp}. M1: DL15000 DNA marker; M2: DL2000 DNA marker; 1: pGBKT7-C35_{1-348bp}. **(B):** Gel electrophoresis of double digested truncated pGBKT7-C35. M3: DL2000 DNA marker; 2-4: pGBKT7-C35_{154-348bp}; 5-7: pGBKT7-C35_{1-153bp}.

corresponding electrophoresis results also showed clear positive bands with 153 bp for C35_{1-153bp} and 195 bp for C35_{154-348bp} respectively (Figure 1B).

3.2. Construction and identification of C35 bait recombinant plasmids

The three kinds of C35 fragments preliminarily amplified by PCR were digested with *EcoR* I/*Sal* I enzymes, then ligated in-frame into the corresponding sites of the bait expression vector pGBKT7 respectively. The three generated recombinants were named as pGBKT7-C35_{1-348bp}, pGBKT7-C35_{1-153bp} and pGBKT7-C35_{154-348bp}. After transformation, the plasmids were extracted from positive colonies and identified by double digestion with *EcoR* I and *Sal* I. The 1% agarose gel electrophoresis results displayed the approximately 7,300 bp empty pGBKT7 and the expected 348 bp (Figure 2A), 153 bp and 195 bp C35 fragments (Figure 2B). All of the three sequencing results were verified to be correct by conducting BLAST database homology searches referred to published C35 sequences in GenBank (data not shown), and proved that the recombinant C35 bait plasmids were successfully established.

3.3. Determination of auto-activation and toxicity of C35 baits

The recombinant C35 bait plasmids were transformed

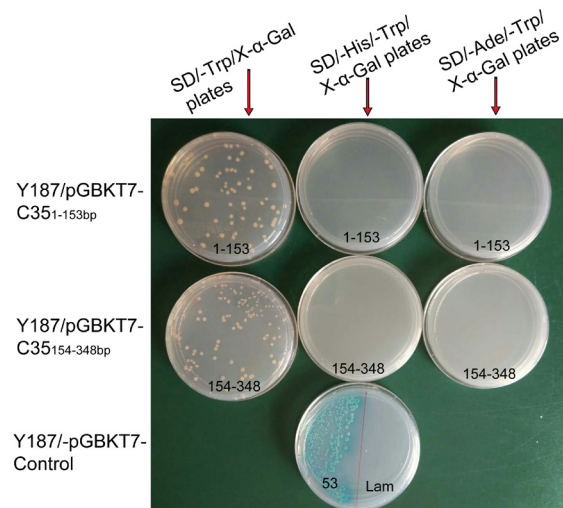


Figure 3. Auto-activation activity detection results of two truncated C35 bait plasmids. The transformation of truncated Y187/pGBKT7-C35 lines showed white colonies on SD/-Trp/X-α-Gal plates but could not grow on SD/-His/-Trp/X-α-Gal and SD/-Ade/-Trp/X-α-Gal plates, indicating the "baits" had no Auto-activation activity and self transcriptional activity. Colonies of Y187/pGBKT7-53 positive control turned blue on SD/-His/-Trp/X-α-Gal plates.

into yeast strain Y187 using the LiAc-mediated method to produce the Y187/pGBKT7-C35 lines. Surprisingly, no visible colony of Y187/pGBKT7-C35_{1-348bp} appeared on SD/-Trp plates, suggesting that the full-length C35 protein had intensive toxicity to the Y187 yeast strain (data not shown). White colonies of Y187/pGBKT7-C35_{1-153bp}, Y187/pGBKT7-C35_{154-348bp} and Y187/pGBKT7-Lam appeared on SD/-Trp/X-α-Gal plates in 3-5 d (Figure 3). At the same time, after being transferred the largest colonies of the two truncated Y187/pGBKT7-C35 lines to SD/-His/-Trp/X-α-Gal and SD/-Ade/-Trp/X-α-Gal plates respectively, showed no background growth on these two kinds of nutritional deficiency plates (Figure 3), suggesting that none of them had an auto-activation effect and were not required for 3-AT inhibition. To determine the baits' toxicity to the yeast strain, the largest colonies of Y187/pGBKT7-C35_{1-153bp} and Y187/pGBKT7-C35_{154-348bp} on SD/-Trp/X-α-Gal plates were picked out and inoculated respectively in 50 mL SD/-Trp/-Kan (20 μg/mL) media for 20 h, the A₆₀₀ value was 0.859 for Y187/pGBKT7-C35_{1-153bp} and 0.807 for Y187/pGBKT7-C35_{154-348bp} respectively, confirming that both of them were nontoxic and thereby the recombinant plasmids pGBKT7-C35_{1-153bp} and pGBKT7-C35_{154-348bp} were eligible to be used as "baits" for yeast two-hybrid analysis.

3.4. Synthesis of T47D cells ds cDNA

The 1.0% agarose electrophoresis results showed that 7 μL LD-PCR product of ds cDNA fractions appeared mainly as a 0.25-2.0 kb smear (Figure 4). More than 3

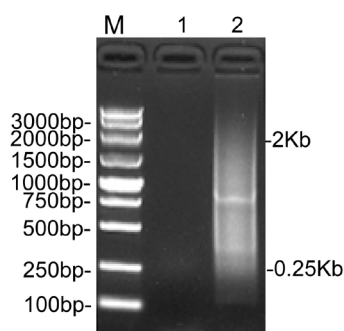


Figure 4. Gel electrophoresis results of the purified ds cDNA fractions of T47D cells by LD-PCR. M: DL 5000 DNA marker; 1: empty lane; 2: ds cDNA. The ds cDNA fractions appeared mainly as a 0.25-2.0 kb smear.

μg of ds cDNA were obtained from the remainder of the 93 μL LD-PCR product after purification on the CHROMA SPINTM+TE-400 Columns. The amount and quality of the amplified ds cDNA were satisfactory for constructing the yeast two-hybrid cDNA library.

3.5. Construction and titering of the T47D cDNA library

After co-transforming the ds cDNA product and pGADT7-Rec into AH109 competent cells, a total of 1.4×10^6 independent colonies which contained the T47D cell cDNA library were harvested on the 100 mm SD/-Leu plates which were spread with gradient dilution transformed cells, and the transformation efficiency was calculated as 1.4×10^6 transformants/3 μg pGADT7-Rec, indicating that the transformation efficiency in this study could yield a satisfactory library with high complexity. Further, after harvesting colonies on all of the 150 mm SD/-Leu plates, the cell density was about $8.2 \times 10^7 - 1.0 \times 10^8$ cells/mL and sufficient enough for screening. The titer of the T47D cell cDNA library was 2×10^7 cfu/mL calculated by colony numbers on the SD/-Leu plates spread with a gradient diluent library aliquot. The electrophoresis results of 20 random colonies showed that the insert size of the ds cDNA was distributed randomly between 0.5 kb-2.0 kb (Figure 5), indicating that our library was homogeneous and the recombination rate of the library was 95% (19/20).

4. Discussion

The C35 gene, also termed as C17orf37/MGC14832, which has a 95% identity compared with the migration and invasion enhancer 1 (MIEN1) protein, is a novel oncogene discovered in various kinds of cancers. Expression of C35 has been reported to positively relate to grade and stage of cancer progression, for example, BC, ovarian cancer, prostate cancer, and colorectal cancer. Yet studies on the function of over-expressed C35 and its interaction factors are still in the initial stage. The known interaction factor of C35 was

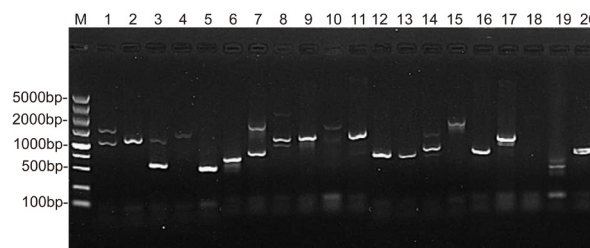


Figure 5. Identification results of insert size of T47D cell cDNA library by PCR. M: DL 5000 DNA marker; 1-20: Gel electrophoresis results of PCR from library colonies selected randomly.

discovered by a Leung *et al.* report (9), in that research, C35 was identified as a potential protein partner of p73 by yeast two-hybrid screen using a HeLa cDNA library and a p73 bait vector. The co-expression of C35 and ΔNp73 , a dominant-negative isoform of p73, which lacks the transactivation domain, could induce greater cisplatin treatment resistance in ovarian cancer cells by activating AKT and nuclear NF- κB p65. Consistently, Dasgupta *et al.* (5) reported that downregulation of C35 in prostate cancer cells suppressed PKB/Akt phosphorylation and NF- κB activity was also reduced by down-regulating downstream target genes MMP-9, uPA and VEGF, suggesting C35 takes part in the regulation of the NF- κB signaling pathway. In addition, Rajendiran *et al.* (10) demonstrated that overexpression of MIEN1 in DOK cells also increased the Akt/NF- κB effectors MMP-9, uPA and VEGF, and thereby further confirmed the correlation between C35 overexpression and the activation of Akt/NF- κB . However, Katz *et al.* (8) discovered that the expression levels of NF- κB markers MMP-9, uPA and VEGF were not correlated with overexpression of C35 in BC cells. These findings suggest that C35 may participate in different signaling pathways in different cancer cell lines. At the same time, they also discovered that high levels of C35 protein expression in primary BC cells could induce transformation in 3D cell cultures by activating Syk kinase, a downstream mediator of signaling from the ITAM motif. Similarly, inhibition of MIEN1 protein expression in BC cells decreased the expression level of matrix metalloproteinase 9 by downregulating the expression of AKT kinase (11). The correlation between C35 and kinase activity suggests that the application value of C35 may not only be the biomarker gene for genetic diagnosis and prognosis, but also be a potential drug target for BC therapy or other cancers. At present, there are a series of reports regarding the inhibition effects of C35. Liu *et al.* (12) have designed two kinds of C35 siRNAs with significant inhibition effects for both mRNA and protein expression levels of C35, and could induce apoptosis of T47D cells *in vitro*. Rajendiran *et al.* (13) proved that inhibiting the expression of MIEN1 protein in prostate cells by microRNA-940 could suppress the migratory and invasive potential of prostate cells. Li *et al.* (14)

reported that microRNA-26b suppressed the metastasis of non-small cell lung cancer by targeting MIEN1 via NF- κ B/MMP-9/VEGF pathways. Therefore C35 is a promising novel diagnostic and therapeutic tool in various kinds of cancers, exploring and screening its interaction factors may elucidate the signaling pathways it takes part in, reveal its mechanisms in inducing cell migration and invasion in different kinds of cancers, and may provide the relevant targets for the development of new drugs.

Notably, the COOH-terminal amino acid sequence "CVIL" of C35 fits the prenylation CAAX motif, and Dasgupta *et al.* (15) demonstrated that this region could be post-translationally modified by protein geranylgeranyltransferase-I (GGTase-I). This C-terminal geranylgeranylation was essential for its membrane, which enhanced cells migratory phenotype by inducing increased filopodia formation, and thus potentiates directional migration. In particular, this "CVIL" motif is completely conserved among all species. Additionally, the ITAM motif was identified to determine the phosphorylation-dependent activation of MIEN1, which regulated filopodia generation, migration and invasion of breast cells (16). These studies indicated that the C-terminal "CVIL" motif and the ITAM domain act as the dominant functional motif of C35. Furthermore, the ITAM-phosphorylation of MIEN1 could be significantly impaired in isoprenylation-deficient MIEN1 mutants, and imply that the post-translational modification of MIEN1 was required for cross-phosphorylation of tyrosine residues (16).

Based on these studies, it is deduced that the functional domains of C35 are mutually independent and functionally interacting in regulating metastatic progression of cancers. Therefore in this study, we have designed three different fragments of C35 for constructing bait vectors for yeast two-hybrid screening according to the results of conserved domain analysis. After transforming the full-length pGBKT7-C35_{1-348bp} into Y187 competent cells, we found that the plasmid intensely inhibited yeast strain Y187 and no visible colony appeared on SD/-Trp/X- α -Gal plates under optimized transformation and recovery conditions, indicating that the full-length of C35 protein has a strong toxicity effect on the yeast strain and potential unknown significant roles on yeast cells. On the contrary, we found that the two C35 truncations (C35_{1-153bp} and C35_{154-348bp}) eliminated the toxicity effects completely. The recombinant baits pGBKT7-C35_{1-153bp} contains the ITAM domain and the pGBKT7-C35_{154-348bp} contains the C-terminal "CVIL" motif, with no observed auto-activation or toxicity effect, and thus could be used for following the screening process in order to figure out their corresponding interaction factors respectively. At the same time, we also constructed the cDNA library of T47D cell lines in which with the C35 gene insert is

over-expressed. The size distribution of T47D ds cDNA in the present study was homogeneous and the amount of independent clones on SD/-Leu was sufficient enough for generating library cells with satisfactory density and high titer. Altogether, our study laid a promising foundation for screening the C35 interaction factors in BC cell lines and exploring the accurate mechanisms of C35 in regulating cancer metastasis and invasion.

Acknowledgements

This study was supported by grants from the National Natural Science Foundation of China (31300617, 81041075, 81702026), and the Innovation Project of Shandong Academy of Medical Sciences, The National Science Foundation of Shandong Province (ZR2015YL024, Q2007D04, BS2013SW015, ZR2014YL039, ZR2014YL036).

References

1. World Health Organization. Breast cancer: Prevention and control. <http://www.who.int/cancer/detection/breastcancer/en/index1.html> (accessed 2013).
2. Fan L, Strasser-Weippl K, Li JJ, St Louis J, Finkelstein DM, Yu KD, Chen WQ, Shao ZM, Goss PE. Breastcancer in China. *Lancet Oncol.* 2014; 15:279-289.
3. Yin K, Ba Z, Li C, Xu C, Zhao G, Zhu S, Yan G. Overexpression of C35 in breast carcinomas is associated with tumor progression and lymph node metastasis. *Biosci Trends* 2015; 9:386-392.
4. Dong X, Huang Y, Kong L, Li J, Kou J, Yin L, Yang J. C35 is overexpressed in colorectal cancer and is associated with tumor invasion and metastasis. *Biosci Trends.* 2015; 9:117-21.
5. Dasgupta S, Wasson LM, Rauniyar N, Prokai L, Borejdo J, Vishwanatha JK. Novel gene C17orf37 in 17q12 amplicon promotes migration and invasion of prostate cancer cells. *Oncogene.* 2009; 28:2860-2872.
6. Evans EE, Henn AD, Jonason A, Paris MJ, Schiffhauer LM, Borrello MA, Smith ES, Sahasrabudhe DM, Zauderer M. C35 (C17orf37) is a novel tumor biomarker abundantly expressed in breast cancer. *Mol Cancer Ther.* 2006; 5:2919-2930.
7. Stein D, Wu J, Fuqua SA, Roonprapunt C, Yajnik V, D'Eustachio P, Moskowitz JJ, Buchberg AM, Osborne CK, Margolis B. The SH2 domain protein GRB-7 is co-amplified, over expressed and in a tight complex with HER2 in breast cancer. *EMBO J.* 1994; 13:1331-1340.
8. Katz E, Dubois-Marshall S, Sims AH, Faratian D, Li J, Smith ES, Quinn JA, Edward M, Meehan RR, Evans EE, Langdon SP, Harrison DJ. A gene on the HER2 amplicon, C35, is an oncogene in breast cancer whose actions are prevented by inhibition of Syk. *Br J Cancer.* 2010; 103:401-410.
9. Leung TH, Wong SC, Chan KK, Chan DW, Cheung AN, Ngan HY. The interaction between C35 and Δ Np73 promotes chemo-resistance in ovarian cancer cells. *Br J Cancer.* 2013; 109:965-975.
10. Rajendiran S, Kpetemey M, Maji S, Gibbs LD, Dasgupta S, Mantsch R, Hare RJ, Vishwanatha JK. MIEN1

- promotes oral cancer progression and implicates poor overall survival. *Cancer Biol Ther.* 2015; 16:876-885.
11. Zhao HB, Zhang XF, Wang HB, Zhang MZ. Migration and invasion enhancer 1 (MIEN1) is overexpressed in breast cancer and is a potential new therapeutic molecular target. *Genet Mol Res.* 2017; 16. (doi: 10.4238/gmr16019380)
 12. Liu Q, Yin K, Zhu S, Zhang L, Wen P, Li C, Zhang D, Liu M, Yan G. Inhibition of C35 gene expression by small interfering RNA induces apoptosis of breast cancer cells. *Biosci Trends.* 2010; 4:254-259.
 13. Rajendiran S, Parwani AV, Hare RJ, Dasgupta S, Roby RK, Vishwanatha JK. MicroRNA-940 suppresses prostate cancer migration and invasion by regulating MIEN1. *Mol Cancer.* 2014; 13:250.
 14. Li D, Wei Y, Wang D, Gao H, Liu K. MicroRNA-26b suppresses the metastasis of non-small cell lung cancer by targeting MIEN1 *via* NF- κ B/MMP-9/VEGF pathways. *Biochem Biophys Res Commun.* 2016; 472:465-470.
 15. Dasgupta S, Cushman I, Kpetemey M, Casey PJ, Vishwanatha JK. Prenylated c17orf37 induces filopodia formation to promote cell migration and metastasis. *J Biol Chem.* 2011; 286:25935-25946.
 16. Kpetemey M, Dasgupta S, Rajendiran S, Das S, Gibbs LD, Shetty P, Gryczynski Z, Vishwanatha JK. MIEN1, a novel interactor of Annexin A2, promotes tumor cell migration by enhancing AnxA2 cell surface expression. *Mol Cancer.* 2015; 14:156.

(Received July 20, 2017; Revised September 28, 2017; Accepted October 3, 2017)

Protective effects of luteolin-7-O-glucoside against starvation-induced injury through upregulation of autophagy in H9c2 Cells

Hong Yao¹, Lichun Zhou¹, Linlin Tang^{1,2}, Yanhui Guan¹, Shang Chen¹, Yu Zhang¹, Xiuzhen Han^{1,3,*}

¹Department of Pharmacology, School of Pharmaceutical Sciences, Shandong University, Jinan, China;

²Department of Pharmacy, Affiliated Hospital of Weifang Medical University, Weifang, China;

³Key Laboratory of Chemical Biology of Natural Products, Ministry of Education, Shandong University, Jinan, China.

Summary

Cardiomyocyte nutrient deprivation is a common clinical event that mediates various cardiac ischemic processes and is associated with autophagy activation and cell survival or death. Luteolin-7-O-glucoside (LUTG) was one of the flavonoid glycosides isolated from *Dracocephalum tanguticum*. Previous research had showed that LUTG pretreatment had significant protective effects against doxorubicin-induced cardiotoxicity. However, whether LUTG could protect cardiomyocytes from starvation-induced injury was not clear. In this study, cardioprotection and mechanisms of LUTG against starvation-induced injury were investigated *in vitro*. 3-(4,5-Dimethyl-2-thiazolyl)-2,5-diphenyl-2-tetrazolium bromide (MTT) assay showed starvation-induced autophagy is a homeostatic and protective response for H9c2 cell survival. LUTG could protect against injury induced by starvation in H9c2 cells. Acridine orange (AO) staining showed that pretreatment with LUTG enhanced lysosomal autophagy. Western blotting indicated that LUTG enhanced autophagy by down-regulating the expression of phospho-extracellular signal regulated kinase1/2 (p-ERK), phospho-protein kinase B (p-Akt) and phospho-mammalian target of rapamycin (p-mTOR). These results suggest that LUTG might act as a promising therapeutic agent for preventing starvation-induced cardiotoxicity by upregulation of autophagy through the Akt/mTOR and ERK signal pathway.

Keywords: Luteolin-7-O-glucoside (LUTG), starvation, autophagy, extracellular signal regulated kinase (ERK), mammalian target of rapamycin (mTOR)

1. Introduction

Cardiomyocyte nutrient deprivation is a common clinical event that mediates various cardiac ischemic processes such as coronary heart disease and heart failure (1,2). In response to starvation, autophagy is upregulated that provides an internal source of nutrients for energy generation and, thus promotes survival (3,4). Autophagy is a process of self-cannibalization in which double-

membrane autophagosomes sequester organelles or portions of cytosol and fuse with lysosomes for breakdown by resident hydrolases (5,6). The resulting breakdown products can be recycled back to the cytosol for reuse during starvation, and are used to generate energy and to build new proteins and membranes (5,6). Autophagy may function primarily as a cytoprotective mechanism, to maintain nutrient and energy homeostasis during starvation conditions (7,8). However, activation of autophagy can also be harmful: excessive autophagy might cause undesirable cell death (9,10). Additional studies are needed to clarify whether autophagy activation serves as an adaptive or maladaptive cardiac response to starvation.

Autophagy is involved in the pathological process of many cardiovascular diseases, and more and more drugs are being studied that can regulate autophagy

Released online in J-STAGE as advance publication October 16, 2017.

*Address correspondence to:

Dr. Xiuzhen Han, Department of Pharmacology, School of Pharmaceutical Sciences, Shandong University, 44 West Wenhua Road, Jinan 250012, Shandong, China.

E-mail: xzyhan@sdu.edu.cn

(2,11). Regulation of autophagy may be an effective mechanism for drug therapy. *Dracocephalum tanguticum* Maxim (Labiatae), a perennial herb distributed in the western region of China, has been used traditionally as folk medicine with a wide range of effects such as anti-hypoxia activity and less toxic side effects for treating gastritis, hepatitis, dizziness, rheumatoid arthritis, and scabies. The herb can effectively scavenge oxygen free radicals to reduce lipid peroxidation and regulate calcium ion stability, and thus protect the myocardial cell from injury. In searching for cardioprotective agents from these natural products, *Dracocephalum tanguticum* Maxim was investigated. We have reported the isolation, structure elucidation and evaluation of antioxidant, and cytoprotective activity of 17 flavonoids along with their preliminary structure-activity relationships (12). The results have demonstrated that flavonoids with OH groups at 3', 4'-position in the B-ring, and a double bond between C-2 and C-3 were necessary for their protective effects against doxorubicin (DOX)-induced cardiotoxicity. LUTG, luteolin-7-O- β -D-glucopyranoside, was isolated from the plants of *Dracocephalum tanguticum* Maxim which had this structure, and the previous study had shown that among all of the tested compounds, LUTG exhibited both a strong antioxidative effect and high protective activity against DOX-induced toxicity. Further investigation found LUTG could decrease DOX-induced death of H9c2 cells, reduce creatine kinase and lactate dehydrogenase levels, and inhibit the elevated intracellular $[Ca^{2+}]$ concentration. LUTG showed a cardioprotective effect by inhibiting the DOX-induced intracellular level of ROS and apoptosis (12,13). Furthermore, pretreatment with LUTG did not decrease the antineoplastic activity of DOX (12). Taken together, LUTG may act as a promising therapeutic agent for preventing the cardiotoxicity induced by DOX. Whether LUTG could protect against starvation-induced cardiomyocyte injury and the underlying mechanisms are not clear.

The mammalian target of rapamycin (mTOR) plays a central role in autophagy by integrating the class I PI3K signaling and amino acid-dependent signaling pathways (10,14). Autophagy is induced by nutrient starvation through the inhibition of mTOR, resulting in translocation of the mTOR substrate complex from the cytosol to certain domains of the endoplasmic reticulum (ER) or closely attached structures (15,16). Otherwise, activation of the phosphatidylinositol 3 kinase/protein kinase B (PI3K/Akt) pathway, by expressing an active form of Akt, or expressing a constitutively active form of 3-phosphoinositide-dependent protein kinase 1 (PDK1), has an inhibitory effect on autophagy (10,17). The mTOR signaling pathway is critical because of its ability to integrate the information from nutrient, metabolic and hormonal signals (10,18). Besides, amino acids inhibit the rapidly accelerated fibrosarcoma-mitogen activated

protein kinase kinase1 (Raf1)/mitogen-activated protein kinase kinase1/2 (MEK1/2)/extracellular signal regulated kinase1/2 (ERK1/2) signaling cascade, leading to inhibition of autophagy (10).

In the present study, we investigated the effects and the related mechanisms of LUTG against starvation-induced cardiotoxicity using H9c2 cells *in vitro*. The results demonstrated that LUTG could prevent cardiomyocytes from starvation-induced injury and the protective effects may be related to upregulation of autophagy through the PI3K/Akt and ERK pathway.

2. Materials and Methods

2.1. Materials and chemicals

LUTG was isolated from *Dracocephalum tanguticum* Maxim by Prof. Ren in our school (12). In the present study, LUTG was dissolved in dimethyl sulfoxide (DMSO) for the *in vitro* assay and stored at a concentration (100 mM) that was diluted with Dulbecco's modified Eagle's medium (DMEM), and a solvent control with DMSO was performed at no more than 2% (v/v).

DMEM and Earle's Balanced Salt Solution (EBSS) were from Gibco BRL (Grand Island, NY, USA). Fetal bovine serum (FBS) was from Tianjin Biotechnology Development Center (Tianjing, China). Bicinchoninic acid (BCA) protein assay kit and radio immunoprecipitation assay (RIPA) buffer were from Beyotime Institute of Biotechnology (Beijing, China). Antibodies against p-Akt and Akt were from Santa Cruz Biotechnology (Santa Cruz, California, USA). Antibody against P44/42-ERK1/2, ERK1/2, P-PTEN, PTEN, P-mTOR, mTOR, P-Beclin1, Beclin1, LC3B and β -actin were from Cell Signaling Technology (Boston, USA). Antibodies against horseradish peroxidase (HRP)-conjugated secondary antibody were from ZSGB-BIO (Beijing, China). 3-Methyladenine (3-MA) was from Millipore (Massachusetts, USA). Phenylmethylsulfonyl fluoride (PMSF), ethylenediamine tetraacetic acid (EDTA), 3-(4,5-dimethyl-2-thiazolyl)-2,5-diphenyl-2-tetrazolium bromide (MTT) and other chemicals were from Sigma.

2.2. Cell Culture

Rat cardiac H9c2 cells (ATCC Rockville, MD, USA) were cultured in DMEM supplemented with 10% heat-inactivated FBS, 100 μ g/mL streptomycin, and 100 U/mL penicillin at 37°C in a humidified atmosphere (5% CO₂-95% air). The cells were fed every 1-2 days, and detached using 0.05 trypsin/0.02% EDTA when they reached about 80-90% confluence. Then cells seeded at an appropriate density according to each experimental design, and the cells used were in the exponential phase of growth before exposure to drugs in all experiments.

2.3. Cell treatment with LUTG

H9c2 cells were seeded at an appropriate density. Following overnight adherence, cells preincubated with or without LUTG (10 and 20 μM) for 24 h followed by starvation (incubation with EBSS) for another 24 h. The concentration of LUTG was used according to the result of the *in vitro* cell proliferation assay. After this incubation, cells were harvested after trypsin digestion by centrifugation (1000 rpm \times 5 min) and parameters were measured as described in materials and methods.

2.4. Cell viability *in vitro*

H9c2 cells were seeded in 96-well plates at a density of 5,000 cells/well. Following overnight adherence, cells were incubated with LUTG (5, 10, 20, 40 and 80 μM) in DMEM supplemented with 10% fetal bovine serum at 37°C for 24 h followed by incubation with EBSS for another 0, 3, 6, 12, and 24 h, and cell viability was determined by MTT assay. Cells were treated with MTT solution (final concentration, 0.5 mg/mL) for 4 h. The supernatants were removed carefully, followed by the addition of 100 μL DMSO to each well to dissolve the precipitate. The absorbance was measured at 570 nm in a microplate reader (Synergy HT).

2.5. Cell cycle measurement

H9c2 cells were cultured in 6-well plates and then starved for 0, 3, 6, 12, 24 h respectively. Cells were harvested and washed, and fixed in cold 70% ethanol overnight, and then suspended in 1 mL propidium iodide (PI) solution (50 $\mu\text{g}/\text{mL}$ DNase-free RNase A) for 30 min. Cell cycle was analyzed using a FACScan Flow Cytometer (Becton Dickinson, New Jersey, USA). The percentages of cells in G0/G1, S and G2/M phases were determined using ModFit LT software 3.0 (Varity Software House, Topsham, USA).

2.6. Detection of intracellular acid phosphatase

The activity of acid phosphatase in the lysosomes increased when the lysosomal degradation (autophagy) was enhanced. To detect the intracellular acid phosphatase, acridine orange (AO) was utilized as an intracellular indicator of acidic phosphatase (19). In this study, H9c2 cells were seeded overnight in 24-well plates, and pretreated without or with LUTG at concentrations of 5, 10 and 20 μM for 24 h, followed by incubation with EBSS for another 12 h. The cells were fixed using 95% ethanol solution for 15 min. H9c2 cells were washed using phosphate buffered saline (PBS) and further incubated with 0.01% AO (500 μL) for another 15 min. The cells were washed 2 times with PBS before being observed and photographed under the fluorescence microscope (IX-7, Olympus, Tokyo, Japan) (400 \times).

2.7. Western blotting analysis

After H9c2 cells were cultured in 6-well plates and treated with conditioned media as indicated, cells were collected and lysed with RIPA buffer on ice for 30 min. The suspension was centrifuged at 13,000 g for 15 min at 4°C, and the supernatant was collected. Protein concentration in total cell lysate was measured using the BCA protein assay kit with bovine serum albumin (BSA) as standard. The other supernatants were stored at -80°C for Western blotting analysis.

After addition of sample loading buffer, protein samples were separated using 12% sodium dodecyl sulfate polyacrylamide gel electrophoresis (SDS-PAGE) and transferred to polyvinylidene difluoride membranes (PVDF) (Millipore Corporation, Massachusetts, USA) in Tris-glycine buffer. The membrane was blocked with 5% (w/v) non-fat dry milk in 20 mM Tris-buffered saline containing 0.1% (v/v) Tween-20 (TBST) for 2 h, followed by incubation with the appropriate primary antibodies at 4°C overnight and then washed three times and exposed to HRP-conjugated secondary antibodies in TBST containing 5% non-fat dry milk for 1 h at room temperature. The primary antibodies included cyclin D1, p21, p-Beclin1, Beclin1, microtubule-associated proteins 1A/1B light chain 3B (MAP1LC3B, LC3B), p-Akt1/2/3, Akt1/2/3, phosphatase and tensin homolog deleted on chromosome ten (PTEN), p-PTEN, p44/42-ERK1/2, ERK1/2, p-mTOR, mTOR and β -actin. The membranes were washed with TBST three times, and the antigen-antibody bands were detected using an enhanced chemiluminescence reagent kit (Millipore, Massachusetts, USA) and quantified by densitometry using a ChemiDoc XRS+ image analyzer (Bio-Rad, California, USA).

2.8. Statistical analyses

Data are described as the mean \pm S.E.M. and analyzed by one-way ANOVA. A *p* value < 0.05 was considered statistically significant. Statistical analysis was performed using the SPSS/Win13.0 software (SPSS, Inc., Chicago, IL).

3. Results

3.1. Effect of starvation on cell viability

To analyze the effects of starvation on the proliferation of H9c2 cells, cell viability was evaluated with the MTT assay. As shown in Figure 1, cell viability was decreased by starvation in a time-dependent manner. There was nearly a 40% decrease in cell viability after 12 hours of starvation compared with the control group (*p* < 0.01).

3.2. Effect of starvation on cell cycle

After H9c2 cells were incubated in starvation medium

for different time durations, cell cycle was measured using flow cytometry and the expression of cell cycle proteins p21 and cyclin D1 were detected by Western blotting. As shown in Figure 2A and 2B, under starvation conditions, the number of myocardial cells in S phase decreased; G0/G1 phase cells increased significantly compared with the normal group. This indicated that starvation induced myocardial cell cycle arrest in the G0/G1 phase, and prevented them from moving to the S phase transformation. As shown in Figure 2C, the

expression of p21 and cyclin D1 continued to decline with time of starvation. This indicated that starvation blocked the myocardial cell cycle by inhibiting the expression of p21 and cyclin D1.

3.3. Effect of starvation on myocardial cell autophagy

To investigate the effect of starvation on myocardial cell autophagy, the expression of p-Beclin1 and LC3B were detected by Western blotting. As shown in Figure 3A, the expression of p-Beclin1 was upregulated, while the expression of LC3B decreased with a longer starvation duration. Autophagy inhibitor 3-MA was used to detect the role of autophagy in the cells under normal and starvation conditions, and validated whether autophagy is conducive to the survival of cells. As shown in Figure 3B, 3-MA and starvation could also decrease the viability of H9c2 cells ($p < 0.01$). Furthermore, 3-MA could more significantly inhibit the viability of H9c2 cells under starvation conditions (compared with starvation, $p < 0.01$). It indicated that autophagy was a protective mechanism for normal cells and cells under starvation.

3.4. Effect of starvation on the expression of Akt and ERK proteins

After H9c2 cells were incubated in starvation medium

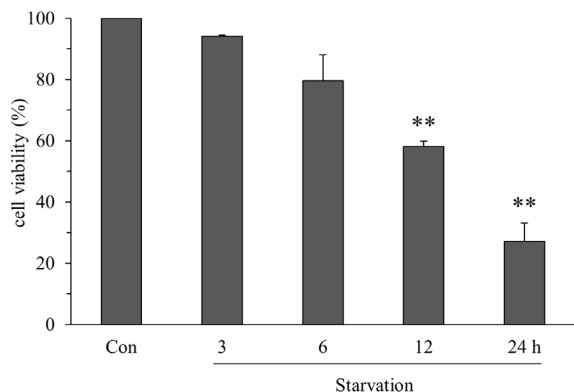


Figure 1. Starvation decreased cell viability in a time-dependent manner. H9c2 cells were incubated in starvation medium (EBSS) for 0, 3, 6, 12, or 24 h respectively. Cell viability was quantified using the MTT assay. ** $p < 0.01$ compared with control.

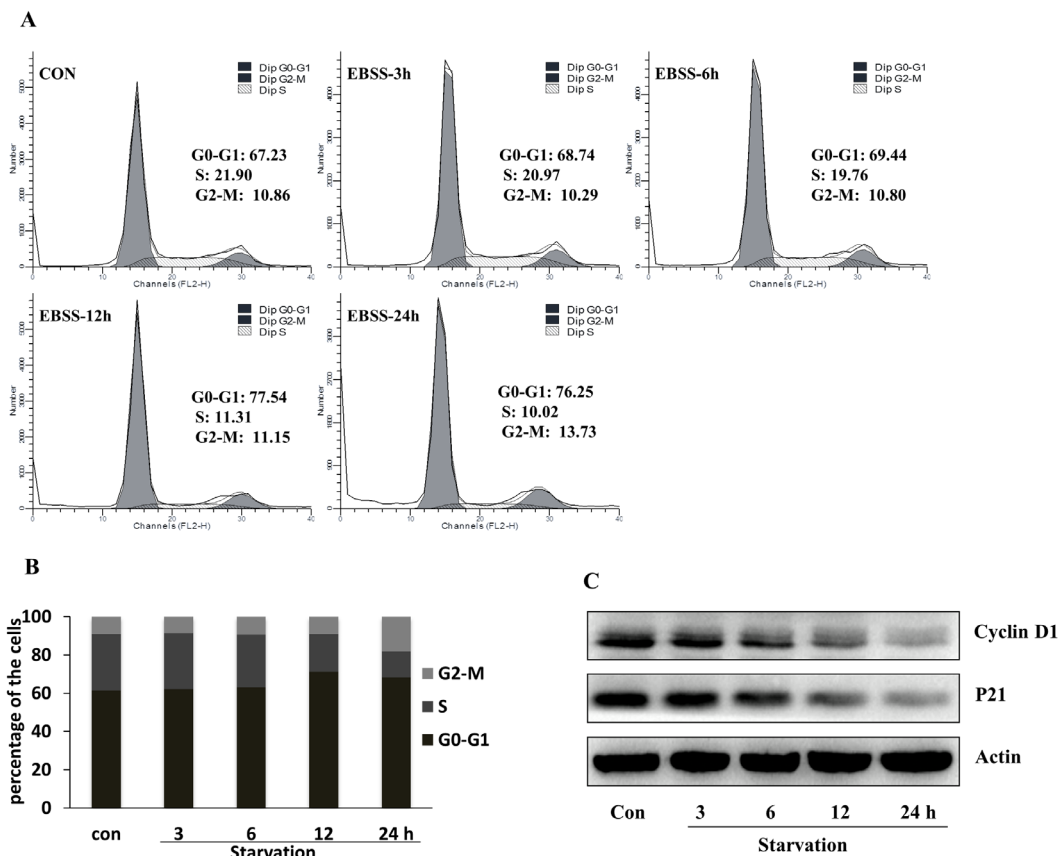


Figure 2. Starvation inhibited the cell cycle. H9c2 cells were incubated in starvation medium for 0, 3, 6, 12, or 24 h respectively, the cell cycle was detected by flow cytometry (A) and the expression of p21 and cyclin D1 were detected by Western blotting (B).

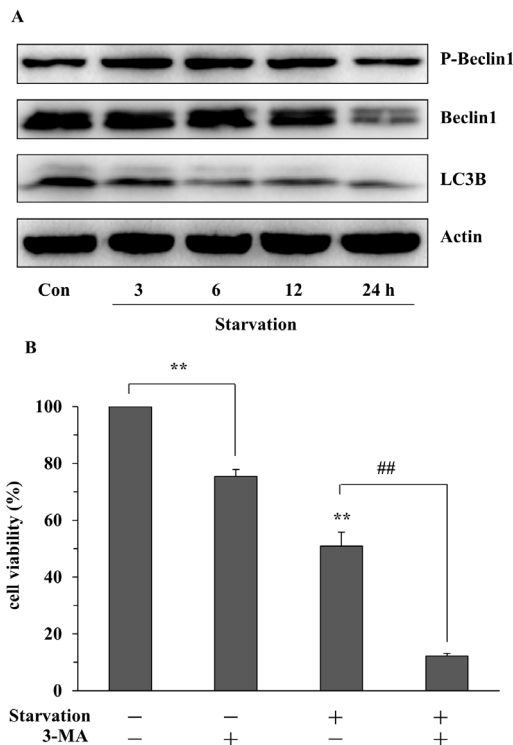


Figure 3. Effects of starvation on autophagy and cell viability. H9c2 cells were incubated in starvation medium for 0, 3, 6, 12, or 24 h respectively, and the expression of autophagy-associated proteins was detected by Western blotting (A). H9c2 cells co-treated with or without 3-MA were incubated in normal or starvation medium. Cell viability was quantified using the MTT assay (B). ** $p < 0.01$ compared with normal group. ### $p < 0.01$ compared with starvation group.

for different durations, the expression of Akt, mTOR, PTEN and ERK were detected by Western blotting. As shown in Figure 4, starvation pretreatment could decrease the expression of p-Akt and p-mTOR. The expression of p-ERK under starvation for 3 h was down-regulated slightly, and was up-regulated after 3 h, but the expression of p-PTEN was not changed. These results indicated that starvation-induced autophagy might be regulating the expression of p-Akt, p-mTOR, and p-ERK.

3.5. Effect of LUTG on cardiomyocyte injury induced by starvation

MTT assay was used to detect the protective effect of LUTG on cell injury induced by starvation. As shown in Figure 5, LUTG (5, 10, and 20 μM) could significantly increase cell viability and protect the H9c2 cells from injury induced by starvation ($p < 0.05$ and $p < 0.01$).

3.6. Effect of LUTG on cardiomyocyte autophagy induced by starvation

To investigate the effect of LUTG on autophagy, the expression of LC3B was detected by Western blotting and autophagy inhibitor 3-MA was used to detect whether the protective effect of LUTG was related to

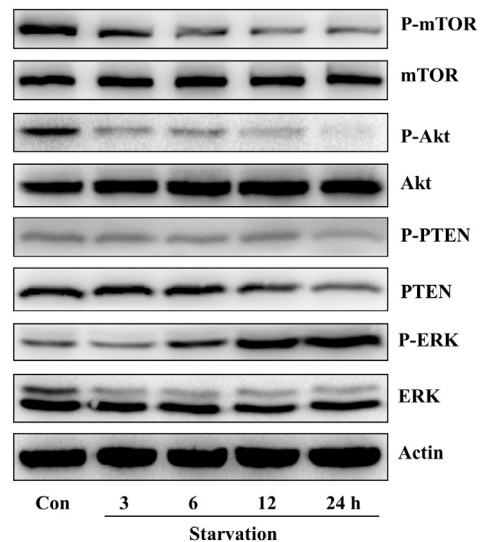


Figure 4. The expression of Akt and ERK proteins in starved H9c2 cells. H9c2 cells were incubated in starvation medium for 0, 3, 6, 12, or 24 h respectively, the expression of Akt and ERK proteins were detected by Western blotting.

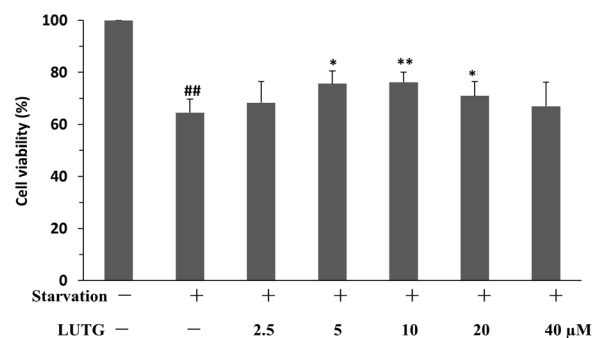


Figure 5. Effects of LUTG on cell viability induced by starvation in H9c2 cells. Cells were incubated without or with LUTG (2.5, 5, 10, 20, and 40 μM) for 24h, followed by incubation with EBSS for another 12h. After this incubation, cell viability was determined with the MTT assay. Values are represented as mean \pm S.E.M. ($n = 6$). ### $p < 0.01$ compared with the normal group; * $p < 0.05$, ** $p < 0.01$ compared with starvation group.

autophagy. As shown in Figures 6A and 6B, LUTG could increase the expression of LC3B and cell viability compared with starvation. 3-MA could reduce the protective effect of LUTG on cell injury induced by starvation. This indicated that LUTG could protect H9c2 cells against starvation-induced injury through enhancing cell autophagy.

To confirm the effect of LUTG on autophagy, AO staining was used to detect lysosomal degradation by measuring the activity of acid phosphatase. AO as an intracellular indicator emits red fluorescence in acidic lysosomes, and displays green fluorescence in neutralized cytosol and nuclei. As shown in Figure 6C, intracellular eosinophilic granules increased under starvation conditions and LUTG further increased the number of red eosinophilic granules in the cell. This indicated that LUTG enhanced lysosomal degradation,

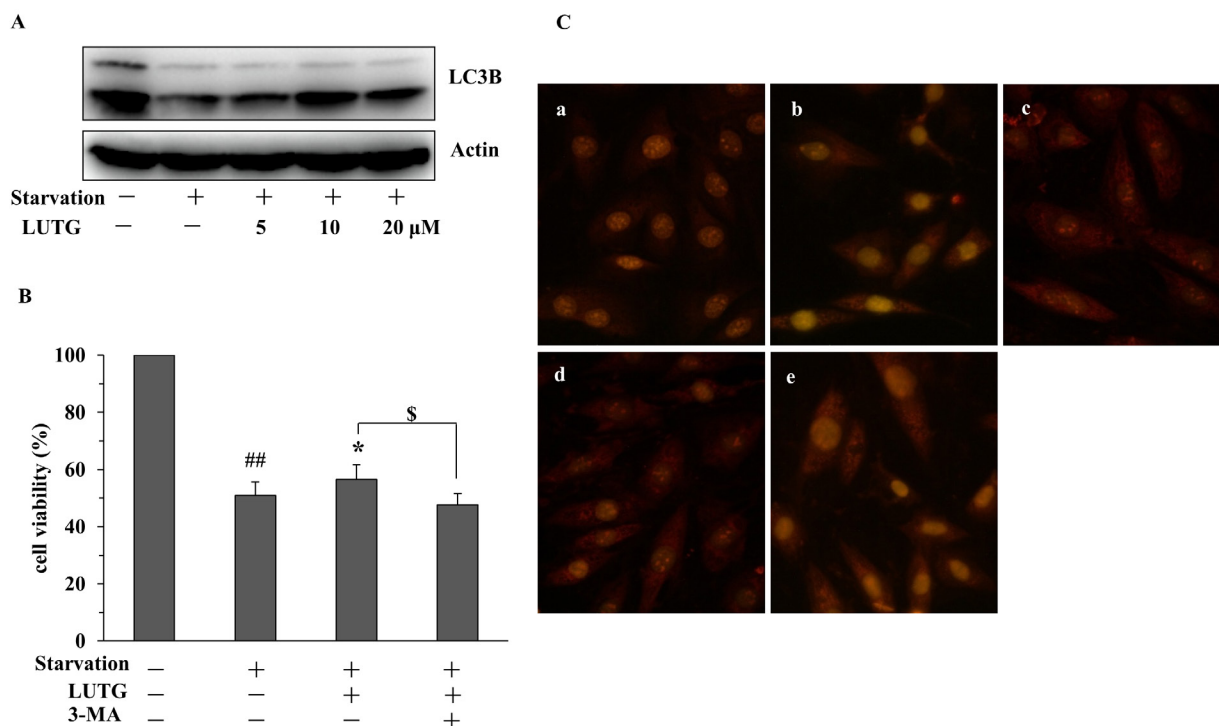


Figure 6. Effect of LUTG on cell autophagy. (A) Western blotting. Cells were incubated without or with LUTG (5, 10, and 20 μM) for 24 h, followed by incubation with EBSS for another 12 h. After this incubation, the expression of LC3B was detected by Western blotting. (B) MTT assay. H9c2 cells pretreated with or without 3-MA and LUTG (10 μM) for 24 h, and incubated in starvation medium for 12 h. Cell viability was detected by MTT assay. ##*p* < 0.01 compared with the normal group; ***p* < 0.01 compared with starvation group; \$*p* < 0.05 compared with LUTG group. (C) Lysosomal degradation. H9c2 cells were pretreated without or with LUTG for 24 h, followed by incubation with EBSS for another 12 h. Morphology of H9c2 cells was assessed using a fluorescence microscope (×400) equipped with quick imaging system without/with AO staining. (a) Control; (b) Starvation; (c) 5 μM LUTG plus starvation; (d) 10 μM LUTG plus starvation; (e) 20 μM LUTG plus starvation.

that is, the enhancement of autophagy.

3.7. Effect of LUTG on the expression of p-Akt, p-mTOR, and p-ERK proteins

To investigate the protective mechanisms of LUTG on H9c2 cell injury induced by starvation, the expression of p-mTOR, p-ERK and p-Akt proteins was detected by Western blotting. As shown in Figure 7, under starvation conditions, the expression of p-ERK increased; and the expression of p-mTOR, p-Akt, and p21 decreased. LUTG upregulated the expression of p21, inhibited the expression of p-ERK and further down regulated the expression of p-Akt and p-mTOR. This indicated that LUTG protected against injury induced by starvation in H9c2 cells by regulating the Akt/mTOR and ERK signaling pathways.

4. Discussion

Autophagy is a conserved cellular pathway that controls protein and organelle degradation, and has essential roles in survival, development and homeostasis (3,10). It is rapidly regulated by nutrient starvation, growth factor withdrawal, or oxidative damage. Because cardiac myocytes are terminally differentiated, cellular degradation *via* autophagy plays an important role in

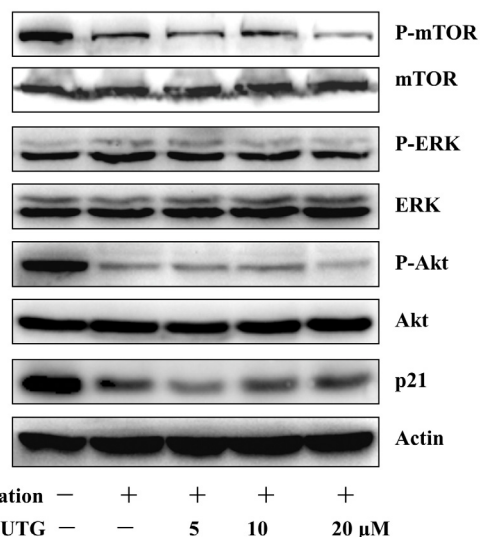


Figure 7. Effects of LUTG on the expression of p-Akt, p-ERK, p-mTOR and p21 in H9c2 cells. After 24 h of treatment without or with LUTG (5, 10, and 20 μM), cardiomyocytes were starved for another 24 h. The expression of p-Akt, p-ERK, p-mTOR, and p21 was detected by Western blotting.

the homeostasis of cardiac cells (20,21). In addition, cardiomyocyte nutrient deprivation is a common clinical event that mediates various cardiac ischemic

References

1. Ahn J, Kim J. Nutritional status and cardiac autophagy. *Diabetes Metab J.* 2013; 37:30-35.
2. Liao LZ, Chen YL, Lu LH, Zhao YH, Guo HL, Wu WK. Polysaccharide from Fuzi likely protects against starvation-induced cytotoxicity in H9c2 cells by increasing autophagy through activation of the AMPK/mTOR pathway. *Am J Chin Med.* 2013; 41:353-367.
3. Jia G, Sowers JR. Autophagy: A housekeeper in cardiorenal metabolic health and disease. *Biochim Biophys Acta.* 2015; 1852:219-224.
4. Ouyang C, You J, Xie Z. The interplay between autophagy and apoptosis in the diabetic heart. *J Mol Cell Cardiol.* 2014; 71:71-80.
5. Gatica D, Chiong M, Lavandero S, Klionsky DJ. Molecular mechanisms of autophagy in the cardiovascular system. *Circ Res.* 2015; 116:456-467.
6. Rabinowitz JD, White E. Autophagy and metabolism. *Science.* 2010; 330:1344-1348.
7. Orogo AM, Gustafsson ÅB. Therapeutic targeting of autophagy: Potential and concerns in treating cardiovascular disease. *Circ Res.* 2015; 116:489-503.
8. Troncoso R, Vicencio JM, Parra V, *et al.* Energy-preserving effects of IGF-1 antagonize starvation-induced cardiac autophagy. *Cardiovasc Res.* 2012; 93:320-329.
9. Schiattarella GG, Hill JA. Therapeutic targeting of autophagy in cardiovascular disease. *J Mol Cell Cardiol.* 2016; 95:86-93.
10. Yang Z, Klionsky DJ. Eaten alive: A history of macroautophagy. *Nat Cell Biol.* 2010; 12:814-822.
11. Salabei JK, Conklin DJ. Cardiovascular autophagy: Crossroads of pathology, pharmacology and toxicology. *Cardiovasc Toxicol.* 2013; 13:220-229.
12. Wang SQ, Han XZ, Li X, Ren DM, Wang XN, Lou HX. Flavonoids from *Dracocephalum tanguticum* and their cardioprotective effects against doxorubicin-induced toxicity in H9c2 cells. *Bioorg Med Chem Lett.* 2010; 20:6411-6415.
13. Yao H, Shang Z, Wang P, Li S, Zhang Q, Tian H, Ren D, Han X. Protection of luteolin-7-O-glucoside against doxorubicin-induced injury through PTEN/Akt and ERK pathway in H9c2 cells. *Cardiovasc Toxicol.* 2016; 16:101-110.
14. Tan VP, Miyamoto S. Nutrient-sensing mTORC1: Integration of metabolic and autophagic signals. *J Mol Cell Cardiol.* 2016; 95:31-41.
15. Levine B, Mizushima N, Virgin HW. Autophagy in immunity and inflammation. *Nature.* 2011; 469:323-335.
16. Kim J, Guan KL. Regulation of the autophagy initiating kinase ULK1 by nutrients: Roles of mTORC1 and AMPK. *Cell Cycle.* 2011; 10:1337-1338.
17. Zhang H, Gong Y, Wang Z, Jiang L, Chen R, Fan X, Zhu H, Han L, Li X, Xiao J, Kong X. Apelin inhibits the proliferation and migration of rat PSMCs *via* the activation of PI3K/Akt/mTOR signal and the inhibition of autophagy under hypoxia. *J Cell Mol Med.* 2014; 18:542-553.
18. Russell RC, Yuan HX, Guan KL. Autophagy regulation by nutrient signaling. *Cell Res.* 2014; 24:42-57.
19. Wan Z, Mao H, Guo M, Li Y, Zhu A, Yang H, He H, Shen J, Zhou L, Jiang Z, Ge C, Chen X, Yang X, Liu G, Chen H. Highly efficient hierarchical micelles integrating photothermal therapy and singlet oxygen-synergized chemotherapy for cancer eradication. *Theranostics.* 2014; 4:399-411.
20. Adams B, Mapanga RF, Essop MF. Partial inhibition of the ubiquitin-proteasome system ameliorates cardiac dysfunction following ischemia-reperfusion in the presence of high glucose. *Cardiovasc Diabetol.* 2015; 14:94.
21. Gurusamy N, Lekli I, Mukherjee S, Ray D, Ahsan MK, Gherghiceanu M, Popescu LM, Das DK. Cardioprotection by resveratrol: A novel mechanism *via* autophagy involving the mTORC2 pathway. *Cardiovasc Res.* 2010; 86:103-112.
22. Jing K, Lim K. Why is autophagy important in human diseases? *Exp Mol Med.* 2012; 44:69-72.
23. Suzuki SW, Onodera J, Ohsumi Y. Starvation induced cell death in autophagy-defective yeast mutants is caused by mitochondria dysfunction. *PLoS One.* 2011; 6:e17412.
24. Aki T, Yamaguchi K, Fujimiya T, Mizukami Y. Phosphoinositide 3-kinase accelerates autophagic cell death during glucose deprivation in the rat cardiomyocyte-derived cell line H9c2. *Oncogene.* 2003; 22:8529-8535.
25. Dunlop EA, Tee AR. mTOR and autophagy: A dynamic relationship governed by nutrients and energy. *Semin Cell Dev Biol.* 2014; 36:121-129.
26. Shinojima N, Yokoyama T, Kondo Y, Kondo S. Roles of the Akt/mTOR/p70S6K and ERK1/2 signaling pathways in curcumin-induced autophagy. *Autophagy.* 2007; 3:635-637.
27. Wang J, Whiteman MW, Lian H, Wang G, Singh A, Huang D, Denmark T. A non-canonical MEK/ERK signaling pathway regulates autophagy *via* regulating Beclin 1. *J Biol Chem.* 2009; 284:21412-21424.
28. Kaminsky VO, Zhivotovsky B. Free radicals in cross talk between autophagy and apoptosis. *Antioxid Redox Signal.* 2014; 21:86-102.
29. Efeyan A, Zoncu R, Chang S, Gumper I, Snitkin H, Wolfson RL, Kirak O, Sabatini DD, Sabatini DM. Regulation of mTORC1 by the Rag GTPases is necessary for neonatal autophagy and survival. *Nature.* 2013; 493:679-683.
30. Yao H, Han X, Han X. The cardioprotection of insulin-mediated PI3K/Akt/mTOR signaling pathway. *Am J Cardiovasc Drugs.* 2014; 14:433-442.
31. Russell RC, Yuan HX, Guan KL. Autophagy regulation by nutrient signaling. *Cell Res.* 2014; 24:42-57.
32. Wu Z, Hu CA, Wu G, Zhaorigetu S, Chand H, Sun K, Ji Y, Wang B, Dai Z, Walton B, Miao Y, Hou Y. Intimacy and a deadly feud: The interplay of autophagy and apoptosis mediated by amino acids. *Amino Acids.* 2015; 47:2089-2099.
33. Ahn J, Kim J. Nutritional status and cardiac autophagy. *Diabetes Metab J.* 2013; 37:30-35.

(Received May 11, 2017; Revised August 26, 2017; Accepted September 26, 2017)

Induction of apoptosis by ethanol extract of *Citrus unshiu* Markovich peel in human bladder cancer T24 cells through ROS-mediated inactivation of the PI3K/Akt pathway

Kyu Im Ahn^{1,2,3}, Eun Ok Choi^{1,2}, Da He Kwon^{1,2}, Hyun HwangBo^{1,2}, Min Yeong Kim^{1,2}, Hong Jae Kim^{1,2}, Seon Yeong Ji^{1,2}, Su-Hyun Hong^{1,2}, Jin-Woo Jeong^{1,2}, Cheol Park⁴, Nam Deuk Kim³, Wun Jae Kim^{5,*}, Yung Hyun Choi^{1,2,*}

¹ Open Laboratory for Muscular and Skeletal Disease, and Department of Biochemistry, Donggeui University College of Korean Medicine, Busan, Korea;

² Anti-Aging Research Center, Donggeui University, Busan, Korea;

³ Department of Pharmacy, Molecular Inflammation Research Center for Aging Intervention, Pusan National University, Busan, Korea;

⁴ Department of Molecular Biology, College of Natural Sciences, Donggeui University, Busan, Korea;

⁵ Personalized Tumor Engineering Research Center, Department of Urology, Chungbuk National University College of Medicine, Cheongju, Korea.

Summary

Citrus unshiu peel has been used to prevent and treat various diseases in traditional East-Asian medicine including in Korea. Extracts of *C. unshiu* peel are known to have various pharmacological effects including antioxidant, anti-inflammatory, and antibacterial properties. Although the possibility of their anti-cancer activity has recently been reported, the exact mechanisms in human cancer cells have not been sufficiently studied. In this study, the inhibitory effect of ethanol extract of *C. unshiu* peel (EECU) on the growth of human bladder cancer T24 cells was evaluated and the underlying mechanism was investigated. The present study demonstrated that the suppression of T24 cell viability by EECU is associated with apoptosis induction. EECU-induced apoptosis was found to correlate with an activation of caspase-8, -9, and -3 in concomitance with a decrease in the expression of the inhibitor of apoptosis family of proteins and an increase in the Bax:Bcl-2 ratio accompanied by the proteolytic degradation of poly(ADP-ribose) polymerase. EECU also increased the generation of reactive oxygen species (ROS), collapse of mitochondrial membrane potential, and cytochrome c release to the cytosol, along with a truncation of Bid. In addition, EECU inactivated phosphatidylinositol 3-kinase (PI3K) as well as Akt, a downstream molecular target of PI3K, and LY294002, a specific PI3K inhibitor significantly enhanced EECU-induced apoptosis and cell viability reduction. However, N-acetyl cysteine, a general ROS scavenger, completely reversed the EECU-induced dephosphorylation of PI3K and Akt, as well as cell apoptosis. Taken together, these findings suggest that EECU inhibits T24 cell proliferation by activating intrinsic and extrinsic apoptosis pathways through a ROS-mediated inactivation of the PI3K/Akt pathway.

Keywords: *Citrus unshiu* peel, apoptosis, PI3K/Akt, ROS

Released online in J-STAGE as advance publication October 24, 2017.

*Address correspondence to:

Dr. Wun-Jae Kim, Department of Urology, Chungbuk National University College of Medicine, Cheongju 28644, Republic of Korea.

E-mail: wjkim@chungbuk.ac.kr

Dr Yung-Hyun Choi, Department of Biochemistry, College of Korean Medicine, Donggeui University, Busan 47227, Republic of Korea.

E-mail: choiyh@deu.ac.kr

1. Introduction

The progression of cancer is a multistep process involving genetic modification, and the deregulation or mutation of particular genes is likely to be a marker for certain cancers. Bladder cancer has been known as one of the most frequent urological malignancies with a high incidence and mortality rate (1,2). Although recent advances in treatment have led to increased survival rates for patients with bladder cancer, the incidence

and mortality rates are still increasing (3,4). Therefore, it is imperative to understand the basic mechanisms of bladder cancer progression and to find new biological targets and effective treatment strategies for bladder cancer prevention and treatment.

Recently, several modes of programmed cell death associated with the inhibition of the proliferation of cancer cells by chemotherapeutic drugs have been described (5,6). Among them, apoptosis, the most typical cell death mechanism, can be triggered through either a death receptor (DR)-initiated extrinsic pathway or a mitochondria-mediated intrinsic pathway characterized by the activation of common caspases (7,8). The extrinsic pathway triggers apoptosis through the binding of death ligands to the DRs, which activates the caspase cascade from the upstream initiator caspase-8 to the downstream effector caspases, including caspase-3 and -7, by recruiting adapter molecules (9,10). The intrinsic pathway is mainly regulated by the interaction between the Bcl-2 family of proteins composed of proteins capable of promoting or inhibiting apoptosis, which is also associated with impaired mitochondrial function. This in turn promotes the release of apoptotic factors such as cytochrome *c* from the mitochondria to the cytoplasm, activating caspase-9, ultimately leading to a caspase cascade pathway that activates the effector caspases (7,11). Although reactive oxygen species (ROS) act as major regulators of cell survival and proliferation, excessive production of ROS causes irreversible cellular damage in various cell death types (12,13). In addition, the induction of cancer cell death associated with mitochondrial dysfunction in the intrinsic apoptosis pathway is often connected with the overproduction of ROS (14,15).

Such apoptosis induction is complexly regulated by the activation and inactivation of various intracellular signal pathways in the cell. Among them, the phosphatidylinositol 3-kinase (PI3K) is abnormally activated or mutated in many tumors, including bladder cancer, and its activation is one of the most important tumorigenic pathways in cancer (16,17). PI3K induces the activation of Akt, a downstream effector of PI3K, through the phosphorylation of major amino acid residues such as Thr 308 and Ser 473 to stimulate cancer proliferation (18,19). Therefore, many clinical trials are urgently needed to find new agents that interfere with the signaling of PI3K pathway components. Interestingly, many previous studies show that increased production of ROS and inactivation of the PI3K/Akt signal pathway are related to the induction of cancer cell apoptosis (20-22). Although studies on the role of ROS production in PI3K/Akt inactivation have not been fully understood, ROS-dependent PI3K/Akt signaling pathway blockade may be a potential therapeutic target for inducing apoptosis in cancer cells (23,24).

Recently, the discovery of cancer substances using natural compounds, especially plant-derived

compounds, has received considerable interest. *Citrus unshiu* Markovich, which belongs to the Rutaceae family, is a citrus fruit that is readily seeded, has no seeds, and is grown in East-Asian countries, including Korea (25,26). For several hundred years, citrus and dried peel have been used as traditional medicines to treat gastrointestinal disorders, colds, indigestion, and bronchial discomfort, and pharmacological activities have been reported for inflammation, allergies, diabetes, and viral infections (27-30). A study on a tumor-bearing mouse model has shown that *C. unshiu* peel (Chimpi) extract inhibits tumor growth, which was associated with an increased production of cytokines such as interferon- γ and tumor necrosis factor- α (31). In addition, Kim *et al.* (32) reported that *C. unshiu* peel reduces systemic inflammation in tumor-bearing mice and inhibits the production of pro-cacheche factors in tumors with the prevention of skeletal muscle atrophy and weight loss. It has also been reported that polysaccharides or flavonoids found in the *C. unshiu* peel can inhibit the metastasis of cancer cells (33,34); however, the evidence for the therapeutic potentials of *C. unshiu* peel against human cancer cells and the molecular pathways involved in suppression of cancer cell apoptosis remain unclear. Therefore, we investigated the anti-cancer effects of ethanol extract of *C. unshiu* peel (EECU) in human bladder cancer T24 cells. In this study, we found for the first time that EECU triggered apoptotic cell death through the ROS-mediated inactivation of the PI3K/Akt pathway.

2. Materials and Methods

2.1. Preparation of EECU

For the preparation of EECU, the dried peel of *C. unshiu* was provided from Dongeui Korean Medical Center (Busan, Republic of Korea) and pulverized into a fine powder. The powder (100 g) was extracted in 1 L of 70% ethanol by sonication for 24 h. After filtering, the filtrate was concentrated with a vacuum rotary evaporator (BUCHI, Switzerland) and the residue was freeze-dried in a freezing-dryer, and then stored at -80°C . The powder was dissolved in dimethyl sulfoxide (DMSO, Sigma-Aldrich Chemical Co., St. Louis, MO, USA) to a final concentration of 100 mg/mL (extract stock solution), and was stored at 4°C . The stock solution was diluted with medium to the desired concentrations prior to use.

2.2. Cell culture

Human urinary bladder transitional cell carcinoma T24 cells were obtained from American Type Culture Collection (Manassas, VA, USA). The cells were maintained in RPMI 1640 medium (WelGENE Inc., Daegu, Republic of Korea), supplemented with 10%

fetal bovine serum (FBS, WelGENE Inc.), 2 mM L-glutamine, 100 U/mL penicillin, and 100 mg/mL streptomycin (WelGENE Inc.) at 37°C in a humidified incubator containing 5% CO₂.

2.3. Cell viability assay and morphological observation

To assess the effects of EECU on T24 cell viability, the cells were plated at a density of 2×10^4 cells per well in a 24-well plate. After overnight incubation, the cells were treated with different concentrations of EECU for 48 h. Following treatment, the culture medium containing EECU was carefully removed and 200 µL of 0.1 mg/mL 3-(4,5-dimethylthiazol)-2,5-diphenyltetrazolium bromide (MTT, Sigma-Aldrich Chemical Co.) solution were added to each well for 2 h at 37°C, prior to dissolving the formazan product using DMSO. The viability of the cells was measured by absorption at 450 nm using an enzyme-linked immunosorbent assay (ELISA) reader (Molecular Devices, Silicon Valley, CA, USA). The mean percentages of viable cells \pm standard deviation (SD) generated from three independent experiments were calculated. The cells in each well were observed under an inverted microscope (Carl Zeiss, Oberkochen, Germany) and were then photographed.

2.4. Colony formation assay

After treatment with different concentrations of EECU for 48 h, single-cell suspensions were prepared by trypsinization and the cells were then seeded into 6-well plates (500 cells/well). The cells were further cultured for two weeks to allow the formation of colonies. The colonies were fixed with 3.7% paraformaldehyde (Sigma-Aldrich Chemical Co.), stained with 0.1% crystal violet solution (Sigma-Aldrich Chemical Co.) for 10 min, washed, and then imaged under an inverted microscope.

2.5. Detection of apoptotic morphological changes

Apoptotic cells containing chromatin condensation and nuclear fragmentation in the nuclei were detected by 4',6-diamidino-2-phenylindole (DAPI, Sigma-Aldrich Chemical Co.) staining. After treatment with EECU, the cells were harvested, washed twice with phosphate-buffered saline (PBS), and fixed with 3.7% paraformaldehyde in PBS for 10 min at 25°C. The cells were washed with PBS, stained with 1 mg/mL of DAPI solution for 10 min, and then washed twice with PBS. The morphology changes in the nucleus were examined using a fluorescence microscope (Carl Zeiss).

2.6. Determination of cell apoptosis by flow cytometry

To determine the magnitude of the apoptosis by EECU, the Annexin V-fluorescein isothiocyanate (FITC)

Apoptosis Detection Kit (BD Biosciences, Franklin Lakes, NJ, USA) was used as described previously (35). Briefly, both attached and floating cells were collected and then washed twice with ice old PBS (resuspended in 500 µL binding buffer). The cells were stained with FITC-conjugated annexin V and propidium iodide (PI) at room temperature for 15 min in the dark. Subsequently, the cells were analyzed using a flow cytometer (Becton Dickinson, San Jose, CA, USA) according to the manufacturer's protocol.

2.7. Protein isolation and Western blot analysis

Following incubation for 48 h with different concentrations of EECU, the cells were lysed in a protein extraction buffer supplemented with a protease inhibitor cocktail (Roche Diagnostics, Basel, Switzerland). For the preparation of mitochondrial and cytosolic extracts of cells, NE-PER nuclear and cytoplasmic extraction reagents (Thermo Fisher Scientific Inc., Waltham, Utah, USA) were applied according to the manufacturer's instructions. Protein concentration was measured with the Bio-Rad protein assay kit (Bio-Rad Laboratories, Hercules, CA, USA) following the manufacturer's instructions. For Western blotting, equal amounts of proteins were separated by sodium dodecyl sulfate (SDS)-polyacrylamide gel electrophoresis and were transferred onto a polyvinylidene fluoride (PVDF) membrane (Schleicher & Schuell, Keene, NH, USA) using an electrophoretic transfer system (Bio-Rad Laboratories). The membranes were blocked in 5% (w/v) skim milk powder in Tris-buffered saline containing 0.1% Tween-20 (TBST buffer) for 1 h at room temperature. After washing with TBST buffer, the membranes were probed with specific primary antibodies purchased from Santa Cruz Biotechnology, Inc. (Santa Cruz, CA, USA) and Cell Signaling Technology, Inc. (Danvers, MA, USA) at 4°C overnight, and then incubated with the appropriate horseradish peroxidase (HRP)-conjugated secondary antibodies (Amersham Life Science, Arlington Heights, IL, USA). The protein bands were visualized using an enhanced chemiluminescence (ECL) kit (Amersham Life Science), according to the manufacturer's instructions.

2.8. Analysis of caspase enzymatic activity

The activities of the caspases (caspase-3, -8, and -9) were detected using colorimetric assay kits (R&D Systems, Minneapolis, MN, USA), according to the manufacturer's protocol. Briefly, the cells were lysed in the supplied lysis buffer. Equal amounts of proteins were incubated with the supplied reaction buffer containing dithiothreitol and synthetic tetrapeptides [Asp-Glu-Val-Asp (DEAD) for caspase-3; Ile-Glu-Thr-Asp (IETD) for caspase-8; and Leu-Glu-His-Asp (LEHD) for caspase-9] labeled with p-nitroaniline

(pNA) that is linked to the end of the caspase-specific substrate at 37°C for 2 h in the dark. The reactions of each sample were measured by changes in absorbance at 405 nm using an ELISA reader.

2.9. Determination of mitochondrial membrane potential ($\Delta\psi_m$)

The changes of the MMP values in the EECU-treated cells were examined using 5,5',6,6'-tetrachloro-1,1',3,3'-tetraethyl-imidacarbocyanine iodide (JC-1, Sigma-Aldrich Chemical Co.), a dual-emission potential-sensitive probe. Briefly, the cells were harvested and washed with cold PBS, and incubated with 10 μ M JC-1 for 30 min at 37°C in the dark. Then, the stained cells were washed twice with PBS to remove unbound dye, and the amount of JC-1 retained by 10,000 cells per sample was measured at 488 nm and 575 nm using a flow cytometer, following the manufacturer's protocol instructions.

2.10. Measurement of ROS generation

For the detection of intracellular ROS production, 2',7'-dichlorofluorescein diacetate (DCF-DA, Molecular Probes, Leiden, Netherlands) dye was used according to the manufacturer's instructions (36). Briefly, after collecting the cells treated with EECU for a certain period of time, the cells were rinsed with PBS and then loaded with 10 μ M DCF-DA for 20 min at 37°C in a dark room. The cells were immediately washed, resuspended in PBS, and analyzed to determine the fluorescence intensity using a flow cytometer. To confirm whether the intracellular ROS levels play a role in the cytotoxicity of EECU, the cells were pre-treated with N-acetyl cysteine (NAC, Sigma-Aldrich Chemicals Co.), a well established antioxidant, for 1 h prior to treatment with EECU. The stained cells were also mounted on a chamber slide with a mounting medium. The images were obtained under a fluorescence microscope.

2.11. Data analysis

The experimental results were presented as mean \pm SD of experiments repeated at least three times. For each treatment group, the statistical significance was compared with that of other groups, and was verified using a one-way ANOVA or Student *t*-test method. A *p* < 0.05 was considered to indicate a statistically significant result.

3. Results

3.1. EECU inhibits cell growth and colony forming property of T24 cells

To determine the inhibitory effect of EECU on T24 cell

growth, an MTT assay was performed. The obtained results indicated that EECU was shown to inhibit the cell survival rate against T24 cells in a concentration-dependent manner (Figure 1A) and accompanied by various morphological changes including membrane blebbing, diminished cell density, poor adherence, and increased number of floating cells (Figure 1B). In the cologenic assay, EECU also significantly reduced the number of colonies of T24 cells that depended on treatment concentration compared with the control group (Figure 1C), indicating that the ability to form colonies by the EECU-treated T24 cells was lost.

3.2. EECU induces apoptosis in T24 cells

To determine whether EECU treatment led to growth reduction due to apoptosis induction, the changes of nucleus morphology by DAPI staining and cell death rate using flow cytometry were investigated. The results of DAPI staining showed that nuclear fragmentation and chromatin condensation found in apoptotic cells increased in the EECU-treated cells compared to the untreated control cells (Figure 1D). In addition, the results from the flow cytometry showed that the

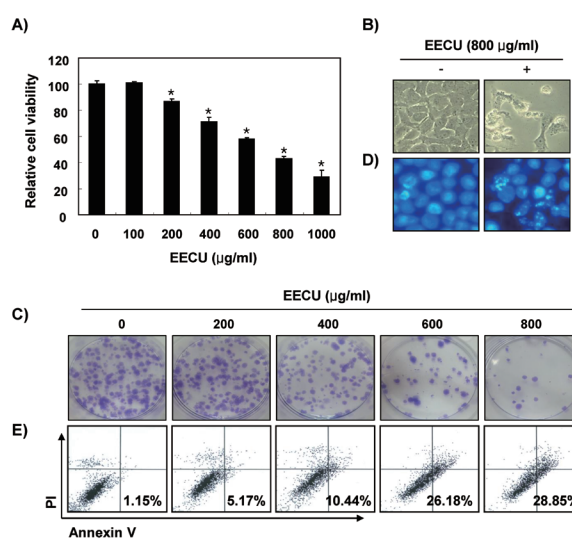


Figure 1. Inhibition of cell viability and induction of apoptosis by EECU in T24 cells. T24 cells were treated with various concentrations of EECU for 48 h. (A) The cell viability was measured by an MTT assay. The data were expressed as the mean \pm SD of three independent experiments (**p* < 0.05 vs. untreated control). (B) The morphological change of MDA-MB-231 cells treated with 800 μ g/mL EECU was observed under an inverted microscope (magnification, \times 200). (C) The cells were exposed to the indicated concentrations of EECU for 48 h and were allowed to form colonies for 14 days. The representative photographs are shown. (D) The cells were fixed and stained with DAPI solution. Stained nuclei were then observed with a fluorescence microscope (original magnification, \times 400). (E) The degree of apoptosis induced by EECU was determined in cells stained with FITC-conjugated Annexin V and PI, and subjected to flow cytometry analysis. Apoptotic cells are determined by counting the % of annexin V/PI cells. Each point represents the means of two independent experiments.

percentage of apoptotic cells was markedly increased in the EECU treatment groups in a concentration-dependent manner (Figure 1E). These data collectively indicate that EECU suppressed cell viability and colony formation by inducing apoptosis in the T24 cells.

3.3. EECU activates caspases in T24 cells

In order to investigate whether the activation of caspases plays a role in EECU-induced T24 cell apoptosis, the levels of caspase-8, -9, and -3 were measured following treatment with various concentrations of EECU. The results revealed that the expression of pro-caspase-8, an initiator caspase of the extrinsic apoptosis pathway, decreased with increasing EECU concentration, while the expression of active-caspase-8 increased (Figure 2A). Although the expression of the active-caspase-9, an initiator caspase of the extrinsic apoptosis pathway, was not detected, the expression of its pro-forms was apparently suppressed depending on the EECU treatment concentration. Our immunoblotting results also revealed a concentration-dependent decrease in caspase-3 pro-form expression, a typical effector caspase, and progressive proteolytic cleavage of poly(ADP-ribose) polymerase (PARP), which is a representative substrate protein of activated effector caspases. Consistent with immunoblotting results, the *in vitro* activity of the three examined caspases was significantly enhanced by EECU treatment (Figure 3B), which was associated with the

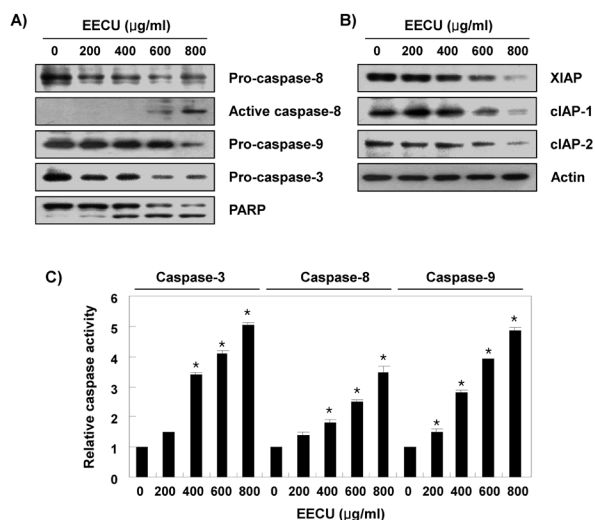


Figure 2. Activation of caspases, degradation of PARP, and inhibition of IAP family proteins expression by EECU in T24 cells. T24 cells were treated with the indicated concentrations of EECU for 48 h. (A and B) The cell lysates were prepared and equal amounts of cellular proteins were separated on SDS-polyacrylamide gels and transferred to PVDF membranes. The membranes were probed with the indicated antibodies and the proteins were visualized using an ECL detection system. Actin was used as an internal control. (C) The activities of caspases were evaluated using caspases colorimetric assay kits. The data were expressed as the mean \pm SD of three independent experiments (* $p < 0.05$ vs. untreated control).

down-regulation of the inhibitor of apoptosis proteins (IAP) family members such as XIAP, cIAP-1, and cIAP-2 (Figure 2C).

3.4. EECU modulates the expression of DR-related and Bcl-2 family proteins in T24 cells

Because the results of Figure 2 show the possibility that two apoptotic pathways may be involved in the induction of apoptosis by EECU, we then evaluated the effect of EECU on the expression of DR-related and Bcl-2 family proteins. The Western blotting data indicated that the expressions of TNF-related apoptosis-inducing ligand (TRAIL), DR4, Fas, and Fas ligand (FasL) increased in response to EECU treatment in a concentration-dependent fashion, even though the expression of DR5 was not changed (Figure 3). In addition, among the Bcl-2 family proteins, the expression of pro-apoptotic Bax was markedly increased when compared with those levels in the control groups, whereas the anti-apoptotic Bcl-2 expression was reduced by EECU treatment. Furthermore, the levels of total Bid expression decreased due to EECU treatment, but truncated Bid (tBid) expression progressively increased depending on the EECU treatment concentration.

3.5. EECU enhances the disruption of MMP and release of cytochrome c in T24 cells

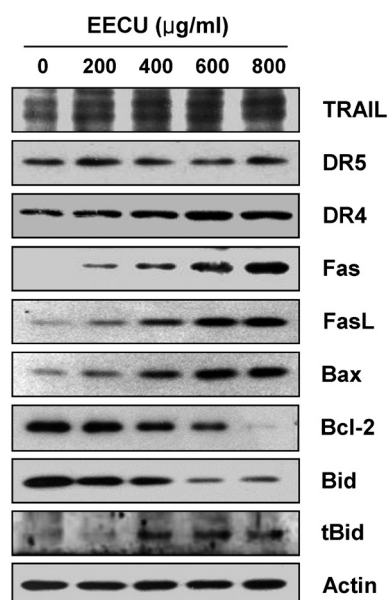


Figure 3. Effects of EECU on the levels of DR-related and Bcl-2 family proteins in T24 cells. After 48 h incubation with the indicated concentrations of EECU, the cells were lysed, and cellular proteins were separated by SDS-polyacrylamide gel electrophoresis and transferred to membranes. The membranes were probed with the indicated antibodies. Proteins were visualized using an ECL detection system. Equal protein loading was confirmed by analysis of actin in the protein extracts.

To further investigate whether mitochondrial dysfunction is involved in the induction of apoptosis by EECU, we determined the effects of EECU on MMP values. As shown in Figure 4A, the frequency of cells with JC-1 monomers, which are predominant in the region with low MMP (lower right quadrant of fluorescence cytogram), the concentration-dependency increased in the EECU-treated T24 cells, revealing that EECU markedly destroys the integrity of the mitochondria measured by the concentration-dependent loss of MMP (Figure 4A). Subsequently, an increase of cytochrome *c* protein level in cytoplasm was obviously observed upon treatment

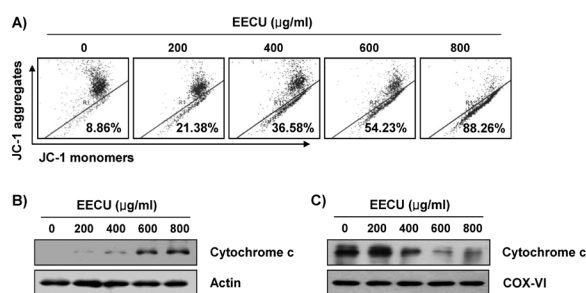


Figure 4. Effects of EECU on the levels of MMP values and cytochrome *c* expression in T24 cells. (A) After 48 h incubation with the indicated concentrations of EECU, the cells were stained with JC-1 dye and were then analyzed on a flow cytometer in order to evaluate the changes in MMP. The data are expressed as the mean of two independent experiments. (B and C) Cells cultured under the same conditions were lysed, and cytosolic and mitochondrial proteins were separated by SDS polyacrylamide gel electrophoresis and transferred to the membranes. The membranes were probed with anti-cytochrome *c* antibody. Proteins were visualized using an ECL detection system. Equal protein loading was confirmed by analysis of actin and cytochrome oxidase subunit VI (COX VI) in each protein extract.

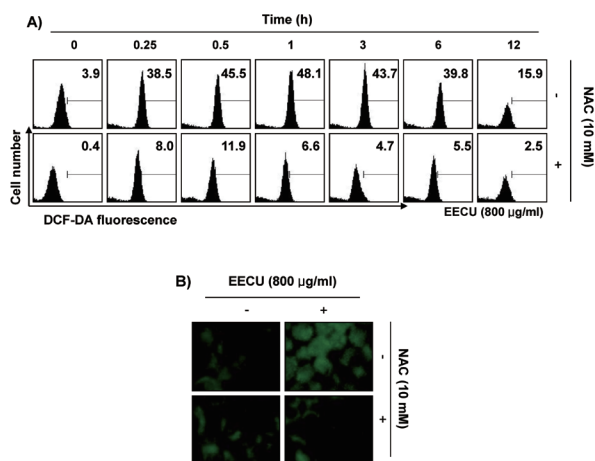


Figure 5. Induction of ROS generation by EECU in T24 cells. (A) T24 cells were either treated with 800 µg/mL EECU for the indicated times or pre-treated with NAC (10 mM) for 1 h before EECU treatment. The medium was discarded and the cells were incubated at 37°C in the dark for 20 min with new culture medium containing 10 µM DCF-DA. ROS generation was measured by a flow cytometer. The data are the means of the two different experiments. (B) Images were obtained using a fluorescence microscope (Original magnifications: ×200). The images presented here are captured from one experiment and are representative of at least three independent experiments.

of increased concentrations of EECU (Figures 4B and 4C), suggesting that mitochondrial dysfunction may also contribute to EECU-induced apoptosis in T24 cells.

3.6. EECU increases the accumulation of ROS in T24 cells

To assess whether EECU-induced mitochondrial dysfunction is associated with ROS production, we quantified the intracellular ROS levels using a DCF-DA probe. Flow cytometry results in Figure 5A demonstrated that the ROS levels elevated sharply within 25 min after EECU treatment, peaked at 1 h of EECU treatment, and then decreased gradually compared to the untreated cells. However, when cells were treated with EECU and NAC, a ROS scavenger, intracellular ROS production was reversed compared to the EECU-treated cells. This phenomenon was also confirmed by fluorescence microscopy analysis (Figure 5B), indicating that ROS production was accompanied by the induction of apoptosis by EECU.

3.7. EECU induces the inactivation of PI3K/Akt pathway in T24 cells

We then examined the effects of EECU on the PI3K/Akt signaling pathway in order to investigate whether EECU-induced apoptosis was affected by PI3K/Akt inactivation, which is indicated by decreased phosphorylation of PI3K and its downstream target molecule Akt, using phosphorylation-specific antibodies. The immunoblotting results demonstrated that EECU remarkably inhibited the phosphorylation of PI3K as well as Akt with increasing EECU concentration (Figure 6A), indicating that they were converted to the inactivated state. Moreover, the addition of LY294002, a specific PI3K inhibitor, enhanced the apoptosis and cytotoxicity induced by EECU (Figure 6B), suggesting that the inactivation of the PI3K/Akt pathway may be involved in EECU-induced cytotoxicity in T24 cells.

3.8. EECU-induced PI3K/Akt inactivation and growth reduction is ROS-dependent in T24 cells

To further test whether the contribution of the ROS generation is mediated in the EECU-induced inactivation of the PI3K/Akt pathway, the effects of EECU on the phosphorylation of PI3K and Akt were tested under conditions of artificially blocked production of ROS with NAC. As shown in Figure 7A, the phosphorylation of PI3K and Akt by EECU was greatly restored in the presence of NAC, which means that EECU-induced inactivation of PI3K/Akt pathway is ROS dependent. Furthermore, after T24 cells were co-incubated with EECU and NAC, the apoptosis phenomenon markedly decreased when compared with the corresponding EECU-treated cells (Figure 7B) and reduction in cell viability was also blocked (Figure 7C). These results

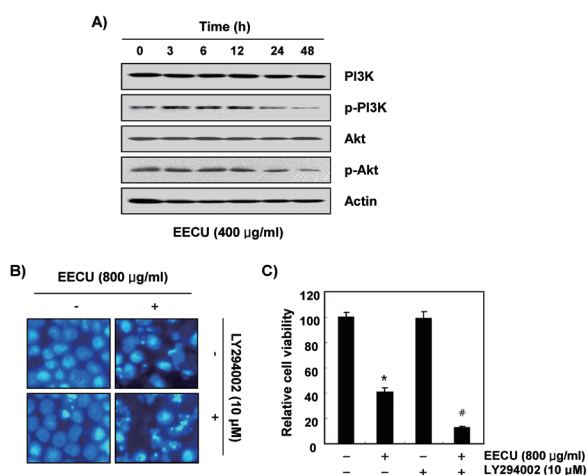


Figure 6. Inactivation of PI3K/Akt pathway by EECU in T24 cells. T24 cells were treated with different concentrations of EECU for 48 h (A) or pre-treated with 10 µM LY294002 for 1 h and then treated with 400 µg/mL EECU for a further 48 h (B and C). (A) Equal amounts of cell lysate were resolved by SDS-polyacrylamide gels, transferred to membranes, and probed with the indicated antibodies. The proteins were visualized using an ECL detection system. Actin was used as an internal control. (B) The DAPI-stained nuclei were then observed with a fluorescence microscope (original magnification, $\times 400$). (C) The cell viability was measured by an MTT assay. The data are expressed as the mean \pm SD of three independent experiments (* $p < 0.05$ vs. untreated control; # $p < 0.05$ vs. EECU-treated cells).

indicate that in addition to the inactivation of PI3K/Akt by EECU, the induction of apoptosis is also ROS dependent.

4. Discussion

In recent decades, considerable interest has been given to discovering anti-cancer drugs from natural products that have been used for a long time for the prevention and treatment of various diseases. Recently, while the possibility of anti-cancer activity of *C. unshiu* peel extract based on the increase of immune activity and anti-inflammatory effect has been raised (31,32), little research has been performed on the mechanism of cancer cell proliferation inhibition. In this study, it was demonstrated that EECU treatment induces the apoptosis of human bladder cancer T24 cells. EECU also considerably causes irreversible damage to the cells because the ability to form colonies by the EECU-treated cells was lost. In addition, the anti-cancer effect of EECU depends on the enhanced ROS generation, and the inactivation of the ROS-dependent PI3K/Akt pathway contributes to the effect of EECU on the apoptosis of T24 cells.

Apoptosis is a highly organized and complex physiological process in which cells destroy themselves, which is carried out mainly through two key pathways in response to various extrinsic and intrinsic signals (7,37). Caspase-8 and -9 are the major initiators of the extrinsic and intrinsic apoptosis pathway, which

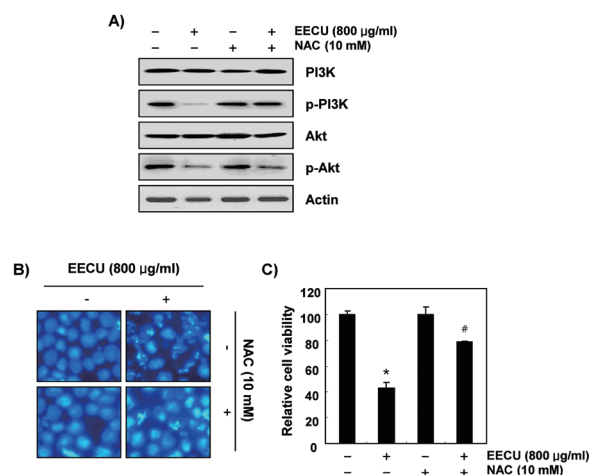


Figure 7. ROS-dependent inactivation of PI3K/Akt pathway in T24 cells. T24 cells were either treated with 800 µg/mL EECU for 48 h or pre-treated with 10 mM NAC for 1 h before EECU treatment and then collected. (A) The cellular proteins were separated by SDS-polyacrylamide gel electrophoresis and transferred to the membranes. The membranes were probed with the indicated antibodies, and the proteins were visualized using an ECL detection system. Actin was used as an internal control. (B) The DAPI-stained nuclei were then observed with a fluorescence microscope (original magnification, $\times 400$). (C) The cell viability was determined by an MTT assay. Each point represents the mean \pm SD of three independent experiments (* $p < 0.05$ vs. untreated control; # $p < 0.05$ vs. EECU-treated cells).

results from binding of the cell-surface DRs of the death ligands and mitochondrial perturbation, respectively (9,11). Activation of caspase-8 and -9 activates effector caspases such as caspase-3 and -7 through the activation of the caspase cascade system to cause apoptosis by causing degradation of the substrate proteins including PARP, which is a DNA repair enzyme (38,39). Thus, the increased activation of caspase-8 and -9 observed in this study indicates that extrinsic and intrinsic pathways may be involved in the induction of apoptosis in T24 cells by EECU. In particular, the increased expression of DR-related proteins by EECU treatment supports the possibility that the extrinsic pathway may be concerned with increased caspase-8 activity. In addition, the loss of mitochondrial membrane integrity was observed with the most typical intrinsic pathway, and the increased translocation of cytochrome *c* from mitochondria to the cytoplasm and increased expression of Bax on Bcl-2 were also observed in the EECU-treated T24 cells. The release of cytochrome *c* requires insertion of mitochondrial membrane and oligomerization of Bax, which is a pro-apoptotic protein belonging to the Bcl-2 family. Thus, the increase in Bax protein expression plays an important role in the activation of the intrinsic pathway, and Bcl-2 is a typical anti-apoptotic protein that suppresses this process (10,11).

EECU also down-regulated the IAP family proteins, which selectively bind to caspases and block apoptosis due to their ability to act directly as inhibitors (40,41). Increased caspase-3 activity and PARP cleavage were

also observed. Furthermore, the expression of truncated Bid, a pro-apoptotic BH3-interacting domain death agonist, in T24 cells exposed to EECU was increased in an EECU-treated concentration-dependent manner. The truncation of Bid is caused by activated caspase-8, which again facilitates caspase-9 activation (42,43). This means that Bid acts as a linker molecule linking DR and mitochondrial dependent pathway. Therefore, the results of this study indicate that the intrinsic pathway activation and the extrinsic pathway were simultaneously involved in the induction of apoptosis of T24 cells by EECU, and that the extrinsic pathway eventually amplified the intrinsic pathway through caspase-8-mediated truncation of Bid.

It is well known that the cellular redox state plays a critical role in regulating cell fate including cell proliferation and death (12,22). ROS, typical products of oxidative stress, are mainly produced in mitochondria and function as mediators of various intracellular cascade signaling (13,14). In addition, the depletion of mitochondrial permeability transition in the apoptosis induction process of cancer cells by various substances having anti-cancer activity is directly related to the abnormal over-production of ROS (15). The attenuation of MMP can induce caspase-9 activation, followed by activation of effector caspases, ultimately resulting in cell apoptosis (13,14). One of the major signal transduction systems that closely regulate cell proliferation related to the production of ROS in the cell is a PI3K/Akt signaling pathway, which is abnormally activated or frequently deregulated in a variety of tumors, including bladder cancer, to increase resistance to apoptosis (17,20,21). According to our results, the production of ROS in the EECU-treated T24 cells was rapidly increased at an early stage, but was almost completely reversed by NAC, a typical antioxidant. In the T24 cells exposed to EECU, the phosphorylation PI3K and Akt also decreased as the EECU treatment time increased, whereas the total PI3K and Akt protein levels remained constant during all treatments. In addition, apoptosis induced by EECU was further increased when the activity of PI3K/Akt was artificially blocked by a specific pharmacological inhibitor of PI3K/Akt, LY294002, indicating that the inhibition of PI3K/Akt signaling was accompanied by apoptosis induced by EECU. Furthermore, T24 cells cultured in medium containing NAC significantly attenuated EECU-induced PI3K, Akt dephosphorylation, and cytotoxicity, suggesting that the production of ROS by EECU was a key step in inhibiting the PI3K/Akt pathway in T24 cells.

The above results demonstrate that EECU induces apoptosis in T24 cells through activation of both intrinsic and extrinsic pathways. Meanwhile, EECU-induced apoptosis in T24 cells is mediated by the inactivation of the ROS-dependent PI3K/Akt signaling axis, indicating that the generation of ROS is a potential upstream molecule for PI3K/Akt inactivation and its cytotoxic

effect. Our findings provide a new perspective on the molecular mechanism of the inhibitory effect of *C. unshiu* Peel extracts on the growth of cancer cells. Nonetheless, further experiments such as determining the EECU efficacy in other cancer cells, the detection of bioactive compounds of EECU, and animal testing should also be performed.

Acknowledgements

This research was supported by the International Science and Business Belt Program through the Ministry of Science, ICT and Future Planning (2016K000297) and Basic Science Research Program through the National Research Foundation of Korea (NRF) grant funded by the Korea government (2015R1A2A2A01004633).

References

- Skeldon SC, Larry Goldenberg S. Bladder cancer: A portal into men's health. *Urol Oncol*. 2015; 33:40-44.
- Dobrush J, Daneshmand S, Fisch M, Lotan Y, Noon AP, Resnick MJ, Shariat SF, Zlotta AR, Boorjian SA. Gender and bladder cancer: A collaborative review of etiology, Biology, and Outcomes. *Eur Urol*. 2016; 69:300-310.
- Jani AB, Efstathiou JA, Shipley WU. Bladder preservation strategies. *Hematol Oncol Clin North Am*. 2015; 29:289-300.
- Pakzad R, Mohammadian-Hafshejani A, Mohammadian M, Pakzad I, Safiri S, Khazaei S, Salehiniya H. Incidence and mortality of bladder cancer and their relationship with development in Asia. *Asian Pac J Cancer Prev*. 2015; 16:7365-7374.
- Ouyang L, Shi Z, Zhao S, Wang FT, Zhou TT, Liu B, Bao JK. Programmed cell death pathways in cancer: A review of apoptosis, autophagy and programmed necrosis. *Cell Prolif*. 2012; 45:487-498.
- Su Z, Yang Z, Xu Y, Chen Y, Yu Q. Apoptosis, autophagy, necroptosis, and cancer metastasis. *Mol Cancer*. 2015; 14:48.
- Fulda S, Debatin KM. Extrinsic versus intrinsic apoptosis pathways in anticancer chemotherapy. *Oncogene*. 2006; 25:4798-4811.
- Nakajima YI, Kuranaga E. Caspase-dependent non-apoptotic processes in development. *Cell Death Differ*. 2017; 24:1422-1430.
- Kaufmann T, Strasser A, Jost PJ. Fas death receptor signalling: Roles of Bid and XIAP. *Cell Death Differ*. 2012; 19:42-50.
- Tummers B, Green DR. Caspase-8: Regulating life and death. *Immunol Rev*. 2017; 277:76-89.
- Hata AN, Engelman JA, Faber AC. The BCL2 family: Key mediators of the apoptotic response to targeted anticancer therapeutics. *Cancer Discov*. 2015; 5:475-487.
- Kaminsky VO, Zhivotovsky B. Free radicals in cross talk between autophagy and apoptosis. *Antioxid Redox Signal*. 2014; 21:86-102.
- Sinha K, Das J, Pal PB, Sil PC. Oxidative stress: The mitochondria-dependent and mitochondria-independent pathways of apoptosis. *Arch Toxicol*. 2013; 87:1157-1180.
- Orrenius S. Reactive oxygen species in mitochondria-

- mediated cell death. *Drug Metab Rev.* 2007; 39:443-455.
15. Giampazolias E, Tait SW. Mitochondria and the hallmarks of cancer. *FEBS J.* 2016; 283:803-814.
 16. Knowles MA, Platt FM, Ross RL, Hurst CD. Phosphatidylinositol 3-kinase (PI3K) pathway activation in bladder cancer. *Cancer Metastasis Rev.* 2009; 28:305-316.
 17. Houédé N, Pourquier P. Targeting the genetic alterations of the PI3K-AKT-mTOR pathway: Its potential use in the treatment of bladder cancers. *Pharmacol Ther.* 2015; 145:1-18.
 18. Hii CS, Moghadammi N, Dunbar A, Ferrante A. Activation of the phosphatidylinositol 3-kinase-Akt/protein kinase B signaling pathway in arachidonic acid-stimulated human myeloid and endothelial cells: Involvement of the ErbB receptor family. *J Biol Chem.* 2001; 276:27246-27255.
 19. Neri LM, Borgatti P, Tazzari PL, Bortul R, Cappellini A, Tabellini G, Bellacosa A, Capitani S, Martelli AM. The phosphoinositide 3-kinase/AKT1 pathway involvement in drug and all-trans-retinoic acid resistance of leukemia cells. *Mol Cancer Res.* 2003; 1:234-246.
 20. Ching CB, Hansel DE. Expanding therapeutic targets in bladder cancer: The PI3K/Akt/mTOR pathway. *Lab Invest.* 2010; 90:1406-1414.
 21. Jin SY, Lee HS, Kim EK, Ha JM, Kim YW, Bae S. Reactive oxygen species and PI3K/Akt signaling in cancer. *Free Radic Biol Med.* 2014; 75(Suppl 1):S34-35.
 22. Kim J, Kim J, Bae JS. ROS homeostasis and metabolism: A critical liaison for cancer therapy. *Exp Mol Med.* 2016; 48:e269.
 23. Li ZY, Yang Y, Ming M, Liu B. Mitochondrial ROS generation for regulation of autophagic pathways in cancer. *Biochem Biophys Res Commun.* 2011; 414:5-8.
 24. Hambright HG, Meng P, Kumar AP, Ghosh R. Inhibition of PI3K/AKT/mTOR axis disrupts oxidative stress-mediated survival of melanoma cells. *Oncotarget.* 2015; 6:7195-7208.
 25. Tanaka T, Yasui Y, Ishigamori-Suzuki R, Oyama T. Citrus compounds inhibit inflammation- and obesity-related colon carcinogenesis in mice. *Nutr Cancer.* 2008; 60:S70-80.
 26. Omura M, Shimada T. Citrus breeding, genetics and genomics in Japan. *Breed Sci.* 2016; 66:3-17.
 27. Min KY, Kim HJ, Lee KA, Kim KT, Paik HD. Antimicrobial activity of acid-hydrolyzed *Citrus unshiu* peel extract in milk. *J Dairy Sci.* 2014; 97:1955-1960.
 28. Park HJ, Jung UJ, Cho SJ, Jung HK, Shim S, Choi MS. *Citrus unshiu* peel extract ameliorates hyperglycemia and hepatic steatosis by altering inflammation and hepatic glucose- and lipid-regulating enzymes in db/db mice. *J Nutr Biochem.* 2013; 24:419-427.
 29. Oh YC, Cho WK, Jeong YH, Im GY, Yang MC, Hwang YH, Ma JY. Anti-inflammatory effect of *Citrus unshiu* peel in LPS-stimulated RAW 264.7 macrophage cells. *Am J Chin Med.* 2012; 40:611-629.
 30. Suzuki M, Sasaki K, Yoshizaki F, Oguchi K, Fujisawa M, Cyong JC. Anti-hepatitis C virus effect of *Citrus unshiu* peel and its active ingredient nobiletin. *Am J Chin Med.* 2005; 33:87-94.
 31. Lee S, Ra J, Song JY, Gwak C, Kwon HJ, Yim SV, Hong SP, Kim J, Lee KH, Cho JJ, Park YS, Park CS, Ahn HJ. Extracts from *Citrus unshiu* promote immune-mediated inhibition of tumor growth in a murine renal cell carcinoma model. *J Ethnopharmacol.* 2011; 133:973-979.
 32. Kim A, Im M, Gu MJ, Ma JY. *Citrus unshiu* peel extract alleviates cancer-induced weight loss in mice bearing CT-26 adenocarcinoma. *Sci Rep.* 2016; 6:24214.
 33. Jin H, Lee WS, Yun JW, Jung JH, Yi SM, Kim HJ, Choi YH, Kim G, Jung JM, Ryu CH, Shin SC, Hong SC. Flavonoids from *Citrus unshiu* Marc. inhibit cancer cell adhesion to endothelial cells by selective inhibition of VCAM-1. *Oncol Rep.* 2013; 30:2336-2342.
 34. Park HR, Park SB, Hong HD, Suh HJ, Shin KS. Structural elucidation of anti-metastatic rhamnogalacturonan II from the pectinase digest of citrus peels (*Citrus unshiu*). *Int J Biol Macromol.* 2017; 94:161-169.
 35. Hengartner MO. The biochemistry of apoptosis. *Nature.* 2000; 407:770-776.
 36. Kim HB, Yoo BS. Propolis inhibits UVA-induced apoptosis of human keratinocyte HaCaT cells by scavenging ROS. *Toxicol Res.* 2016; 32:345-351.
 37. Hajra KM, Liu JR. Apoptosome dysfunction in human cancer. *Apoptosis.* 2004; 9:691-704.
 38. Lee PY, Park BC, Chi SW, Bae KH, Kim S, Cho S, Kang S, Kim JH, Park SG. Histone H4 is cleaved by granzyme A during staurosporine-induced cell death in B-lymphoid Raji cells. *BMB Rep.* 2016; 49:560-565.
 39. Decker P, Muller S. Modulating poly (ADP-ribose) polymerase activity: Potential for the prevention and therapy of pathogenic situations involving DNA damage and oxidative stress. *Curr Pharm Biotechnol.* 2002; 3:275-283.
 40. Nachmias B, Ashhab Y, Ben-Yehuda D. The inhibitor of apoptosis protein family (IAPs): An emerging therapeutic target in cancer. *Semin Cancer Biol.* 2004; 14:231-243.
 41. Fulda S, Vucic D. Targeting IAP proteins for therapeutic intervention in cancer. *Nat Rev Drug Discov.* 2012; 11:109-124.
 42. Billen LP, Shamas-Din A, Andrews DW. Bid: A Bax-like BH3 protein. *Oncogene.* 2008; 27:S93-104.
 43. Kantari C, Walczak H. Caspase-8 and bid: Caught in the act between death receptors and mitochondria. *Biochim Biophys Acta.* 2011; 1813:558-563.

(Received September 5, 2017; Revised October 12, 2017; Accepted October 19, 2017)

Statin use is associated with a reduced risk of hepatocellular carcinoma recurrence after initial liver resection

Yoshikuni Kawaguchi¹, Yoshihiro Sakamoto¹, Daisuke Ito¹, Kyoji Ito¹, Junichi Arita¹, Nobuhisa Akamatsu¹, Junichi Kaneko¹, Kiyoshi Hasegawa¹, Kyoji Moriya², Norihiro Kokudo^{1,3,*}

¹ Hepato-Biliary-Pancreatic Surgery Division, Department of Surgery, Graduate School of Medicine, The University of Tokyo, Tokyo, Japan;

² Department of Infection Control and Prevention, Graduate School of Medicine, The University of Tokyo, Tokyo, Japan;

³ National Center for Global Health and Medicine, Tokyo, Japan.

Summary

Effective adjuvant therapies have not been established for hepatocellular carcinoma (HCC). The study aimed to determine prognostic influence of statin against HCC recurrence after initial resection. From 2003 to 2013, 734 patients underwent initial HCC resection. Exposure to statins was defined as the use at the recommended daily dosage for > 90 days after surgery. Outcomes were compared between patients who did and did not receive statins. Of 734 patients, 31 (4.2%) received statins for dyslipidemia (statin group) and 703 (95.8%) did not (non-statin group). The proportions of hepatitis B (6.5% vs. 22.8%, $P = 0.032$), C (19.4% vs. 45.0%, $P = 0.005$), and a fibrosis score of F3-4 (16.1 % vs. 39.8%, $P = 0.008$) were significantly lower in the statin than non-statin group. The recurrence-free survival rate was significantly higher in the statin than non-statin group ($P < 0.001$), without significant difference of the overall survival rate ($P = 0.142$). A multivariable Cox proportional hazards model revealed that the use of statins (hazard ratio, 0.34; $P = 0.005$) was associated with a significantly lower risk of HCC recurrence. After one-to-two propensity score matching, the RFS rate was also significantly higher in the statin group ($n = 31$) than in the non-statin group ($n = 62$) ($P = 0.008$). In conclusion: The statins use reduced the risk of HCC recurrence after initial resection. Statins may have protective influences on HCC recurrence in patients who undergo initial liver resection.

Keywords: Statin, liver resection, hepatocellular carcinoma

1. Introduction

Hepatocellular carcinoma (HCC) is the fifth most common cancer worldwide and the second among causes of cancer-related deaths among men, whereas among women, it is the seventh most common cancer and the sixth leading cause of cancer death (1). Liver resection remains the optimal treatment for HCC. Previously reported overall survival rates are 40% to

80% at 3 years and 20% to 70% at 5 years after HCC resection (2-4). Cumulative recurrence rates remain high (50-60% at 3 years and 70-100% at 5 years) (2-6). Adjuvant therapy has been expected to reduce HCC recurrence and prolong postsurgical survival. Indeed, several drugs including interferon, sorafenib, and acyclic retinoid have been examined to determine their protective effect against HCC recurrence (7-10). However, effective adjuvant therapies for use after HCC resection have yet to be established.

The protective effects of statins against the development of HCC were recently indicated in patients with hepatitis B (11-13) and hepatitis C (14,15), although conflicting results have also been reported (16). Use of nucleoside analogues, statins, and nonsteroidal anti-inflammatory drugs (NSAIDs)/

Released online in J-STAGE as advance publication October 29, 2017.

*Address correspondence to:

Dr. Norihiro Kokudo, National Center for Global Health and Medicine, 1-21-1 Toyama, Shinjuku-ku, Tokyo 162-8655, Japan.
E-mail: nkokudo@hosp.ncgm.go.jp

aspirin were reportedly associated with a reduced risk of HCC recurrence in patients with hepatitis B, who underwent liver resection (17). However, few studies have focused on the effectiveness of statin use against HCC recurrence after liver resection. We hypothesized that statin use can influence HCC recurrence after liver resection even in patients who receive statins on a daily basis for the treatment of dyslipidemia.

The aim of the present study was to determine the prognostic influence of statin use on initial liver resection of HCC by comparing long-term outcomes between patients who did and did not receive statins.

2. Methods

2.1. Study population

From January 2003 to December 2013, a total of 1,337 consecutive patients with HCC underwent liver resection at the University of Tokyo Hospital. The collected data were retrieved from prospectively maintained databases and included baseline patient characteristics such as specific drug use (statins), operative characteristics, histopathological data, and postoperative outcomes. Exposure to statins was defined as the use of statins at the recommended daily dosages for > 90 days after surgery. These recommended daily dosages were as follows: pravastatin, 10 mg/day; simvastatin, 5 mg/day; fluvastatin, 20 mg/day; pitavastatin, 1 mg/day; atorvastatin, 5 mg/day; and rosuvastatin, 2.5 mg/day. Patients who underwent repeated hepatectomy ($n = 603$) were excluded from the present study. The remaining 734 patients were included in the analysis. This study was conducted with the approval of the Institutional Ethics Review Board of The University of Tokyo (ID: 2158-5). Written informed consent was obtained from all patients.

2.2. Surgical procedures and histopathological assessments

Chest and abdominal contrast-enhanced computed tomography, and ultrasonography were routinely performed before surgical resection. Additionally, magnetic resonance imaging with Gd-EOB-DTPA (Bayer Schering Pharma, Berlin, Germany) had been performed since 2007. Liver resection was indicated according to specific criteria based on preoperative liver function parameters, such as the presence/absence of uncontrolled ascites, serum bilirubin concentration, and indocyanine green retention rate at 15 min (ICG-R15). (18,19) Briefly, if the serum bilirubin concentration was normal, our criteria permitted right hepatectomy or trisectoriectomy when the ICG-R15 was < 10%, left hepatectomy or sectoriectomy when the ICG-R15 was < 20%, subsegmentectomy or monosegmentectomy when the ICG-R15 was < 30%, limited resection when

the ICG-R15 was < 40%, and enucleation when the ICG-R15 was > 40%.

The histologic classification of tumors and the background liver was based on the system established by the Liver Cancer Study Group of Japan (20). The histologic differentiation of HCC (well, moderate, or poor) was determined according to the Edmondson grade (20,21). Both the fibrotic stage and the activity of hepatitis in the background liver were also recorded according to the classification proposed by Desmet *et al.* (22).

2.3. Postoperative management

Morbidity and mortality were defined as postoperative complications and death within 90 days after surgery, respectively. Postoperative morbidity was graded according to the Clavien-Dindo classification (23).

2.4. Patient follow-up

Measurement of blood tumor marker [alpha-fetoprotein (AFP) and des- γ -carboxyprothrombin (DCP)] were performed every month for six months after hospital discharge. Contrast-enhanced computed tomography or magnetic resonance imaging was performed every 3 to 4 months.

Recurrence was diagnosed as the appearance of a new lesion with radiographic features compatible with HCC. Recurrence-free survival (RFS) was defined as the interval between the operation and the date of diagnosis of the first recurrence, and overall survival (OS) was calculated based on the time from surgery to death or last follow-up.

2.5. Statistical analysis

Categorical variables are expressed as numerical figures (%), and were compared between groups using Fisher's exact test or the chi-square test as appropriate. Continuous variables are expressed as median (interquartile range, IQR) and were compared using the Wilcoxon's rank-sum test. OS and RFS curves were constructed using the Kaplan-Meier method and compared using the log-rank test. Factors with a P value of < 0.10 in a Cox proportional hazard model under univariable analysis were considered potential risk factors and were further analyzed in a multivariable Cox model. Hazard ratios (HRs) and 95% confidence intervals (CIs) were calculated for each factor. Based on previously reported evidence, we chose potential confounders and dichotomized their cutoff levels of continuous variables (5,24-30). A propensity score-matching analysis (31,32) was used to build a matched group of patients. The propensity score model was estimated using a logistic regression model. A 1:2 match without replacement was performed using

logit (propensity score) through the nearest available matching, setting the caliper at 0.20. A P value of < 0.05 was considered to indicate statistical significance. Statistical analysis was conducted using JMP software (version 11.0; SAS Institute Inc., Cary, NC).

3. Results

3.1. Patient characteristics

Of the 734 patients, 31 (4.2%) received statins for the treatment of dyslipidemia before surgery. There were no patients that received statin at the recommended daily dosages for ≤ 90 days after surgery. The median statin administration period was 37.2 (32.4 – 51.6) months postoperatively. The background characteristics were compared between patients who received statins (statin group) and patients who did not (non-statin group) (Table 1). The proportions of patients with hepatitis B surface antigen (HBsAg) positivity and hepatitis C virus antibody (HCVAb) positivity were significantly lower in the statin than non-statin group (HBsAg, 6.5% vs. 22.8%, $P = 0.032$; HCVAb, 19.4% vs. 45.0%, $P = 0.005$). The level of triglyceride was significantly higher in the statin groups than the non-statin group: [104 (81-150) vs. 89 (68-122) mg/dL, $P = 0.030$]. The preoperative AFP concentration was significantly lower in the statin than non-statin group [3.5 (2.3-8.0) vs. 15.0 (5.0-65.3) ng/mL, $P < 0.001$]. There were no significant differences in age, male/female ratio, proportion of patients with hepatitis B core antibody (HBcAb) positivity, Child-Pugh class/score, number of tumors, maximum tumor diameter, liver functional parameters, or ICG-R15 between the two groups.

3.2. Surgical, histopathological, and postoperative factors

Surgical, histopathological, and postoperative factors are summarized in Table 2. Red blood cell transfusion were performed more frequently in the statin than non-statin group (16.1% vs. 3.1%, $P = 0.004$). There were no significant differences in the operative time, estimated blood loss, or positive surgical margins between the two groups. With respect to histopathological factors, the proportion of patients with a fibrosis score of F3-4 was significantly lower in the statin than non-statin group (16.1% vs. 39.8%, $P = 0.008$). The proportions of tumor differentiation (poor) and major/minor vascular invasion were similar between the groups. The operative mortality rate was 0.0% in the statin group and 0.3% in the non-statin group ($P > 0.999$). The morbidity and major complication rates were similar between the groups. The postoperative hospital stay was significantly shorter in the statin than non-statin group [13 (10-16) days vs. 15 (12-19) days, $P = 0.022$].

3.3. Patient survival

The median follow-up time was 37.2 (32.4-51.6) months in the statin group and 31.2 (16.8-67.2) months in the non-statin group, demonstrating no significant difference ($P = 0.598$). The RFS rate was significantly higher in the statin than non-statin group ($P < 0.001$): the 1-, 3-, and 5- year RFS rates were 87.1%, 76.7%, and 76.7%, respectively, in the statin group, and 65.3%, 40.6%, and 32.9%, respectively, in the non-statin group (Figure 1). The OS rate was not significantly different between the groups: the 1-, 3-, and 5- year OS rates were 96.7%,

Table 1. Patient demographic and clinical characteristics

Variables	Statin group, $n = 31$	Non-statin group, $n = 703$	P value
Age, years	68 (64 - 75)	67 (59 - 73)	0.233
Sex, male : female	25:6	542:161	0.827
HBsAg, positive	2 (6.5)	160 (22.8)	0.032
HBcAb, positive	8 (25.8)	239 (34.0)	0.439
HCVAb, positive	6 (19.4)	316 (45.0)	0.005
Child-Pugh class*, A/B/C	28 (90.3)/3 (9.7)/0	650 (92.5)/52 (7.4)/1 (0.1)	0.876
Medications			
Statins [†]	31 (100)	-	-
No. of tumors, multiple	7 (22.6)	236 (33.6)	0.245
Maximum diameter of the tumors, mm	32 (18 - 106)	37 (23 - 60)	0.461
AST, IU/L	31 (28 - 39)	38 (26 - 53)	0.191
ALT, IU/L	29 (16 - 42)	35 (22 - 54)	0.152
Total bilirubin, mg/dL	0.7 (0.5 - 0.8)	0.7 (0.5 - 0.9)	0.494
Total cholesterol, mg/dL	163 (146 - 195)	166 (144 - 191)	0.822
Triglyceride, mg/dL	104 (81 - 150)	89 (68 - 122)	0.030
PT, %	100.0 (77.6 - 100.0)	89.0 (76.3 - 100)	0.085
ICG-R15, %	10.5 (6.4 - 16.7)	12.1 (8.0 - 18.9)	0.207
AFP, ng/mL	3.5 (2.3 - 8.0)	15.0 (5.0 - 65.3)	< 0.001
DCP, mAU/mL	635.0 (20.0 - 5076.0)	102.0 (22.0 - 1057.5)	0.103

Abbreviations: HBsAg, hepatitis B surface antigen; HBcAb, hepatitis B core antibody; HCVAb, hepatitis C virus antibody; AST, aspartate aminotransferase; ALT, alanine aminotransferase; PT, prothrombin time; ICG-R15, indocyanine green retention rate at 15 minutes; AFP, α -fetoprotein; DCP, des- γ -carboxyprothrombin. *Child-Pugh score, 5 (5-6) vs. 5 (5-6), $P = 0.570$. [†]Recommended dosages for statins: pravastatin, 10 mg/day ($n = 5$); simvastatin, 5 mg/day ($n = 1$); pitavastatin, 1mg/day ($n = 1$); atorvastatin, 5 mg/day ($n = 19$); and rosuvastatin, 2.5 mg/day ($n = 5$).

Table 2. Surgical, histopathological, and postoperative factors

Variables	Statin group, n = 31	Non-statin group, n = 703	P value
Surgical factors			
Operative time, minutes	317 (228 - 457)	356 (275 - 460)	0.160
Estimated blood loss, mL	430 (210 - 1001)	650 (370 - 1144)	0.059
Red blood cell transfusion	5 (16.1)	22 (3.1)	0.004
Surgical margin, positive	1 (3.2)	18 (2.6)	0.564
Histopathological factors			
Fibrosis score, F3-4*	5 (16.1)	280 (39.8)	0.008
Tumor differentiation, poor†	1 (3.2)	52 (7.4)	0.719
Vascular invasion	11 (35.5)	271 (38.6)	0.851
Postoperative factors			
Morbidity	4 (12.9)	162 (23.0)	0.271
Major complication	1 (3.2)	32 (4.6)	> 0.999
Mortality	0	2 (0.3)	> 0.999
Postoperative hospital stay, days	13 (10-16)	15 (12-19)	0.022

*Based on the classification by Desmet *et al.* (22). †vs. well/moderate, based on modification of the Edmondson grade (21).

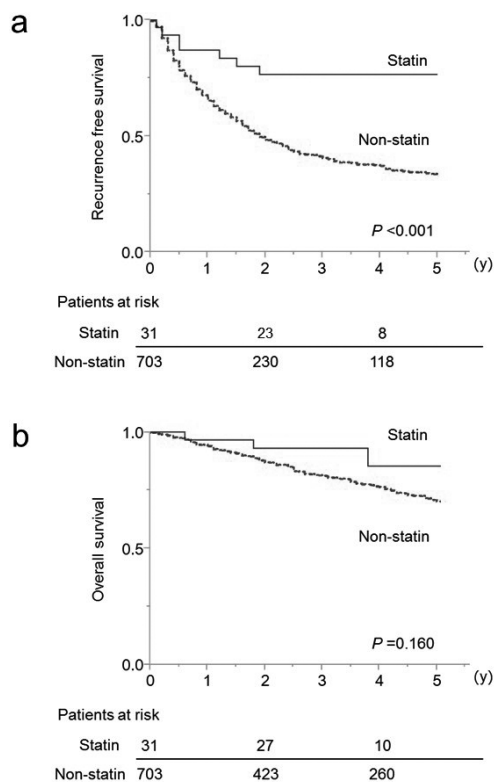


Figure 1. Long-term outcomes between the groups. (a) Recurrence-free survival rate was significantly higher in the statin than non-statin group ($P < 0.001$); **(b)** Overall survival rate was similar between the groups ($P = 0.160$).

93.1%, and 85.3%, respectively, in the statin group, and 94.2%, 87.1%, and 70.2%, respectively, in the non-statin group ($P = 0.142$).

3.4. Factors associated with recurrence and overall survival

HCVAb positivity, use of statins, an ICG-R15 of > 15%, a concentration of > 40 IU/L, an AFP concentration of > 20 ng/mL, a DCP concentration of > 40 mAU/mL, multiple

tumors, tumor size of > 2 cm, and vascular invasion were found to be factors that potentially influenced RFS (Table 3). The multivariable Cox proportional hazards model revealed that use of statins (HR, 0.34; 95% CI, 0.12-0.75; $P = 0.005$) was associated with a significantly lower risk of HCC recurrence. Additionally, an ICG-R15 of > 15% (HR, 1.27), ALT concentration of > 40 IU/L (HR, 1.46), AFP concentration of > 20 ng/mL (HR, 1.39), DCP concentration of > 40 mAU/mL (HR, 1.34), multiple tumors (HR, 1.94), tumor size of > 2 cm (HR, 1.38), and vascular invasion (HR, 1.22) were independent risk factors for RFS. Use of statins was not a significant risk factor for OS (HR, 0.44; 95% CI, 0.11-1.15; $P = 0.102$) (Table 4). HCVAb positivity (HR, 1.55), an ICG-R15 of > 15% (HR, 1.39), AFP concentration of > 20 ng/mL (HR, 1.37), multiple tumors (HR, 2.22), tumor size of > 2 cm (HR, 1.72), poor tumor differentiation (HR, 1.79), and vascular invasion (HR, 1.47) were independent risk factors for OS.

3.5. Patient survival evaluation using propensity score-matching analysis

After 1:2 case propensity score matching, 31 patients in the statin group and 62 patients in the non-statin group were analyzed. Patient demographics, and surgical, histopathological, and postoperative outcomes were comparable after the matching (Supplementary Tables S1 and S2, <http://www.biosciencetrends.com/action/getSupplementalData.php?ID=15>). The RFS rate was significantly higher in the statin than non-statin group ($P = 0.008$) (Figure 2). The OS rate was not significantly different between the groups ($P = 0.581$).

4. Discussion

In the present study, the use of statins was significantly associated with a lower HCC recurrence rate. This finding is consistent with the RFS rates in the cohort after excluding patients with hepatitis B and C. The

Table 3. Cox proportional hazards model analysis for recurrence free survival

Variables	Univariable Analysis			Multivariable Analysis		
	HR	95% CI	P value	HR	95% CI	P value
Age > 65 years	0.92	0.76 - 1.12	0.414			
Male	0.86	0.69 - 1.08	0.186			
HBsAg, positive	1.06	0.84 - 1.34	0.603			
HBcAb, positive	0.98	0.80 - 1.20	0.866			
HCVAb, positive	1.20	0.99 - 1.46	0.062	1.05	0.85-1.30	0.662
Fibrosis (F3-4) vs. (F0-2)	1.11	0.91 - 1.35	0.292			
Use of statin	0.30	0.13 - 0.58	< 0.001	0.32	0.11-0.70	0.002
ICG-R15 > 15%	1.34	1.10 - 1.64	0.004	1.27	1.02-1.58	0.031
ALT > 40 IU/L	1.57	1.28 - 1.91	< 0.001	1.46	1.18-1.80	< 0.001
AFP > 20 ng/mL	1.66	1.37 - 2.02	< 0.001	1.39	1.14-1.70	0.001
DCP > 40 mAU/mL	1.39	1.14 - 1.71	0.001	1.34	1.07-1.68	0.009
Red blood cell transfusion	0.84	0.40 - 1.53	0.592			
Surgical margin, positive	1.62	0.80 - 2.87	0.165			
Multiple tumor vs. solitary tumor	1.97	1.61 - 2.40	< 0.001	1.94	1.58-2.38	< 0.001
Tumor size > 2 cm	1.49	1.15 - 1.97	0.002	1.38	1.05-1.84	0.022
Tumor differentiation, poor	1.18	0.81 - 1.66	0.384			
Vascular invasion, positive	1.31	1.07 - 1.60	0.008	1.22	0.99-1.49	0.059

Abbreviations: HBcAb, hepatitis B core antibody; HVCAB, hepatitis C virus antibody; ICG-R15, Indocyanine green retention rate at 15 minutes; ALT, alanine aminotransferase; AFP, α -fetoprotein; DCP, des- γ -carboxyprothrombin.

Table 4. Cox proportional hazards model analysis for overall survival

Variables	Univariable Analysis			Multivariable Analysis		
	HR	95% CI	P value	HR	95% CI	P value
Age > 65 years	1.21	0.90 - 1.64	0.213			
Male	0.80	0.58 - 1.09	0.152			
HBsAg, positive	0.69	0.46 - 1.00	0.049	0.80	0.49 - 1.25	0.329
HBcAb, positive	0.98	0.80 - 1.20	0.866			
HCVAb, positive	1.82	1.35 - 2.47	< 0.001	1.55	1.08 - 2.24	0.017
Fibrosis (F3-4) vs. (F0-2)*	1.13	0.84 - 1.52	0.417			
Use of statin	0.44	0.11 - 1.15	0.102			
ICG-R15 > 15%	1.65	1.21 - 2.18	0.001	1.39	1.01 - 1.92	0.045
ALT > 40 IU/L	1.54	1.15 - 2.07	0.005	1.35	0.98 - 1.86	0.067
AFP > 20 ng/mL	1.76	1.31 - 2.36	< 0.001	1.37	1.00 - 1.87	0.047
DCP > 40 mAU/mL	1.27	0.94 - 1.72	0.119			
Red blood cell transfusion	1.94	0.76 - 4.03	0.152			
Surgical margin, positive	2.69	0.95 - 5.95	0.061	1.80	0.54 - 4.50	0.301
Multiple tumor vs. solitary tumor	2.24	1.66 - 3.00	< 0.001	2.22	1.64 - 3.01	< 0.001
Tumor size > 2 cm	1.50	1.01 - 2.31	0.042	1.72	1.15 - 2.66	0.008
Tumor differentiation, poor†	1.62	0.99 - 2.52	0.055	1.79	1.04 - 2.93	0.037
Vascular invasion, positive	1.51	1.12 - 20.2	0.007	1.47	1.08 - 2.00	0.016

*Based on the classification by Desmet *et al.* (22). †vs. well/moderate, based on modification of the Edmondson grade (21). Abbreviations: HBcAb, hepatitis B core antibody; HVCAB, hepatitis C virus antibody; ICG-R15, Indocyanine green retention rate at 15 minutes; ALT, alanine aminotransferase; AFP, α -fetoprotein; DCP, des- γ -carboxyprothrombin.

multivariable analysis revealed that the use of statins reduced the risk of HCC recurrence after initial liver resection.

Certain drugs, including statins, metformin, and aspirins/NSAIDs, have been reported to alter the risk of HCC development (11,13,15-17). One previous study revealed a protective effect of statin use after liver resection (17). The study demonstrated that in patients with hepatitis B virus-related HCC, the use of nucleoside analogues after liver resection was associated with a significantly lower risk of HCC recurrence. Additionally, use of statins (HR, 0.68) and NSAIDs or aspirins (HR, 0.80) were found to be significantly associated with a

lower risk of hepatitis B virus-related HCC recurrence. In the present study, use of statins was an independent factor associated with a 0.32-fold lower risk of HCC recurrence in patients including all etiological backgrounds, whereas an ICG-R15 of > 15%, preoperative ALT concentration of > 40 IU/L, preoperative AFP concentration of > 20 ng/mL, preoperative DCP concentration of > 40 mAU/mL, multiple tumors, tumor size of > 2 cm, and vascular invasion were found to be independent risk factors for HCC recurrence.

The underlying mechanism of the protective effect of statins against the development of HCC has not been fully explained. Some possible mechanisms of

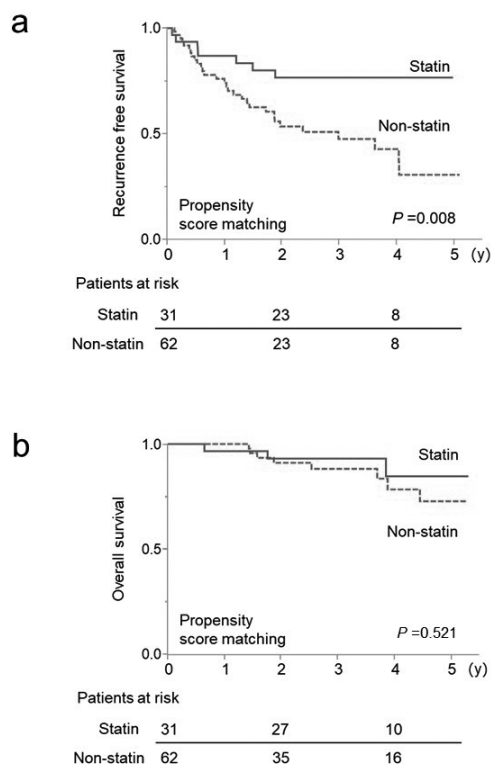


Figure 2. Long-term outcomes between the groups using propensity score-matching analysis. (a) Recurrence-free survival rate was significantly higher in the statin ($n = 31$) than non-statin group ($n = 62$) ($P = 0.008$); **(b)** Overall survival rate was similar between the groups ($P = 0.521$).

the anticancer effect of statins include inhibition of downstream products of the mevalonate pathway (33,34), triggering of tumor apoptosis (35), inhibition of the proteasome pathway (36), and induction of autophagy (37). Approximately half of patients develop HCC recurrence 3 years after liver resection (2-6). Although adjuvant therapies for HCC have been investigated (7), an effective therapeutic option has not yet been established. Prospective randomized trials are needed to confirm the influence of statin use on patients who have undergone liver resection for HCC.

The main limitation of our study is its retrospective nature and the fact that not all confounders could be completely adjusted for despite the use of a multivariable analysis and a propensity score-matching analysis. The proportion of patients who received statins in our series was small (4.2%); however, this is in line with the limited proportion of patients who underwent liver resection and received statins (3.8%) in a previous report (17). Additionally, the influence of statins was unclear according to each statin type based on the results and the previous studies (11,13,15-17). Second, the protective effects of statins against the development of HCC are not well defined. Additionally, the adverse effects of statins are unclear when they are used for patients without dyslipidemia. Statins are generally contraindicated for patients with liver damage. Finally, we dichotomized

continuous variables of potential confounders for HCC prognosis based on previous reports and conducted a multivariable analysis. Such dichotomization may have resulted in lower statistical power.

In conclusion, the risk of HCC recurrence after initial liver resection was lower in patients who received statins than those who did not. Statins may have protective influences on HCC recurrence in patients who undergo initial liver resection, although further studies are needed to elucidate their adverse effects and influences on HCC recurrence.

Acknowledgements

This work was supported by the Program on the Innovative Development and the Application of New Drugs for Hepatitis B from Japan Agency for Medical Research and Development, AMED (to N.K. and K.M.)

References

- Jemal A, Bray F, Center MM, Ferlay J, Ward E, Forman D. Global cancer statistics. *CA Cancer J Clin.* 2011; 61:69-90.
- Belghiti J, Panis Y, Farges O, Benhamou JP, Fekete F. Intrahepatic recurrence after resection of hepatocellular carcinoma complicating cirrhosis. *Ann Surg.* 1991; 214:114-117.
- Grazi GL, Ercolani G, Pierangeli F, Del Gaudio M, Cescon M, Cavallari A, Mazziotti A. Improved results of liver resection for hepatocellular carcinoma on cirrhosis give the procedure added value. *Ann Surg.* 2001; 234:71-78.
- Poon RT, Fan ST, Lo CM, Liu CL, Wong J. Long-term survival and pattern of recurrence after resection of small hepatocellular carcinoma in patients with preserved liver function: implications for a strategy of salvage transplantation. *Ann Surg.* 2002; 235:373-382.
- Imamura H, Matsuyama Y, Miyagawa Y, Ishida K, Shimada R, Miyagawa S, Makuuchi M, Kawasaki S. Prognostic significance of anatomical resection and des-gamma-carboxy prothrombin in patients with hepatocellular carcinoma. *Br J Surg.* 1999; 86:1032-1038.
- Nakajima Y, Ko S, Kanamura T, Nagao M, Kanehiro H, Hisanaga M, Aomatsu Y, Ikeda N, Nakano H. Repeat liver resection for hepatocellular carcinoma. *J Am Coll Surg.* 2001; 192:339-344.
- Zhu GQ, Shi KQ, Yu HJ, He SY, Braddock M, Zhou MT, Chen YP, Zheng MH. Optimal adjuvant therapy for resected hepatocellular carcinoma: A systematic review with network meta-analysis. *Oncotarget.* 2015; 6:18151-18161.
- Printz C. Clinical trials of note. Sorafenib as adjuvant treatment in the prevention of disease recurrence in patients with hepatocellular carcinoma (HCC) (STORM). *Cancer.* 2009; 115:4646.
- Shirakami Y, Sakai H, Shimizu M. Retinoid roles in blocking hepatocellular carcinoma. *Hepatobiliary Surg Nutr.* 2015; 4:222-228.
- Okita K, Izumi N, Ikeda K, *et al.* Survey of survival among patients with hepatitis C virus-related hepatocellular carcinoma treated with peretinoin, an

- acyclic retinoid, after the completion of a randomized, placebo-controlled trial. *J Gastroenterol.* 2015; 50:667-674.
11. Tsan YT, Lee CH, Wang JD, Chen PC. Statins and the risk of hepatocellular carcinoma in patients with hepatitis B virus infection. *J Clin Oncol.* 2012; 30:623-630.
 12. Hsiang JC, Wong GL, Tse YK, Wong VW, Yip TC, Chan HL. Statin and the risk of hepatocellular carcinoma and death in a hospital-based hepatitis B-infected population: A propensity score landmark analysis. *J Hepatol.* 2015; 63:1190-1197.
 13. Chen CI, Kuan CF, Fang YA, Liu SH, Liu JC, Wu LL, Chang CJ, Yang HC, Hwang J, Miser JS, Wu SY. Cancer risk in HBV patients with statin and metformin use: a population-based cohort study. *Medicine (Baltimore)* 2015; 94:e462.
 14. Butt AA, Yan P, Bonilla H, Abou-Samra AB, Shaikh OS, Simon TG, Chung RT, Rogal SS; ERCHIVES (Electronically Retrieved Cohort of HCV Infected Veterans) Study Team. Effect of addition of statins to antiviral therapy in hepatitis C virus-infected persons: Results from ERCHIVES. *Hepatology.* 2015; 62:365-374.
 15. Tsan YT, Lee CH, Ho WC, Lin MH, Wang JD, Chen PC. Statins and the risk of hepatocellular carcinoma in patients with hepatitis C virus infection. *J Clin Oncol.* 2013; 31:1514-1521.
 16. Singh S, Singh PP, Singh AG, Murad MH, Sanchez W. Statins are associated with a reduced risk of hepatocellular cancer: A systematic review and meta-analysis. *Gastroenterology.* 2013; 144:323-332.
 17. Wu CY, Chen YJ, Ho HJ, Hsu YC, Kuo KN, Wu MS, Lin JT. Association Between Nucleoside Analogues and Risk of Hepatitis B Virus-Related Hepatocellular Carcinoma Recurrence Following Liver Resection. *JAMA.* 2012; 308:1906.
 18. Makuuchi M, Kosuge T, Takayama T, Yamazaki S, Kakazu T, Miyagawa S, Kawasaki S. Surgery for small liver cancers. *Semin Surg Oncol.* 1993; 9:298-304.
 19. Kubota K, Makuuchi M, Kusaka K, Kobayashi T, Miki K, Hasegawa K, Harihara Y, Takayama T. Measurement of liver volume and hepatic functional reserve as a guide to decision-making in resectional surgery for hepatic tumors. *Hepatology.* 1997; 26:1176-1181.
 20. Kudo M, Kitano M, Sakurai T, Nishida N. General Rules for the Clinical and Pathological Study of Primary Liver Cancer, Nationwide Follow-Up Survey and Clinical Practice Guidelines: The Outstanding Achievements of the Liver Cancer Study Group of Japan. *Dig Dis.* 2015; 33:765-770.
 21. Edmondson HA, Steiner PE. Primary carcinoma of the liver: A study of 100 cases among 48,900 necropsies. *Cancer.* 1954; 7:462-503.
 22. Desmet VJ, Gerber M, Hoofnagle JH, Manns M, Scheuer PJ. Classification of chronic hepatitis: Diagnosis, grading and staging. *Hepatology.* 1994; 19:1513-1520.
 23. Dindo D, Demartines N, Clavien PA. Classification of surgical complications: A new proposal with evaluation in a cohort of 6336 patients and results of a survey. *Ann Surg.* 2004; 240:205-213.
 24. Yamanaka N, Okamoto E, Toyosaka A, Mitunobu M, Fujihara S, Kato T, Fujimoto J, Oriyama T, Furukawa K, Kawamura E. Prognostic factors after hepatectomy for hepatocellular carcinomas. A univariate and multivariate analysis. *Cancer.* 1990; 65:1104-1110.
 25. Yamamoto J, Kosuge T, Takayama T, Shimada K, Yamasaki S, Ozaki H, Yamaguchi N, Makuuchi M. Recurrence of hepatocellular carcinoma after surgery. *Br J Surg.* 1996; 83:1219-1222.
 26. Lee CS, Sheu JC, Wang M, Hsu HC. Long-term outcome after surgery for asymptomatic small hepatocellular carcinoma. *Br J Surg.* 1996; 83:330-333.
 27. Fuster J, García-Valdecasas JC, Grande L, Tabet J, Bruix J, Anglada T, Taurá P, Lacy AM, González X, Vilana R, Bru C, Solé M, Visa J. Hepatocellular carcinoma and cirrhosis. Results of surgical treatment in a European series. *Ann Surg.* 1996; 223:297-302.
 28. Fan ST, Ng IO, Poon RT, Lo CM, Liu CL, Wong J. Hepatectomy for hepatocellular carcinoma: the surgeon's role in long-term survival. *Arch Surg.* 1999; 134:1124-1130.
 29. Vauthey JN, Lauwers GY, Esnaola NF, Do KA, Belghiti J, Mirza N, Curley SA, Ellis LM, Regimbeau JM, Rashid A, Cleary KR, Nagorney DM. Simplified staging for hepatocellular carcinoma. *J Clin Oncol.* 2002; 20:1527-1536.
 30. Ikeda K, Marusawa H, Osaki Y, Nakamura T, Kitajima N, Yamashita Y, Kudo M, Sato T, Chiba T. Antibody to hepatitis B core antigen and risk for hepatitis C-related hepatocellular carcinoma: a prospective study. *Ann Intern Med.* 2007; 146:649-656.
 31. Austin PC. Statistical criteria for selecting the optimal number of untreated subjects matched to each treated subject when using many-to-one matching on the propensity score. *Am J Epidemiol.* 2010; 172:1092-1097.
 32. D'Agostino RB, Jr. Propensity score methods for bias reduction in the comparison of a treatment to a non-randomized control group. *Stat Med.* 1998; 17:2265-2281.
 33. Danesh FR, Sadeghi MM, Amro N, Philips C, Zeng L, Lin S, Sahai A, Kanwar YS. 3-Hydroxy-3-methylglutaryl CoA reductase inhibitors prevent high glucose-induced proliferation of mesangial cells via modulation of Rho GTPase/ p21 signaling pathway: Implications for diabetic nephropathy. *Proc Natl Acad Sci U S A.* 2002; 99:8301-8305.
 34. Wong WW, Dimitroulakos J, Minden MD, Penn LZ. HMG-CoA reductase inhibitors and the malignant cell: The statin family of drugs as triggers of tumor-specific apoptosis. *Leukemia.* 2002; 16:508-519.
 35. Chan KK, Oza AM, Siu LL. The statins as anticancer agents. *Clin Cancer Res.* 2003; 9:10-19.
 36. Rao S, Porter DC, Chen X, Herliczek T, Lowe M, Keyomarsi K. Lovastatin-mediated G1 arrest is through inhibition of the proteasome, independent of hydroxymethyl glutaryl-CoA reductase. *Proc Natl Acad Sci U S A.* 1999; 96:7797-7802.
 37. Yang PM, Liu YL, Lin YC, Shun CT, Wu MS, Chen CC. Inhibition of autophagy enhances anticancer effects of atorvastatin in digestive malignancies. *Cancer Res.* 2010; 70:7699-7709.

(Received August 20, 2017; Revised October 17, 2017; Accepted October 18, 2017)

Indication for surgical resection in patients with hepatocellular carcinoma with major vascular invasion

Tokio Higaki, Shintaro Yamazaki*, Masamichi Moriguchi, Hisashi Nakayama, Tomoharu Kurokawa, Tadatoshi Takayama

Department of Digestive Surgery, Nihon University School of Medicine, Tokyo, Japan.

Summary Major portal vein invasion (MVI) by hepatocellular carcinoma (HCC) carries an extremely poor prognosis. Our aim was to clarify the indications of hepatic resection in the presence of MVI by HCC. Between 2001 and 2015, 1,306 patients undergoing primary treatment for HCC were analyzed (866 hepatic resections and 440 transarterial therapies). Significant prognostic factors were identified by retrospectively analyzing tumor status, liver function and treatment. Overall survival was compared in terms of the degree of vascular invasion and treatment. The 5-year survival rates according to the degree of vascular invasion (Vp) were Vp0: 51.9%, Vp1: 33.0%, Vp2: 16.7%, Vp3: 21.8%, and Vp4: 0%, respectively. Overall survival (OS) did not differ significantly between patients with Vp3 and Vp4 MVI ($p = 0.153$). Median survival following hepatic resection of Vp3 cases was significantly better than that for Vp4 cases (1,913 vs. 258 days, $p = 0.014$), while OS following transarterial therapy was not significantly different (164 vs. 254 days in Vp3 vs. Vp4, $p = 0.137$). Multivariate analysis revealed hepatic resection (Odds: 2.335 [95%CI: 1.236-4.718], $p = 0.008$) and multiple tumors (1.698 [1.029-2.826], $p = 0.038$) as independent predictors of survival. Hepatic resection in HCC patients with MVI should be indicate in patients with Vp3 invasion.

Keywords: Hepatocellular carcinoma, vascular invasion, survival, liver resection

1. Introduction

Major portal vein invasion (MVI) in patients with hepatocellular carcinoma (HCC), in which tumor thrombi extend to the main or first order branches of the portal trunk, is known to be associated with a poor prognosis. MVI is detected in 30-62% of advanced HCC cases (1-6). The median survival time of untreated patients with MVI is reportedly 2.7 to 4 months (6-8). Although hepatic resection is the only potentially curative treatment in patients with MVI, most patients rapidly develop recurrence in the remnant liver (1-4,5,8). Therefore, MVI is a contraindication for hepatic

resection according to the American Association for the Study of Liver Disease (AASLD) and Barcelona Clinic for Liver Cancer (BCLC) guidelines, which instead recommend treatment with intra-arterial/portal chemotherapy or sorafenib (9-11).

However, recent advances in surgical techniques allow hepatic resection to be performed safely even for more severe cancers (3,5,12,13). Some studies showed that hepatic resection for MVI may be advantageous in terms of avoiding liver failure secondary to tumor thrombus (13-17). However, the indications for hepatic resection and transarterial therapy in HCC cases with MVI differ among institutions (2,3,12,18-20). Thus, the treatment for MVI is still controversial and few reports have documented the limits and clinical benefits of hepatic resection and other therapies.

This study aimed to identify categories of HCC patients with MVI who are likely to obtain survival benefits from hepatic resection. We retrospectively analyzed a large number of HCC patients at a single institution who were treated using uniform treatment criteria.

Released online in J-STAGE as advance publication October 11, 2017.

*Address correspondence to:

Dr. Shintaro Yamazaki, eapartment of Digestive Surgery, Nihon University School of Medicine, 30-1 Oyaguchikami-machi, Itabashi-ku, Tokyo 173-8610, Japan.
E-mail: yamazaki-nmed@umin.ac.jp

2. Patients and Methods

2.1. Patients

Between April 2001 and December 2015, a total of 2,299 patients were treated for HCC at our hospital (1,459 patients underwent hepatic resection and 840 patients underwent transarterial therapy) (Figure 1). Among hepatic resection cases, 593 patients were excluded (407 patients who underwent repeat resection and 186 patients in whom pathology revealed that the tumor was not HCC) from this study. Four hundred of the transarterial therapy patients were excluded (319 patients with repeat transarterial therapy and 81 patients' whose tumor did not seem to be classical type HCC). Thus, the data from the remaining 1,306 HCC cases who underwent primary treatment of HCC at our hospital were analyzed.

Based on the degree of portal vein invasion (Vp), these patients were divided into 5 groups according to the classification of the Liver Cancer Study Group of Japan (21), as Vp0 (no tumor thrombus), Vp1 (tumor thrombus in the third or lower order portal vein branch), Vp2 (tumor thrombus in the second order branch), Vp3 (tumor thrombus in the first order portal vein branch), and Vp4 (tumor thrombus extending to the main portal trunk or counter side of portal branch of tumor thrombus). We defined Vp1 and Vp2 as minor vascular invasion, and Vp3 and Vp4 as MVI.

2.2. Indications

The indication for hepatic resection was less than 3 HCCs with adequate liver functional reserve (21).

The location and number of tumors were confirmed using three different imaging modalities (abdominal ultrasonography, enhanced CT and magnetic resonance imaging). The upper limit of liver volume to be resected was defined on the basis of Makuuchi's criteria, which are based on assessment of the indocyanine green retention rate at 15 minutes (22).

The first-line treatment for transarterial therapy is chemoembolization with cisplatin (CDDP), 50-100 mg/body, or epirubicin, 30-50 mg/body, in a gel form. Total bilirubin levels exceeding 3 mg/dL and Vp4 are contraindications to embolization, and performed transarterial chemotherapy alone (CDDP, 5-fluorouracil (5FU), 500 mg/body/5days or CDDP, 50-100 mg/body) performed to avoid hepatic failure. This study included only typical HCC cases, as assessed using radiological examinations.

2.3. Surgical procedures

Hepatic parenchymal transection was performed using the clamp-crushing method with the inflow blood occlusion technique (23-25). Anatomic resection of Couinaud's segment was the first-line operative procedure for HCC in patients with Child-Pugh class A liver function (21). Intraoperative ultrasonography was routinely performed to check for minor vascular invasion (25). When the tumor thrombus was found by intraoperative ultrasonography, extended hepatic resection was performed to remove the entire tumor thrombus as far as possible. In case of Vp3 and Vp4 MVI, entire tumor thrombectomy was performed using the peel off technique under inflow occlusion (2,15).

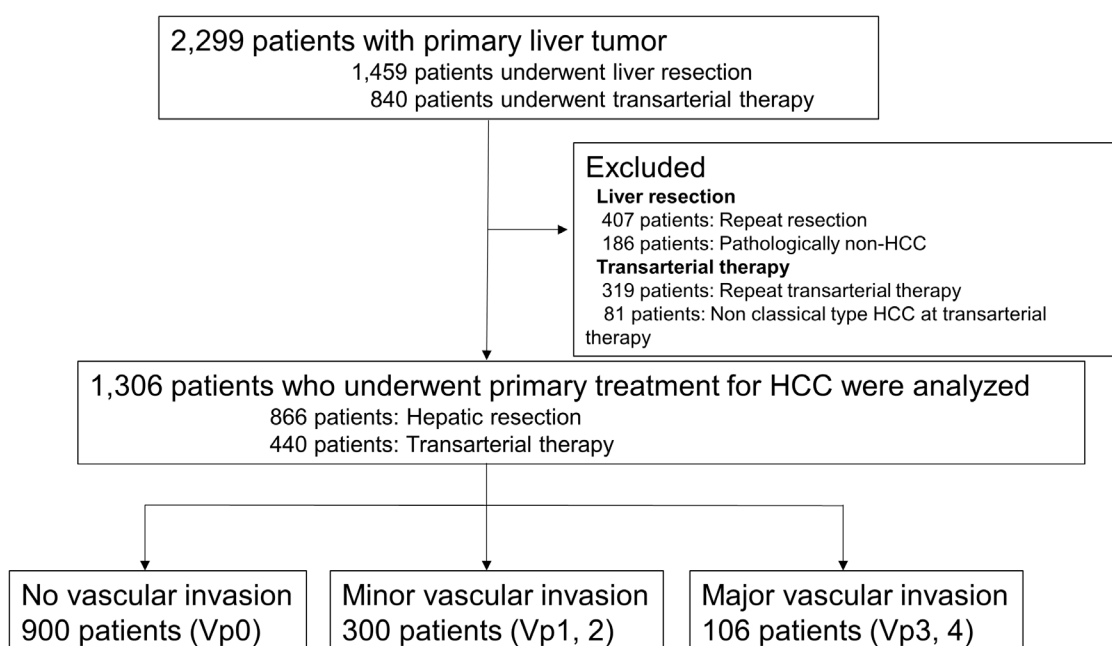


Figure 1. Flow chart of patient inclusion in the study.

Table 1. Patients' characteristics according to the degree of vascular invasion

Degree of vascular invasion	vp0 (n = 900)	vp1 (n = 241)	vp2 (n = 59)	vp3 (n = 72)	vp4 (n = 34)	Total (n = 1306)
Treatment (Hepatic resection)	660 (73.3%)	161 (66.8%)	21(35.6%)	19 (26.4%)	8 (23.5%)	869 (66.5%)
Gender (male)	645 (71.7%)	192 (79.7%)	44 (74.6%)	65 (90.3%)	29 (85.3%)	975 (74.7%)
Age (year)	70 (32-87)	69 (31-86)	70 (47-86)	72(52-88)	69(44-82)	69 (44-88)
Tumor diameter (cm)	2.5 (1.8-3.7)	4.5 (1.4-17.0)	6.5 (2.0-20.0)	10.0 (4.0-23.0)	8.0 (2.4-20.0)	2.7 (1.84-23.0)
Multiple tumors (%)	250 (27.8%)	102 (42.3%)	29 (49.2%)	34 (47.2%)	19 (55.9%)	434 (33.2%)
Hepatitis virus infection (%)	613 (68.1%)	157 (65.1%)	36 (61.0%)	53 (73.6%)	27 (79.4%)	886 (67.8%)
Platelet count (mm ³ /dL)	13.6 (3.7-41.2)	15.3 (4.0-51.0)	15.9 (9.5-68.6)	15.5 (3.9-49.8)	17.5 (8.1-45.5)	14.0 (3.9-49.8)
Albumin (g/dL)	3.8 (2.1-4.8)	3.8 (1.8-5.0)	3.5 (2.1-4.6)	3.5 (1.6-4.8)	3.6 (2.4-4.9)	3.8 (1.6-4.9)
Bilirubin (mg/dL)	0.65 (0.19-2.87)	0.66 (0.26-3.32)	0.69 (0.24-2.71)	0.79 (0.24-8.3)	0.82 (0.44-2.7)	0.63 (0.24-2.70)
Prothrombin activity (%)	96 (43-100)	98 (36-100)	95 (57-100)	93 (48-100)	93 (60-100)	96 (36-100)
IGCR15* (%)	12.9 (8.9-19.4)	12.2 (8.2-17.5)	11.1 (9.3-14.2)	11.3 (9.3-13.7)	17.0 (11.9-22.1)	12.7 (8.8-22.1)
AFP (ng/mL)	13.1 (0.8-10,618)	33.2 (0.6-145,900)	207.1 (2.1-425,700)	991.5 (1.0-365,400)	640.0 (1.4-235,099)	15.4 (0.6-425,700)
PIVKA-II (mAU/mL)	63 (1.0-75,000)	287 (4.3-75,000)	1633 (17.0-114,100)	4582 (15.0-75,000)	4297 (15.0-89,380)	127.0 (1.0-114,100)

*: Only operated cases, AFP, alpha-fetoprotein; PIVKA-II, protein induced by Vitamin K absence/antagonists-II.

2.4. Measurements

Patient status (age, gender, presence of hepatic viral infection and liver functional reserve), tumor status (tumor diameter, number, and tumor marker levels) and patient survival were compared in terms of the degree of vascular invasion. Postoperatively, the specimens were separately checked by a pathologist without access to the clinical information, and the degree of vascular invasion was estimated.

2.5. Measurements

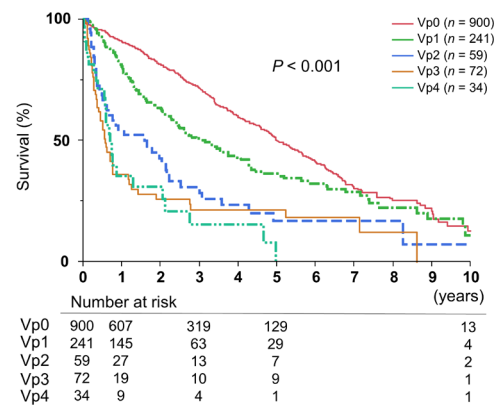
Student's *t*-test, χ^2 test, Mann-Whitney *U* test, and Fisher's exact test were used for univariate analysis, as required. The Cox hazard model was used to calculate survival rates, Kaplan-Meier method was used to obtain survival curves, and all comparisons were made using the log-rank test. *P* values < 0.05 were considered to indicate statistical significance. All the analyses were performed using a statistical software package (JMP version 10.0, SAS Institute Inc., CA).

3. Results

3.1. Survival in cases with major vascular invasion

There were 900 patients with no vascular invasion (Vp0), 241 patients with Vp1, 59 patients with Vp2, 72 patients with Vp3 and 34 patients with Vp4 invasion (Table 1). The 1-, 3-, and 5-year survival rates according to the degree of vascular invasion were Vp0: 91.5%, 72.6% and 51.9%, Vp1: 78.8%, 46.7% and 33.0%, Vp2: 54.8%, 30.0% and 16.7%, Vp3: 36.4%, 21.8% and 21.8%, and Vp4: 35.3%, 15.4% and 0%, respectively ($p < 0.001$) (Figure 2A). The 1-, 3-, and 5-year survival rates in patients with major Vp were significantly worse than in those with minor Vp (37.1%, 21.8% and 12.4% vs. 74.6%, 43.4% and 31.3%, respectively, $p < 0.001$) (Figure 2B).

(A) Overall survival according to the degree of vascular invasion (Vp)



(B) Overall survival in patients with major vascular invasion

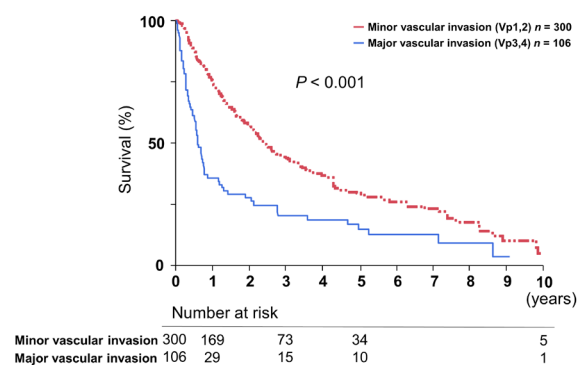


Figure 2. Cumulative survival rates based on the degree of vascular invasion. The 1-, 3-, and 5-year survival rates according to the degree of vascular invasion were distinct among the five groups (A). The 1-, 3-, and 5-year survival rates with major vascular invasion were significantly worse than those with minor vascular invasion (B).

3.2. Characteristics of patients with major vascular invasion

In the MVI group, there were 72 patients with Vp3 and 34 patients with Vp4 invasion (Table 2). The number of tumors were significantly smaller in the hepatic

Table 2. Characteristics of patients stratified according to the degree of major vascular invasion (Vp) and the treatment received

Items	vp3 (n = 72)			vp4 (n = 34)		
	Hepatic resection (n = 19)	TATx (n = 53)	p-value	Hepatic resection (n = 8)	TATx (n = 26)	p-value
Gender (male)	19 (100%)	46 (86.8%)	0.033	8 (100%)	21 (80.8%)	0.179
Age (year)	63 (53-78)	73 (52-88)	0.001	64 (44-81)	70 (58-82)	0.132
Multiple tumors (%)	5 (26.3%)	29 (54.7%)	0.017	1 (12.5%)	18 (69.2%)	0.005
Tumor diameter (cm)	7.7 (1.7-18.0)	10.0 (5.7-23.0)	0.116	7.0 (1.0-12.0)	8.5 (1.5-20.0)	0.163
Hepatitis virus infection (%)	12 (63.2%)	41 (76.9%)	0.246	7 (87.5%)	20 (76.9%)	0.518
Albumin (g/dL)	4.0 (2.5-4.8)	3.4 (1.6-4.6)	0.004	3.9 (3.7-4.4)	3.5 (2.4-4.9)	0.012
Bilirubin (mg/dL)	0.62 (0.24-2.9)	0.81(0.39-10.7)	0.172	0.71 (0.5-1.1)	0.92 (0.44-2.7)	0.234
Prothrombin activity (%)	96 (69-100)	89 (48-100)	0.051	100 (88-100)	92 (60-100)	0.113
Platelet count (mm ³ /dL)	19.1 (8.1-49.8)	15.1 (3.9-41.2)	0.052	12.9 (10.9-18.4)	17.8 (8.1-45.5)	0.139
AFP (ng/mL)	677 (1-100500)	1593 (3-365400)	0.256	26 (2.4-17541.1)	1114 (1.4-235099)	0.520
PIVKA-II (mAU/mL)	2905 (15-75000)	5776 (22-75000)	0.413	2848 (404-178000)	5007 (15-89380)	0.351

TATx, transarterial therapy; AFP, alfa fetoprotein; PIVKA-II, prothrombin induced by Vitamin K absence/antagonists-II.

resection than the transarterial therapy groups [Vp3: 5 (26.3%) vs. 29 (54.7%) patients, $p = 0.017$, and Vp4; 1 (12.5%) vs. 18 (69.2%) patients, respectively, $p = 0.005$]. Serum albumin levels were significantly higher in the hepatic resection than in the transarterial therapy group (Vp3: median 4.0 g/dL [range: 2.5-4.8g/dL] vs. 3.4 [1.6-4.6], $p = 0.004$, Vp4: 3.9 g/dL [3.7-4.4g/dL] vs. 3.5 [2.4-4.9], respectively, $p = 0.012$). There were no significant differences in serum bilirubin levels, prothrombin activity and platelet count between the two treatment groups. Also, median alfa fetoprotein (AFP) levels ($p = 0.256$ and $p = 0.520$) and median prothrombin induced by Vitamin K absence/antagonists-II (PIVKA-II) levels ($p = 0.413$ and $p = 0.351$) did not differ significantly between the two treatment groups for both Vp3 and Vp4 invasion.

3.3. Survival in HCC patients with major vascular invasion stratified according to treatment

Analysis of patients with MVI showed that there were no significant differences in survival rates between patients with Vp3 and Vp4 invasion (1-, 3- and 5-year survival rates: 36.4%, 21.8% and 21.8% vs. 35.3%, 15.4% and 0%, respectively, $p = 0.153$). Median survival did not differ significantly according to the degree of MVI (Vp3 vs. Vp4: 254 days vs. 206, $p = 0.696$) (Figure 3A). In contrast, median survival with Vp3 invasion was significantly better than that with Vp4 invasion among patients who underwent hepatic resection (1,913 days vs. 258, $p = 0.014$), while median survival did not differ significantly between patients with Vp3 and Vp4 invasion who underwent transarterial therapy (164 days vs. 254, $p = 0.137$) (Figures 3B, C). In patients with Vp4 invasion, seven out of 8 patients (87.5%) rapidly developed recurrence of tumor thrombus in the remnant liver within 1 year.

4. Prognostic factors in patients with major vascular invasion

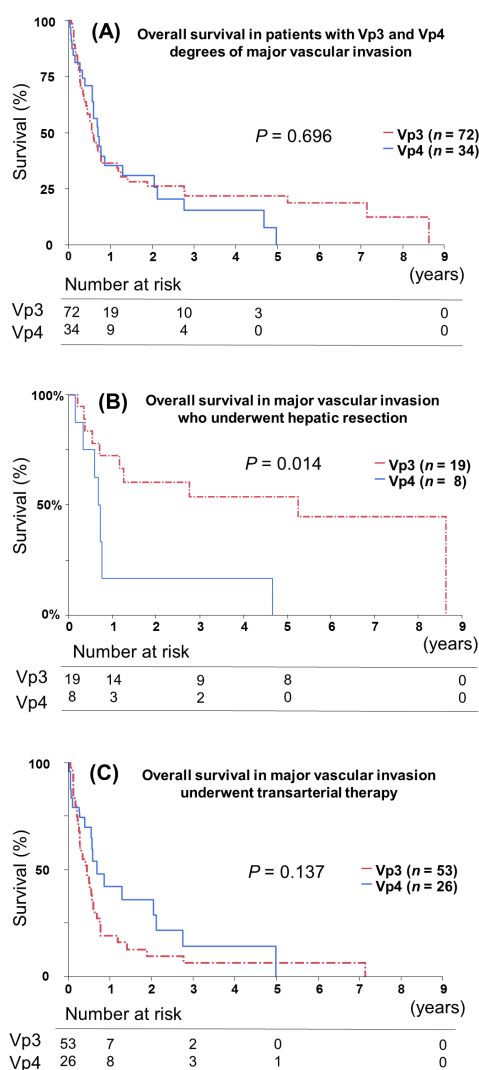


Figure 3. Cumulative survival rates in patients with major vascular invasion based on the treatment given. The 1-, 3- and 5-year survival rates did not differ significantly between Vp3 vs. Vp4 invasion, (36.4%, 21.8% and 21.8% vs. 35.3%, 15.4% and 0%, respectively, $p = 0.696$) (A). Median survival among patients who underwent hepatic resection was significantly higher in those with Vp3 versus Vp4 invasion (1,913 vs. 258 days, $p = 0.014$) (B), while median survival did not differ significantly in patients with Vp3 and Vp4 invasion who underwent transarterial therapy (164 vs. 254 days, $p = 0.137$) (C).

Table 3 Uni- and multivariate analysis of prognostic factors in patients with hepatocellular carcinoma with major vascular invasion

Variables	Univariate analysis			Multivariate analysis		
	Odds	95% CI (Low-High)	p-value	Odds	95% CI (Low-High)	p-value
Treatment (surgery)	2.641	1.535 - 4.823	< 0.001	2.335	1.236 - 4.718	0.008
Gender (male)	0.555	0.310 - 1.083	0.815			
Age (> 70 yr.)	0.983	0.627 - 1.543	0.940			
Multiple tumors	1.984	1.239 - 3.197	0.004	1.698	1.029 - 2.826	0.038
Tumor diameter (> 50 mm)	1.834	1.004 - 3.692	0.049			
Hepatitis virus infection	1.149	0.732 - 1.821	0.548			
Platelet count (mm ⁴ /dL)	1.049	0.431 - 2.171	0.907			
Albumin (< 3.0 g)	1.793	1.105 - 3.014	0.046	1.060	0.484 - 2.112	0.877
Bilirubin (> 2 mg/dL)	2.848	1.178 - 5.867	0.023	1.910	0.622 - 5.593	0.250
Child Pugh class (B)	2.480	0.950 - 5.353	0.062			
AFP (> 400 ng/mL)	1.408	0.896 - 2.215	0.137			
PIVKA-II (>1000 mAU/mL)	1.361	0.747 - 2.732	0.330			

AFP, alpha-fetoprotein; PIVKA-II, protein induced by Vitamin K absence/antagonists-II.

Univariate analysis revealed five factors that affect the prognosis of HCC with MVI (Table 3): hepatic resection (Odds ratio: 2.641 [95%CI; 1.535-4.823], $p < 0.001$), multiple tumors (Odds ratio: 1.984 [1.239-3.197], $p = 0.004$), tumor diameter (Odds ratio: 1.834 [1.004-3.692], $p = 0.049$), albumin level (Odds ratio: 1.793 [1.105-3.014], $p = 0.046$) and bilirubin level (Odds ratio: 2.848 [1.178-5.862], $p = 0.023$). Multivariate analysis revealed that only two factors contribute to survival in patients with MVI. Hepatic resection is the strongest predictor of survival (Odds ratio: 2.335 [1.236-4.718], $p = 0.008$), while the presence of multiple tumors is the second predictor (Odds ratio: 1.698 [1.029-2.826], $p = 0.038$).

4. Discussion

We found that the vascular invasion by HCC is an unfavorable factor for survival. In particular, in the MVI group, only patients with Vp3 invasion experience survival benefits with hepatic resection, while there is no clinical benefit of performing hepatic resection in patients with Vp4 invasion. Thus, patients with Vp4 invasion should be treated by transarterial therapy or other treatments.

Anatomic resection is the primary therapeutic strategy in patients with minor vascular invasion. This results in simultaneous treatment of potential intrahepatic metastasis *via* the portal vein (25). Thus, hepatic resection provides significant local tumor control in case of minor vascular invasion (26,27). In contrast, in patients with MVI, the risk of recurrence after liver resection remains disappointingly high despite hepatic resection (1,28-30). Therefore, the ideal treatment strategy for surgical control of vascular invasion in patients with MVI is still debatable.

Multivariate analysis in our study revealed that performing hepatic resection is the strongest predictor for survival in MVI. Hepatic resection significantly

contributed to OS in patients with Vp3, while it had no prognostic benefit in patients with Vp4 invasion (31-34). In our study, seven out of 8 patients with Vp4 invasion (87.5%) developed rapid recurrence of tumor thrombus in the remnant liver within 1 year. We speculate that Vp4 invasion may result in occult intrahepatic metastasis prior to development of the visible thrombus, even though the tumor may be single or small. Hepatic resection for MVI itself may be one of the risk factors for intrahepatic metastasis *via* the portal vein. Therefore, hepatic resection alone does not improve the outcomes of HCC with Vp4 invasion. Thus, Vp3 is the only degree of invasion that has potential survival benefits following hepatic resection. Perioperative transarterial chemotherapy, including molecularly-targeted therapy, may be a possible treatment option for improving survival in patients with Vp4 invasion (18,29-35).

Our study is limited by its retrospective nature, which would probably have introduced a selection bias between patients who underwent hepatic resection and transarterial therapy. However, all treatment protocols were decided using uniform criteria, which is a merit of this being a single institution study.

In conclusion, the present study revealed that among HCC with MVI patients, only those with Vp3 invasion are likely to benefit from hepatic resection. Surgical resection in patients with Vp4 invasion should be strictly limited, even if the tumor seems completely removable by surgery, because of the high incidence of early intrahepatic recurrence in the remnant liver. Careful consideration of the indications for surgery in patients with major Vp contributes to the quality of life in patients with advanced HCC.

Acknowledgement

This work was supported by a grants-in-aid of The 106th Annual Congress of JS Memorial Surgical Research Fund, Tokyo, Japan.

References

- Kokudo T, Hasegawa K, Matsuyama Y, Takayama T, Izumi N, Kadoya M, Kudo M, Ku Y, Sakamoto M, Nakashima O, Kaneko S, Kokudo N; Liver Cancer Study Group of Japan. Survival benefit of liver resection for hepatocellular carcinoma associated with portal vein invasion. *J Hepatol.* 2016; 65:938-943.
- Minagawa M, Makuuchi M, Takayama T, Ohtomo K. Selection criteria for hepatectomy in patients with hepatocellular carcinoma and portal vein tumor thrombus. *Ann Surg.* 2001; 233:379-384.
- Torzilli G, Belghiti J, Kokudo N, Takayama T, Capussotti L, Nuzzo G, Vauthey JN, Choti MA, De Santibanes E, Donadon M, Morengi E, Makuuchi M. A snapshot of the effective indications and results of surgery for hepatocellular carcinoma in tertiary referral centers: Is it adherent to the EASL/AASLD recommendations?: An observational study of the HCC East-West study group. *Ann Surg.* 2013; 257:929-937.
- Pesi B, Ferrero A, Grazi GL, Cescon M, Russolillo N, Leo F, Boni L, Pinna AD, Capussotti L, Batignani G. Liver resection with thrombectomy as a treatment of hepatocellular carcinoma with major vascular invasion: Results from a retrospective multicentric study. *Am J Surg.* 2015; 210:35-44.
- Shi J, Lai EC, Li N, Guo WX, Xue J, Lau WY, Wu MC, Cheng SQ. Surgical treatment of hepatocellular carcinoma with portal vein tumor thrombus. *Ann Surg Oncol.* 2010; 17:2073-2080.
- Llovet JM, Bustamante J, Castells A, Vilana R, Ayuso Mdel C, Sala M, Brú C, Rodés J, Bruix J. Natural history of untreated nonsurgical hepatocellular carcinoma: Rationale for the design and evaluation of therapeutic trials. *Hepatology.* 1999; 29:62-67.
- Villa E, Moles A, Ferretti I, Buttafoco P, Grottola A, Del Buono M, De Santis M, Manenti F. Natural history of inoperable hepatocellular carcinoma: Estrogen receptors' status in the tumor is the strongest prognostic factor for survival. *Hepatology.* 2000; 32:233-238.
- Shuqun C, Mengchao W, Han C, Feng S, Jiahe Y, Guanghui D, Wenming C, Peijun W, Yuxiang Z. Tumor thrombus types influence the prognosis of hepatocellular carcinoma with the tumor thrombi in the portal vein. *Hepatogastroenterology.* 2007; 54:499-502.
- Thomas MB, Jaffe D, Choti MM, *et al.* Hepatocellular carcinoma: Consensus recommendations of the National Cancer Institute Clinical Trials Planning Meeting. *J Clin Oncol.* 2010; 28:3994-4005.
- Llovet JM, Ricci S, Mazzaferro V, *et al.* Sorafenib in advanced hepatocellular carcinoma. *N Engl J Med.* 2008; 359:378-390.
- Llovet JM, Bru C, Bruix J. Prognosis of hepatocellular carcinoma: The BCLC staging classification. *Semin Liver Dis.* 1999; 19:329-338.
- Zhong JH, Ke Y, Gong WF, Xiang BD, Ma L, Ye XP, Peng T, Xie GS, Li LQ. Hepatic resection associated with good survival for selected patients with intermediate and advanced-stage hepatocellular carcinoma. *Ann Surg.* 2014; 260:329-340.
- Imamura H, Seyama Y, Kokudo N, Maema A, Sugawara Y, Sano K, Takayama T, Makuuchi M. One thousand fifty-six hepatectomies without mortality in 8 years. *Arch Surg.* 2003; 138:1198-1206.
- Shaohua L, Qiaoxuan W, Peng S, Qing L, Zhongyuan Y, Ming S, Wei W, Rongping G. Surgical Strategy for Hepatocellular Carcinoma Patients with Portal/Hepatic Vein Tumor Thrombosis. *PLoS One.* 2015; 10:e0130021.
- Inoue Y, Hasegawa K, Ishizawa T, Aoki T, Sano K, Beck Y, Imamura H, Sugawara Y, Kokudo N, Makuuchi M. Is there any difference in survival according to the portal tumor thrombectomy method in patients with hepatocellular carcinoma? *Surgery.* 2009; 145:9-19.
- Roayaie S, Jibara G, Taouli B, Schwartz M. Resection of hepatocellular carcinoma with macroscopic vascular invasion. *Ann Surg Oncol.* 2013; 20:3754-3760.
- Chen XP, Qiu FZ, Wu ZD, Zhang ZW, Huang ZY, Chen YF, Zhang BX, He SQ, Zhang WG. Effects of location and extension of portal vein tumor thrombus on long-term outcomes of surgical treatment for hepatocellular carcinoma. *Ann Surg Oncol.* 2006; 13:940-946.
- Takayasu K, Arii S, Ikai I, Omata M, Okita K, Ichida T, Matsuyama Y, Nakanuma Y, Kojiro M, Makuuchi M, Yamaoka Y; Liver Cancer Study Group of Japan. Prospective cohort study of transarterial chemoembolization for unresectable hepatocellular carcinoma in 8510 patients. *Gastroenterology.* 2006; 131:461-469.
- Li N, Feng S, Xue J, Wei XB, Shi J, Guo WX, Lau WY, Wu MC, Cheng SQ, Meng Y. Hepatocellular carcinoma with main portal vein tumor thrombus: A comparative study comparing hepatectomy with or without neoadjuvant radiotherapy. *HPB (Oxford).* 2016; 18:549-556.
- Sakon M, Umeshita K, Nagano H, Eguchi H, Kishimoto S, Miyamoto A, Ohshima S, Dono K, Nakamori S, Gotoh M, Monden M. Clinical significance of hepatic resection in hepatocellular carcinoma: Analysis by disease-free survival curves. *Arch Surg.* 2000; 135:1456-1459.
- Liver cancer study group of Japan. The general rules for the clinical and pathological study of primary liver cancer, 2nd English edition Tokyo: Kanehara & Co., Ltd.; 2003.
- Makuuchi M, Kosuge T, Takayama T, Yamazaki S, Kakazu T, Miyagawa S, Kawasaki S. Surgery for small liver cancers. *Semin Surg Oncol.* 1993; 9:298-304
- Imamura H, Takayama T, Sugawara Y, Kokudo N, Aoki T, Kaneko J, Matsuyama Y, Sano K, Maema A, Makuuchi M. Pringle's maneuver in living donors. *Lancet.* 2002; 360:2049-2050.
- Takayama T, Makuuchi M, Kubota K, Harihara Y, Hui AM, Sano K, Ijichi M, Hasegawa K. Randomized comparison of ultrasonic vs clamp transection of the liver. *Arch Surg.* 2001; 136:922-928.
- Makuuchi M, Hasegawa H, Yamazaki S. Ultrasonically guided subsegmentectomy. *Surg Gynecol Obstet.* 1985; 161:346-350.
- Hasegawa K, Kokudo N, Imamura H, Matsuyama Y, Aoki T, Minagawa M, Sano K, Sugawara Y, Takayama T, Makuuchi M. Prognostic impact of anatomic resection for hepatocellular carcinoma. *Ann Surg.* 2005; 242:252-259.
- Shindoh J, Makuuchi M, Matsuyama Y, Mise Y, Arita J, Sakamoto Y, Hasegawa K, Kokudo N. Complete removal of the tumor-bearing portal territory decreases local tumor recurrence and improves disease-specific survival of patients with hepatocellular carcinoma. *J Hepatol.* 2016; 64:594-600.
- Irtan S, Chopin-Laly X, Ronot M, Faivre S, Paradis V, Belghiti J. Complete regression of locally advanced hepatocellular carcinoma induced by sorafenib allowing

- curative resection. *Liver Int.* 2011; 31:740-743.
29. Ueno M, Uchiyama K, Ozawa S, Hayami S, Shigekawa Y, Tani M, Yamaue H. Adjuvant chemolipiodolization reduces early recurrence derived from intrahepatic metastasis of hepatocellular carcinoma after hepatectomy. *Ann Surg Oncol.* 2011; 18:3624-3631.
 30. Wu CC, Hsieh SR, Chen JT, Ho WL, Lin MC, Yeh DC, Liu TJ, P'eng FK. An appraisal of liver and portal vein resection for hepatocellular carcinoma with tumor thrombi extending to portal bifurcation. *Arch Surg.* 2000; 135:1273-1279.
 31. Ishikura S, Ogino T, Furuse J, Satake M, Baba S, Kawashima M, Nihei K, Ito Y, Maru Y, Ikeda H. Radiotherapy after transcatheter arterial chemoembolization for patients with hepatocellular carcinoma and portal vein tumor thrombus. *Am J Clin Oncol.* 2002; 25:189-193.
 32. Nitta H, Beppu T, Imai K, Hayashi H, Chikamoto A, Baba H. Adjuvant hepatic arterial infusion chemotherapy after hepatic resection of hepatocellular carcinoma with macroscopic vascular invasion. *World J Surg.* 2013; 37:1034-1042.
 33. Luo , Peng ZW, Guo RP, Zhang YQ, Li JQ, Chen MS, Shi M. Hepatic resection versus transarterial lipiodol chemoembolization as the initial treatment for large, multiple, and resectable hepatocellular carcinomas: A prospective nonrandomized analysis. *Radiology.* 2011; 259:286-295.
 34. Peng ZW, Guo RP, Zhang YJ, Lin XJ, Chen MS, Lau WY. Hepatic resection versus transcatheter arterial chemoembolization for the treatment of hepatocellular carcinoma with portal vein tumor thrombus. *Cancer.* 2012; 118:4725-4736.
 35. Zhang YF, Guo RP, Zou RH, Shen JX, Wei W, Li SH, OuYang HY, Zhu HB, Xu L, Lao XM, Shi M. Efficacy and safety of preoperative chemoembolization for resectable hepatocellular carcinoma with portal vein invasion: A prospective comparative study. *Eur Radiol.* 2016; 26:2078-2088.
- (Received September 1, 2017; Revised September 25, 2017; Accepted September 30, 2017)

Total bilirubin amount in drainage fluid can be an early predictor for severe biliary fistula after hepatobiliary surgery

Toshitaka Sugawara^{1,*}, Junichi Shindoh^{1,2}, Yujiro Nishioka³, Masaji Hashimoto¹

¹Hepatobiliary-Pancreatic Surgery Division, Department of Digestive Surgery, Toranomon Hospital, Tokyo, Japan;

²Okinaka Memorial Institute for Medical Disease, Tokyo, Japan;

³Hepato-Biliary-Pancreatic Surgery Division, Department of Surgery, Graduate School of Medicine, The University of Tokyo, Tokyo, Japan.

Summary

The ratio of the bilirubin concentration in abdominal drainage fluid to the serum bilirubin concentration (d-Bil/s-Bil) has been used as a predictor of biliary fistula (BF) formation after hepatobiliary surgery. The d-Bil/s-Bil ratio is highly influenced by the amount of drainage and is not always reliable, especially when the amount of drainage is large. In this study, the usefulness of the d-Bil/s-Bil ratio and total bilirubin amount in the drainage fluid (TBA) (bilirubin concentration in the drainage fluid x the amount of drainage) as predictors of severe BF (sBF) formation was evaluated retrospectively from the data of 306 patients who had undergone hepatobiliary surgery. Of the 306 patients, 201 patients were included in the training set and the remaining 105 in the validation set, to determine the best parameter to predict sBF formation after hepatobiliary surgery. Receiver-operating characteristic curve analysis revealed that the predictive power of TBA was superior to that of the d-Bil/s-Bil ratio throughout the postoperative period, and that the TBA on postoperative day (POD) 1 showed the highest discriminatory power in the training set (area under the curve, 0.789; cutoff value, 470 mg/day). The TBA on POD 1 also showed the highest predictive power for sBF formation in the validation set, with a sensitivity of 100%, specificity of 97.1%, and accuracy of 97.1%. In conclusion, TBA may be a more reliable predictor of sBF than the conventionally used d-Bil/s-Bil ratio. Early prediction of sBF may be useful for early removal of unnecessary prophylactic drainage tubes after hepatobiliary surgery.

Keywords: Total bilirubin amount, biliary fistula, hepatobiliary surgery, drainage

1. Introduction

Despite the advances in the surgical and postoperative management techniques, the risk of development of biliary fistula remains a problem after complex hepatobiliary surgery (1-5). An undrained biliary fistula may be further complicated by abdominal abscess formation and sepsis, necessitating long-term

drainage or even surgical intervention (6). Therefore, an abdominal drain is routinely placed prophylactically in many institutions to prevent this postoperative morbidity sequence (7,8). On the contrary, however, several recent studies have reported that prophylactic drainage after hepatic resection may not reduce morbidity, but may, in fact, increase the risk of reactive ascites and/or retrograde infections, resulting in prolongation of the patient's hospital stay (9-15). Early removal of drainage can minimize the risk of drainage related infection without neglecting bleeding or obvious bile leakage. Thus, early removal, at the optimal time, of unnecessary abdominal drains is necessary even after complex hepatobiliary surgery.

The International Study Group of Liver Surgery (ISGLS) defined biliary fistula and classified it into three grades in 2011 (Table 1); biliary fistula after

Released online in J-STAGE as advance publication October 24, 2017.

*Address correspondence to:

Dr. Toshitaka Sugawara, Hepatobiliary-pancreatic Surgery Division, Department of Digestive Surgery, Toranomon Hospital, 2-2-2 Toranomon, Minato-ku, Tokyo 105-8470, Japan. E-mail: s.tishitaka@gmail.com

Table 1. The International Study Group of Liver Surgery classification of biliary fistula*

Definition	Bile leakage is defined as fluid with an increased bilirubin concentration in the abdominal drain or in the intra-abdominal fluid on or after postoperative day 3, or as the need for radiologic intervention (<i>i.e.</i> , interventional drainage) because of biliary collections or relaparotomy resulting from bile peritonitis. Increased bilirubin concentration in the drain or intra-abdominal fluid is defined as a bilirubin concentration at least 3 times greater than the serum bilirubin concentration measured at the same time.
Grade	
A	Bile leakage requiring no or little change in patients' clinical management.
B	Bile leakage requiring a change in patients clinical management (eg, additional diagnostic or interventional procedures) but manageable without relaparotomy, or a Grade A bile leakage lasting for >1 week.
C	Bile leakage requiring relaparotomy.

*Adapted from Koch 2011.

hepatobiliary and pancreatic surgery was defined as an at least threefold higher bilirubin concentration in the drainage fluid than the serum bilirubin concentration on postoperative day (POD) 3 or later, or as the need for radiologic or operative intervention resulting from biliary collections or bile peritonitis (16). However, the bilirubin concentration in the drainage fluid may be influenced by the amount of drainage, especially in patients with liver cirrhosis and those undergoing extended hepatectomy (17). Nevertheless, little is known yet about whether the bilirubin "concentration" is actually the most reliable measure of the risk of development of major biliary fistula or not (18). Therefore, this study sought to compare the predictive power of the ratio of the bilirubin concentration in abdominal drainage fluid to the serum bilirubin concentration (d-Bil/s-Bil), the conventionally used criterion proposed by the ISGLS, and that of the new parameter "total bilirubin amount", to determine the best measure for predicting severe biliary fistula formation requiring long-term management with drainage.

2. Materials and Methods

2.1. Materials

Data of a total of 306 patients who underwent liver resections or bilioenteric anastomoses at Toranomon Hospital between January 2011 and January 2016 were retrospectively reviewed. Of the 306 patients, the initial 201 patients who underwent surgery from January 2011 through March 2015 were included in the training cohort to determine the cutoff values of the drainage parameters, and the remaining 104 patients who underwent surgery between April 2015 and January 2016 were included in the split-sample internal validation cohort.

Data obtained from the clinical records were used to calculate the d-Bil/s-Bil ratio, the conventionally used criterion recommended by the ISGLS, and the total bilirubin amount (bilirubin concentration in the

drainage fluid x the amount of drainage) on PODs 1, 3 and 5. The predictive powers of the two parameters for severe biliary fistula formation were compared to identify the best clinical measure for this prediction. The study was conducted with the approval of the institutional review board of Toranomon hospital, and all the analyses were performed in accordance with the ethical guidelines for clinical research at the hospital.

2.2. Surgery

Hepatic parenchymal transection in all the patients was performed by the clamp crushing method using Pringle's maneuver or by the microwave precoagulation method without vascular occlusion. Bile leakage was routinely checked at the final step of the parenchymal transection, and a tissue sealant sheet or fibrin glue was applied to the raw surface of the liver. Bilioenteric anastomosis was performed by intermittent suture using 5-0 absorbable suture. A closed suction drain was routinely placed near the transected plane or behind the biliary anastomosis. Both the amount of drainage and the bilirubin concentration in the drainage fluid (and serum) were measured on alternate days (PODs 1,3,5,...) until the drain was removed.

2.3. Postoperative management

A prophylactic antibiotic, cefmetazole sodium, was routinely administered for 2 to 5 days after the surgery. The drain was usually removed within 5 days of surgery when the d-Bil/s-Bil ratio was < 3, the amount of drainage was < 200 mL/day, and there was no evidence of infection. In case that the drainage was poor and with less fluid, the drain was removed at that point.

Biliary fistula was defined according to the ISGLS classification. The total bilirubin amount (TBA) was calculated by multiplying the drainage volume by the bilirubin concentration of the drainage fluid. The d-Bil/s-Bil ratio was calculated by dividing the bilirubin concentration of the drainage fluid by the serum bilirubin concentration.

Table 2. Patient characteristics and data related with biliary fistula in training set

Items	sBF* (n = 14)	Non-sBF (n = 187)	P
Male/female	9/5	131/56	0.764
Age (years)	68 (58 – 76)	67 (60 – 73)	0.487
BMI (kg/m ²)	26.4 (19.8 – 22.0)	22.3 (19.9 – 24.6)	0.611
Operation type			0.001
Hepatectomy	13	87	
Biliary tract reconstruction	1	100	
Blood loss	765 (474 – 1107)	531.5 (250 – 1038)	0.253
Operation time	307.5 (208 – 381)	271 (175 – 370)	0.364
Grade of BF			
A		52	
B	13		
C	1		
Duration of drainage (d)	20 (15 – 30)	8 (6 – 10)	< 0.001
Discharge bilirubin concentration (mg/dL)			
POD1	6.4 (1.5 – 40.6)	1.1 (0.9 – 1.6)	0.001
POD3	4.9 (1.8 – 20.4)	1.7 (1.3 – 2.6)	0.002
POD5	8.0 (3.0 – 30.5)	2.0 (1.3 – 2.9)	< 0.001
Discharge amount (mL)			
POD1	277 (214 – 463)	175 (95 – 294)	0.026
POD3	66 (24 – 191)	50 (15 – 138)	0.388
POD5	114 (26.5 – 171)	49 (8.5 – 186.5)	0.483

Data are median (interquartile range) or numbers of patients unless otherwise indicated. *Biliary fistula was defined according to the international study group of liver surgery classification. *Abbreviations:* sBF, severe biliary fistula; BMI body mass index; POD postoperative day.

2.4. Statistical Analysis

Data are expressed as median with range. Statistical analysis was performed using the Mann–Whitney *U* test for continuous variables and the Chi-square test or Fisher's exact test for categorical variables, as appropriate.

The receiver operating characteristic (ROC) curve was used to determine the predictive powers of the TBA and d-Bil/s-Bil ratio for severe biliary fistula formation (grade B or greater according to the ISGLS classification) in the training set, and the predictive powers of these drainage parameters were then compared in the validation set. All data were analyzed using SPSS, version 13.0 (SPSS, Chicago, IL). *P* < 0.05 was considered as denoting statistical significance, and all the tests were two-sided.

3. Results

The 201 patients of the training cohort consisted of 100 patients who underwent hepatic resections and 101 patients who underwent bilioenteric anastomoses. Biliary fistula (of any grade) was observed in 66 (32.8%) patients, including grade A biliary fistula in 52 (25.8%) patients, grade B biliary fistula in 13 (6.4%) patients and grade C biliary fistula in one (0.5%) patient. There was only one patient with late-onset bile leakage, who developed severe biliary fistula on POD 23 after discharge. The other patients were diagnosed as severe biliary fistula before removal of drainage. Drainage was mostly removed after POD 3. There were not any patients who developed sever postoperative hepatic failure. The incidence of severe biliary fistula was

Table 3. Predictive power for severe biliary fistula in training set

Items	AUC	P	Cut-off value
Bilirubin concentration ratio			
POD1	0.701	0.005	3.3
POD3	0.636	0.106	3.2
POD5	0.712	0.012	5.4
Total bilirubin amount			
POD1	0.789	0.001	470
POD3	0.665	0.007	923
POD5	0.776	0.001	469

Abbreviations. POD, postoperative day; AUC, area under the curve; LR+, positive likelihood ratio; LR-, negative likelihood ratio.

significantly higher in the hepatectomy group than in the bilioenteric anastomosis group in the training cohort. The drainage fluid bilirubin concentration and the amount of drainage on POD 1 were significantly higher in the patient group with severe biliary fistula formation than in the patient group not showing severe biliary fistula formation. On the other hand, amounts of drainage on POD 3 and POD 5 were equivalent between the two groups (Table 2). TBA both after hepatectomy and after bilioenteric anastomoses had similar tendency in non-severe biliary fistula group, though in severe biliary fistula group, TBA after bilioenteric anastomoses were lower.

Table 3 and Figure 1 show the results of the ROC analysis conducted to determine the predictive powers of the d-Bil/s-Bil ratio and TBA for severe biliary fistula formation. The area under the curve (AUC) was the highest on POD 1 for TBA (AUC, 0.789) and on POD 5 for the d-Bil/s-Bil ratio (AUC 0.712). The cutoff value of the TBA on POD 1 was 470 mg/day (positive

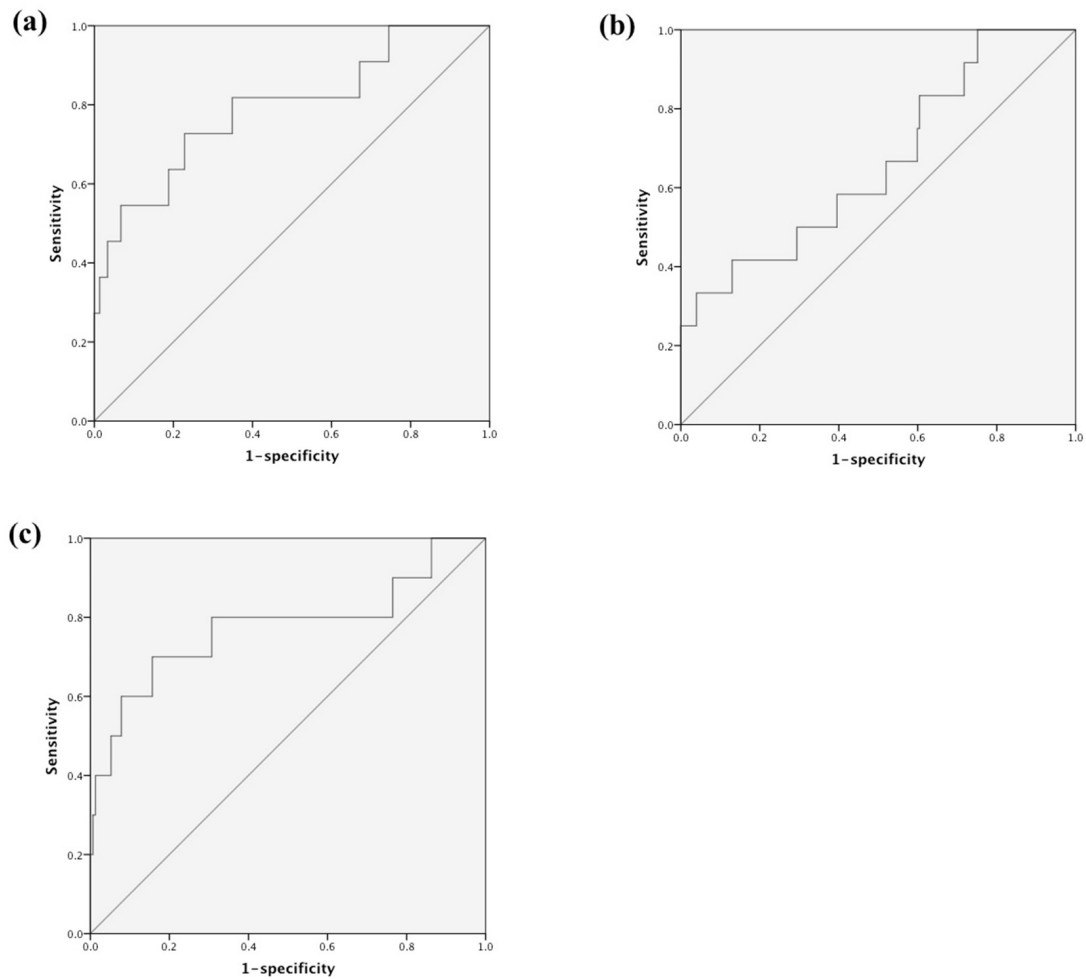


Figure 1. Receiver-operating characteristic curve of the total bilirubin amount. (a), Total bilirubin amount on POD 1 (AUC 0.789); (b), Total bilirubin amount on POD 3 (AUC 0.665); (c), Total bilirubin amount on POD 5 (AUC 0.776).

Table 4. Patient characteristics and data related with biliary fistula in validation set

Items	sBF* (n = 5)	Non-sBF (n = 99)
Male/female	5/0	66/33
Age (years)	65 (59 – 69)	67 (62 – 74)
BMI (kg/m ²)	20.3 (19.9 – 24.5)	21.2 (19.5 – 24.1)
Operation type		
Hepatectomy	3	63
Biliary tract reconstruction	2	36
Blood loss	950 (426 – 978)	851.5 (479 – 1390)
Operation time	238 (184 – 285)	246 (175 – 330)
Grade of BF		
A		13
B	5	
C	0	
Duration of drainage (d)	32 (34 – 65)	5 (4 – 7)
Discharge bilirubin concentration (mg/dL)		
POD1	52.3 (9.4 – 83.9)	1.2 (0.9 – 2.1)
POD3	18.1 (6.9 – 19.6)	1.85 (1.1 – 2.8)
POD5	3.4 (3.4 – 5.6)	1.9 (1.1 – 2.9)
Discharge amount (mL)		
POD1	330 (280 – 473)	176.5 (102 – 270)
POD3	72 (31 – 145)	53.5 (25 – 220)
POD5	181 (155 – 212)	50 (13 – 170)

Data are median (interquartile range) or numbers of patients unless otherwise indicated. *Biliary fistula was defined according to the international study group of liver surgery classification. *Abbreviations:* sBF, severe biliary fistula; BMI body mass index; POD postoperative day.

Table 5. Predictive power of drainage variables for severe biliary fistula in validation set

Items	Cut-off value	Sensitivity	Specificity	Accuracy	LR+	LR-
Bilirubin concentration ratio						
POD1	3.3	26.7	98.9	88.5	23.7	0.74
POD3	3.2	16.7	97.6	83.5	7.08	0.85
POD5	5.4	14.3	94.0	86.5	2.39	0.91
Total bilirubin amount						
POD1	470	100	97.1	97.1	34	0
POD3	923	N/A	N/A	N/A	N/A	N/A
POD5	469	0	92.8	91.4	0	1.08

Abbreviations: POD, postoperative day; LR+ positive likelihood ratio; LR- negative likelihood ratio; NA, not assessible.

likelihood ratio, 3.10; negative likelihood ratio, 0.36), and that of the d-Bil/s-Bil ratio on POD 5 was 5.4 (positive likelihood ratio, 6.95; negative likelihood ratio, 0.54). Of the 6 tested variables, TBA on POD 1 showed the highest predictive power for severe biliary fistula formation, based on the AUC value.

The clinical usefulness of the cutoff values determined in Figure 1 was then tested in the validation cohort. Table 4 reveals the demographic and clinical characteristics of the validation group. Of the 105 patients, biliary fistula formation was observed in 18 (17.1%) patients, including 13 patients who developed grade A biliary fistula and 5 who developed Grade B biliary fistula. Table 5 shows the predictive power of each of the aforementioned cutoff values in the validation set.

Of the tested variables, the TBA on POD 1 showed the highest sensitivity (100%) and specificity (97.1%), with an accuracy of 97.1%, for severe biliary fistula formation. The positive likelihood ratio was 34 and the negative likelihood ratio was 0. On the other hand, the d-Bil/s-Bil ratio had good specificity on PODs 1, 3 and 5 (98.9%, 97.6%, 94%), but the sensitivity was insufficient.

4. Discussion

In the present study, the predictive power of a new measure, the TBA in the drainage fluid, was compared with that of the conventionally used d-Bil/s-Bil ratio for severe biliary fistula formation after hepatobiliary surgery. The ROC curve analyses confirmed the superior predictive power of the TBA to that of the d-Bil/s-Bil ratio on PODs 1, 3 and 5, and revealed that TBA > 470 mg/day on POD 1 was the most sensitive measure to predict the formation of severe biliary fistula requiring continuous drainage, in both the training set and the validation set.

Prophylactic placement of an abdominal drain after hepatobiliary surgery can be useful for early detection of hemorrhage, biliary fistula formation, or infection. It can also be useful for the treatment of these complications (7,8). With the recent advances in surgical and perioperative management techniques, however, several studies have suggested that prophylactic placement of a

drain is not always necessary after hepatobiliary surgery and that prophylactic drainage may, in fact, increase the risk of complications, including retrograde infection (19). Because late-onset bile leakage is relatively rare and difficult to predict (20), these authors have recommended against the routine use of prophylactic abdominal drains after hepatobiliary surgery.

Yamasaki *et al.* proposed the "3 x 3 rule" (drainage fluid bilirubin concentration less than 3 mg/dL on day 3 after the operation) as an accurate criterion for the removal of a prophylactically placed drain after liver resection (21). Tanaka *et al.* calculated the drainage fluid/serum bilirubin concentration ratio multiplied by the volume of the drainage fluid, and determined that a reliable cutoff value for this parameter on POD 2 was 200 (18). Although some authors have focused on the volume of discharge drainage to determine the cutoff value for removal of a prophylactically placed drain, the predictive power of the total amount of bilirubin drained has not yet been investigated. In this study, the drainage fluid bilirubin concentration on POD 1, 3, and 5 were significantly higher in the patient group with severe biliary fistula formation than in the patient group not showing severe biliary fistula formation. On the other hand, amounts of drainage on POD 3 and POD 5 were equivalent between the two groups. This may be an evidence of that the bilirubin concentration in the drainage fluid may be influenced by the amount of drainage. That is, the effusion increases over time, and the bilirubin concentration may change.

The novelty of the current study lies in the comparison of the actual predictive powers of the conventionally used criterion of the d-Bil/s-Bil ratio and the TBA on PODs 1, 3 and 5 for severe biliary fistula formation, and in the validation of the measure in a different study population. As shown in both in Table 3 and Table 5, the TBA showed a better predictive power than the d-Bil/s-Bil ratio for severe biliary fistula formation, and the TBA on POD 1 showed the highest predictive power. However, in this very early period, the problem of false positive should be concerned. In fact, the false positive rate was 2.9%, and this is sufficient as a predictor. Moreover, since patients who have false positive results will be re-assessed on POD 3 and receive removal of drains, the negative effect may be minimal.

These results suggest that the risk of severe biliary fistula formation could be predicted or detected from the TBA on POD 1, and that TBA may be a direct parameter that shows the severity of biliary fistula. That is, the greater TBA increases, the severer the biliary fistula becomes. Therefore, TBA may also serve as a criterion for the removal of unnecessary prophylactic drains. Migita *et al* (22). reported that retrograde drain infection could be detected from as early as POD 2 after surgery, and that early prediction of a drain-related infectious complication sequence can aid in the decision making process during postoperative management.

Limitations of this study include its retrospective nature and its being based on data from a single institution. On the other hand, the clinical management procedures were constant during the study period and similar outcomes were confirmed in both the training set and the validation set. The current results are clinically important in that early prediction of severe biliary fistula formation might be possible with measurement of the TBA. Because the bilirubin concentration in the drainage fluid is highly influenced by the amount of drainage, TBA may serve as a more accurate and direct measure of the amount of bile leakage, which might determine the risk of severe complication sequences.

It is better to differentiate the bile leak situations, such as hepatectomy without bilioenteric anastomoses, hepatectomy with bilioenteric anastomoses, and bilioenteric anastomoses. Since the incidence of severe biliary fistula was low in each situation, it was impossible to do this analysis in this study. A validation study using a larger prospective database is warranted to confirm the current results. However, we think TBA is a direct parameter and thus may not be affected by the reasons and mechanism for biliary fistula.

In conclusion, TBA may be a more reliable measure for predicting severe biliary fistula formation than the conventionally used d-Bil/s-Bil ratio. Early prediction of severe biliary fistula formation may allow early removal of unnecessary prophylactic drains placed after hepatobiliary and pancreatic surgery.

Acknowledgement

This study was supported by JSPS KAKENHI Grant No. 26861063.

References

- Jarnagin WR, Gonen M, Fong Y, DeMatteo RP, Ben-Porat L, Little S, Corvera C, Weber S, Blumgart LH. Improvement in perioperative outcome after hepatic resection: Analysis of 1,803 consecutive cases over the past decade. *Ann Surg.* 2002; 236:397-406; discussion 406-397.
- Poon RT, Fan ST, Lo CM, Liu CL, Lam CM, Yuen WK, Yeung C, Wong J. Improving Perioperative Outcome Expands the Role of Hepatectomy in Management of Benign and Malignant Hepatobiliary Diseases. *Transactions of the Meeting of the American Surgical Association.* 2004; CXXII:296-308.
- Ke S, Ding XM, Gao J, Zhao AM, Deng GY, Ma RL, Xin ZH, Ning CM, Sun WB. A prospective, randomized trial of Roux-en-Y reconstruction with isolated pancreatic drainage versus conventional loop reconstruction after pancreaticoduodenectomy. *Surgery.* 2013; 153:743-752.
- El Nakeeb A, Hamdy E, Sultan AM, Salah T, Askr W, Ezzat H, Said M, Zeied MA, Abdallah T. Isolated Roux loop pancreaticojejunostomy versus pancreaticogastrostomy after pancreaticoduodenectomy: A prospective randomized study. *HPB (Oxford).* 2014; 16:713-722.
- Tani M, Kawai M, Hirono S, Okada KI, Miyazawa M, Shimizu A, Kitahata Y, Yamaue H. Randomized clinical trial of isolated Roux-en-Y versus conventional reconstruction after pancreaticoduodenectomy. *Br J Surg.* 2014; 101:1084-1091.
- Sakamoto K, Tamesa T, Yukio T, Tokuhisa Y, Maeda Y, Oka M. Risk Factors and Managements of Bile Leakage After Hepatectomy. *World J Surg.* 2016; 40:182-189.
- Bona S, Gavelli A, Huguet C. The role of abdominal drainage after major hepatic resection. *Am J Surg.* 1994; 167:593-595.
- Kyoden Y, Imamura H, Sano K, Beck Y, Sugawara Y, Kokudo N, Makuuchi M. Value of prophylactic abdominal drainage in 1269 consecutive cases of elective liver resection. *J Hepatobiliary Pancreat Sci.* 2010; 17:186-192.
- Liu CL, Fan ST, Lo CM, Wong Y, Ng IO, Lam CM, Poon RT, Wong J. Abdominal drainage after hepatic resection is contraindicated in patients with chronic liver diseases. *Ann Surg.* 2004; 239:194-201.
- Fuster J, Llovet JM, Garcia-Valdecasas JC, Grande L, Fondevila C, Vilana R, Palacin J, Tabet J, Ferrer J, Bruix J, Visa J. Abdominal drainage after liver resection for hepatocellular carcinoma in cirrhotic patients: A randomized controlled study. *Hepatogastroenterology.* 2004; 51:536-540.
- Sun HC, Qin LX, Lu L, Wang L, Ye QH, Ren N, Fan J, Tang ZY. Randomized clinical trial of the effects of abdominal drainage after elective hepatectomy using the crushing clamp method. *Br J Surg.* 2006; 93:422-426.
- Hirokawa F, Hayashi M, Miyamoto Y, Asakuma M, Shimizu T, Komeda K, Inoue Y, Tanigawa N. Re-evaluation of the necessity of prophylactic drainage after liver resection. *Am Surg.* 2011; 77:539-544.
- Gurusamy KS, Samraj K, Davidson BR. Routine abdominal drainage for uncomplicated liver resection. *Cochrane Database Syst Rev.* 2007; CD006232.
- Butte JM, Grendar J, Bathe O, Sutherland F, Grondin S, Ball CG, Dixon E. The role of peri-hepatic drain placement in liver surgery: A prospective analysis. *HPB (Oxford).* 2014; 16:936-942.
- Kim YI, Fujita S, Hwang VJ, Nagase Y. Comparison of Abdominal Drainage and No-drainage after Elective Hepatectomy: A Randomized Study. *Hepatogastroenterology.* 2014; 61:707-711.
- Koch M, Garden OJ, Padbury R, *et al.* Bile leakage after hepatobiliary and pancreatic surgery: A definition and grading of severity by the International Study Group of Liver Surgery. *Surgery.* 2011; 149:680-688.
- Chan KM, Lee CF, Wu TJ, Chou HS, Yu MC, Lee WC, Chen MF. Adverse outcomes in patients with postoperative ascites after liver resection for

- hepatocellular carcinoma. *World J Surg.* 2012; 36:392-400.
18. Tanaka K, Kumamoto T, Nojiri K, Takeda K, Endo I. The effectiveness and appropriate management of abdominal drains in patients undergoing elective liver resection: A retrospective analysis and prospective case series. *Surg Today.* 2013; 43:372-380.
 19. Belghiti J, Kabbej M, Sauvanet A, Vilgrain V, Panis Y, Fekete F. Drainage after elective hepatic resection. A randomized trial. *Ann Surg.* 1993; 218:748-753.
 20. Kaibori M, Shimizu J, Hayashi M, Nakai T, Ishizaki M, Matsui K, Kim YK, Hirokawa F, Nakata Y, Noda T, Dono K, Nozawa A, Kwon M, Uchiyama K, Kubo S. Late-onset bile leakage after hepatic resection. *Surgery.* 2015; 157:37-44.
 21. Yamazaki S, Takayama T, Moriguchi M, Mitsuka Y, Okada S, Midorikawa Y, Nakayama H, Higaki T. Criteria for drain removal following liver resection. *Br J Surg.* 2012; 99:1584-1590.
 22. Migita K, Takayama T, Matsumoto S, Wakatsuki K, Tanaka T, Ito M, Nakajima Y. Impact of bacterial culture positivity of the drainage fluid during the early postoperative period on the development of intra-abdominal abscesses after gastrectomy. *Surg Today.* 2014; 44:2138-2145.
- (Received August 31, 2017; Revised October 15, 2017; Accepted October 18, 2017)*

5-aminolevulinic acid (5-ALA) fluorescence-guided Mohs surgery resection of penile-scrotal extramammary Paget's disease

Xiaoqiong Peng[§], Wei Qian[§], Jiangang Hou^{*}

Department of Urology Research Institute, Huashan Hospital Affiliated to Fudan University, Shanghai, China.

Summary

This report aims to evaluate the usefulness of 5-aminolevulinic acid (5-ALA) fluorescence-guided Mohs surgery resection of penile-scrotal extramammary Paget's disease for achieving maximum tumor resection. Between January 2014 and December 2015, 5 patients underwent surgical resection of a penile-scrotal extramammary Paget's disease in department of urology, Huashan hospital, Fudan University. All patients were coated with 5-ALA (concentration of 20%) throughout the scrotum and the visible range of the lesion plus a 2cm margin 3 hours before the induction of anesthesia. 5-ALA fluorescence was visualized using an ultraviolet (UV) light at 405 nm. Surgical margin was determined in a standardized manner. The extent of resection was evaluated on the basis of frozen and histology sections. If the fluorescence positive punctate lesions were found outside the resection range, we removed the lesions and sent them for pathological examination. All data were prospectively collected, and the short- and long-term outcomes of the treatment strategy were analyzed. Lesions in the blue light turns red after irradiation, the fluorescence-guided surgery delineated range is less than the naked eye, intraoperative frozen prompted negative margins, postoperative pathological diagnosis. A total of 31 scattered lesions were found. After biopsy pathology prompted four were positive. In conclusion, 5-ALA fluorescence-guided minimum range can be completely removed in penile-scrotal Paget's lesions, and it is able to detect distant scattered lesions.

Keywords: 5-aminolevulinic acid, fluorescence, Mohs surgery, extramammary Paget's disease

1. Introduction

Extramammary Paget's disease (EMPD) is a rare malignancy that mainly affects the anogenital region in elderly people, first described by Crocker in 1889 (1). The disease is usually misdiagnosed as eczema and the lesions commonly develop in the vulva, penis, scrotum, perineum, perianal area, umbilicus and axilla.

The method of surgical excision and defining the surgical margin of EMPD remain controversial. At present, surgical modalities including Mohs micrographic surgery, fluorescent dyes and frozen section examination (FSE) are recommended to ensure clear margins. With regard to treatment, neither the

method of surgical excision nor the size of the surgical margin has been standardized because of the anatomical complexity of genital lesions. Even extensive resections are complicated by a high local recurrence rate (15-44%) due to several characteristics of EMPD, such as multicentricity and ill-defined margins (2-3).

While many attempts to increase the rate of complete resection have been made, conclusive evidence supporting the efficacy of these approaches is limited. Studies using photodynamic therapy have been published, however achieving solely palliative results (4). Imiquimod cream at 5% concentration, 5% 5-fluorouracil cream, CO₂ laser and the association of two or more therapeutic approaches may also be used, with variable results (5). Increasing the incidence of complete resection, without causing excess morbidity, requires new methods to accurately identify neoplastic tissue intraoperatively, such as use of the drug 5-aminolevulinic acid (5-ALA). It is utilized as a precursor of a photosensitizer for performing a photodynamic diagnosis (PDD) and photodynamic therapy (PDT) to confirm and kill tumor cells (6-8). In

Released online in J-STAGE as advance publication October 16, 2017.

[§]These authors contributed equally to this work.

^{*}Address correspondence to:

Dr. Jiangang Hou, Department of Urology Research Institute, Huashan Hospital Affiliated to Fudan University, Shanghai, 200040, China.

E-mail: hou_jiangang@126.com

addition to the utilization of PDD and PDT, 5-ALA has been used to treat inflammatory disease, autoimmune disease and transplantation due to the anti-inflammation and immunoregulation properties by upregulation of heme oxygenase (HO)-1 expression and release of heme metabolites (9,10). Monitoring the distribution of PpIX is a useful tool for visualizing tumor locations, since the ALA-induced PpIX fluorescence accumulates primarily in malignant tumor tissue and its fluorescence is much stronger than that in normal skin. However, the clinical demarcation of the lesion is still a frequent problem. 5-ALA has been widely used to aid intraoperative identification of malignant gliomas, showing better cytoreduction and marked benefits for patients (11). Chan et al reported that 5-ALA is a useful intraoperative guide for resection. It increases the percentage of total removal of the tumor (12). According to the above results, we want to demonstrate for the first time a case of penile-scrotal EMPD was treated effectively by Mohs surgery resection guided by 5-ALA fluorescence.

This study allowed us to examine the usefulness of these techniques for detecting tumor border and distant scattered lesions. To evaluate the characteristics and efficacy of 5-ALA fluorescence-guided resection of EMPD, we report a clinical series of 5 patients during surgical resection of the lesions.

2. Materials and Methods

2.1. Inclusive criteria

According to the experience of the department of dermatology on the therapy in skin disease using the 5-ALA (13), the present study included 5 patients with penile-scrotal extramammary Paget's disease at our department between January 2014 and December 2015. All patients were diagnosed by biopsy in the department of dermatology and without prior chemotherapy radiotherapy or biological therapy, or laser, frozen, or focal drug application.

2.2. Exclusive criteria

Those patients with severe light allergy, cardiac or cerebral vascular disease, severe liver or heart failure, other malignant tumor or hematologic disease, systemic immune disease, infectious disease, or inflammatory disease. Those patients who could not finish follow-up, died accidentally, or had incomplete clinical information.

2.3. Major equipment and reagent

The 5-aminolevulinic acid (5-ALA) (Shanghai Fudan-zhangjiang Bio-Pharmaceutical Co., Ltd. Shanghai, China) was obtained from the hospital. The photodynamic diagnosis instrument used the ultraviolet torch.

2.4. Surgical procedures

All patient's penile-scrotal lesions were coated with 5-ALA (concentration of 20%) throughout the visible range of the lesion plus a 2 cm margin 3 hours before the induction of anesthesia. Surgical margin was determined in a standardized manner. The extent of resection was evaluated on the basis of frozen and histology sections. If the fluorescence positive punctate lesions were found outside the resection range, we removed the lesions and sent them for pathological examination. Each biopsy site was sutured with 4-0 nylon.

2.5. Case Illustration

A 72-year-old male patient with recurrent penile-scrotal extramammary Paget's disease was initially admitted to the Urology Department of our hospital. Physical examination showed that there was sporadic edema erythema, popular eruption over an area of $6.0 \times 3.0 \text{ cm}^2$ in the penile-scrotal region (Figure 1A). Histopathological examination biopsy confirmed extramammary Paget's disease. We prepared a fresh solution of 5-aminolevulinic acid (5-ALA) solution (20%) by dissolving 5-ALA powder in physiological saline solution. The lesion plus a 2 cm margin were covered by ALA-soaked gauze for 3 h (Figure 1B). Before surgery, lesion locations were visualized by fluorescence examination using a light emitting diode (LED) emitting ultraviolet (UV) light at 405 nm. 5-ALA's fluorescent product, protoporphyrin IX (PpIX), showed a characteristic bright brick-red color (Figure 1C). Under light visualization, the fluorescing areas were marked (Figures. 2A, 2B). Lesions in the blue light turn red after irradiation, the fluorescence-guided surgery delineated range is less than the naked eye can see, intraoperative frozen prompted negative margins, A total of 7 scattered lesions were found and resected (Figures 2C, 2D).

2.6. Tumor pathology

Tissue samples first underwent immediate frozen section analysis. After the operation all samples including scattered lesions were sent for routine histology.

2.7. Postoperative complications and follow-up

Follow-ups were performed every 3 months after treatment via telephone or outpatient clinic visits, and follow-up lasted for 12-24 months (average follow-up 17.8 months). Side-effects such as photosensitivity reactions or inflammation and recrudescence were observed.

3. Results and Discussion

Clinical and histological characteristics including

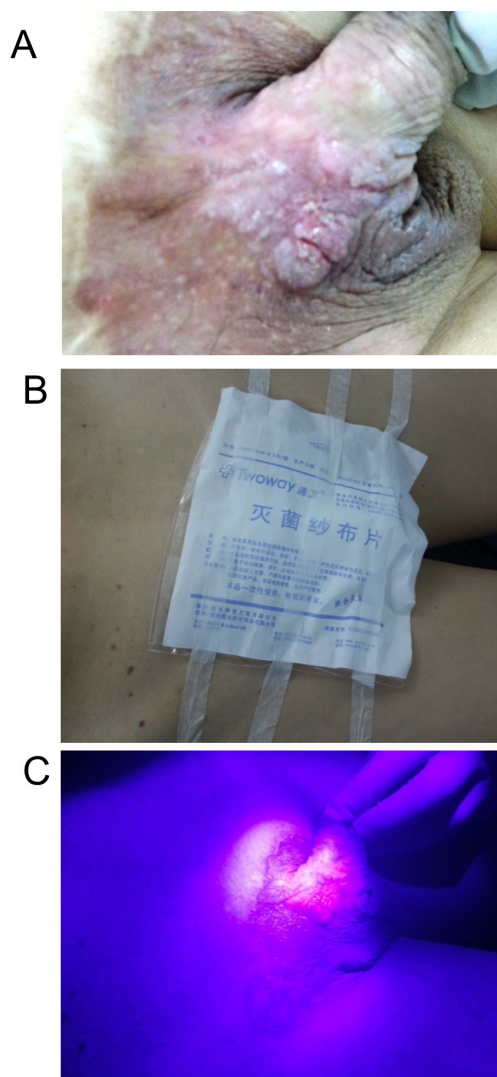


Figure 1. Surgical procedures. (A) A 72-year-old male patient with recurrence of penile-scrotal extramammary Paget's disease showed that there was sporadic edema erythema, popular eruption over an area $6.0 \times 3.0 \text{ cm}^2$ in the penile-scrotal region. (B) The penile-scrotal lesion was coated with 5-ALA (concentration of 20%) throughout the visible range of lesion plus a 2cm margin 3 hours before the induction of anesthesia. (C) Before surgery, lesion locations were visualized by fluorescence examination using a light emitting diode (LED) emitting ultraviolet (UV) light at 405 nm. Under light visualization, the fluorescing areas were marked. Lesions in the blue light turned red after irradiation.

surgical results are summarized in Table 1. Five patients with penile-scrotal extramammary Paget's disease (all men, median age, 69.8 years; range, 65- 77 years) were enrolled in the analysis. Tumors were diagnosed based on biopsy by department of dermatology. The mean maximal tumor diameter of all surgical specimens was 5.6 cm (range, 4-7cm) (pre-PDD) and 4.8 cm (range, 3.5-6cm) (post-PDD). All 5 patients underwent the surgical procedures described above, and no side-effects were attributed to 5-ALA. Lesions in the blue light turn red after irradiation, the fluorescence-guided surgery delineated range is less than the naked eye can see, intraoperative frozen sections prompted negative

margins, for a postoperative pathological diagnosis. A total of 31 scattered lesions were found. After serial biopsies pathology prompted that four were positive. Surgical margins were negative in all patients.

The median follow-up duration was 17.8 months (range, 12-24 months). All patients were alive with no evidence of side-effects (photosensitivity reaction or inflammation) and local recurrence or metastasis at the end of the follow-up period.

Extramammary Paget disease (EMPD) is a cutaneous neoplasm presenting with erythematous spread, mainly on the genitals. As the tumor margin sometimes presents as ill-defined and multicentric, local recurrence after surgical excision is an important issue to overcome. Although surgical treatment with wide local excision (WLE) has been the standard choice of treatment, the recurrence rate is reported to be 33-60% (14). The significant morbidity and deformity after WLE is also problematic.

Differentiation of EMPD of the penoscrotal area from normal tissue is clearly frequently difficult, and setting a clear surgical margin is also difficult because of scrotal tissue redundancy. Therefore, various trials, such as intraoperative frozen sections or Mohs micrographic surgery (MMS), were performed to achieve tumor-free margins. However, frozen sections have a false-negative rate of 10.4%, up to as high as 40%, and is known to have no improvement in disease outcome (15,16). MMS may lower local recurrence rate (17-20) but is time-consuming and requires additional faculty for use.

As the tumor margin sometimes presents as ill-defined and multicentric, local recurrence after surgical excision is an important issue to overcome. Photodynamic diagnosis has been utilized intraoperatively to detect positive surgical margins (21). Over the last decade, 5-aminolevulinic acid (5-ALA) has acquired considerable attention as a feasible agent for photodynamic diagnosis and therapy.

ALA is a precursor to heme in the heme cycle. When excess ALA is supplied to tissues, malignant tumor cells can take up the exogenous 5-ALA and convert it to a fluorescent photosensitizer, protoporphyrin IX (PpIX). Monitoring the distribution of PpIX is a useful tool for visualizing tumor locations, since the 5-ALA-induced PpIX fluorescence accumulates primarily in malignant tumor tissue and its fluorescence is much stronger than that in normal skin (22).

This report demonstrates for the first time the effective treatment of penile-scrotal extramammary Paget's disease with Mohs surgery resection guided by 5-ALA-induced fluorescence. To define clinically the apparent borders of the tumor as well as the extent of the tumor invasiveness 5-ALA was used. Biopsies from all the fluorescing lesions showed some histological extramammary Paget's disease, indicating the efficiency of ALA-induced fluorescence in detection and demarcation of EMPD.

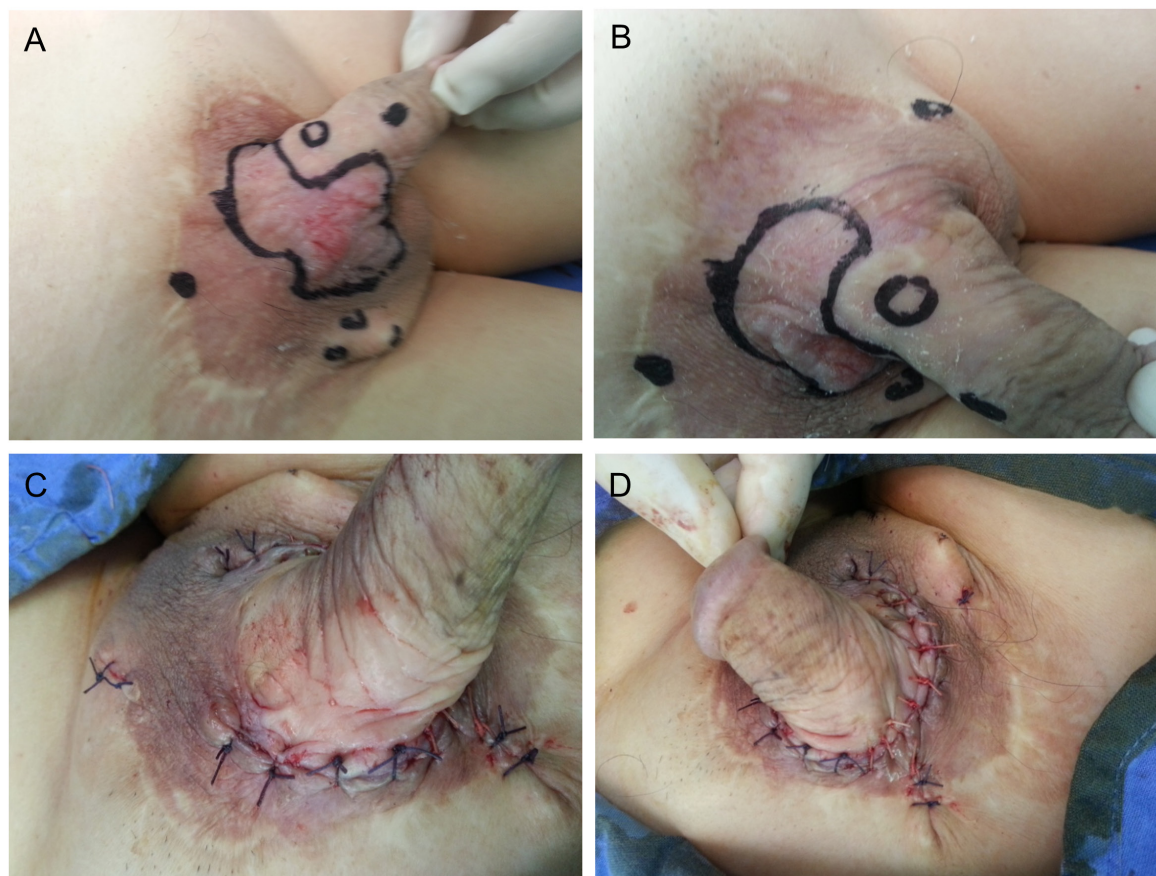


Figure 2. Lesions in the blue light turns red after irradiation, the fluorescence-guided surgery delineated range is less than the naked eye can see (A, B), intraoperative frozen sections prompted negative margins, scattered lesions were found and resected (C, D).

Table 1. Surgical characteristics, pathological findings, short and long-term outcomes of patients with penile-scrotal extramammary Paget's disease

No.	Age (yr)	Biopsy	Tumor size (cm) Pre-PDD	Tumor size (cm) Post-PDD	Scattered lesions (PDD+)	Pathology positive	follow-up (mo)
1	67	Paget	5.0 × 6.0	4.0 × 5.0	7	1	12
2	65	Paget	5.0 × 6.5	5.0 × 6.0	6	0	16
3	69	Paget	4.0 × 5.5	5.0 × 6.0	5	0	24
4	77	Paget	5.0 × 7.0	4.5 × 5.0	7	2	21
5	71	Paget	5.0 × 6.5	3.5 × 4.0	6	1	15

Protoporphyrin seems to be the metabolite mainly responsible for tissue fluorescence. Slight fluorescence is always present in normal skin especially that of the intertriginous areas. This is due to the normal presence of propionibacteria, which are able to produce porphyrins (23). The fluorescence of these bacteria is pale and ill defined. In addition, after ALA application, normal unaffected skin of any area is also able to produce porphyrins, showing a slightly ill defined fluorescence. In contrast, the fluorescence of the tumor tissue is intense and sharply demarcated. When using 5-aminolevulinic acid (5-ALA)-mediated Photodynamic diagnosis (PDD), many studies have obtained better results (24-28).

However, in some cases it is difficult to excise the

lesion completely, especially if it is distant or located in a critical anatomical site. In this study, we revealed feasibility of photodynamic diagnosis using 5-ALA for scattered lesions or those located in a critical anatomical site resection by direct intraoperative inspection of the tumor. We showed that the use of 5-ALA led to a higher frequency of complete resection of the scattered lesions and avoided large-scale resections. Intraoperatively, 5-ALA fluorescence-guided resection was useful especially when a tumor was distant or located in a critical anatomical site.

The study had some limitations such as small sample size and a short follow-up period. However, our results indicate that 5-ALA fluorescence-guided resection of penile-scrotal extramammary Paget's lesions was a

feasible strategy for visualizing margins and maximum tumor resection was achieved with satisfactory outcomes.

In conclusion 5-ALA fluorescence-guided minimum range can completely remove penile-scrotal extramammary Paget's lesions, and it is able to detect distant scattered lesions.

References

- Crocker HR. Paget's disease affecting the scrotum and penis. *Trans Pathol Soc London*. 1889; 40:187-191.
- Zollo JD, Zeitouni NC. The Roswell Park Cancer Institute experience with extramammary Paget's disease. *Br J Dermatol*. 2000; 142:59-65.
- Hendi A, Brodland DG, Zitelli JA. Extramammary Paget's disease: Surgical treatment with Mohs' micrographic surgery. *J Am Acad Dermatol*. 2004; 51:767-773.
- Nardelli AA, Stafinski T, Menon D. Effectiveness of photodynamic therapy for mammary and extra-mammary Paget's disease: A state of the science review. *BMC Dermatol*. 2011; 11:13.
- Cohen PR, Schulze KE, Tschen JA, Hetherington GW, Nelson BR. Treatment of extramammary Paget disease with topical imiquimod cream: Case report and literature review. *South Med J*. 2006; 99:396-402.
- Thunshelle C, Yin R, Chen Q, Hamblin MR. Current Advances in 5-Aminolevulinic Acid Mediated Photodynamic Therapy. *Curr Dermatol Rep*. 2016; 5:179-190.
- Lv T, Zhang JC, Miao F, Wang HW. Aminolevulinic acid photodynamic therapy (ALA-PDT) for Bowen's disease in a SLE patient: Case report and literature review. *Photodiagnosis Photodyn Ther*. 2017; 18:20-23.
- Ang JM, Riaz IB, Kamal MU, Paragh G, Zeitouni NC. Photodynamic Therapy and Pain: A Systematic Review. *Photodiagnosis Photodyn Ther*. 2017; 19:308-344.
- Hou J, Zhang Q, Fujino M, Cai S, Ito H, Takahashi K, Abe F, Nakajima M, Tanaka T, Xu J, Zou H, Ding Q, Li XK. 5-Aminolevulinic acid with ferrous iron induces permanent cardiac allograft acceptance in mice via induction of regulatory cells. *J Heart Lung Transplant*. 2015; 34:254-263.
- Fujino M, Nishio Y, Ito H, Tanaka T, Li XK. 5-Aminolevulinic acid regulates the inflammatory response and alloimmune reaction. *Int Immunopharmacol*. 2016; 37:71-78.
- Stummer W, Pichlmeier U, Meinel T, Wiestler OD, Zanella F, Reulen HJ. Fluorescence-guided surgery with 5-aminolevulinic acid for resection of malignant glioma: A randomized controlled multicentre phase III trial. *Lancet Oncol*. 2006; 7:392-401.
- Chan DTM, Yi-Pin Sonia H, Poon WS. 5-Aminolevulinic acid fluorescence guided resection of malignant glioma: Hong Kong experience. *Asian J Surg*. 2017; pii: S1015-9584(17)30247-6.
- Zhang Z, Lu XN, Liang J, Tang H, Yang YS, Zhu XH, Du J, Shen YY, Xu JH. Evaluation of photodynamic therapy using topical aminolevulinic acid hydrochloride in the treatment of condylomata acuminata. *Int J Clin Exp Med*. 2015; 8:6517-6521.
- Lam C, Funaro D. Extramammary Paget's disease: Summary of current knowledge. *Dermatol Clin*. 2010; 28:807-826.
- Gunn RA, Gallager HS. Vulvar Paget's disease: A topographic study. *Cancer*. 1980; 46:590-594.
- Chan JYW, Li GKH, Chung JHP, Chow VLY. Extramammary Paget's disease: 20 years of experience in Chinese population. *Int J Surg Oncol*. 2012; 2012:1-5.
- O'Connor WJ, Lim KK, Zalla MJ, Gagnot M, Otley CC, Nguyen TH, Roenigk RK. Comparison of Mohs micrographic surgery and wide excision for extramammary Paget's disease. *Dermatol Surg*. 2003; 29:723-727.
- Lee KY, Roh MR, Chung WG, Chung KY. Comparison of Mohs micrographic surgery and wide excision for extramammary Paget's Disease: Korean experience. *Dermatol Surg*. 2009; 35:34-40.
- Bae JM, Choi YY, Kim H, Oh BH, Roh MR, Nam K, Chung KY. Mohs micrographic surgery for extramammary Paget disease: A pooled analysis of individual patient data. *J Am Acad Dermatol*. 2013; 68:632-637.
- Kim SJ, Thompson AK, Zubair AS, Otley CC, Arpey CJ, Baum CL, Roenigk RK, Lohse CM, Brewer JD. Surgical Treatment and Outcomes of Patients With Extramammary Paget Disease: A Cohort Study. *Dermatol Surg*. 2017; 43:708-714.
- Thunshelle C, Yin R, Chen Q, Hamblin MR. Current Advances in 5-Aminolevulinic Acid Mediated Photodynamic Therapy. *Curr Dermatol Rep*. 2016; 5:179-190.
- Yang X, Palasuberniam P, Kraus D, Chen B. Aminolevulinic Acid-Based Tumor Detection and Therapy: Molecular Mechanisms and Strategies for Enhancement. *Int J Mol Sci*. 2015; 16:25865-25880.
- Flohil SC, van Lee CB, Beisenherz J, Mureau MA, Overbeek LI, Nijsten T, van den Bos RR. Mohs micrographic surgery of rare cutaneous tumours. *J Eur Acad Dermatol Venereol*. 2017; 31:1285-1288.
- Wang W, Tabu K, Hagiya Y, Sugiyama Y, Kokubu Y, Murota Y, Ogura SI, Taga T. Enhancement of 5-aminolevulinic acid-based fluorescence detection of side population-defined glioma stem cells by iron chelation. *Sci Rep*. 2017; 7:42070.
- Inoue Y, Imai Y, Fujii K, Hirokawa F, Hayashi M, Uchiyama K. The utility of 5-aminolevulinic acid-mediated photodynamic diagnosis in the detection of intraoperative bile leakage. *Am J Surg*. 2017; 213:1077-1082.
- Hillemanns P, Wimberger P, Reif J, Stepp H, Klapdor R. Photodynamic diagnosis with 5-aminolevulinic acid for intraoperative detection of peritoneal metastases of ovarian cancer: A feasibility and dose finding study. *Lasers Surg Med*. 2017; 49:169-176.
- Kishi K, Fujiwara Y, Yano M, Motoori M, Sugimura K, Takahashi H, Ohue M, Sakon M. Usefulness of diagnostic laparoscopy with 5-aminolevulinic acid (ALA)-mediated photodynamic diagnosis for the detection of peritoneal micrometastasis in advanced gastric cancer after chemotherapy. *Surg Today*. 2016; 46:1427-1434.
- Motoori M, Yano M, Tanaka K, Kishi K, Takahashi H, Inoue M, Saito T, Sugimura K, Fujiwara Y, Ishikawa O, Sakon M. Intraoperative photodynamic diagnosis of lymph node metastasis in esophageal cancer patients using 5-aminolevulinic acid. *Oncol Lett*. 2015; 10:3035-3039.

(Received August 29, 2017; Revised October 5, 2017; Accepted October 9, 2017)

Non-linear association between alcohol and incident frailty among community-dwelling older people: A dose-response meta-analysis

Gotaro Kojima*, Steve Iliffe, Ann Liljas, Kate Walters

Department of Primary Care and Population Health, University College London, London, UK.

Summary

A recent systematic review and meta-analysis study suggested that higher alcohol consumption is associated with lower risks for frailty. However the apparent protective effect may not be true because of some limitations. Therefore we further explored potential linear and non-linear associations using a two-stage dose-response meta-analysis. Restricted cubic splines were applied with three fixed knots at percentiles (10%, 50%, and 90%). A two-stage dose-response meta-analysis showed a significant non-linear association (p for non-linearity < 0.001); incident frailty risk decreased until around 15 g/day of alcohol consumption and increased thereafter. This suggests that while moderate alcohol consumption is associated with a lower risk of frailty, at higher consumption levels this apparent protect effect is lost. Given these findings, non-linear associations should be considered in future research on alcohol and frailty.

Keywords: Frailty, alcohol, dose-response meta-analysis, older people

Beneficial effects of light-to-moderate alcohol consumption against various diseases suggested by numerous population-based studies have been controversial and debated in the literature (1). There has been limited evidence regarding whether light-to-moderate alcohol consumption is also protective against frailty (2). Frailty is a state characterized by decreased physiological reserve resulting from age-related accumulated deficits across multiple systems, with increased risks of various negative health outcomes (3). Although a few prospective cohort studies have examined associations between alcohol and risk of frailty, the results are mixed and inconclusive (4-6). Our recent systematic review and meta-analysis study suggested that alcohol consumption is associated with lower risks for frailty (pooled odds ratio (OR) of incident frailty among the highest alcohol use categories compared with non-drinkers = 0.44, 95% confidence interval (CI) = 0.19-1.00, $p = 0.05$) (2). However, only

data of the heaviest drinkers were used in the main meta-analysis and the association of intermediate alcohol use categories with incident frailty has not been investigated (2). Therefore, to further explore potential linear and non-linear associations between alcohol consumption and incident frailty risk, we conducted a two-stage dose-response meta-analysis using the data from the same longitudinal cohort studies.

The data used come from three prospective studies examining associations between quantity of alcohol consumption and incident frailty (4-6), identified in our previous systematic review and meta-analysis study, that provided data on frailty risk according to quantity of alcohol consumption (2). A value (in grams of alcohol per day) assigned to each alcohol consumption category was based on a mid-point of the upper and lower boundary values of the category. When the ranges of the alcohol consumption were different by gender in the same category, the assigned value was modified based on the gender proportion in the category. For the highest alcohol consumption category with only the lower boundary value, the boundary value multiplied by 1.2 was assigned (7). All three studies included had defined frailty according to the Fried phenotype (8). Crude relative risk (RR) and 95% CI of incident frailty for each alcohol consumption category compared with non-drinking category were calculated and used for the meta-

Released online in J-STAGE as advance publication October 11, 2017.

*Address correspondence to:

Dr. Gotaro Kojima, Department of Primary Care and Population Health, University College London (Royal Free Campus), Rowland Hill Street, London, NW3 2PF, UK.
E-mail: gotarokojima@yahoo.co.jp

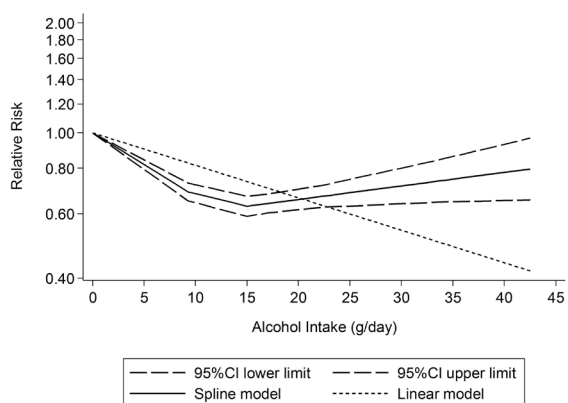


Figure 1. Dose-response linear and non-linear relationships between alcohol consumption and incident frailty risk. CI: confidence interval.

analyses.

Potential linear and non-linear dose-response associations between alcohol consumption and incident frailty were estimated using a two-stage dose-response meta-analysis (9). A random-effect model was used when heterogeneity was detected using the chi-square test, and a fixed-effect model was used otherwise. For the non-linear association, in the first stage, the restricted cubic spline method was applied with three fixed knots at percentiles (10%, 50%, and 90%) of the alcohol consumption distribution. In the second stage, the regression coefficients and the variance/covariance matrix were combined. Non-linearity was examined by the null hypothesis that the coefficient of the second spline is equal to zero. All statistical analyses were conducted using StataSE 14 (StataCorp LP, College Station, Texas, USA).

We included three studies examining incident frailty risks according to alcohol consumption among a total of 30,929 community-dwelling older people (age ≥ 60 years old) with 4,433 incident frailty cases (4-6). These studies categorized alcohol consumption into three or four categories with various cut-points (4-6).

For the linear association, a two-stage fixed-effect dose-response meta-analysis was conducted because of absence of significant heterogeneity ($p = 0.27$). There was a significant inverse linear association (pooled RR = 0.83 per 10 g/day increase in alcohol, 95% CI = 0.80-0.85, $p < 0.001$). However there was also a significant non-linear association between alcohol consumption and incident frailty risk (p for non-linearity < 0.001). In the model, the incident frailty risk by alcohol consumption showed a U-shaped association. The frailty risk decreased until around 15 g/day of alcohol consumption and increased thereafter. Predicted linear and non-linear incident frailty risk estimates by alcohol consumption are depicted in Figure 1. The non-linear model had a better fit, based on Akaike's information criterion (AIC) and Bayesian information criterion (BIC); AIC and BIC of the linear model were 82.6 and 81.7, respectively, while AIC and BIC of the non-linear model were 21.5 and

21.4, respectively.

We found a significant non-linear dose-response association between alcohol consumption and incident frailty among community-dwelling older people. Our analysis showed a U-shaped association, with the lowest risk with drinking around 15 g of alcohol per day (equivalent to approximately 2 UK units of alcohol or approximately 1 standard drink in the US). The incident frailty risk slowly increased at consumption above 15 g/day, however remained below that of non-drinkers until the highest alcohol value in our dataset (40 g/day).

These results should be interpreted with caution because of some limitations. First, only three studies were included in the analysis. The small number of the included studies also limited us in undertaking flexible non-linear dose-response analysis with more knots. Second, the highest alcohol consumption category was approximately 40 g/day (4) and it was not possible to examine frailty risk above that limit. Alcohol consumption less than 40 g/day may be too low to cause any clinically meaningful worsening of frailty even in older people (10). Third, all RRs used in the dose-response meta-analyses were unadjusted since they were calculated based on data from the included studies. Therefore our findings may be confounded by important factors like age, gender, smoking and socioeconomic status.

More research on the associations between alcohol consumption and frailty is needed. Future research should consider using higher cut-points to categorize alcohol consumption than 40 g/day, and use such statistical methods to examine potential dose-response non-linear associations. It is also vital to that future studies control for potential confounders.

Acknowledgements

We are grateful to the authors of the original study for sharing the data (5).

Funding

GK is funded by a University College London (UCL) Overseas Research Scholarship, which did not have any influence on the study design, the collection, analysis, and interpretation of data, the writing of the article or the decision to submit it for publication.

References

1. Nova E, Bacchan GC, Veses A, Zapatera B, Marcos A. Potential health benefits of moderate alcohol consumption: Current perspectives in research. *Proc Nutr Soc.* 2012; 71:307-315.
2. Kojima G, Liljas A, Iliffe S, Jivraj S, Walters K. A systematic review and meta-analysis of prospective associations between alcohol consumption and incident

- frailty. *Age Ageing*. 2017;1-9.
3. Clegg A, Young J, Iliffe S, Rikkert MO, Rockwood K. Frailty in elderly people. *Lancet*. 2013; 381:752-762.
 4. Ortola R, Garcia-Esquinas E, Leon-Munoz LM, Guallar-Castillon P, Valencia-Martin JL, Galan I, Rodriguez-Artalejo F. Patterns of alcohol consumption and risk of frailty in community-dwelling older adults. *J Gerontol A Biol Sci Med Sci*. 2016; 71:251-258.
 5. Seematter-Bagnoud L, Spagnoli J, Bula C, Santos-Eggimann B. Alcohol use and frailty in community-dwelling older persons aged 65 to 70 years. *J Frailty Aging*. 2014; 3:9-14.
 6. Woods NF, LaCroix AZ, Gray SL, Aragaki A, Cochrane BB, Brunner RL, Masaki K, Murray A, Newman AB; Women's Health Initiative. Frailty: Emergence and consequences in women aged 65 and older in the Women's Health Initiative Observational Study. *J Am Geriatr Soc*. 2005; 53:1321-1330.
 7. Berlin JA, Longnecker MP, Greenland S. Meta-analysis of epidemiologic dose-response data. *Epidemiology*. 1993; 4:218-228.
 8. Fried LP, Tangen CM, Walston J, Newman AB, Hirsch C, Gottdiener J, Seeman T, Tracy R, Kop WJ, Burke G, McBurnie MA; Cardiovascular Health Study Collaborative Research Group. Frailty in older adults: Evidence for a phenotype. *J Gerontol A Biol Sci Med Sci*. 2001; 56:M146-156.
 9. Orsini N, Li R, Wolk A, Khudyakov P, Spiegelman D. Meta-analysis for linear and nonlinear dose-response relations: Examples, an evaluation of approximations, and software. *Am J Epidemiol*. 2012; 175:66-73.
 10. Crome I, Li TK, Rao R, Wu LT. Alcohol limits in older people. *Addiction*. 2012; 107:1541-1543.

(Received September 23, 2017; Revised October 3, 2017; Accepted October 5, 2017)

Activity outside the home, environmental barriers, and healthy aging for community-dwelling elderly individuals in China

Yuhong Niu^{1,§}, Na Li^{1,§}, Chunlin Jin¹, Duo Chen¹, Yitong Yang², Hansheng Ding^{1,*}

¹Shanghai Health Development Research Center, Shanghai, China;

²University of Finance and Economics, Shanghai, China.

Summary

Elderly individuals benefit from frequently engaging in activities outside the home because such activities sustain the overall health and functioning of an aging body. However, environmental barriers can limit participation in activities outside the home by elderly individuals. The current study examined the factors that influence the frequency with which elderly individuals living in China engage in activity outside the home. Data were collected from 2,402 elderly individuals residing in the Jiangning district of Shanghai, China in 2015. Face-to-face interviews were conducted based on a questionnaire, and multiple regression analysis was used to measure influencing factors. Results revealed that elderly respondents with a better self-reported health status ($p = 0.2499$) engaged in activities outside the home more frequently. In addition, elderly respondents residing on higher floors of multi-floor residential buildings ($p < 0.001$) were less likely to participate in activities outside of the home. This effect was virtually eliminated, however, when the residence in question was equipped with an elevator ($p < 0.001$).

Keywords: Floor of residence, multi-floor residential building, activities outside the home, elevator, elderly individuals

Activity outside the home plays an important role in maintaining health among the elderly. Activity outside the home refers to activities performed in daily life and includes activities related to social networking, work, and transportation (1-3). Regular outings from a limited "living area" (*i.e.* an area where a person spends large amounts of time engaged in everyday activity) facilitates participation in meaningful activities within a society (4). These social activities may help the elderly ameliorate feelings of loneliness, build social networks, and satisfy social needs. In addition to the social aspects, elderly individuals engage in the most intense levels of physical activity outside of the home (5). Previous studies have suggested that going outside less frequently is associated with poorer overall health and mental problems in the elderly. Therefore, the elderly benefit from engaging in activities outside the home with a certain frequency since such activities sustain overall health and functioning in comparison to individuals who do not engage in activities

outside the home (6-8).

In 2007, the World Health Organization collected basic information on elderly people in 33 nations and then published *Global age-friendly cities: A guide* (9). This guide suggests that multi-floor residential buildings be equipped with an elevator if residents are elderly individuals. An age-friendly city has buildings that are more accessible to meet the varying needs of elderly people. Accordingly, elderly individuals need to reside on lower floors of residential buildings or have access to an elevator in a multi-floor residential building to remain able to engage in activities outside the home. Moreover, the 2015 *World Report on Aging and Health* outlines a framework for action to foster *Healthy Aging* built around the new concept of functional ability (10). The report indicated that architectural obstacles need to be reduced in order to facilitate activity by the elderly and it also revealed that varying levels of physical functioning and mental ability may limit activity by the elderly. Therefore, architectural plans need to feature ramps, handrails, elevators, and appropriated signage to facilitate use by the elderly, regardless of their level of activity.

Environmental barriers are associated with unsatisfactory living conditions or inadequate infrastructure. The elderly are predicted to have

[§]These authors contributed equally to this work.

*Address correspondence to:

Dr. Hansheng Ding, Development Research Center, Shanghai Health Development Research Center, Beijing (W) Road No.1477, Jingan District, Shanghai 200040, China.
E-mail: dinghansheng@hotmail.com

significantly lower scores for activities of daily living (ADL) and instrumental activities of daily living (IADL) if environmental barriers restrict their ability to engage in activities outside the home (11). This finding is substantiated by correlations between environmental barriers and restricted ability to engage in activities outside the home. In addition, many studies have provided evidence of an association between depressive mood and engaging in activities outside the home less frequently due to environmental barriers (5,7,8). A European study on how environmental barriers influence activities outside the home found that an environment of poor quality and poor street connectivity led to elderly individuals being unwilling go outside (12). In contrast, a Tokyo study found that green spaces near the residence of elderly individuals encourage their desire to engage in activities outside the home and may decrease their risk of mortality (11).

Unquestionably, Chinese elderly are faced with the environmental barriers mentioned earlier. However, there is one particular environmental barrier that many

Chinese elderly are likely to face but that Western elderly may not encounter. This particular environmental barrier is living in an apartment building that is not equipped with an elevator because of the age of many residential buildings in China. Descending stairs may hamper elderly individuals from engaging in activities outside the home, and thus eventually lead to inactivity. This inactivity, in turn, results in a decline in health and functioning. For this population, environmental pressure may decrease the desire to engage in activities outside the home.

According to *China's Design Code for Residential Buildings* promulgated in 1987, a building with more than 7 floors must be equipped with an elevator. In 2016, the elderly population (\geq the age of 60) in Shanghai totaled 4.58 million (13). Recent statistics indicated that 1.8 million elderly people resided in old buildings in Shanghai in 2013 (14). Old buildings referred to a three- (or four-) story house or an older style building with fewer than seven floors. None of these old buildings were equipped with an elevator.

In order to investigate whether the floor of residence

Table 1. Baseline characteristics of elderly individuals who had to descend stairs or who lived on the ground floor/had access to an elevator

Items	Descended stairs to engage in exercise outside the home, N (%)	Live on the ground floor or used an elevator to engage in exercise outside the home, N (%)	p value
Gender			0.9762
Male	668 (58.09)	482 (41.91)	
Female	728 (58.15)	524 (41.85)	
Age	71.24 \pm 7.34	70.57 \pm 7.01	0.0441
ADL	19.62 \pm 0.84	19.74 \pm 0.88	< 0.0001
IADL	7.67 \pm 0.94	7.72 \pm 0.86	0.1754
Self-reported health*			0.2499
Unhealthy	612 (59.48)	417 (40.52)	
Healthy	781 (57.13)	586 (42.87)	
Floor of residence			< 0.0001
Ground floor	0 (0)	509 (100)	
Second floor	471 (97.52)	12 (2.48)	
Third floor	310 (95.98)	13 (4.02)	
Fourth floor	232 (91.7)	21 (8.3)	
Fifth floor	182 (83.49)	36 (16.51)	
Sixth floor	169 (81.25)	39 (18.75)	
Seventh floor	32 (43.84)	41 (56.16)	
> Seventh floor	0 (0)	335 (100)	
Activities			< 0.0001
Inside only	237 (69.1)	106 (30.9)	
Outside the home	1,159 (56.29)	900 (43.71)	

ADL refers to routine activities in daily life that people are capable of performing, without assistance. These necessary functions include eating, bathing, dressing, and toileting; IADL refers to instrumental activities of daily living, including light housework, food preparation, shopping, and managing one's finances. *6 of 2,402 respondents did not respond to the question about self-reported health on the questionnaire.

Table 2. Factors influencing the desire of respondents to engage in activities outside the home

Effects	Point Estimate	95% Wald Confidence Interval	p value
Age	0.913	0.896 - 0.930	< 0.0001
Gender (Female vs. Male)	1.139	0.875 - 1.483	0.3323
Self-reported health status (Healthy vs. Unhealthy)	3.048	2.304 - 4.034	< 0.0001
ADL	1.068	0.936 - 1.219	0.3296
IADL	1.480	1.303 - 1.682	< 0.0001
Elevator (Yes vs. No)	2.051	1.519 - 2.768	< 0.0001
Floor of residence	0.968	0.939 - 0.998	0.0342

ADL refers to routine activities in daily life that people are capable of performing, without assistance. These necessary functions include eating, bathing, dressing, and toileting; IADL refers to instrumental activities of daily living, including light housework, food preparation, shopping, and managing one's finances. *6 of 2,402 respondents did not respond to the question about self-reported health on the questionnaire.

influences the desire of community-dwelling elderly to engage in activities outside the home, 2,402 active individuals age 60 or older residing in the Jiangning district of Shanghai, China were surveyed. Face-to-face interviews were conducted in 2015 based on a questionnaire. Respondents were divided into two groups: respondents who had to descend stairs to go outside and respondents who lived on the ground floor or who did not need to descend stairs as a result of access to an elevator. Demographic characteristics including age, gender, and self-reported health status and physical status including scores for both ADL and IADL were obtained. Multiple regression analysis was used to identify the factors influencing the desire of respondents to engage in activities outside the home.

As shown in Tables 1 and 2, the results yielded three interesting findings. First, elderly respondents with a better self-reported health status engaged in activities outside the home more frequently. Second, the floor on which a respondent resided was associated with the frequency with which the respondent engaged in activities outside the home. Further, the current study found that residing on a higher floor of a building resulted in less desire to engage in activities outside the home. Interestingly, respondents residing in an apartment building equipped with an elevator retained the desire to go outside and remain active, and these individuals were less influenced by the floor on which they resided. The results indicate that an elevator is extremely important within this context, enabling improvement of a less than ideal situation.

Activity outside the home is quite important to successful aging. Environmental barriers predict a significant decline in activity outside the home. In the current study, descending stairs represented a substantial environmental barrier to engaging in activities outside the home. Unfortunately, most of the old apartment buildings in China lack an elevator, so residents must descend stairs to go outside. However, an elevator can eliminate that problem. In light of this information, multi-floor residential buildings with elderly residents should be equipped with an elevator. Moreover, results of the self-reported health status indicated that elderly individuals with a better self-reported health status engaged in activities outside the home more frequently. This suggests that relatives, and society at large, should encourage those individuals to engage in activities outside of the home.

Acknowledgements

The study was supported by grants from the National Natural Science Foundation of China (grant no. 71073104/G0308), the China Medical Board's Program for Collaboration in Healthcare Research and Policymaking (CMB-CP 14-190), and Projects in the Three-year Action Plan of the Shanghai Health and Family Planning Commission (grant no. 43). The sponsor had no role in the design or conduct of the study; collection, management,

analysis, or interpretation of the data; or the preparation, review, or approval of the manuscript.

References

1. Simonsick EM, Guralnik JM, Volpato S, Balfour J, Fried LP. Just get out the door! Importance of walking outside the home for maintaining mobility: Findings from the Women's Health and Aging Study. *J Am Geriatr Soc.* 2005; 53:198-203.
2. Brach JS, Simonsick EM, Kritchevsky S, Yaffe K, Newman AB; Health, Aging and Body Composition Study Research Group. The association between physical function and lifestyle activity and exercise in the health aging and body composition study. *J Am Geriatr Soc.* 2004; 52:502-509.
3. Varma VR, Tan EJ, Wang T, Xue QL, Fried LP, Seplaki CL, King AC, Seeman TE, Rebok GW, Carlson MC. Low-intensity walking activity is associated with better health. *J Appl Gerontol.* 2014; 33:870-887.
4. Portegijs E, Tsai LT, Rantanen T, Rantakokko M. Moving through life-space areas and objectively measured physical activity of older people. *PLoS One.* 2015; 10:e0135308.
5. Kerr J, Sallis JF, Saelens BE, Cain KL, Conway TL, Frank LD, King AC. Outdoor physical activity and self-rated health in older adults living in two regions of the U.S. *Int J Behav Nutr Phys Act.* 2012; 9:89.
6. Jacobs JM, Cohen A, Hammerman-Rozenberg R, Azoulay D, Maaravi Y, Stessman J. Going outdoors daily predicts long-term functional and health benefits among ambulatory older people. *J Aging Health.* 2008; 20:259-272.
7. Shimada H, Ishizaki T, Kato M, Morimoto A, Tamate A, Uchiyama Y, Yasumura S. How often and how far do frail elderly people need to go outdoors to maintain functional capacity? *Arch Gerontol Geriatr.* 2010; 50:140-146.
8. Fujita K, Fujiwara Y, Chaves PH, Motohashi Y, Shinkai S. Frequency of going outdoors as a good predictors for incident disability of physical function as well as disability recovery in community-dwelling older adults in rural Japan. *J Epidemiol.* 2006; 16:261-270.
9. WHO. Aging and Life Course, Global age-friendly cities: A guide. http://www.who.int/ageing/age_friendly_cities_guide/en/ (accessed October 5, 2017).
10. WHO, Aging and Life Course, World report on ageing and health 2015. <http://www.who.int/ageing/events/world-report-2015-launch/en/> (accessed September 30, 2017).
11. Rantakokko M, Törmäkangas T, Rantanen T, Haak M, Iwarsson S. Environmental barriers, person-environment fit and mortality among community-dwelling very old people. *BMC Public Health.* 2013; 13:783.
12. Golant SM. Handbook of Aging and the Social Sciences, United States, 2011; pp. 207-212
13. Wu ZD. People's daily online. data show: By the end of December 2016, the elderly will account for over 31% of the population of Shanghai. http://www.cssn.cn/shx/shx_sjzx/201703/t20170329_3470307.shtml (accessed September 29, 2017) (in Chinese)
14. The evening news, Elderly people despair without access to an elevator to go outside and cool off. http://newspaper.jfdaily.com/xwwb/html/2013-08/05/content_1071120.htm (accessed September 5, 2017) (in Chinese)

(Received September 26, 2017; Revised October 16, 2017; Accepted October 18, 2017)

Guide for Authors

1. Scope of Articles

BioScience Trends is an international peer-reviewed journal. BioScience Trends devotes to publishing the latest and most exciting advances in scientific research. Articles cover fields of life science such as biochemistry, molecular biology, clinical research, public health, medical care system, and social science in order to encourage cooperation and exchange among scientists and clinical researchers.

2. Submission Types

Original Articles should be well-documented, novel, and significant to the field as a whole. An Original Article should be arranged into the following sections: Title page, Abstract, Introduction, Materials and Methods, Results, Discussion, Acknowledgments, and References. Original articles should not exceed 5,000 words in length (excluding references) and should be limited to a maximum of 50 references. Articles may contain a maximum of 10 figures and/or tables.

Brief Reports definitively documenting either experimental results or informative clinical observations will be considered for publication in this category. Brief Reports are not intended for publication of incomplete or preliminary findings. Brief Reports should not exceed 3,000 words in length (excluding references) and should be limited to a maximum of 4 figures and/or tables and 30 references. A Brief Report contains the same sections as an Original Article, but the Results and Discussion sections should be combined.

Reviews should present a full and up-to-date account of recent developments within an area of research. Normally, reviews should not exceed 8,000 words in length (excluding references) and should be limited to a maximum of 100 references. Mini reviews are also accepted.

Policy Forum articles discuss research and policy issues in areas related to life science such as public health, the medical care system, and social science and may address governmental issues at district, national, and international levels of discourse. Policy Forum articles should not exceed 2,000 words in length (excluding references).

Case Reports should be detailed reports of the symptoms, signs, diagnosis, treatment, and follow-up of an individual patient. Case reports may contain a demographic profile of the patient but usually describe an unusual or novel occurrence. Unreported or unusual

side effects or adverse interactions involving medications will also be considered. Case Reports should not exceed 3,000 words in length (excluding references).

News articles should report the latest events in health sciences and medical research from around the world. News should not exceed 500 words in length.

Letters should present considered opinions in response to articles published in BioScience Trends in the last 6 months or issues of general interest. Letters should not exceed 800 words in length and may contain a maximum of 10 references.

3. Editorial Policies

Ethics: BioScience Trends requires that authors of reports of investigations in humans or animals indicate that those studies were formally approved by a relevant ethics committee or review board.

Conflict of Interest: All authors are required to disclose any actual or potential conflict of interest including financial interests or relationships with other people or organizations that might raise questions of bias in the work reported. If no conflict of interest exists for each author, please state "There is no conflict of interest to disclose".

Submission Declaration: When a manuscript is considered for submission to BioScience Trends, the authors should confirm that 1) no part of this manuscript is currently under consideration for publication elsewhere; 2) this manuscript does not contain the same information in whole or in part as manuscripts that have been published, accepted, or are under review elsewhere, except in the form of an abstract, a letter to the editor, or part of a published lecture or academic thesis; 3) authorization for publication has been obtained from the authors' employer or institution; and 4) all contributing authors have agreed to submit this manuscript.

Cover Letter: The manuscript must be accompanied by a cover letter signed by the corresponding author on behalf of all authors. The letter should indicate the basic findings of the work and their significance. The letter should also include a statement affirming that all authors concur with the submission and that the material submitted for publication has not been published previously or is not under consideration for publication elsewhere. The cover letter should be submitted in PDF format. For example of Cover Letter, please visit <http://www.biosciencetrends.com/downcentre.php> (Download Centre).

Copyright: A signed JOURNAL PUBLISHING AGREEMENT (JPA) form must be provided by post, fax, or as a scanned file before acceptance of the article. Only forms with a hand-written signature are accepted. This copyright will ensure the widest possible dissemination of information. A form facilitating transfer of copyright can be downloaded by clicking the

appropriate link and can be returned to the e-mail address or fax number noted on the form (Please visit [Download Centre](#)). Please note that your manuscript will not proceed to the next step in publication until the JPA Form is received. In addition, if excerpts from other copyrighted works are included, the author(s) must obtain written permission from the copyright owners and credit the source(s) in the article.

Suggested Reviewers: A list of up to 3 reviewers who are qualified to assess the scientific merit of the study is welcomed. Reviewer information including names, affiliations, addresses, and e-mail should be provided at the same time the manuscript is submitted online. Please do not suggest reviewers with known conflicts of interest, including participants or anyone with a stake in the proposed research; anyone from the same institution; former students, advisors, or research collaborators (within the last three years); or close personal contacts. Please note that the Editor-in-Chief may accept one or more of the proposed reviewers or may request a review by other qualified persons.

Language Editing: Manuscripts prepared by authors whose native language is not English should have their work proofread by a native English speaker before submission. If not, this might delay the publication of your manuscript in BioScience Trends.

The Editing Support Organization can provide English proofreading, Japanese-English translation, and Chinese-English translation services to authors who want to publish in BioScience Trends and need assistance before submitting a manuscript. Authors can visit this organization directly at <http://www.iacmhr.com/iac-eso/support.php?lang=en>. IAC-ESO was established to facilitate manuscript preparation by researchers whose native language is not English and to help edit works intended for international academic journals.

4. Manuscript Preparation

Manuscripts should be written in clear, grammatically correct English and submitted as a Microsoft Word file in a single-column format. Manuscripts must be paginated and typed in 12-point Times New Roman font with 24-point line spacing. Please do not embed figures in the text. Abbreviations should be used as little as possible and should be explained at first mention unless the term is a well-known abbreviation (e.g. DNA). Single words should not be abbreviated.

Title Page: The title page must include 1) the title of the paper (Please note the title should be short, informative, and contain the major key words); 2) full name(s) and affiliation(s) of the author(s), 3) abbreviated names of the author(s), 4) full name, mailing address, telephone/fax numbers, and e-mail address of the corresponding author; and 5) conflicts of interest (if you have an actual or potential conflict of interest to disclose, it must be included as a footnote on the title page of the manuscript; if no conflict of

interest exists for each author, please state "There is no conflict of interest to disclose"). Please visit [Download Centre](#) and refer to the title page of the manuscript sample.

Abstract: The abstract should briefly state the purpose of the study, methods, main findings, and conclusions. For article types including Original Article, Brief Report, Review, Policy Forum, and Case Report, a one-paragraph abstract consisting of no more than 250 words must be included in the manuscript. For News and Letters, a brief summary of main content in 150 words or fewer should be included in the manuscript. Abbreviations must be kept to a minimum and non-standard abbreviations explained in brackets at first mention. References should be avoided in the abstract. Key words or phrases that do not occur in the title should be included in the Abstract page.

Introduction: The introduction should be a concise statement of the basis for the study and its scientific context.

Materials and Methods: The description should be brief but with sufficient detail to enable others to reproduce the experiments. Procedures that have been published previously should not be described in detail but appropriate references should simply be cited. Only new and significant modifications of previously published procedures require complete description. Names of products and manufacturers with their locations (city and state/country) should be given and sources of animals and cell lines should always be indicated. All clinical investigations must have been conducted in accordance with Declaration of Helsinki principles. All human and animal studies must have been approved by the appropriate institutional review board(s) and a specific declaration of approval must be made within this section.

Results: The description of the experimental results should be succinct but in sufficient detail to allow the experiments to be analyzed and interpreted by an independent reader. If necessary, subheadings may be used for an orderly presentation. All figures and tables must be referred to in the text.

Discussion: The data should be interpreted concisely without repeating material already presented in the Results section. Speculation is permissible, but it must be well-founded, and discussion of the wider implications of the findings is encouraged. Conclusions derived from the study should be included in this section.

Acknowledgments: All funding sources should be credited in the Acknowledgments section. In addition, people who contributed to the work but who do not meet the criteria for authors should be listed along with their contributions.

References: References should be numbered in the order in which they appear in the text. Citing of unpublished results, personal communications, conference abstracts, and theses in the reference list is not recommended but these sources may be mentioned in the text. In the reference list,

cite the names of all authors when there are fifteen or fewer authors; if there are sixteen or more authors, list the first three followed by *et al.* Names of journals should be abbreviated in the style used in PubMed. Authors are responsible for the accuracy of the references. Examples are given below:

Example 1 (Sample journal reference): Inagaki Y, Tang W, Zhang L, Du GH, Xu WF, Kokudo N. Novel aminopeptidase N (APN/CD13) inhibitor 24F can suppress invasion of hepatocellular carcinoma cells as well as angiogenesis. *Biosci Trends*. 2010; 4:56-60.

Example 2 (Sample journal reference with more than 15 authors): Darby S, Hill D, Auvinen A, *et al.* Radon in homes and risk of lung cancer: Collaborative analysis of individual data from 13 European case-control studies. *BMJ*. 2005; 330:223.

Example 3 (Sample book reference): Shalev AY. Post-traumatic stress disorder: diagnosis, history and life course. In: Post-traumatic Stress Disorder, Diagnosis, Management and Treatment (Nutt DJ, Davidson JR, Zohar J, eds.). Martin Dunitz, London, UK, 2000; pp. 1-15.

Example 4 (Sample web page reference): Ministry of Health, Labour and Welfare of Japan. Dietary reference intakes for Japanese. <http://www.mhlw.go.jp/houdou/2004/11/h1122-2a.html> (accessed June 14, 2010).

Tables: All tables should be prepared in Microsoft Word or Excel and should be arranged at the end of the manuscript after the References section. Please note that tables should not be image format. All tables should have a concise title and should be numbered consecutively with Arabic numerals. If necessary, additional information should be given below the table.

Figure Legend: The figure legend should be typed on a separate page of the main manuscript and should include a short title and explanation. The legend should be concise but comprehensive and should be understood without referring to the text. Symbols used in figures must be explained.

Figure Preparation: All figures should be clear and cited in numerical order in the text. Figures must fit a one- or two-column format on the journal page: 8.3 cm (3.3 in.) wide for a single column, 17.3 cm (6.8 in.) wide for a double column; maximum height: 24.0 cm (9.5 in.). Please make sure that the symbols and numbers appeared in the figures should be clear. Please make sure that artwork files are in an acceptable format (TIFF or JPEG) at minimum resolution (600 dpi for illustrations, graphs, and annotated artwork, and 300 dpi for micrographs and photographs). Please provide all figures as separate files. Please note that low-resolution images are one of the leading causes of article resubmission and schedule delays. All color figures will be reproduced in full color in the online edition of the journal at no cost to authors.

Units and Symbols: Units and symbols

conforming to the International System of Units (SI) should be used for physicochemical quantities. Solidus notation (*e.g.* mg/kg, mg/mL, mol/mm²/min) should be used. Please refer to the SI Guide www.bipm.org/en/si/ for standard units.

Supplemental data: Supplemental data might be useful for supporting and enhancing your scientific research and BioScience Trends accepts the submission of these materials which will be only published online alongside the electronic version of your article. Supplemental files (figures, tables, and other text materials) should be prepared according to the above guidelines, numbered in Arabic numerals (*e.g.*, Figure S1, Figure S2, and Table S1, Table S2) and referred to in the text. All figures and tables should have titles and legends. All figure legends, tables and supplemental text materials should be placed at the end of the paper. Please note all of these supplemental data should be provided at the time of initial submission and note that the editors reserve the right to limit the size and length of Supplemental Data.

5. Submission Checklist

The Submission Checklist will be useful during the final checking of a manuscript prior to sending it to BioScience Trends for review. Please visit [Download Centre](#) and download the Submission Checklist file.

6. Online Submission

Manuscripts should be submitted to BioScience Trends online at <http://www.biosciencetrends.com>. The manuscript file should be smaller than 5 MB in size. If for any reason you are unable to submit a file online, please contact the Editorial Office by e-mail at office@biosciencetrends.com.

7. Accepted Manuscripts

Proofs: Galley proofs in PDF format will be sent to the corresponding author via e-mail. Corrections must be returned to the editor (proof-editing@biosciencetrends.com) within 3 working days.

Offprints: Authors will be provided with electronic offprints of their article. Paper offprints can be ordered at prices quoted on the order form that accompanies the proofs.

Page Charge: Page charges will be levied on all manuscripts accepted for publication in BioScience Trends (\$140 per page for black white pages; \$340 per page for color pages). Under exceptional circumstances, the author(s) may apply to the editorial office for a waiver of the publication charges at the time of submission.

(Revised February 2013)

Editorial and Head Office:

Pearl City Koishikawa 603
2-4-5 Kasuga, Bunkyo-ku
Tokyo 112-0003 Japan
Tel: +81-3-5840-8764
Fax: +81-3-5840-8765
E-mail: office@biosciencetrends.com

JOURNAL PUBLISHING AGREEMENT (JPA)

Manuscript No.:

Title:

Corresponding Author:

The International Advancement Center for Medicine & Health Research Co., Ltd. (IACMHR Co., Ltd.) is pleased to accept the above article for publication in BioScience Trends. The International Research and Cooperation Association for Bio & Socio-Sciences Advancement (IRCA-BSSA) reserves all rights to the published article. Your written acceptance of this JOURNAL PUBLISHING AGREEMENT is required before the article can be published. Please read this form carefully and sign it if you agree to its terms. The signed JOURNAL PUBLISHING AGREEMENT should be sent to the BioScience Trends office (Pearl City Koishikawa 603, 2-4-5 Kasuga, Bunkyo-ku, Tokyo 112-0003, Japan; E-mail: office@biosciencetrends.com; Tel: +81-3-5840-8764; Fax: +81-3-5840-8765).

1. Authorship Criteria

As the corresponding author, I certify on behalf of all of the authors that:

- 1) The article is an original work and does not involve fraud, fabrication, or plagiarism.
- 2) The article has not been published previously and is not currently under consideration for publication elsewhere. If accepted by BioScience Trends, the article will not be submitted for publication to any other journal.
- 3) The article contains no libelous or other unlawful statements and does not contain any materials that infringes upon individual privacy or proprietary rights or any statutory copyright.
- 4) I have obtained written permission from copyright owners for any excerpts from copyrighted works that are included and have credited the sources in my article.
- 5) All authors have made significant contributions to the study including the conception and design of this work, the analysis of the data, and the writing of the manuscript.
- 6) All authors have reviewed this manuscript and take responsibility for its content and approve its publication.
- 7) I have informed all of the authors of the terms of this publishing agreement and I am signing on their behalf as their agent.

2. Copyright Transfer Agreement

I hereby assign and transfer to IACMHR Co., Ltd. all exclusive rights of copyright ownership to the above work in the journal BioScience Trends, including but not limited to the right 1) to publish, republish, derivate, distribute, transmit, sell, and otherwise use the work and other related material worldwide, in whole or in part, in all languages, in electronic, printed, or any other forms of media now known or hereafter developed and the right 2) to authorize or license third parties to do any of the above.

I understand that these exclusive rights will become the property of IACMHR Co., Ltd., from the date the article is accepted for publication in the journal BioScience Trends. I also understand that IACMHR Co., Ltd. as a copyright owner has sole authority to license and permit reproductions of the article.

I understand that except for copyright, other proprietary rights related to the Work (e.g. patent or other rights to any process or procedure) shall be retained by the authors. To reproduce any text, figures, tables, or illustrations from this Work in future works of their own, the authors must obtain written permission from IACMHR Co., Ltd.; such permission cannot be unreasonably withheld by IACMHR Co., Ltd.

3. Conflict of Interest Disclosure

I confirm that all funding sources supporting the work and all institutions or people who contributed to the work but who do not meet the criteria for authors are acknowledged. I also confirm that all commercial affiliations, stock ownership, equity interests, or patent-licensing arrangements that could be considered to pose a financial conflict of interest in connection with the article have been disclosed.

Corresponding Author's Name (Signature):

Date:

